UNIVERSITY OF CALIFORNIA SAN DIEGO

Loss of *GTF2I* promotes synaptic dysfunction and impaired connectivity in human cellular models of neurodevelopment

A Dissertation submitted in partial satisfaction of the requirements
for the degree Doctor of Philosophy

in

Neurosciences with a Specialization in Anthropogeny

by

Jason William Adams

Committee in charge:

Professor Alysson Muotri, Chair
Professor Pascal Gagneux
Professor Jeffrey Gold
Professor Robert Hevner
Professor Prashant Mali
Professor Karl Wahlin

2022

The Dissertation of Jason William Adams is approved, and it is acceptable in quality and form for publication on microfilm and electronically.

University of California San Diego

2022

DEDICATION

This dissertation and, far more important, any development it might earnestly hope to represent can only be dedicated to Brandon Gavett, PhD, who, 10 years ago nearly to the day, opened the door to the future.

EPIGRAPH

"When my information changes, I change my mind. What do you do?"

—*John Maynard Keynes* (supposedly)

TABLE OF CONTENTS

LIST OF FIGURES

LIST OF ABBREVIATIONS

ASD	Autism spectrum disorder
GTF2I	General transcription factor 2I
hiPSC	Human induced pluripotent stem cell
MEA	multi-electrode array
NPC	neural progenitor cell
WS	Williams-Beuren (William) syndrome
7dup	7q11.23 microduplication syndrome

ACKNOWLEDGEMENTS

In any endeavor, it is the people involved who ultimately shape its quality, and I would be incapable of proceeding without first acknowledging the principal characters among the high-caliber cast with whom I have been fortunate enough to work.

First among many, I gratefully acknowledge the generous and enduring support of my advisor, Dr. Alysson Muotri. Something I contemplate regularly, and am particularly grateful for, is your ready willingness, eagerness in fact, to extend opportunity. With an astonishing, admirable, and very much appreciated measure of trust, you have allowed and often even encouraged my pursuits or antics, and only rarely doused them (these, I suspect, were times when I was at the sheerest heights of idiocy). This is one of the things I have most appreciated about our interactions and discussions—for example, when I've come to you with ideas about how we want to proceed or whether I should pursue some particular new direction—is that the focus is on the science, be it scientific plausibility or the value (i.e., the purpose) of the science being proposed, rather than other non-scientific encumbrances (e.g., shortsighted technical hindrances). Another thing I would like to acknowledge my appreciation of and respect for (particularly given that I suspect it was of key importance for my scientific development or, rather, how I get "brought up" as a trainee) is your general open-mindedness to scientific progress in general, an outlook I think is very valuable for trainees, or at least it certainly was for this trainee. Moreover, I appreciate that your ethos, and hence that of the lab, is very much to move the great ball of science forward, into where the waters are choppier, rather than being trapped in the safer, calmer waters of the past. Overall, to put it simply, I consider myself incredibly fortunate to have had an advisor who foremost sees opportunities rather than barriers, who sees the promising potential of an undertaking rather than the

potential pitfalls. And, if for no better reason than I've already noticed it happen, I know that this perspective will greatly influence how I think about scientific and clinical problems in the future.

A successful production requires more than a visionary director, however, and it has been an inspiration for this nascently developing scientist to work with such an immensely talented group of people. Well, *characters* is really the appropriate word. To Cleber Trujillo and Priscilla Negraes, I genuinely appreciate indescribably the tutelage and opportunities you've provided to help me develop as a scientist, but even more so, I will be forever grateful that we have transformed our successful work partnerships into solid personal friendships, emboldened by apartment-moving, Thanksgiving, a speakeasy outing, and a baby shower, to which someone brought homemade quindim.

To the great Fabio Papes and Simoni Avansini, it was excellent getting to work with both of you in the lab and having the opportunity to share dinners (Christmas!), other activities, and conversations outside of lab. The two of you surely rank among the world's most caring people, and the loss of your energy from the lab has left an unfillable void. I am so grateful for the friendship we've established; we must keep it well tended and vigorously defended across decades. I'm already looking forward to the next trip to Brazil…and this time the amazing Francesca Puppo is coming, too. Francesca, I'm so glad our tenures in the lab overlapped so perfectly, you're one of my favorite colleagues with whom I've ever had the pleasure to work. Your radiant personality and tireless energy always brighten any work day or event, whether it's a lab sunset bonfire at the beach or hour three and counting in the TC. I hope we continue to cross paths for many years into the future and can start working together on some more projects.

For two more people who command special mention, Fernanda Cugola and Angels Almenar-Queralt, I wish our time in the lab had been more overlapping. To Fernanda, who left too soon, I'm very glad that we got to work together on a couple projects, writing and presenting, and that we continue to encounter each other at get-togethers outside of lab. It must be said that, among other things, I've been very appreciative of your candid perspectives as an entertaining *raconteuse* on the joys of the PhD experience. Seldom have the words "best years of my life" been deployed to greater effect… On the opposing end of the lab-timing-overlap spectrum, meanwhile, has been the more recent arrival of Angels. Professionally, it is a gift given to few to be able to inspire one's colleagues via the raw caliber of one's work on its own. With her intellect, scientific logic, disciplined experimental talent, and creativity, Angels is one of them. Angels, even in such a short number of months (not counting individual hours in the TC, each of which is capable of lasting its own month) of being able to work alongside you and glean your insight, I have been able to appreciate changes in my own patterns of scientific thinking, to say nothing of how you've helped me improve my technical scientific skills. I am unable to express the depth of my gratitude to you for your willingness to share your scientific expertise and perspective, they have transformatively enriched this past year of my PhD and have challenged me to try and improve each dimension of my own work. Moreover, I'm glad we got to share so many laughs in the TC, it wouldn't have been the same without you.

Beyond those mentioned thus far, I cannot fail to acknowledge my gratitude to Pinar Mesci for the experimental guidance, scientific opinions, and the other conversations we have shared across the years. It has been a genuine pleasure to work with you, and I'm looking forward to seeing where your next career step takes you. Critically, I must recognize the other

PhD students in the lab—Cedric Snethlage, Gabriela Goldberg, Erin LaMontagne, Tiffany Chu, and Blanca Martin-burgos. For me, the support we all offer to one another, pandemic or otherwise, has provided a consistent handhold of solidarity, even when things have felt at their most ridiculous, and will be the necessary and durable element to get us over the finish line. In addition to the other PhD students, it has been a great pleasure, and constant source of entertainment, to work with a number of other talented and remarkable collaborators, techs, and students. In particular, Richard Gao, Lucas Henry, Ryan Szeto, and Justin Truong, I hope we can continue to work together and that our paths cross again many times in the future. And to the diligent and persistent students who have had the misfortune of working with me, Annabelle Vinokur and Charles Austria, hopefully I've been able to make even a slight contribution to your progress in the world.

Outside the Muotri lab, I am immensely grateful for the dedication of time and persistent assistance of Karl Wahlin, without whom this PhD would have been immeasurably more brutal and immeasurably less valuable. My gratitude extends not just to the tutelage and assistance you provided with gene editing human stem cells and the molecular biology inherent to that undertaking (a debt of such magnificent magnitude that words to accurately quantify it do not exist and which I shall never be able to properly repay), but also to the discussions, scientific and otherwise, and *very* late nights in the TC and making constructs.

It is with further gratitude that I acknowledge the additional training and support provided by Pascal Gagneux and the UCSD Center for Academic Research and Training in Anthropogeny (CARTA). I can very easily bring to mind the memory of being a brand-new medical student, the first day—indeed, the opening lecture—in the earliest (dare I say embryonic?) stages of my medical and graduate education and listening to Ajit Varki's

presentation on the evolutionary foundation of many of modern humans' pathologies. I made mental note of the "decals" on the slides and carefully stored them for future pursuit: Here was a Center for research that seemed to encapsulate all of my academic interests—from human origins to neuroscience to medicine—and, into the bargain, fostered interdisciplinary discourse on the study of humans. It perhaps goes without saying, but I will of course say it anyways, that my CARTA interactions have been a consistent bright spot throughout my graduate education, and I will seek to keep that spirit alive as I embark on future endeavors in science and medicine.

I say often that I am fortunate to have such incredible friends, in San Diego and elsewhere, and failure to include such a statement here would render these Acknowledgements woefully incomplete. Regarding my MSTP cohort, I think often how lucky I was to get placed with such a remarkable group of people, such a remarkable group of friends, with our laughs and get-togethers and stories and conversation that can rekindle the inner fire. It's difficult to think what the experience would be like to go through the duration of this program with a different group…my suspicion is that it would be far less rewarding. In addition to my San Diego compatriots, I am likewise unable to express how grateful I am for the support of my friends outside of San Diego, who are, each in turn, pursuing different career fields, thus offering interesting stories and a crucial tether to the world outside of science and medicine.

Alas, I must close these acknowledgements with an admission, or perhaps a confession, and a declaration. In paraphrase, Theodore Roosevelt supposedly pointed out that the only people who never make mistakes are people who never do anything. This, by way of confession, is essentially the same outlook with which I naïvely approached the PhD.

Sometimes for better and other times for worse, I suppose, but the unavoidable result—well, better say *consequence*—of this approach has been an ever-persistent, yet-exponentially accumulating pile of innumerable failures and mistakes. Some of these are larger failures; many, in hindsight, verge on the comical. But others are smaller and, by mistaken oversight, some are surely still hiding within this document, the result of my failure to sufficiently purge them from its pages. Thus, while any successes that may be contained or implied within this document, and indeed within the entirety of my PhD, could not have been achieved without the people listed above (in addition to countless others), I declare at the outset that culpability for any mistakes, inadequacies, or outright failures is mine alone.

Chapter/Appendix co-author acknowledgements:

The main body of the dissertation is currently being prepared for submission for publication of the material. Adams, J. W., Vinokur, A., Austria, C., Guerra, B. S., Herai, R. H., Wahlin, K. J., & Muotri, A. R. **Loss of *GTF2I* promotes synaptic dysfunction and impaired connectivity in human cellular models of neurodevelopment**. The dissertation author was the primary investigator and author of this material.

Appendix 1, in full, is a reprint of the material as it appears in the following manuscript, published in *Physiology*: Adams, J. W., Cugola, F. R., & Muotri, A. R. (2019). **Brain Organoids as Tools for Modeling Human Neurodevelopmental Disorders**. The dissertation author was the primary author of this paper.

Appendix 2, in full, is a reprint of the material as it appears in the following manuscript, published in *EMBO Molecular Medicine*: Trujillo, C. A.*, Adams, J. W.*, Negraes, P. D., Carromeu, C., Tejwani, L., Acab, A., Tsuda, B., Thomas, C. A., Sodhi, N.,

Fichter, K. M., Romero, S., Zanella, F., Sejnowski, T. J., Ulrich, H., & Muotri, A. R. (2021). **Pharmacological reversal of synaptic and network pathology in human *MECP2*-KO neurons and cortical organoids.** The dissertation author was one of the primary investigators and co-first authors of this paper.

Appendix 3, in full, has been submitted for publication of the material as it may appear in *Molecular Psychiatry*: Adams, J. W., Negraes, P. D., Truong, J., Tran, T., Szeto, R. A., Teodorof-Diedrich, C., Spector, S. A., Del Campo, M., Jones, K. L., Muotri, A. R.*, & Trujillo, C. A.* (2022). **Impact of alcohol exposure on neural development and network formation in human cortical organoids.** The dissertation author was the primary researcher and author of this paper.

VITA

2014	Bachelor of Science in Biology, University of Colorado Colorado Springs
2014	Bachelor of Arts in Psychology, University of Colorado Colorado Springs
2014-2016	Research Assistant, Boston University School of Medicine
2022	Doctor of Philosophy in Neurosciences with a Specialization in Anthropogeny, University of California San Diego
2024	Doctor of Medicine (expected), University of California San Diego

PUBLICATIONS

Raposo-Amaral, C. E., Raposo-Amaral, C. A., **Adams, J. W.**, & Ghizoni, E. (2022). Posterior Vault Distraction Outcomes in Patients with Severe Crouzon Syndrome Resulting from Ser347Cys and Ser354Cys Mutations. *Journal of Craniofacial Surgery, 33*.

Avansini, S. H., Puppo, F., **Adams, J.W.**, et al. (2021). Junctional instability in neuroepithelium and network hyperexcitability in a focal cortical dysplasia human model. *Brain*.

Trujillo, C. A.*, **Adams, J. W.***, Negraes, P. D., et al. (2021). Pharmacological reversal of synaptic and network pathology in human *MECP2*-KO neurons and cortical organoids. *EMBO Molecular Medicine*, *13(*1*)*: e12523.

Adams, J. W., Alosco, M. L., Mez, J., et al. (2020). Association of probable REM sleep behavior disorder with pathology and years of contact sports play in chronic traumatic encephalopathy. *Acta Neuropathologica*, *140*, 851-862.

Adams, J. W., Cugola, F. R., & Muotri, A. R. (2019). Brain organoids as tools for modeling neurodevelopmental disorders. *Physiology*, *34*(5): 365-375.

Adams, J. W., Mahar, I., & McKee, A. C. (2019). Chronic traumatic encephalopathy. In M. L. Alosco & R. A. Stern (Eds.), *The Oxford handbook of adult cognitive disorders* (pp. 631-644). Oxford University Press.

Adams, J. W., Alvarez, V. E., Mez, J., et al. (2018). Lewy body pathology and chronic traumatic encephalopathy associated with contact sports. *Journal of Neuropathology & Experimental Neurology*, *77*(9), 757–768.

Griffin, J. W., John, S. E., **Adams, J. W.**, Bussell, C. A., Saurman, J. L., & Gavett, B. E. (2017). The effects of age on the learning and forgetting of primacy, middle, and

recency components of a multi-trial word list. *Journal of Clinical and Experimental Neuropsychology*, *39*(9), 900-912.

Mez, J., Solomon, T. M., Daneshvar, D. H., Murphy, L., Kiernan, P. T., Montenigro, P. H., Kriegel, J., Abdolmohammadi, B., Fry, B., Babcock, K. J., **Adams, J. W.**, et al. (2015). Assessing clinicopathological correlation in chronic traumatic encephalopathy: rationale and methods for the UNITE study. *Alzheimer's Research & Therapy*, *7*(1):62.

Gavett, B. E., Vudy, V., Jeffrey, M., John, S. E., Gurnani, A., & **Adams, J. W.** (2015). The δ latent dementia phenotype in the Uniform Data Set: Cross-validation and extension. *Neuropsychology*, *29*(3), 344-352.

Silk-Eglit, G. M., Stenclik, J. H., Gavett, B. E., **Adams, J. W.**, Lynch, J. K., & McCaffrey, R. J. (2014). Base rate of performance invalidity among non-clinical undergraduate research participants. *Archives of Clinical Neuropsychology*, *29*(5), 415-421.

ABSTRACT OF THE DISSERTATION

Loss of *GTF2I* promotes synaptic dysfunction and impaired connectivity in human cellular models of neurodevelopment

by

Jason William Adams

Doctor of Philosophy in Neurosciences with a Specialization in Anthropogeny

University of California San Diego, 2022

Professor Alysson Muotri, Chair

Individuals with Williams syndrome (WS), a multisystemic neurodevelopmental disorder, characteristically portray a hypersocial phenotype. WS is caused by the hemizygous loss of ~26 genes at chromosomal locus 7q11.23, one of which is *GTF2I*. Copy number variations and mutations in *GTF2I* are associated with altered sociality and have been proposed to underlie the hypersocial expression of WS. However, the contribution of *GTF2I* to human neurodevelopment remains incompletely understood. Here, human cellular models

of neurodevelopment, including neural progenitors, neurons, and three-dimensional cortical organoids, were differentiated from CRISPR-Cas9-edited *GTF2I*-knockout (*GTF2I*-KO) isogenic pluripotent stem cells (hiPSCs) to investigate the role of *GTF2I* in human neurodevelopment. Compared to controls, *GTF2I*-KO progenitors exhibited an increased proliferation rate and an altered cell cycle profile. Cortical organoids and neurons demonstrated increased cell death and synaptic dysregulation, including synaptic structural dysfunction and electrophysiological impairment on multi-electrode array. Overall, our findings show loss of *GTF2I* promotes synaptic defects, increased cell death, and impaired neuronal network function in human cellular models of neurodevelopment, suggesting changes in synaptic circuit integrity may be a prominent mediator of the link between alterations in *GTF2I* and variation in the phenotypic expression of human sociality.

INTRODUCTION

Deletion or duplication of ~26-28 genes in the 7q11.23 chromosomal region results in Williams syndrome (WS) or 7q11.23 microduplication syndrome (7dup), respectively (Pober, 2010; Somerville et al., 2005). These multisystemic disorders exhibit a constellation of symptoms with frequently opposing phenotypic expression, a reflection of the dose-dependent effects of copy number alterations of the underlying genes that also renders them excellent portraits of genotype-phenotype correlation (Kozel et al., 2021; Morris et al., 2015; Preus, 1984). Among these symptoms are notably contrasting neurocognitive phenotypes, in particular differences in social expressivity (López-Tobón et al., 2020; Pober, 2010; Somerville et al., 2005). Whereas individuals with 7dup customarily portray hyposocial symptoms of autism spectrum disorder (ASD; Barak & Feng, 2016; Depienne et al., 2007; Somerville et al., 2005), patients with WS, in which haploinsufficiency affects the full set of ~26-28 genes, feature the unique behavioral trait of pronounced hypersociality (Bellugi et al., 2000; Doyle et al., 2004). In contrast to these individuals with classical or "typical" WS, however, some "atypical" WS patients have smaller deletions and consequently present with partial WS clinical profiles that spare particular phenotypes (Kozel et al., 2021). On this basis, previous studies have indicated the altered social phenotype of WS may be attributable to haploinsufficiency of *GTF2I* (Chailangkarn et al., 2018; Karmiloff-Smith et al., 2012), a gene located in the WS chromosomal region (Kozel et al., 2021; Osborne et al., 2001; Pober, 2010; Scherer et al., 2003). Most notable was the observation of a patient who near-selectively preserved both copies of *GTF2I* and, in association, retained a normal social phenotype (Dai et al., 2009). Similarly, a separate study reported two single-nucleotide polymorphisms in

GTF2I in an ASD cohort (Malenfant et al., 2012), further argument for the role of this gene as a mediator of social expression.

GTF2I encodes the general transcription factor 2I (GTF2I), a protein with multiple functions in both the cytoplasm and nucleus of the cell (Parker et al., 2001; Roy, 2001). Foremost among these, GTF2I is thought to be a prominent regulator of signal-induced gene transcription, a process in which stimulation via extracellular signals activates GTF2I, thereby inducing its translocation to the nucleus (Desgranges & Roy, 2006; Roy, 2001, 2007). GTF2I can influence gene expression both directly—for example, by binding to initiator element-containing promoters at the transcription start sites of target genes or an upstream E-box element (Roy et al., 1991, 1997)—or indirectly, such as via association with chromatin modifier complexes (Adamo et al., 2015).

To date, most studies that have investigated the effects of *GTF2I* on neurodevelopment have been conducted in animal models (Danoff et al., 2004; Deurloo et al., 2019). These have affirmed the association of heterozygous *GTF2I* deletion with hypersociality and, furthermore, demonstrated the essentiality of *GTF2I* for viability (Enkhmandakh et al., 2009; Lucena et al., 2010; Sakurai et al., 2011). Additionally, Barak and colleagues showed that selective deletion of *GTF2I* from excitatory neurons in the brains of mice resulted in impaired myelination as well as motor and behavioral deficits (Barak et al., 2019). Despite this progress, however, recapitulation of aspects of human cortical development by animal models may be suboptimal (Hodge et al., 2019), a subtle yet perhaps salient difference given the preeminent association between humans and social expression. The use of human pluripotent stem cells (hiPSCs) has facilitated the study of mechanisms of neurodevelopmental disease in a human context (Adams et al., 2019), but prior studies that

have investigated this spectrum of disorders have mainly been limited to WS and 7dup (Adamo et al., 2015; Chailangkarn et al., 2016). In consequence, the role of *GTF2I* in human neurodevelopment has yet to be comprehensively defined.

Here, we used differentiated neural cell models—including neural progenitor cells (NPCs), human neurons, and three-dimensional cortical organoids—from isogenic *GTF2I*-knockout (*GTF2I*-KO) hiPSCs to investigate the contribution of *GTF2I* to human neurodevelopment. Loss of *GTF2I* resulted in progenitors with altered cell cycle and proliferation and promoted the development of neurons and cortical organoids with synaptic defects, increased cell death, and neuronal network impairment. Overall, our findings tentatively support a model in which alterations in NPCs induced by loss of *GTF2I* give rise to neurons and networks with synaptic defects, reduced connectivity, and impaired neuronal health.

Acknowledgments

The main body of the dissertation is currently being prepared for submission for publication of the material. Adams, J. W., Vinokur, A., Austria, C., Guerra, B. S., Herai, R. H., Wahlin, K. J., & Muotri, A. R. **Loss of *GTF2I* promotes synaptic dysfunction and impaired connectivity in human cellular models of neurodevelopment**. The dissertation author was the primary investigator and author of this material.

MATERIALS & METHODS

hiPS cell lines and cell culture

Control CVB and WT83 hiPS cell lines were generated and characterized as has been described (Chaves et al., 2021; Gore et al., 2011; Trujillo et al., 2019). CRISPR-Cas9 editing was performed similarly to as described (Wahlin et al., 2021), with guide RNAs delivered using a U6-guide-scaffold cassette to introduce frameshift mutations and knockout *GTF2I* function (Figure 5). As we have described (Chailangkarn et al., 2016), hiPSC colonies were maintained on 6-cm dishes coated with Matrigel (BD-Biosciences, San Jose, CA, USA) and were fed daily with mTeSR1 (StemCell Technologies, Vancouver, Canada); only mycoplasma-negative cell cultures were used.

Generation of cortical organoids

Cortical organoids were generated as has previously been described (Trujillo et al., 2019). Briefly, PSCs were cultured for approximately six days and then dissociated with 1:1 Accutase (Life Technologies):PBS, and cells were then plated into a 6-well plate ($4x10^6$ cells/well) in mTeSR1 supplemented with 10 μM SB431542 (SB; Stemgent, Cambridge, MA, USA), 1 μM Dorsomorphin (Dorso; R&D Systems, Minneapolis, MN, USA), and 5 μM Y-27632 (EMD-Millipore, Burlington, MA, USA) and subsequently cultured in shaker suspension (95 rpm at 37°C). Emergent spheres were fed mTeSR1 (supplemented with 10 μM SB and 1 μM Dorso) for three days, after which medium was changed to Media1 [Neurobasal (Life Technologies), 1x Glutamax (Life Technologies), 2% Gem21-NeuroPlex (Gem21; Gemini Bio-Products, Sacramento, CA, USA), 1% N2-NeuroPlex (N2; Gemini Bio-Products), 1% non-essential amino acids (NEAA; Life Technologies), 1%

penicillin/streptomycin (P/S; Life Technologies), 10 μM SB, and 1 μM Dorso] for six days, every other day; then Media2 (Neurobasal, 1x Glutamax, 2% Gem21, 1% NEAA, and 1% P/S) supplemented with 20 ng/mL FGF-2 (Life Technologies) for seven days, daily; followed by Media2 supplemented with 20 ng/mL each of FGF-2 and EGF (PeproTech, Rocky Hill, NJ, USA) for six days, every other day; and then Media2 with 10 ng/mL each of BDNF, GDNF, and NT-3 (all PeproTech), 200 μM L-ascorbic acid (Sigma-Aldrich, St. Louis, MO, USA), and 1 mM dibutyryl-cAMP (Sigma-Aldrich) for six days, every other day. Cortical organoids were subsequently maintained indefinitely in Media2 without supplementation.

Progenitor and neuronal differentiation of hiPSCs

hiPSC colonies cultured for approximately six days were dissociated in 50:50 Accutase (Life Technologies):PBS, and ~$4x10^6$ hiPSCs were plated per well of a 6-well plate in suspension in 3mL mTeSR1 supplemented with 5 μM Y-27632 (EMD-Millipore) and cultured in shaker suspension (95 rpm at 37°C) to form embryoid bodies (EBs). Medium was replaced the following day with Neural Induction Medium (NIM; StemCell Technologies) and fed with NIM daily or every other day. After seven days, EBs were plated on Matrigel-coated 6-cm plates and fed with NIM for another week. Emergent rosettes were picked manually with a P1000 tip and transferred to a new Matrigel-coated 6-cm dish. After 2-3 days, rosettes with neurite outgrowth were manually picked again, transferred to a 15mL conical tube, and dissociated by incubating them in 1-2mL Accutase (Life Technologies) at 37°C for ~5-10 minutes followed by manual dissociation with a P1000 pipette to single-cell suspension. Cells (NPCs) were centrifuged for four mins at 1.1 rpm, resuspended in NGF medium [DMEM/F12 (Life Technologies), 1x N2 (Gemini), 1x Gem21 (Gemini), 1% P/S

(Life Technologies), and supplemented with 20 ng/mL FGF-2], and seeded on poly-L-ornithine/laminin plates. NPCs were expanded and maintained in NGF medium with feeding on alternate days. Neuronal differentiation was induced by withdrawing FGF-2 supplementation.

Western blotting

Western blotting was performed as detailed in (Trujillo, Adams, et al., 2021). Briefly, total protein was extracted and quantified (Pierce BCA Protein Assay Kit, ThermoScientific) after cell lysis in RIPA buffer (ThermoScientific) with cOmplete ULTRA mini protease inhibitor (Roche, Mannheim, Germany) and PhosSTOP phosphatase inhibitor (Roche). Total protein (20µg) was separated on a Bolt 4–12% Bis-Tris Plus Gel (Life Technologies) and subsequently transferred to a nitrocellulose membrane using an iBlot2 dry blotting system (ThermoScientific). Membranes were blocked at room temperature for 1-4 hours (Rockland Immunochemicals, VWR International, Arlington Heights, IL, USA); primary antibodies (rabbit anti-Synapsin1, EMD-Millipore AB1543P, 1:1500; mouse anti-PSD-95, Neuromab, 1:1500; rabbit anti-GTF2I, Abcam (Cambridge, UK) ab129025, 1:250; mouse anti-β-actin, Abcam ab8226, 1:10,000) in blocking buffer incubated, shaking, overnight at 4°C. Membranes underwent three five-minute washes with PBS + 0.1% Tween-20, followed by the application of secondary antibodies (IRDye 680RD and IRDye 800CW, 1:5000 in blocking buffer) incubated at room temperature, shaking and protected from light, for one hour. Membranes underwent three more washes, after which an Odyssey CLx infrared imaging system (LiCOR Biosciences, Lincoln, NE, USA) was used to detect proteins, and signal intensity was normalized relative to intensity quantification of β-actin.

Immunofluorescence staining of monolayer cells and cortical organoids

Immunofluorescence was performed in accordance with how was previously described (Chailangkarn et al., 2016; Trujillo et al., 2019; Trujillo et al., 2020). Cells were fixed in 4% paraformaldehyde, washed three times with PBS (five minutes each), and then permeabilized and blocked (0.1% Triton X-100 and 3% BSA in PBS). Cortical organoids were fixed overnight in 4% paraformaldehyde and subsequently transferred to, and sunken in, 30% sucrose, embedded in O.C.T. (Sakura, Tokyo, Japan), and sectioned at 20 µm on a cryostat. Slides with organoid sections were air-dried and then permeabilized and blocked (0.1% Triton X-100 and 3% BSA in PBS). Primary antibodies (goat anti-Nanog, Abcam ab77095, 1:500; rabbit anti-Oct4, Abcam ab19857, 1:500; mouse anti-Nestin, Abcam ab22035, 1:200 (organoid: 1:250); rat anti-CTIP2, Abcam ab18465, 1:250 (organoid: 1:500); chicken anti-MAP2, Abcam ab5392, 1:1000 (organoid: 1:2000); rabbit anti-Synapsin1, EMD-Millipore AB1543P, 1:500; mouse anti-Vglut1, Synaptic Systems (Goettingen, Germany) 135311, 1:500; rabbit anti-Homer1, Synaptic Systems 160003, 1:500; mouse anti-NeuN, EMD-Millipore MAB377, 1:500; rabbit anti-Ki67, Abcam ab15580, 1:1000; rabbit anti-SOX2, Cell Signaling Technology (Danvers, MA, USA) 2748, 1:500) in blocking buffer incubated overnight at 4°C. Slides were washed three times with PBS (five minutes each) and then incubated with secondary antibodies (Alexa Fluor 488, 555, and 647, Life Technologies, 1:1000 in blocking buffer). Nuclei were stained with DAPI for 10 minutes (1:10,000 in PBS). Slides were mounted with ProLong Gold anti-fade mountant (Life Technologies) and imaged and analyzed with a Z1 Axio Observer Apotome fluorescence microscope (Zeiss, Oberkochen, Germany).

RNA sequencing analyses

RNA was isolated, via an RNeasy Mini kit (Qiagen), for library preparation (Illumina TruSeq RNA Sample Preparation Kit; San Diego, CA, USA) and sequencing (Illumina HiSeq2000, 50bp paired-end reads, 50 million high-quality sequencing fragments per sample, on average). Data was analyzed by ROSALIND® (https://rosalind.onramp.bio/), with a HyperScale architecture developed by ROSALIND, Inc. (San Diego, CA). Reads were trimmed using cutadapt (Martin, 2011). Quality scores were assessed using FastQC (Andrews, 2010). Reads were aligned to the *Homo sapiens* genome build hg19 using STAR (Dobin et al., 2013). Individual sample reads were quantified using HTseq (Anders et al., 2015) and normalized via Relative Log Expression using DESeq2 R library (Love et al., 2014). Read Distribution percentages, violin plots, identity heatmaps, and sample MDS plots were generated as part of the QC step using RSeQC (Wang et al., 2012). DEseq2 was also used to calculate fold changes and p-values and perform optional covariate correction. Clustering of genes for the final heatmap of differentially expressed genes was done using the PAM (Partitioning Around Medoids) method using the fpc R library (Hennig, 2020). Hypergeometric distribution was used to analyze the enrichment of pathways, gene ontology, domain structure, and other ontologies. Enrichment was calculated relative to a set of background genes relevant for the experiment. Gene ontology analysis was performed using WebGestalt (Liao et al., 2019; Zhang et al., 2005), and networks of alternatively enriched pathways were constructed in Cytoscape (Shannon et al., 2003) using the ClueGO (Bindea et al., 2009) and BiNGO (Maere et al., 2005) plugins.

Cell cycle assay

Cell cycle assay was performed in accordance with how was previously described (Griesi-Oliveira et al., 2015; Negraes et al., 2021; Trujillo, Rice, et al., 2021). Cortical organoids and NPCs were dissociated and quantified using a Via1-Cassette with the NucleoCounter NC-3000 (Chemometec, Allerod, Denmark). Dissociated cells were fixed on ice or at 4°C with 70% ethanol for at least two hours. Cells were subsequently resuspended in a solution of 0.5 µg/ml DAPI and 0.1% Triton X-100 in PBS, and incubated at 37ºC for five minutes. Cells were then distributed onto an NC-Slide A2 chamber (Chemometec), and fluorescence was quantified with the NucleoCounter NC-3000 according to the manufacturer's protocol.

Annexin V assay

Annexin V assay was performed as described (Negraes et al., 2021; Trujillo, Rice, et al., 2021). Dissociated cortical organoids and monolayer neurons were resuspended in Annexin V binding buffer (Invitrogen) with Annexin V-CF488A conjugate (Biotium, Inc., Hayward, CA, USA) and Hoechst 33342 (Chemometec) and incubated for 15 minutes at 37°C. After a PBS wash, the cells were resuspended in Annexin V binding buffer (Invitrogen) supplemented by 10 µg/mL propidium iodide (Chemometec). Cells were loaded into NC-Slide A2 chambers and assessed with a Chemometec NucleoCounter NC-3000 cytometer, using the preoptimized Annexin V assay.

DNA fragmentation assay

The DNA fragmentation assay was performed as previously described (Negraes et al., 2021). Briefly, single-cell NPCs were collected and suspended in PBS and fixed with 70%

ethanol for 24 hours at 4°C. Cells subsequently were washed with PBS, resuspended in DAPI staining solution (0.1% (v/v) Triton X-100, 1 μg/mL DAPI in PBS), and incubated for five minutes at 37°C. Samples were analyzed with a Chemometec NC-3000 cytometer, using the preoptimized DNA Fragmentation Assay.

Synaptic puncta quantification

Co-localized Vglut1 (presynaptic) and Homer1 (postsynaptic) immunostained puncta along MAP2-positive processes were quantified as described (Chailangkarn et al., 2016; Nageshappa et al., 2016; Trujillo, Adams, et al., 2021). Primary antibodies incubated overnight at 4°C, secondary antibodies incubated at room temperature for one hour, and coverslips were mounted; see above for complete immunofluorescence methodology. *GTF2I* rescue experiments were performed by transfecting $3x10^6$ NPCs with a Nucleofector 2b (Lonza Bioscience, Morristown, NJ, USA) with 1μg of the commercially obtained plasmid eGFP-CAG>hGTF2I (VectorBuilder, Chicago, IL, USA) or a GFP-expressing control plasmid (Lonza Bioscience) according to the Neural Stem Cell Nucleofection kit protocol using the preoptimized A-033 program. Cells were resuspended in NGF medium (see above) and subsequently seeded on poly-L-ornithine/laminin-coated chamber slides (ThermoFisher). The slides were imaged using a Z1 Axio Observer Apotome fluorescence microscope (Zeiss), and a blinded investigator manually quantified co-localized synaptic puncta along 50μm segments of randomly selected MAP2-positive processes.

Multi-electrode array (MEA) recording

Multi-electrode array recordings were achieved as previously described (Negraes et al., 2021; Sirenko et al., 2019; Trujillo et al., 2019; Trujillo, Adams, et al., 2021). Six-week-old cortical organoids were plated in 6-, 12-, or 48-well (each well with an 8x8 grid of electrodes) MEA plates (Axion Biosystems, Atlanta, GA, USA) pre-coated with 100 µg/mL poly-L-ornithine and 10 µg/mL laminin. Cellular cultures were fed twice per week with Medium 2 (see above) and, 7-14 days after plating, were incrementally switched to BrainPhys medium (StemCell Technologies; Bardy et al., 2015) supplemented with 10 ng/mL of BDNF (PeproTech) and 200 µM L-ascorbic acid (Sigma-Aldrich). Recordings were conducted in a Maestro MEA system with AxIS Software Spontaneous Neural Configuration (Axion Biosystems). Using Axion Biosystems' Neural Metrics Tool, active electrodes required at least five spikes/min. Bursts/electrode used an inter-spike interval (ISI) threshold requiring minimally five spikes with a maximum ISI of 100 milliseconds (ms). Network bursts required at least 10 spikes under the same ISI with >25% active electrodes in the well. The synchrony index utilized a cross-correlogram window of 20 ms.

Statistical analysis

Statistical analyses were performed using GraphPad Prism v9 (GraphPad Software, La Jolla, CA). Sample sizes were determined based on previous publications from this lab and others. Experiment-specific information for samples and cell lines is detailed in the figure legends. Samples were allocated and evaluated according to genotype; no randomization was applied. Analyses of synaptic puncta was performed by blinded investigators. Data exclusion in MEA datasets (outliers) was carried out automatically using pre-established criteria as described above. Outliers in other experiments were determined using GraphPad criteria and

excluded. Results for continuous variables were expressed as mean ± standard error of the mean and 95% confidence intervals were normal-based. Normality was assessed visually or via analysis in GraphPad, and variance was accounted for in all analyses. Means for continuous variables were compared between groups using, where appropriate, unpaired Student's *t*-test, one-way, or two-way analyses of variance, and nonparametric distributions were compared using Mann Whitney *U* test. Tests were performed two-sided with α throughout set as 0.05.

Acknowledgments

The main body of the dissertation is currently being prepared for submission for publication of the material. Adams, J. W., Vinokur, A., Austria, C., Guerra, B. S., Herai, R. H., Wahlin, K. J., & Muotri, A. R. **Loss of *GTF2I* promotes synaptic dysfunction and impaired connectivity in human cellular models of neurodevelopment**. The dissertation author was the primary investigator and author of this material.

RESULTS

Loss of GTF2I *induces transcriptomic alterations in cortical organoids*

To investigate the role of *GTF2I* in human neurodevelopment, two hiPSC lines (CVB and WT83) were CRISPR-edited into isogenic *GTF2I*-KO pairs (Figure 1A, Figure 4, Figure 5; Wahlin et al., 2021) and subsequently differentiated into neural cell types (Figure 4A). Control and *GTF2I*-KO hiPSCs were differentiated into cortical organoids (Figure 1B; Trujillo et al., 2019), a cytoarchitecturally complex human cellular model of neurodevelopment that develops in close alignment to the human fetal developing brain (Camp et al., 2015; Luo et al., 2016; Urresti et al., 2021). Immunostaining of cortical organoids portrayed a characteristic neurodevelopmental spatial pattern in which Ki67+ progenitor regions gave rise to NeuN+ and MAP2+ neurons (Figure 1C; Trujillo et al., 2019). Immunostaining further confirmed pronounced GTF2I expression in control cortical organoids that was absent in organoids differentiated from *GTF2I*-KO hiPSCs (Figure 1D).

A prior investigation of transcriptomic variation in 7q11.23 cell lines strategically estimated that 10-20% of the differential expression could be attributed to *GTF2I*, with that variance particularly enriched in biological categories most relevant to disease-specific phenotypes (Adamo et al., 2015). Similarly, we predicted that removal of *GTF2I* would be associated with transcriptomic changes in cortical organoids and that this dysregulation would be particularly enriched in pathways critical for neurodevelopment. Comparison of the transcriptomic profiles of two-month-old organoids showed markedly altered expression, with upregulation (≥ 1.5-fold) of 456 genes and downregulation (≤ -1.5-fold) of 404 genes in *GTF2I*-KO cortical organoids compared to controls (Figure 1E and Figure 6A). Summary gene ontology analyses of top differentially expressed pathways for “Cellular Component”

and “Biological Process” showed downregulation of synaptic processes and synaptic signaling, particularly of glutamatergic transmission, and upregulation of pathways relevant to apoptotic signaling (Figure 1F,G and Figure 6B,C).

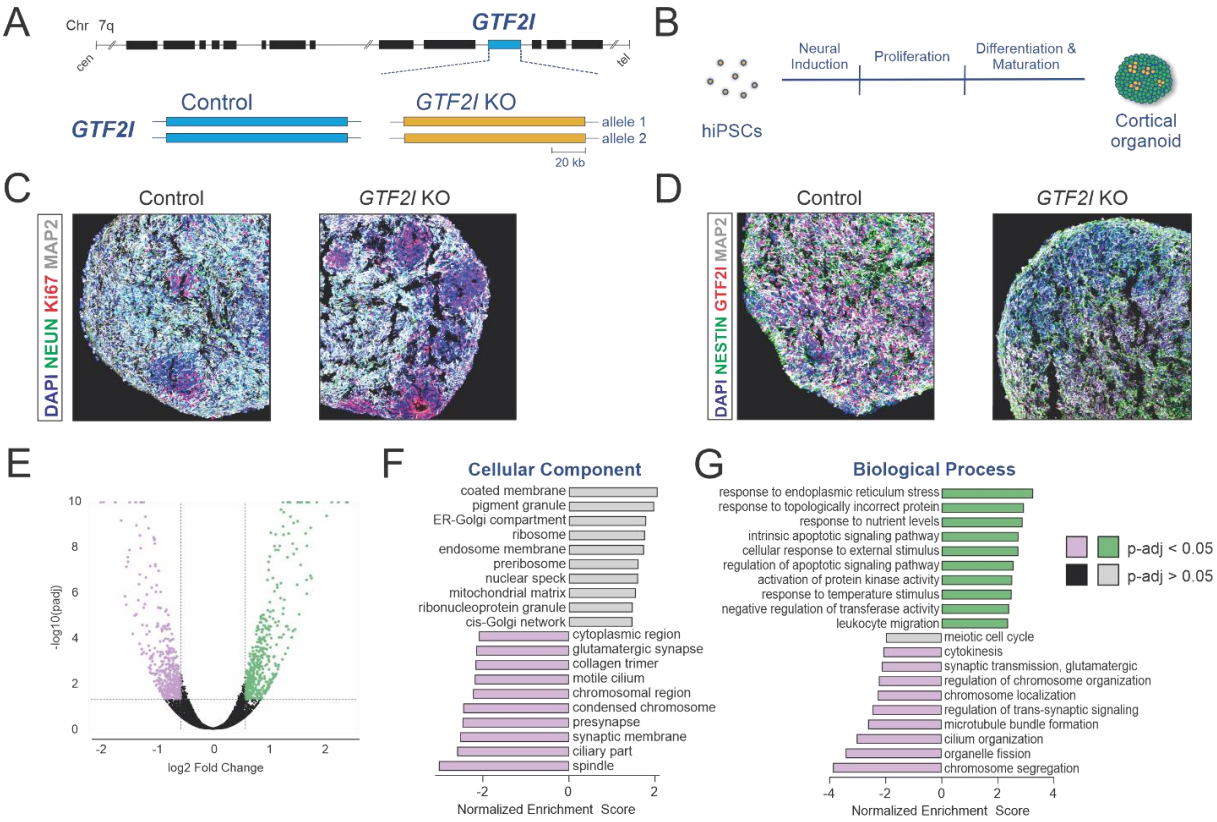

Figure 1: Transcriptomic alterations in *GTF2I*-KO cortical organoids. (**A**) Depiction of the *GTF2I* locus on chromosome 7 (top) and representation of its alleles in the control and *GTF2I*-KO conditions (bottom). (**B**) Schematic showing the differentiation protocol of cortical organoids from hiPSCs. (**C**) Immunostaining of two-month-old organoids showed progenitor regions of Ki67 positivity that give rise to mature neurons immunopositive for NeuN and MAP2. (**D**) GTF2I is robustly expressed in two-month-old control organoids. (**E**) Volcano plot showing differentially expressed genes detected by RNA sequencing of two-month-old control and *GTF2I*-KO organoids. (**F** and **G**) Gene ontology analyses of top ten and bottom ten altered gene expression pathways within the categories “Cellular Component” (**F**) and “Biological Process” (**G**).

GTF2I-*KO alters cell cycle, proliferation, and survival*

Consistent with increased expression of apoptotic signaling pathways, neuronal deletion of *GTF2I* is associated with decreased brain weight and cortical thickness in mice

(Barak et al., 2019), and we likewise observed that two-month-old *GTF2I*-KO organoids were decreased in diameter compared to controls ($P<0.0001$; Figure 2A). To further evaluate their apoptotic phenotype, two- and three-month-old organoids were dissociated and assessed via an annexin assay. *GTF2I*-KO organoids at two months ($P=0.004$) and three months of age ($P=0.019$) exhibited a higher frequency of apoptotic cells compared to controls (Figure 2B).

Previous work in other experimental systems has documented the involvement of *GTF2I* in proliferation and cell cycle regulation (Desgranges et al., 2005; Desgranges & Roy, 2006; Shen et al., 2018), suggesting it may likewise affect these processes during neurodevelopment. To study these properties in neural cells, control and *GTF2I*-KO hiPSCs were differentiated into NPCs (Figure 2C). To compare their proliferative propensities, $1x10^5$ NPCs were plated per well of a 6-well plate and allowed to proliferate for a set number of days, after which total cells per well were collected. Quantification revealed a higher rate of proliferation per day of *GTF2I*-KO NPCs compared to controls ($P=0.001$; Figure 2D). In pursuit of an explanation for the increased proliferation rate, the cell cycle profiles and frequencies of cells with DNA fragmentation were compared between control and *GTF2I*-KO NPCs (Figure 2E). *GTF2I*-KO and control NPCs exhibited distinct cell cycle profiles ($P=0.001$; Figure 2F), but rates of DNA fragmentation were similar between genotypes ($P=0.23$; Figure 2G).

Neural progenitor cells were subsequently differentiated into neurons that stained immunopositive for the neuronal markers β-tubulin (Tuj1), Synapsin, and MAP2 (Figure 3A). In agreement with our findings in two- and three-month-old organoids, 8-week neurons exhibited a higher frequency of apoptotic cells ($P=0.016$; Figure 3B).

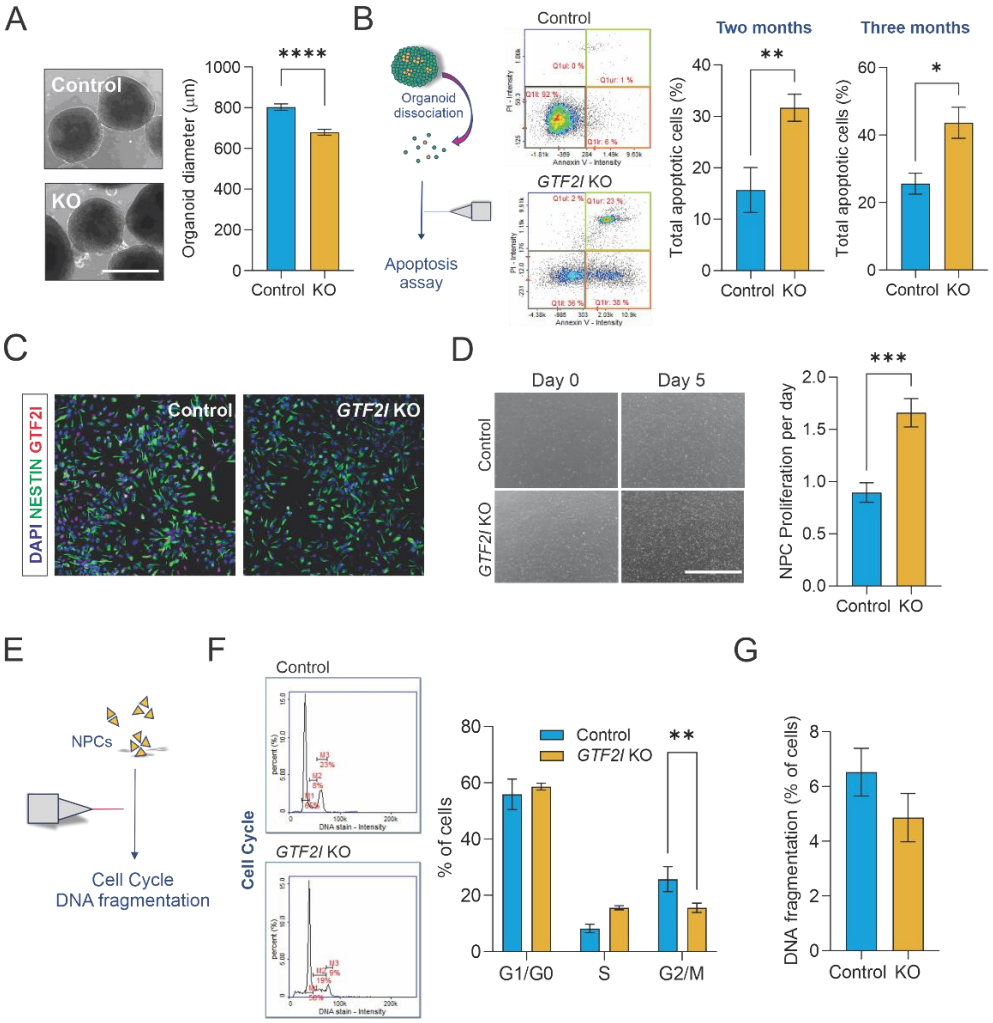

Figure 2: Loss of *GTF2I* alters proliferation dynamics and survival in human cell models. (**A**) Reduced diameter of *GTF2I*-KO cortical organoids compared to controls (Student's *t*-test, t_{96} = 5.73, *P*<0.0001; *N*=43 control and 55 *GTF2I*-KO organoids); scale bar=1,000µm. (**B**) Left, organoid dissociation into single-cell suspension to analyze apoptotic cell frequency. Right, compared to controls, *GTF2I*-KO organoids have a higher frequency of apoptotic cells at two months (Student's *t*-test, t_{17} = 3.35, *P*=0.004; *N*=7 replicates of ~5-10 control organoids and 12 replicates of ~5-10 *GTF2I*-KO organoids) and three months (Student's *t*-test, t_{12} = 2.71, *P*=0.019; *N*=5 replicates of ~5-10 control organoids and 9 replicates of ~5-10 *GTF2I*-KO organoids) of age. (**C**) Immunostaining portrays Nestin+ NPCs. (**D**) *GTF2I*-KO NPCs exhibited a higher proliferation rate per day (Student's *t*-test, t_{14} = 4.37, *P*=0.001; *N*=7 wells of control NPCs and 9 wells of *GTF2I*-KO NPCs); scale bar=1,000µm. (**E**) NPCs evaluated with cell cycle and DNA fragmentation assays. (**F**) *GTF2I*-KO NPCs show an altered cell cycle profile compared to controls (two-way analysis of variance (ANOVA), $F_{2,54}$ = 7.829, *P*=0.001; *N*=6 10-cm plates of control NPCs and 14 10-cm plates of *GTF2I*-KO NPCs). (**G**) *GTF2I*-KO and control NPCs showed a similar frequency of cells with fragmented DNA (Student's *t*-test, t_{11} = 1.26, *P*=0.23; *N*=5 10-cm plates of control NPCs and 8 10-cm plates of *GTF2I*-KO NPCs). Data are presented as mean ± standard error of the mean (s.e.m.)

GTF2I-*KO is associated with synaptic dysfunction and impaired connectivity*

Given the results of our RNA sequencing analyses showing downregulated expression of synaptic pathways in *GTF2I*-KO cortical organoids, we sought to further evaluate these phenotypes. Western blot analysis of synaptic proteins demonstrated a decrease of the presynaptic protein Synapsin (*P*=0.026), albeit not the postsynaptic protein PSD-95 (*P*=0.69), in two-month-old *GTF2I*-KO cortical organoids compared to controls (Figure 3C). Concordantly, immunostaining of presynaptic Vglut1 and postsynaptic Homer1 showed a reduction of co-localized synaptic puncta in *GTF2I*-KO 8-week neurons compared to controls (*P*= 0.0001), a deficiency that was rescuable by re-expression of *GTF2I* (*P*=0.026; Figure 3D).

To interrogate the functional connectivity of human neurons in circuits, organoids were plated for evaluation on MEA electrophysiology (Figure 3E,F). Compared to controls, *GTF2I*-KO organoids showed fewer spikes per minute (*P*=0.007), a decreased mean firing rate (*P*=0.007), and fewer bursts per minute (*P*=0.001), but the difference in the synchronous network burst rate did not reach statistical significance (*P*=0.15) and no difference in the synchrony index was detected (*P*=0.92; Figure 3G).

Acknowledgments

The main body of the dissertation is currently being prepared for submission for publication of the material. Adams, J. W., Vinokur, A., Austria, C., Guerra, B. S., Herai, R. H., Wahlin, K. J., & Muotri, A. R. **Loss of *GTF2I* promotes synaptic dysfunction and impaired connectivity in human cellular models of neurodevelopment**. The dissertation author was the primary investigator and author of this material.

Figure 3: Loss of *GTF2I* impairs synaptic structure and network connectivity in neurons and cortical organoids. (**A**) Representative images of neurons differentiated from NPCs immunostained positive for the mature neuronal markers β-tubulin (Tuj1), Synapsin, and MAP2. (**B**) Compared to controls, *GTF2I*-KO neurons exhibited a higher frequency of apoptotic cells (Student's *t*-test, $t_7 = 3.16$, P=0.016; N=5 10-cm plates of CVB control neurons and 4 10-cm plates of CVB *GTF2I*-KO neurons). (**C**) Representative Western blots (left) and quantification (right) of the presynaptic protein Synapsin (Mann Whitney *U* test, P=0.026; N=6 control samples and 6 *GTF2I*-KO samples from CVB and WT83 hiPSC lines) and the postsynaptic protein PSD-95 (Mann Whitney *U* test, P=0.69; N=4 control samples and 4 *GTF2I*-KO samples from CVB and WT83 hiPSC lines); samples are independent protein extractions of ~10 organoids, with intensity normalized by actin and averaged from duplicate lanes. (**D**) Co-localized synaptic puncta density was reduced in *GTF2I*-KO neurons and reversable by *GTF2I* re-expression (one-way ANOVA, $F_{3,90} = 7.703$, P=0.0001, with Dunnett's multiple comparison's test: Control vs KO: P=0.0001, KO vs +*GTF2I*: P=0.026, KO vs +ctrl: P=0.99; N=16-33 neurons from CVB and WT83 hiPSC lines). (**E**) Representation and top-down image of organoid plated for multi-electrode array (MEA) electrophysiology. (**F**) Representative MEA raster plots for control and *GTF2I*-KO organoids. Pink rectangles generated by Axion NeuralMetric software denote network bursts. (**G**) Compared to controls, *GTF2I*-KO organoids show fewer spikes per minute (Student's *t*-test, Welch-corrected, $t_{71.5}$=2.80, P=0.007; N=50 control and 44 *GTF2I*-KO MEA-plate wells), a decreased firing rate (Student's *t*-test, Welch-corrected, $t_{56.9}$=2.80, P=0.007; N=41 control and 37 *GTF2I*-KO MEA-plate wells), and fewer bursts per minute (Student's *t*-test, Welch-corrected, $t_{49.7}$=3.61, P=0.001; N=37 control and 33 *GTF2I*-KO MEA-plate wells), with less difference in the network burst rate (Student's *t*-test, Welch-corrected, $t_{15.3}$=1.51, P=0.15; N=13 control and 6 *GTF2I*-KO MEA-plate wells) or the synchrony index (Student's *t*-test, t_{63}=0.11, P=0.92; N=31 control and 34 *GTF2I*-KO MEA-plate wells); samples include organoids from CVB and WT83 hiPSC lines, pooled from multiple experiments. Data are presented as mean ± s.e.m.

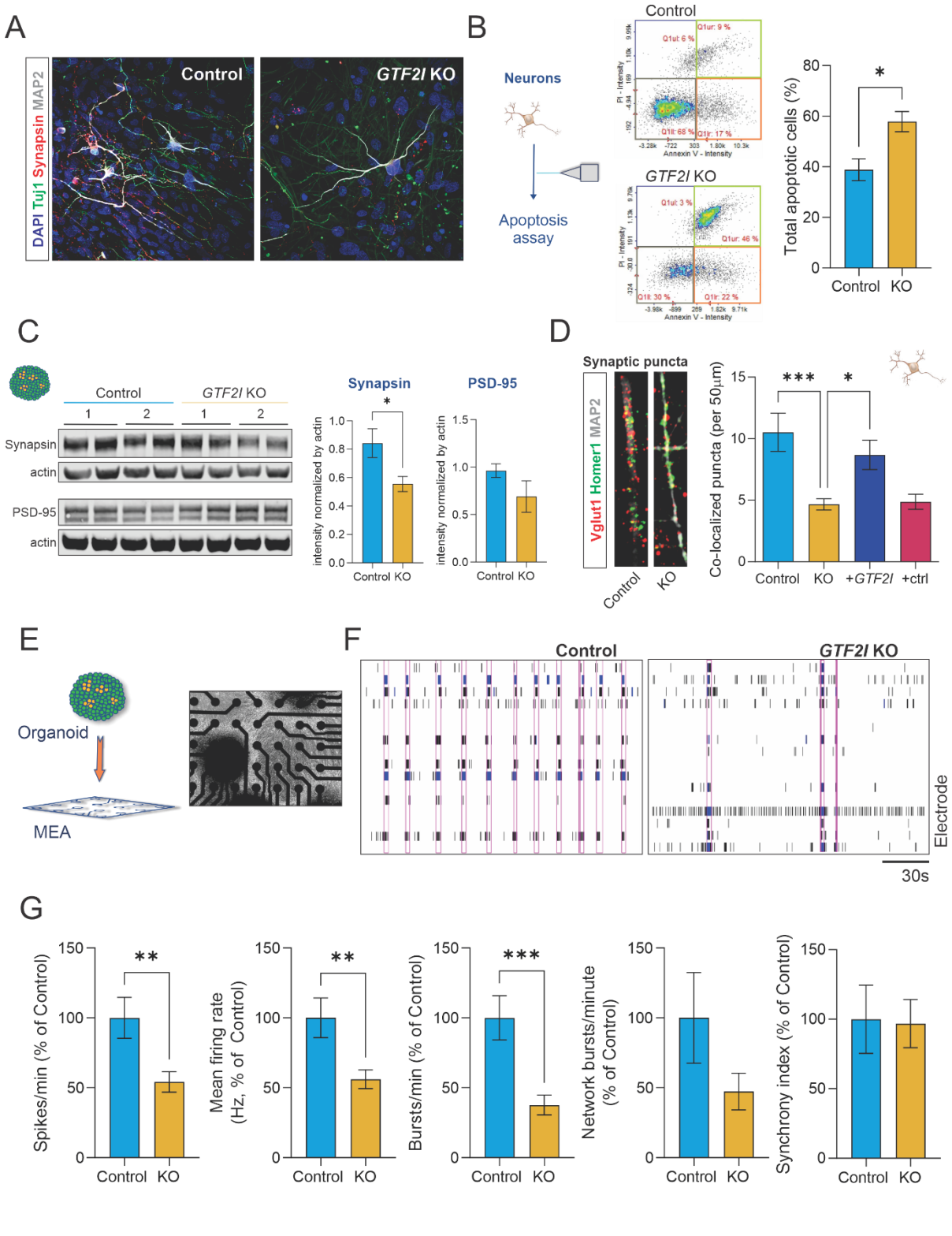
A
DAPI Tuj1 Synapsin MAP2
Control
GTF2I KO
B
Neurons
Apoptosis assay
Control
GTF2I KO
Annexin V - Intensity
PI - Intensity
Total apoptotic cells (%)
Control KO
C
Control
GTF2I KO
1 2 1 2
Synapsin
actin
PSD-95
actin
Synapsin
PSD-95
intensity normalized by actin
Control KO
D
Synaptic puncta
Vglut1 Homer1 MAP2
Control
KO
Co-localized puncta (per 50µm)
Control KO +GTF2I +ctrl
E
Organoid
MEA
F
Control
GTF2I KO
Electrode
30s
G
Spikes/min (% of Control)
Mean firing rate (Hz, % of Control)
Bursts/min (% of Control)
Network bursts/minute (% of Control)
Synchrony index (% of Control)
Control KO

DISCUSSION

In the present study, cortical organoids, NPCs, and neurons were differentiated from *GTF2I*-KO hiPSCs to investigate the impact of *GTF2I* during human neurodevelopment. Transcriptomic analyses in cortical organoids revealed decreased expression of pathways relevant to synaptic signaling, particularly glutamatergic transmission, and increased expression of apoptotic pathways. In concordance, *GTF2I*-KO organoids and neurons exhibited higher frequencies of apoptotic cells and synaptic impairment, the functional consequence of which was further reflected by the decreased electrophysiological activity of *GTF2I*-KO organoids on MEA. Compared to control NPCs, *GTF2I*-KO NPCs portray an altered cell cycle profile and an increased proliferation rate. Together, these results suggest a summary model of *GTF2I*'s function during neurodevelopment in which *GTF2I* helps regulate the growth and proliferation of neural progenitors but subsequently, at the mature neuronal stage, becomes critical for neuronal health and the maintenance of neuronal function.

GTF2I is included among the ~26-28 genes at the Williams-Beuren chromosomal locus at 7q11.23 (Osborne et al., 2001; Pober, 2010; Scherer et al., 2003), and mutations of it are associated with variation in the phenotypic expression of human sociality (Chailangkarn et al., 2018; Roy, 2017). Although our group previously employed patient-derived hiPSCs differentiated into neural cell types to investigate WS (Chailangkarn et al., 2016), little is understood about the specific effects of GTF2I on human neurodevelopment. Here we used two pairs of isogenic *GTF2I*-KO hiPSC lines differentiated into an array of neural cell platforms to isolate the neurodevelopmental effects of *GTF2I*.

Cortical organoids offer an invaluable platform to study neurodevelopmental disease (Adams et al., 2019; Avansini et al., 2021; Trujillo, Adams, et al., 2021) and may offer insight into molecular mechanisms predicted to underlie variation in human sociality, particularly its aberrant phenotypic expression in WS (Chailangkarn et al., 2018). We found that, compared to controls, *GTF2I*-KO cortical organoids show transcriptomic dysregulation, with decreased expression of genes involved in synaptic structure and function, particularly glutamatergic function, and enriched expression of genes in pathways involved in cell death. This observation was matched by further findings showing decreased organoid size and, via subsequent assays, increased apoptosis and impaired electrophysiological function. Our findings of synaptic impairment in *GTF2I*-KO organoids and neurons contrast with our group's previous observations of synaptic hyperactivity in WS neurons (Chailangkarn et al., 2016), but direct comparison of these studies' results may be improper given that the hiPSC lines used here are isogenic whereas those utilized in the previous study were derived from WS patients and hence were hemizygously deficient in the whole complement of WS genes. However, although the present study seeks to identify the neurodevelopmental effects of *GTF2I* in isolation, seeking to understand the effects of altering *GTF2I* along with combinations of neighboring genes may be valuable for future efforts.

Interestingly, in contrast to the increased frequency of apoptotic cells in *GTF2I*-KO organoids and neurons, *GTF2I*-KO NPCs demonstrated a frequency of DNA fragmentation—the sub-G_1 proportion of the cell population—that was equivalent to that observed for the controls. One explanation for this difference may be that the cellular functions of GTF2I in neural progenitors and in mature neurons are distinct (Desgranges & Roy, 2006). While the findings of increased NPC proliferation and unchanged or decreased cell death are expected

(Massagué, 2004), it has likewise previously been demonstrated that increased proliferation of human NPCs increases stress and promotes genomic instability (Wang et al., 2020). Replication-stress affected progenitors that are differentiated into neurons with GTF2I dysfunction may be incapable of coping with the DNA damage (Desgranges et al., 2005; Desgranges & Roy, 2006). Future studies that investigate this plausibility may be warranted.

Our study has several intrinsic limitations. The differentiation protocols utilized here principally guide cells towards an excitatory forebrain neuronal fate (Nageshappa et al., 2016; Trujillo et al., 2019), limiting the diversity of cell types and cellular interactions under investigation in the present study. Previous studies in animal models have argued that loss of *GTF2I* may indirectly affect GABAergic cells (Barak & Feng, 2016; Levi et al., 2021) and neuronal interactions with oligodendrocytes (Barak et al., 2019), suggesting that including a wider array of human neural cell types will be an important objective for future studies. Nevertheless, we have sought to minimize this limitation by including an array of human cell models of neurodevelopment, the convergent results of which increase our confidence in our phenotypic findings. In addition to restricted cellular diversity, our cellular models capture a narrow window of early neurodevelopment (Camp et al., 2015; Luo et al., 2016; Trujillo et al., 2019; Urresti et al., 2021) that may inadequately portray the full involvement of *GTF2I* across the spectrum of human neurodevelopment. However, our concern regarding how severely this shortcoming limits our findings is lessened by the observation that *GTF2I* expression in the brain appears to be concentrated during the prenatal period of neurodevelopment (Tebbenkamp et al., 2018), supporting a prediction that the effects of its absence would be most pronounced in this period.

In summary, compared to control organoids, *GTF2I*-KO cortical organoids showed synaptic dysregulation, altered electrophysiological connectivity, and increased cell death. *GTF2I*-KO neurons likewise exhibited synaptic impairment and increased apoptosis, following differentiation from *GTF2I*-KO neural progenitors that have a higher rate of proliferation and altered cell cycle. Overall, our findings suggest loss of *GTF2I* induces alterations in neural progenitors which give rise to neurons and networks characterized by synaptic defects, reduced connectivity, and impaired neuronal health.

Acknowledgments

The main body of the dissertation is currently being prepared for submission for publication of the material. Adams, J. W., Vinokur, A., Austria, C., Guerra, B. S., Herai, R. H., Wahlin, K. J., & Muotri, A. R. **Loss of *GTF2I* promotes synaptic dysfunction and impaired connectivity in human cellular models of neurodevelopment**. The dissertation author was the primary investigator and author of this material.

SUPPLEMENTARY FIGURES

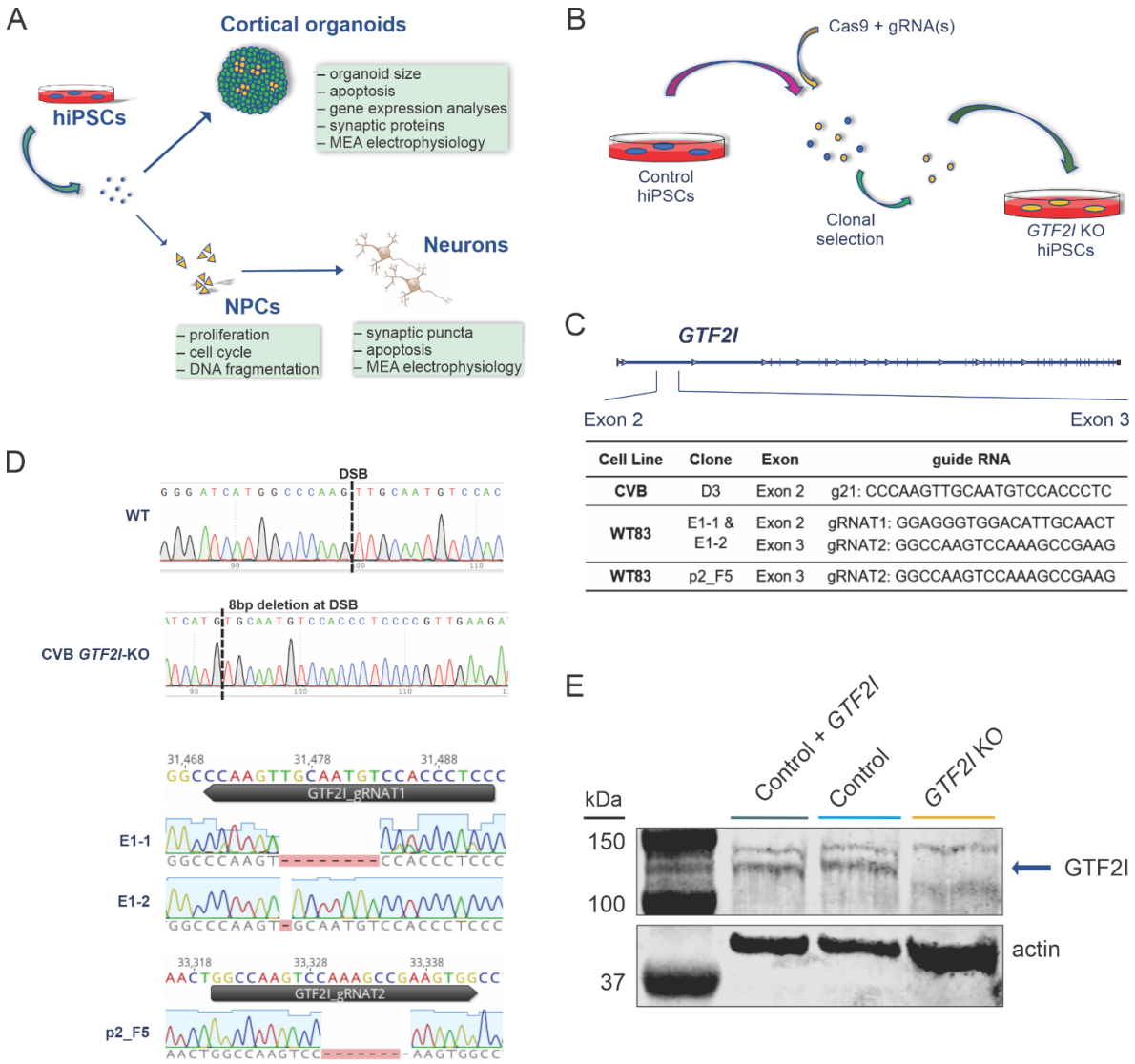

Cell Line	Clone	Exon	guide RNA
CVB	D3	Exon 2	g21: CCCAAGTTGCAATGTCCACCCTC
WT83	E1-1 & E1-2	Exon 2 Exon 3	gRNAT1: GGAGGGTGGACATTGCAACT gRNAT2: GGCCAAGTCCAAAGCCGAAG
WT83	p2_F5	Exon 3	gRNAT2: GGCCAAGTCCAAAGCCGAAG

Figure 4: Generation of *GTF2I*-KO human cellular models of neurodevelopment. (**A**) Schematic of study design. (**B, C**) hiPSCs underwent CRISPR-Cas9 editing with clonal selection (**B**), using guide RNAs (gRNAs) against exons 2 and/or 3 (**C**). (**D**) DNA sequencing confirmed the induction of frameshift mutations. Western blot of protein extracted from NPCs; protein samples are from control NPCs further transfected with *GTF2I*, control NPCs, and pooled *GTF2I*-KO NPCs. *GTF2I*-KO total protein was overloaded to confirm successful knockout of GTF2I.

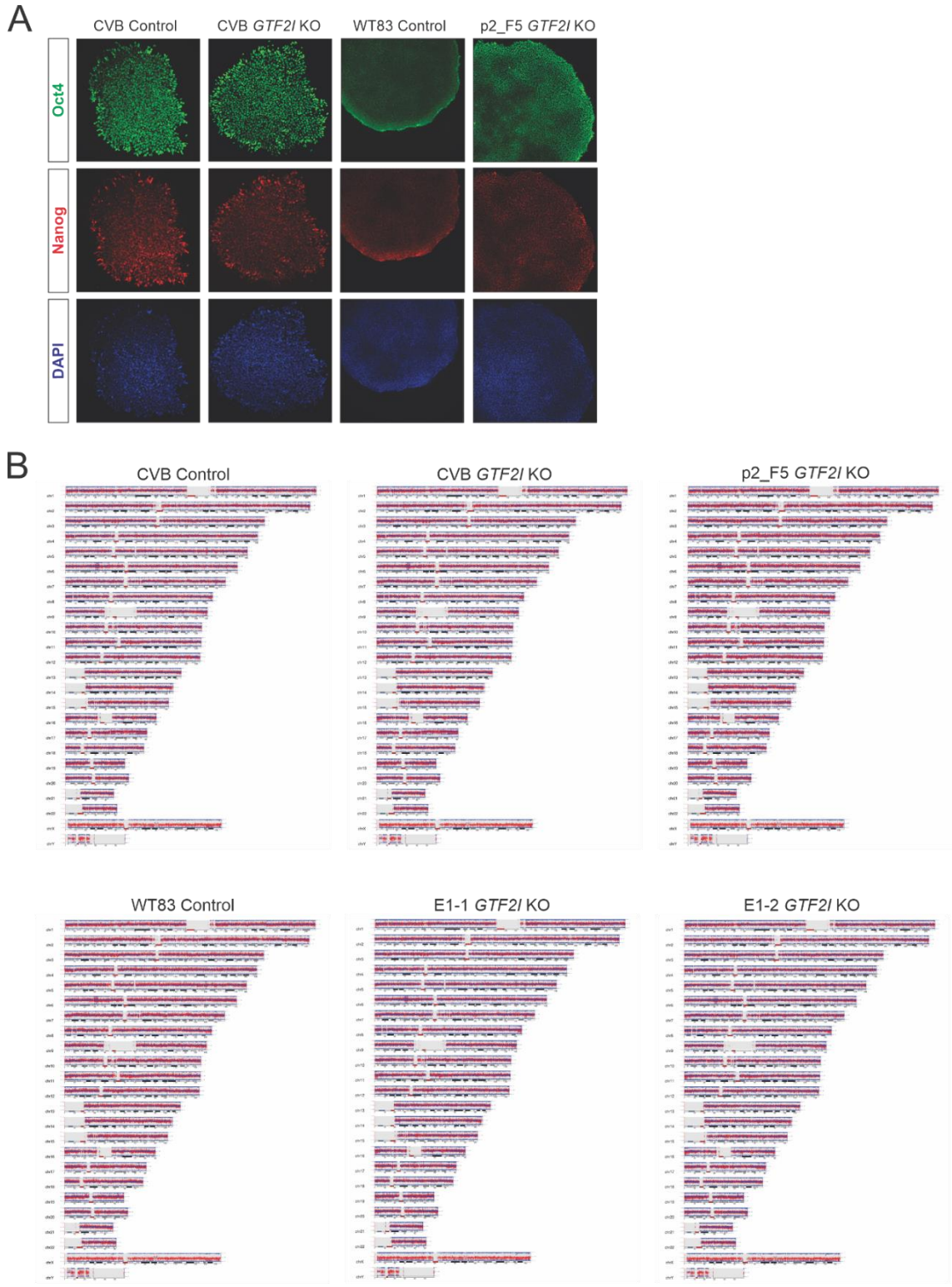

Figure 5: Characterization of *GTF2I*-KO hiPSCs. (**A**) Representative images of immunohistochemical characterization of pluripotency of control and *GTF2I*-KO hiPSCs. (**B**) Karyotyping of control and *GTF2I*-KO hiPSCs.

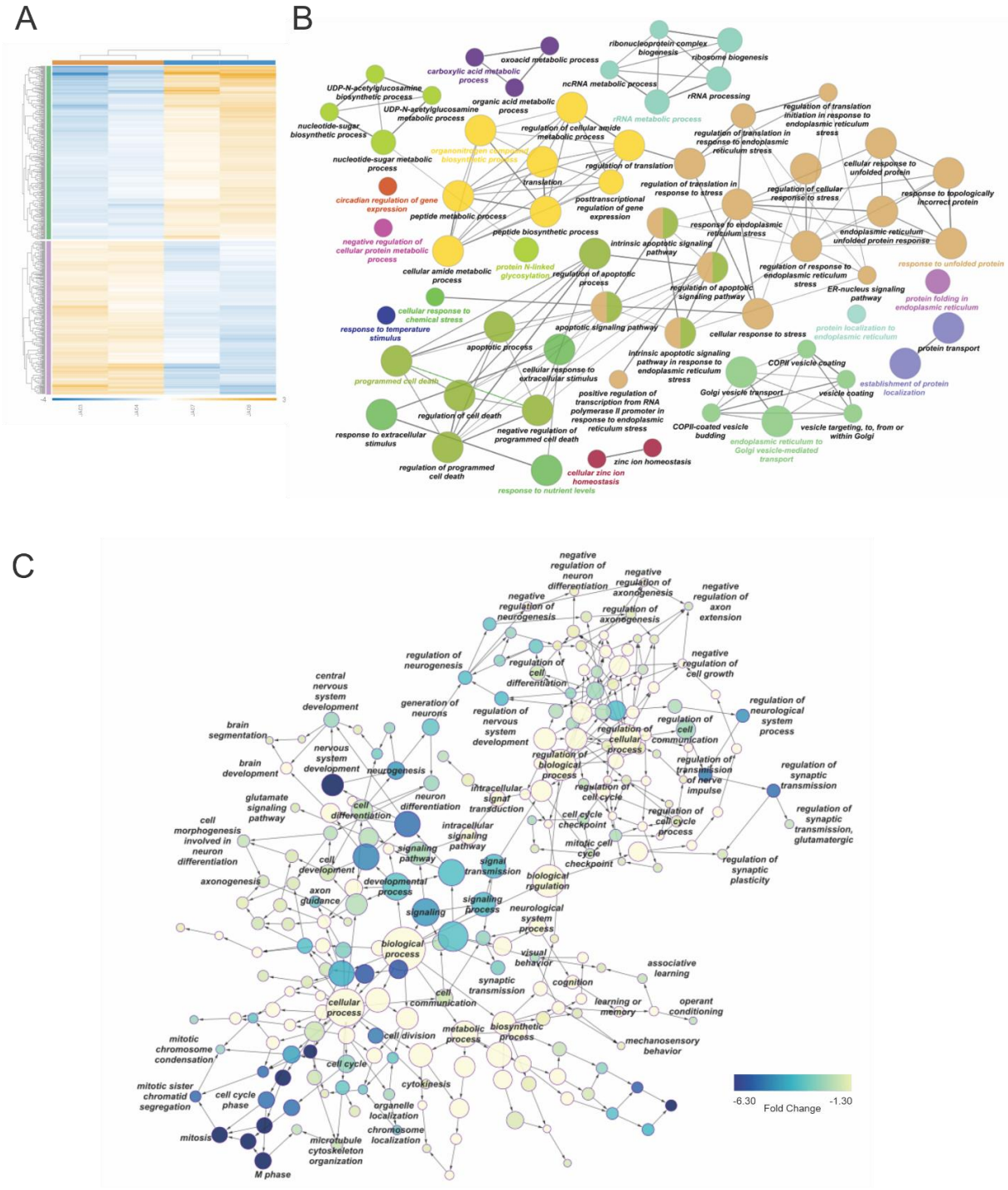

Figure 6: Network analyses of dysregulated gene expression pathways in *GTF2I*-KO cortical organoids. (**A**) Heatmap of RNA sequencing of two-month-old CVB control and *GTF2I*-KO cortical organoids. (**B**) ClueGO network analysis of pathways of upregulated (≥ 1.5-fold) genes in *GTF2I*-KO organoids. (**C**) Bingo network analysis of pathways of downregulated (≤ -1.5-fold) genes in *GTF2I*-KO organoids.

REFERENCES

Adamo, A., Atashpaz, S., Germain, P. L., Zanella, M., D'Agostino, G., Albertin, V., Chenoweth, J., Micale, L., Fusco, C., Unger, C., Augello, B., Palumbo, O., Hamilton, B., Carella, M., Donti, E., Pruneri, G., Selicorni, A., Biamino, E., Prontera, P., McKay, R., Merla, G., & Testa, G. (2015). 7Q11.23 Dosage-Dependent Dysregulation in Human Pluripotent Stem Cells Affects Transcriptional Programs in Disease-Relevant Lineages. *Nature Genetics*, *47*(2), 132–141. https://doi.org/10.1038/ng.3169

Adams, J. W., Cugola, F. R., & Muotri, A. R. (2019). Brain organoids as tools for modeling human neurodevelopmental disorders. *Physiology*, *34*(5), 365–375. https://doi.org/10.1152/physiol.00005.2019

Anders, S., Pyl, P. T., & Huber, W. (2015). HTSeq-A Python framework to work with high-throughput sequencing data. *Bioinformatics*, *31*(2), 166–169. https://doi.org/10.1093/bioinformatics/btu638

Andrews, S. (2010). *FastQC: a quality control tool for high throughput sequence data.*

Avansini, S. H., Puppo, F., Adams, J. W., Vieira, A. S., Coan, A. C., Rogerio, F., Torres, F. R., Araújo, P. A. O. R., Martin, M., Montenegro, M. A., Yasuda, C. L., Tedeschi, H., Ghizoni, E., França, A. F. E. C., Alvim, M. K. M., Athié, M. C., Rocha, C. S., Almeida, V. S., Dias, E. V, Delay, L., Molina, E., Yaksh, T. L., Cendes, F., Lopes Cendes, I., & Muotri, A. R. (2021). Junctional instability in neuroepithelium and network hyperexcitability in a focal cortical dysplasia human model. *Brain*. https://doi.org/10.1093/brain/awab479

Barak, B., & Feng, G. (2016). Neurobiology of social behavior abnormalities in autism and Williams syndrome. *Nature Neuroscience*, *19*(6), 647–655. https://doi.org/10.1038/nn.4276

Barak, B., Zhang, Z., Liu, Y., Nir, A., Trangle, S. S., Ennis, M., Levandowski, K. M., Wang, D., Quast, K., Boulting, G. L., Li, Y., Bayarsaihan, D., He, Z., & Feng, G. (2019). Neuronal deletion of Gtf2i, associated with Williams syndrome, causes behavioral and myelin alterations rescuable by a remyelinating drug. *Nature Neuroscience*, *22*(5), 700–708. https://doi.org/10.1038/s41593-019-0380-9

Bardy, C., Van Den Hurk, M., Eames, T., Marchand, C., Hernandez, R. V., Kellogg, M., Gorris, M., Galet, B., Palomares, V., Brown, J., Bang, A. G., Mertens, J., Böhnke, L., Boyer, L., Simon, S., & Gage, F. H. (2015). Neuronal medium that supports basic synaptic functions and activity of human neurons in vitro. *Proceedings of the National Academy of Sciences of the United States of America*, *112*(20), E2725–E2734. https://doi.org/10.1073/pnas.1504393112

Bellugi, U., Lichtenberger, L., Jones, W., Lai, Z., & St. George, M. (2000). I. The neurocognitive profile of Williams syndrome: A complex pattern of strengths and weaknesses. *Journal of Cognitive Neuroscience*, *12*(SUPPL. 1), 7–29. https://doi.org/10.1162/089892900561959

Bindea, G., Mlecnik, B., Hackl, H., Charoentong, P., Tosolini, M., Kirilovsky, A., Fridman, W. H., Pagès, F., Trajanoski, Z., & Galon, J. (2009). ClueGO: A Cytoscape plug-in to decipher functionally grouped gene ontology and pathway annotation networks. *Bioinformatics*, *25*(8), 1091–1093. https://doi.org/10.1093/bioinformatics/btp101

Camp, J. G., Badsha, F., Florio, M., Kanton, S., Gerber, T., Wilsch-Bräuninger, M., Lewitus, E., Sykes, A., Hevers, W., Lancaster, M., Knoblich, J. A., Lachmann, R., Pääbo, S., Huttner, W. B., & Treutlein, B. (2015a). Human cerebral organoids recapitulate gene expression programs of fetal neocortex development. *Proceedings of the National Academy of Sciences*, *112*(51), 201520760. https://doi.org/10.1073/pnas.1520760112

Chailangkarn, T., Noree, C., & Muotri, A. R. (2018). The contribution of GTF2I haploinsufficiency to Williams syndrome. *Molecular and Cellular Probes*, *40*, 45–51. https://doi.org/10.1016/j.mcp.2017.12.005

Chailangkarn, T., Trujillo, C. A., Freitas, B. C., Hrvoj-Mihic, B., Herai, R. H., Yu, D. X., Brown, T. T., Marchetto, M. C., Bardy, C., McHenry, L., Stefanacci, L., Järvinen, A., Searcy, Y. M., Dewitt, M., Wong, W., Lai, P., Ard, M. C., Hanson, K. L., Romero, S., Jacobs, B., Dale, A. M., Dai, L., Korenberg, J. R., Gage, F. H., Bellugi, U., Halgren, E., Semendeferi, K., & Muotri, A. R. (2016). A human neurodevelopmental model for Williams syndrome. *Nature*, *536*(7616), 338–343. https://doi.org/10.1038/nature19067

Chaves, R. S., Tran, M., Holder, A. R., Balcer, A. M., Dickey, A. M., Roberts, E. A., Bober, B. G., Gutierrez, E., Head, B. P., Groisman, A., Goldstein, L. S. B., Almenar-Queralt, A., & Shah, S. B. (2021). Amyloidogenic Processing of Amyloid Precursor Protein Drives Stretch-Induced Disruption of Axonal Transport in hiPSC-Derived Neurons. *The Journal of Neuroscience : The Official Journal of the Society for Neuroscience*, *41*(49), 10034–10053. https://doi.org/10.1523/JNEUROSCI.2553-20.2021

Dai, L., Bellugi, U., Chen, X. N., Pulst-Korenberg, A. M., Järvinen-Pasley, A., Tirosh-Wagner, T., Eis, P. S., Graham, J., Mills, D., Searcy, Y., & Korenberg, J. R. (2009). Is it williams syndrome? GTF2IRD1 implicated in visual-spatial construction and GTF2I in sociability revealed by high resolution arrays. *American Journal of Medical Genetics, Part A*, *149*(3), 302–314. https://doi.org/10.1002/ajmg.a.32652

Danoff, S. K., Taylor, H. E., Blackshaw, S., & Desiderio, S. (2004). TFII-I, a candidate gene for Williams syndrome cognitive profile: Parallels between regional expression in mouse brain and human phenotype. *Neuroscience*, *123*(4), 931–938. https://doi.org/10.1016/j.neuroscience.2003.08.038

Depienne, C., Heron, D., Betancur, C., Benyahia, B., Trouillard, O., Bouteiller, D., Verloes, A., LeGuern, E., Leboyer, M., & Brice, A. (2007). Autism, language delay and mental retardation in a patient with 7q11 duplication. *Journal of Medical Genetics*, *44*(7), 452–458. https://doi.org/10.1136/jmg.2006.047092

Desgranges, Z. P., Ahn, J., Lazebnik, M. B., Ashworth, T., Lee, C., Pestell, R. C., Rosenberg, N., Prives, C., & Roy, A. L. (2005). Inhibition of TFII-I-Dependent Cell Cycle Regulation by p53. *Molecular and Cellular Biology*, *25*(24), 10940–10952.

https://doi.org/10.1128/mcb.25.24.10940-10952.2005

Desgranges, Z. P., & Roy, A. L. (2006). TFII-I: Connecting mitogenic signals to cell cycle regulation. *Cell Cycle*, *5*(4), 356–359. https://doi.org/10.4161/cc.5.4.2442

Deurloo, M. H. S., Turlova, E., Chen, W. L., Lin, Y. W., Tam, E., Tassew, N. G., Wu, M., Huang, Y. C., Crawley, J. N., Monnier, P. P., Groffen, A. J. A., Sun, H. S., Osborne, L. R., & Feng, Z. P. (2019). Transcription Factor 2I Regulates Neuronal Development via TRPC3 in 7q11.23 Disorder Models. *Molecular Neurobiology*, *56*(5), 3313–3325. https://doi.org/10.1007/s12035-018-1290-7

Dobin, A., Davis, C. A., Schlesinger, F., Drenkow, J., Zaleski, C., Jha, S., Batut, P., Chaisson, M., & Gingeras, T. R. (2013). STAR: Ultrafast universal RNA-seq aligner. *Bioinformatics*, *29*(1), 15–21. https://doi.org/10.1093/bioinformatics/bts635

Doyle, T. F., Bellugi, U., Korenberg, J. R., & Graham, J. (2004). "Everybody in the World Is My Friend" Hypersociability in Young Children with Williams Syndrome. *American Journal of Medical Genetics*, *124 A*(3), 263–273. https://doi.org/10.1002/ajmg.a.20416

Enkhmandakh, B., Makeyev, A. V., Erdenechimeg, L., Ruddle, F. H., Chimge, N. O., Tussie-Luna, M. I., Roy, A. L., & Bayarsaihan, D. (2009). Essential functions of the Williams-Beuren syndrome-associated TFII-I genes in embryonic development. *Proceedings of the National Academy of Sciences of the United States of America*, *106*(1), 181–186. https://doi.org/10.1073/pnas.0811531106

Gore, A., Li, Z., Fung, H. L., Young, J. E., Agarwal, S., Antosiewicz-Bourget, J., Canto, I., Giorgetti, A., Israel, M. A., Kiskinis, E., Lee, J. H., Loh, Y. H., Manos, P. D., Montserrat, N., Panopoulos, A. D., Ruiz, S., Wilbert, M. L., Yu, J., Kirkness, E. F., Belmonte, J. C. I., Rossi, D. J., Thomson, J. A., Eggan, K., Daley, G. Q., Goldstein, L. S. B., & Zhang, K. (2011). Somatic coding mutations in human induced pluripotent stem cells. *Nature*, *471*(7336), 63–67. https://doi.org/10.1038/nature09805

Griesi-Oliveira, K., Acab, A., Gupta, A. R., Sunaga, D. Y., Chailangkarn, T., Nicol, X., Nunez, Y., Walker, M. F., Murdoch, J. D., Sanders, S. J., Fernandez, T. V., Ji, W., Lifton, R. P., Vadasz, E., Dietrich, A., Pradhan, D., Song, H., Ming, G. L., Gu, X., Haddad, G., Marchetto, M. C. N., Spitzer, N., Passos-Bueno, M. R., State, M. W., & Muotri, A. R. (2015). Modeling non-syndromic autism and the impact of TRPC6 disruption in human neurons. *Molecular Psychiatry*, *20*(11), 1350–1365. https://doi.org/10.1038/mp.2014.141

Hennig, C. (2020). *fpc: Flexible Procedures for Clustering*.

Hodge, R. D., Bakken, T. E., Miller, J. A., Smith, K. A., Barkan, E. R., Graybuck, L. T., Close, J. L., Long, B., Johansen, N., Penn, O., Yao, Z., Eggermont, J., Höllt, T., Levi, B. P., Shehata, S. I., Aevermann, B., Beller, A., Bertagnolli, D., Brouner, K., Casper, T., Cobbs, C., Dalley, R., Dee, N., Ding, S. L., Ellenbogen, R. G., Fong, O., Garren, E., Goldy, J., Gwinn, R. P., Hirschstein, D., Keene, C. D., Keshk, M., Ko, A. L., Lathia, K., Mahfouz, A., Maltzer, Z., McGraw, M., Nguyen, T. N., Nyhus, J., Ojemann, J. G., Oldre,

A., Parry, S., Reynolds, S., Rimorin, C., Shapovalova, N. V., Somasundaram, S., Szafer, A., Thomsen, E. R., Tieu, M., Quon, G., Scheuermann, R. H., Yuste, R., Sunkin, S. M., Lelieveldt, B., Feng, D., Ng, L., Bernard, A., Hawrylycz, M., Phillips, J. W., Tasic, B., Zeng, H., Jones, A. R., Koch, C., & Lein, E. S. (2019). Conserved cell types with divergent features in human versus mouse cortex. *Nature*, *573*(7772), 61–68. https://doi.org/10.1038/s41586-019-1506-7

Karmiloff-Smith, A., Broadbent, H., Farran, E. K., Longhi, E., D'Souza, D., Metcalfe, K., Tassabehji, M., Wu, R., Senju, A., Happé, F., Turnpenny, P., & Sansbury, F. (2012). Social cognition in Williams syndrome: Genotype/phenotype insights from partial deletion patients. *Frontiers in Psychology*, *3*, 1–8. https://doi.org/10.3389/fpsyg.2012.00168

Kozel, B. A., Barak, B., Kim, C. A., Mervis, C. B., Osborne, L. R., Porter, M., & Pober, B. R. (2021). Williams syndrome. *Nature Reviews Disease Primers*, *7*(1). https://doi.org/10.1038/s41572-021-00276-z

Levi, G., De Lombares, C., Giuliani, C., Iannuzzi, V., Aouci, R., Garagnani, P., Franceschi, C., Grimaud-Hervé, D., & Narboux-Nême, N. (2021). DLX5/6 GABAergic Expression Affects Social Vocalization: Implications for Human Evolution. *Molecular Biology and Evolution*, *38*(11), 4748–4764. https://doi.org/10.1093/molbev/msab181

Liao, Y., Wang, J., Jaehnig, E. J., Shi, Z., & Zhang, B. (2019). WebGestalt 2019: gene set analysis toolkit with revamped UIs and APIs. *Nucleic Acids Research*, *47*(W1), W199–W205. https://doi.org/10.1093/nar/gkz401

López-Tobón, A., Trattaro, S., & Testa, G. (2020). The sociability spectrum: Evidence from reciprocal genetic copy number variations. *Molecular Autism*, *11*(1), 1–13. https://doi.org/10.1186/s13229-020-00347-0

Love, M. I., Huber, W., & Anders, S. (2014). Moderated estimation of fold change and dispersion for RNA-seq data with DESeq2. *Genome Biology*, *15*(12), 1–21. https://doi.org/10.1186/s13059-014-0550-8

Lucena, J., Pezzi, S., Aso, E., Valero, M. C., Carreiro, C., Dubus, P., Sampaio, A., Segura, M., Barthelemy, I., Zindel, M. Y., Sousa, N., Barbero, J. L., Maldonado, R., Pérez-, L. A., & Campuzano, V. (2010). Essential role of the N-terminal region of TFII-I in viability and behavior. *BMC Medical Genetics*, *11*(61). https://doi.org/10.1186/1471-2350-11-61

Luo, C., Lancaster, M. A., Castanon, R., Nery, J. R., Knoblich, J. A., & Ecker, J. R. (2016). Cerebral Organoids Recapitulate Epigenomic Signatures of the Human Fetal Brain. *Cell Reports*, *17*(12), 3369–3384. https://doi.org/10.1016/j.celrep.2016.12.001

Maere, S., Heymans, K., & Kuiper, M. (2005). BiNGO: A Cytoscape plugin to assess overrepresentation of Gene Ontology categories in Biological Networks. *Bioinformatics*, *21*(16), 3448–3449. https://doi.org/10.1093/bioinformatics/bti551

Malenfant, P., Liu, X., Hudson, M. L., Qiao, Y., Hrynchak, M., Riendeau, N., Hildebrand, M. J., Cohen, I. L., Chudley, A. E., Forster-Gibson, C., Mickelson, E. C. R., Rajcan-Separovic, E., Lewis, M. E. S., & Holden, J. J. A. (2012). Association of GTF2i in the Williams-Beuren Syndrome critical region with autism spectrum disorders. *Journal of Autism and Developmental Disorders*, *42*(7), 1459–1469. https://doi.org/10.1007/s10803-011-1389-4

Martin, M. (2011). Cutadapt removes adapter sequences from high-throughput sequencing reads. *EMBnet.Journal*, *17*(1), 10–12.

Massagué, J. (2004). G1 cell-cycle control and cancer. *Nature*, *432*, 298–306. https://doi.org/doi:10.1038/nature03094

Morris, C. A., Mervis, C. B., Paciorkowski, A. P., Abdul-Rahman, O., Dugan, S. L., Rope, A. F., Bader, P., Hendon, L. G., Velleman, S. L., Klein-Tasman, B. P., & Osborne, L. R. (2015). 7q11.23 Duplication syndrome: Physical characteristics and natural history. *American Journal of Medical Genetics, Part A*, *167*(12), 2916–2935. https://doi.org/10.1002/ajmg.a.37340

Nageshappa, S., Carromeu, C., Trujillo, C. A., Mesci, P., Espuny-Camacho, I., Pasciuto, E., Vanderhaeghen, P., Verfaillie, C. M., Raitano, S., Kumar, A., Carvalho, C. M. B., Bagni, C., Ramocki, M. B., Araujo, B. H. S., Torres, L. B., Lupski, J. R., Van Esch, H., & Muotri, A. R. (2016). Altered neuronal network and rescue in a human MECP2 duplication model. *Molecular Psychiatry*, *21*(2), 178–188. https://doi.org/10.1038/mp.2015.128

Negraes, P. D., Trujillo, C. A., Yu, N. K., Wu, W., Yao, H., Liang, N., Lautz, J. D., Kwok, E., McClatchy, D., Diedrich, J., de Bartolome, S. M., Truong, J., Szeto, R., Tran, T., Herai, R. H., Smith, S. E. P., Haddad, G. G., Yates, J. R., & Muotri, A. R. (2021). Altered network and rescue of human neurons derived from individuals with early-onset genetic epilepsy. *Molecular Psychiatry*, *26*(11), 7047–7068. https://doi.org/10.1038/s41380-021-01104-2

Osborne, L. R., Li, M., Pober, B., Chitayat, D., Bodurtha, J., Mandel, A., Costa, T., Grebe, T., Cox, S., Tsui, L. C., & Scherer, S. W. (2001). A 1.5 million-base pair inversion polymorphism in families with Williams-Beuren syndrome. *Nature Genetics*, *29*(3), 321–325. https://doi.org/10.1038/ng753

Parker, R., Phan, T., Baumeister, P., Roy, B., Cheriyath, V., Roy, A. L., & Lee, A. S. (2001). Identification of TFII-I as the Endoplasmic Reticulum Stress Response Element Binding Factor ERSF: Its Autoregulation by Stress and Interaction with ATF6. *Molecular and Cellular Biology*, *21*(9), 3220–3233. https://doi.org/10.1128/mcb.21.9.3220-3233.2001

Pober, B. R. (2010). Williams–Beuren Syndrome. *New England Journal of Medicine*, *362*(3), 239–252. https://doi.org/10.1056/NEJMra0903074

Preus, M. (1984). The Williams syndrome: objective definition and diagnosis. *Clinical Genetics*, *25*(5), 422–428. https://doi.org/10.1111/j.1399-0004.1984.tb02011.x

Roy, A. L. (2001). Biochemistry and biology of the inducible multifunctional transcription factor TFII-I. *Gene*, *274*(1), 1–13. https://doi.org/10.1016/s0378-1119(01)00625-4

Roy, A. L. (2007). Signal-induced functions of the transcription factor TFII-I. *Biochimica et Biophysica Acta - Gene Structure and Expression*, *1769*(11–12), 613–621. https://doi.org/10.1016/j.bbaexp.2007.10.002

Roy, A. L. (2017). Pathophysiology of TFII-I: Old Guard Wearing New Hats. *Trends in Molecular Medicine*, *23*(6), 501–511. https://doi.org/10.1016/j.molmed.2017.04.002

Roy, A. L., Du, H., Gregor, P. D., Novina, C. D., Martinez, E., & Roeder, R. G. (1997). Cloning of an inr- and E-box-binding protein, TFII-I, that interacts physically and functionally with USF1. *EMBO Journal*, *16*(23), 7091–7104. https://doi.org/10.1093/emboj/16.23.7091

Roy, A. L., Meisterernst, M., Pognonec, P., & Roeder, R. G. (1991). Cooperative interaction of an initiator-binding transcription initiation factor and the helix-loop-helix activator USF. *Nature*, *354*(6350), 245–248. https://doi.org/10.1038/354245a0

Sakurai, T., Dorr, N. P., Takahashi, N., McInnes, L. A., Elder, G. A., & Buxbaum, J. D. (2011). Haploinsufficiency of Gtf2i, a gene deleted in Williams Syndrome, leads to increases in social interactions. *Autism Research*, *4*(1), 28–39. https://doi.org/10.1002/aur.169

Scherer, S. W., Cheung, J., MacDonald, J. R., Osborne, L. R., Nakabayashi, K., Herbrick, J. A., Carson, A. R., Parker-Katiraee, L., Skaug, J., Khaja, R., Zhang, J., Hudek, A. K., Li, M., Haddad, M., Duggan, G. E., Fernandez, B. A., Kanematsu, E., Gentles, S., Christopoulos, C. C., Choufani, S., Kwasnicka, D., Zheng, X. H., Lai, Z., Nusskern, D., Zhang, Q., Gu, Z., Lu, F., Zeesman, S., Nowaczyk, M. J., Teshima, I., Chitayat, D., Shuman, C., Weksberg, R., Zackai, E. H., Grebe, T. A., Cox, S. R., Kirkpatrick, S. J., Rahman, N., Friedman, J. M., Heng, H. H. Q., Pelicci, P. G., Lo-Coco, F., Belloni, E., Shaffer, L. G., Pober, B., Morton, C. C., Gusella, J. F., Bruns, G. A. P., Korf, B. R., Quade, B. J., Ligon, A. H., Ferguson, H., Higgins, A. W., Leach, N. T., Herrick, S. R., Lemyre, E., Farra, C. G., Kim, H. G., Summers, A. M., Gripp, K. W., Roberts, W., Szatmari, P., Winsor, E. J. T., Grzeschik, K. H., Teebi, A., Minassian, B. A., Kere, J., Armengol, L., Pujana, M. A., Estivill, X., Wilson, M. D., Koop, B. F., Tosi, S., Moore, G. E., Boright, A. P., Zlotorynski, E., Kerem, B., Kroisel, P. M., Petek, E., Oscier, D. G., Mould, S. J., Döhner, H., Döhner, K., Rommens, J. M., Vincent, J. B., Venter, J. C., Li, P. W., Mural, R. J., Adams, M. D., & Tsui, L. C. (2003). Human chromosome 7: DNA sequence and biology. *Science*, *300*(5620), 767–772. https://doi.org/10.1126/science.1083423

Shannon, P., Markiel, A., Ozier, O., Baliga, N. S., Wang, J. T., Ramage, D., Amin, N., Schwikowski, B., & Ideker, T. (2003). Cytoscape: A Software Environment for Integrated Models of Biomolecular Interaction Networks. *Genome Research*, *13*, 2498–2504. https://doi.org/10.1101/gr.1239303.metabolite

Shen, Y., Nar, R., Fan, A. X., Aryan, M., Hossain, M. A., Gurumurthy, A., Wassel, P. C.,

Tang, M., Lu, J., Strouboulis, J., & Bungert, J. (2018). Functional interrelationship between TFII-I and E2F transcription factors at specific cell cycle gene loci. *Journal of Cellular Biochemistry*, *119*(1), 712–722. https://doi.org/10.1002/jcb.26235

Sirenko, O., Parham, F., Dea, S., Sodhi, N., Biesmans, S., Mora-Castilla, S., Ryan, K., Behl, M., Chandy, G., Crittenden, C., Vargas-Hurlston, S., Guicherit, O., Gordon, R., Zanella, F., & Carromeu, C. (2019). Functional and mechanistic neurotoxicity profiling using human iPSC-Derived neural 3D cultures. *Toxicological Sciences*, *167*(1), 249–257. https://doi.org/10.1093/toxsci/kfy218

Somerville, M. J., Mervis, C. B., Young, E. J., Seo, E.-J., del Campo, M., Bamforth, S., Peregrine, E., Loo, W., Lilley, M., Pérez-Jurado, L. A., Morris, C. A., Scherer, S. W., & Osborne, L. R. (2005). Severe Expressive-Language Delay Related to Duplication of the Williams–Beuren Locus. *New England Journal of Medicine*, *353*(16), 1694–1701. https://doi.org/10.1056/nejmoa051962

Tebbenkamp, A. T. N., Varela, L., Choi, J., Paredes, M. I., Giani, A. M., Song, J. E., Sestan-Pesa, M., Franjic, D., Sousa, A. M. M., Liu, Z. W., Li, M., Bichsel, C., Koch, M., Szigeti-Buck, K., Liu, F., Li, Z., Kawasawa, Y. I., Paspalas, C. D., Mineur, Y. S., Prontera, P., Merla, G., Picciotto, M. R., Arnsten, A. F. T., Horvath, T. L., & Sestan, N. (2018). The 7q11.23 Protein DNAJC30 Interacts with ATP Synthase and Links Mitochondria to Brain Development. *Cell*, *175*(4), 1088-1104.e23. https://doi.org/10.1016/j.cell.2018.09.014

Trujillo, C. A., Adams, J. W., Negraes, P. D., Carromeu, C., Tejwani, L., Acab, A., Tsuda, B., Thomas, C. A., Sodhi, N., Fichter, K. M., Romero, S., Zanella, F., Sejnowski, T. J., Ulrich, H., & Muotri, A. R. (2021). Pharmacological reversal of synaptic and network pathology in human MECP2 -KO neurons and cortical organoids. *EMBO Molecular Medicine*, *13:e12523*. https://doi.org/10.15252/emmm.202012523

Trujillo, C. A., Gao, R., Negraes, P. D., Gu, J., Buchanan, J., Preissl, S., Wang, A., Wu, W., Haddad, G. G., Chaim, I. A., Domissy, A., Vandenberghe, M., Devor, A., Yeo, G. W., Voytek, B., & Muotri, A. R. (2019). Complex Oscillatory Waves Emerging from Cortical Organoids Model Early Human Brain Network Development. *Cell Stem Cell*, *25*(4), 558-569.e7. https://doi.org/10.1016/j.stem.2019.08.002

Trujillo, C. A., Rice, E. S., Schaefer, N. K., Chaim, I. A., Wheeler, E. C., Madrigal, A. A., Buchanan, J., Preissl, S., Wang, A., Negraes, P. D., Szeto, R. A., Herai, R. H., Huseynov, A., Ferraz, M. S. A., Borges, F. S., Kihara, A. H., Byrne, A., Marin, M., Vollmers, C., Brooks, A. N., Lautz, J. D., Semendeferi, K., Shapiro, B., Yeo, G. W., Smith, S. E. P., Green, R. E., & Muotri, A. R. (2021). Reintroduction of the archaic variant of NOVA1 in cortical organoids alters neurodevelopment. *Science*, *371*(6530). https://doi.org/10.1126/science.aax2537

Urresti, J., Zhang, P., Moran-Losada, P., Yu, N. K., Negraes, P. D., Trujillo, C. A., Antaki, D., Amar, M., Chau, K., Pramod, A. B., Diedrich, J., Tejwani, L., Romero, S., Sebat, J., Yates, J. R., Muotri, A. R., & Iakoucheva, L. M. (2021). Cortical organoids model early

brain development disrupted by 16p11.2 copy number variants in autism. *Molecular Psychiatry*, *26*(12), 7560–7580. https://doi.org/10.1038/s41380-021-01243-6

Wahlin, K. J., Cheng, J., Jurlina, S. L., Jones, M. K., Dash, N. R., Ogata, A., Kibria, N., Ray, S., Eldred, K. C., Kim, C., Heng, J. S., Phillips, J., Johnston, R. J., Gamm, D. M., Berlinicke, C., & Zack, D. J. (2021). CRISPR Generated SIX6 and POU4F2 Reporters Allow Identification of Brain and Optic Transcriptional Differences in Human PSC-Derived Organoids. *Frontiers in Cell and Developmental Biology*, *9*(764725). https://doi.org/10.3389/fcell.2021.764725

Wang, L., Wang, S., & Li, W. (2012). RSeQC: Quality control of RNA-seq experiments. *Bioinformatics*, *28*(16), 2184–2185. https://doi.org/10.1093/bioinformatics/bts356

Wang, M., Wei, P. C., Lim, C. K., Gallina, I. S., Marshall, S., Marchetto, M. C., Alt, F. W., & Gage, F. H. (2020). Increased Neural Progenitor Proliferation in a hiPSC Model of Autism Induces Replication Stress-Associated Genome Instability. *Cell Stem Cell*, *26*(2), 221-233.e6. https://doi.org/10.1016/j.stem.2019.12.013

Zhang, B., Kirov, S., & Snoddy, J. (2005). WebGestalt: An integrated system for exploring gene sets in various biological contexts. *Nucleic Acids Research*, *33*(SUPPL. 2), 741–748. https://doi.org/10.1093/nar/gki475

APPENDIX 1 Brain organoids as tools for modeling human neurodevelopmental disorders

Abstract

Brain organoids recapitulate *in vitro* the specific stages of *in vivo* human brain development, thus offering an innovative tool by which to model human neurodevelopmental disease. We review here how brain organoids have been used to study neurodevelopmental disease and consider their potential for both technological advancement and therapeutic development.

Introduction

Investigating neurodevelopmental disease pathogenesis presents considerable challenge due to limited accessibility of human central nervous system (CNS) tissue and poor recapitulation of animal models. The considerable variability in neuroanatomy and connectivity that exists between individuals because of disparate genetic background and environmental exposure (Geschwind & Flint, 2015) introduces another barrier to understanding disease progression. Our understanding of cellular phenotypes in neuropathological conditions has historically derived primarily from postmortem analysis of CNS tissue, but tissue represents only a single disease time point and may not be well-preserved. Functional neuroimaging and animal models have provided noninvasive alternatives for modeling human neurological diseases, but these models are limited by age, sex, pathological heterogeneity, and inconsistent translatability between species (Figure 7; Muotri, 2016).

Recent advancement of stem cell technology has introduced a new model by which to study the human brain. Human embryonic stem cells (hESCs) can be induced into neural stem cells and further differentiated into neurons and glia. Due to their ethically controversial origin, however, hESCs have been only loosely adopted. Cellular reprogramming—a technique that reverts patient-specific somatic cells to a pluripotent state, the induced pluripotent stem cells (iPSCs; Takahashi et al., 2007)—offers a way around this problem. iPSCs carry the genotype of the patient donor and, like hESCs, can be differentiated into many different cell types—including neurons and glia. iPSCs thus enable direct *in vitro* manipulation of relevant cellular phenotypes affected in nervous system diseases.

Initial efforts to model neurological diseases *in vitro* consisted of neuronal culturing in monolayer. Neurons and glia can be obtained by differentiating neural progenitor cells (NPCs) that are, in turn, directed from iPSCs or ESCs by dual SMAD inhibition (Chambers et al., 2009). NPCs self-organize into rosettes resembling the embryonic neural tube—thereby mimicking *in vivo* neocortical development—and are thus a predominant method in several differentiation protocols (Paşca et al., 2014). Alternatively, neurons can be induced directly from fibroblasts via forcible expression of several transcription factors—Brn2, Ascl1, and MytL1—or even a single transcription factor, Ngn2 (Caiazzo et al., 2011; Pang et al., 2011; Y. Zhang et al., 2013). Regardless, culturing neural cells in a 2D environment limits the opportunity for cells to create the structure and organized network connectivity observed *in vivo* (Kirwan et al., 2015). The need for improved *in vitro* models that more accurately recapitulate human brain complexity and overcome the limitations of 2D models led to the development of 3D brain organoids (Figure 7).

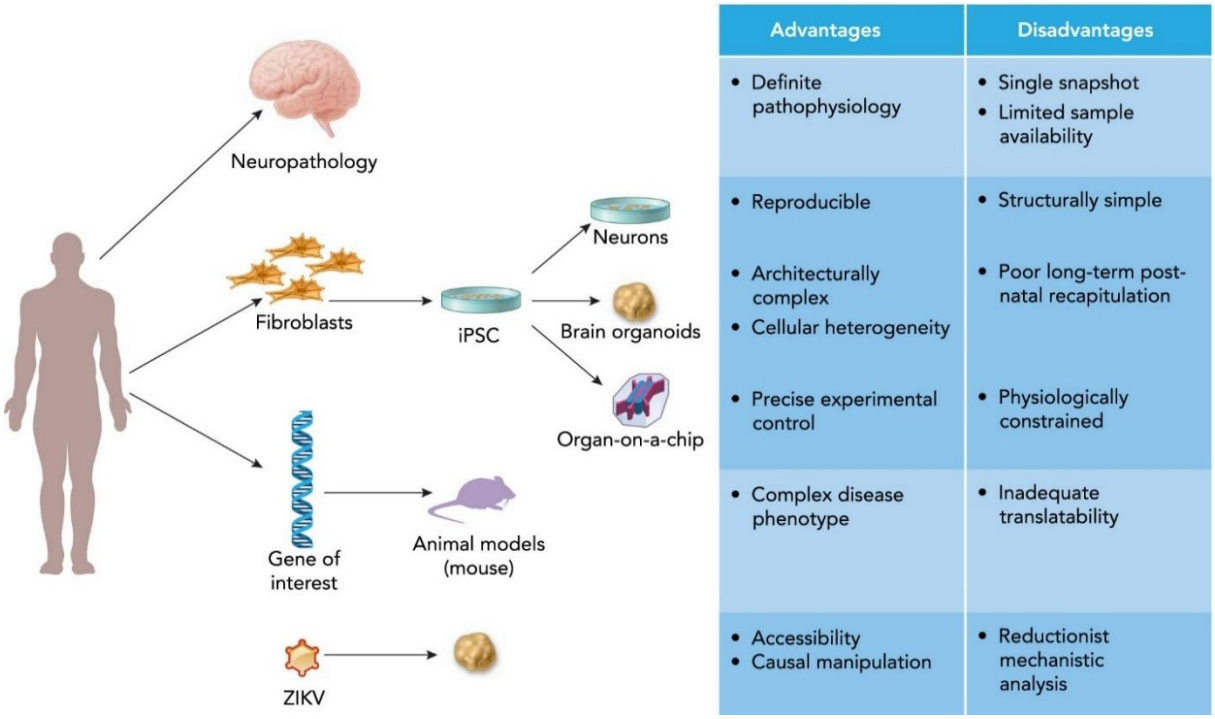

Figure 7: Advantages and disadvantages of methods of neurodevelopmental disease analysis. Neurodevelopmental disease mechanisms can be assessed using various modalities, each of which has unique and complementary strengths, with selection dependent on desired read-out.

The founding discovery of what would come to be called an ‘organoid’ was made by the Sasai laboratory, a pioneering stem cell research group upon whose shoulders all subsequent organoid research stands. They observed that ESCs and iPSCs could self-organize and aggregate in a manner remarkably recapitulative of *in vivo* development (Eiraku et al., 2011; Nakano et al., 2012). Indeed, although the Sasai group’s initial monographs detailed the self-formation of optic tissue (Eiraku et al., 2011; Nakano et al., 2012), organoids of other neural fate likewise display highly similar organization, gene expression profiling, topographical induction, and temporal development to that seen during fetal neural development (Camp et al., 2015; Cederquist et al., 2019; Lancaster et al., 2013; Luo et al.,

2016; Xiang et al., 2019). Currently, brain organoids can be generated in two ways: non-patterned or patterned. Non-patterned organoids, generally grown embedded in an extracellular matrix, self-organize into different brain regions via endogenous patterning cues (Lancaster et al., 2013; Renner et al., 2017). Patterned organoids, in contrast, are differentiated into specific brain regions—forebrain or midbrain, for example—by adding external growth factors (Mariani et al., 2015; Pasca et al., 2015; Qian et al., 2016).

Brain organoids, patterned or otherwise, confer investigative ability unavailable *in vivo*. Evaluation of normal cellular migration and organoid maturation with immunofluorescence and live imaging can be used to examine tissue stratification and detect early signs of pathology (Birey et al., 2017; Camp et al., 2015). Genomic engineering tools can modify patient-derived stem cells to investigate gene-function relation (Sloan et al., 2018), regionally patterned organoids can be fused to investigate complex interregional dynamics (Birey et al., 2017; Sloan et al., 2018; Xiang et al., 2017), and patch-clamp electrophysiology and optogenetics can assess functional integration (Figure 8; Mansour et al., 2018). Furthermore, recent detection of spontaneous network activity with regular oscillatory waves, similar to that observed in preterm human electroencephalography, demonstrated the capacity of multi-electrode array to dynamically assess network activity in long-term mature organoids (Trujillo et al., 2018). The accessibility of iPSCs and brain organoids has thus introduced unprecedented possibility for *in vitro* neurodevelopmental disease modeling.

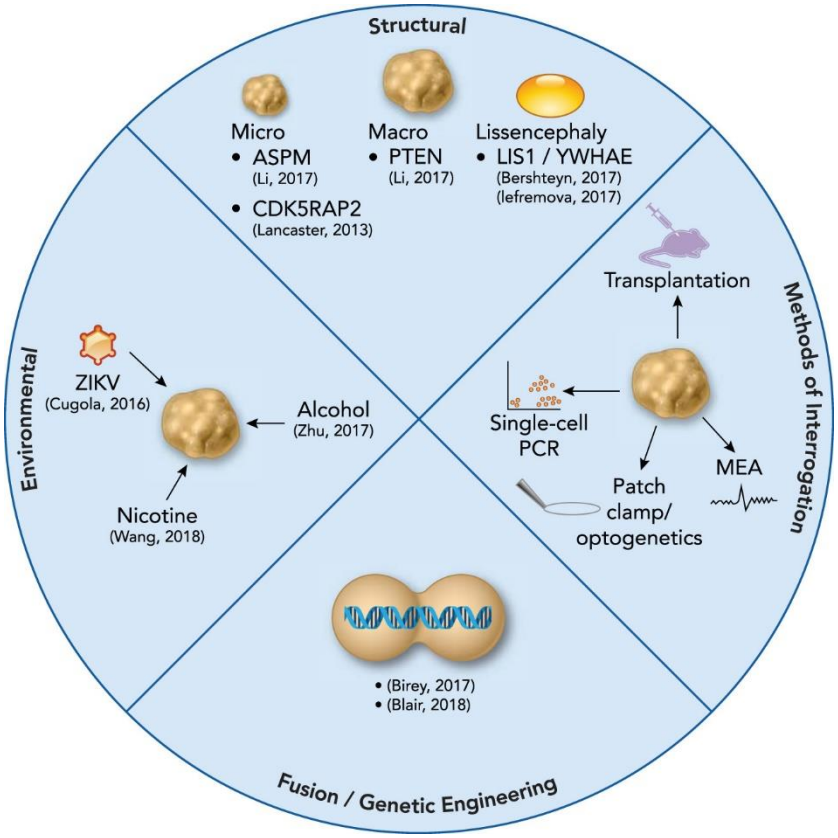

Figure 8: Brain organoid disease modeling and analytic techniques. Brain organoids can model congenital structural deficits or be subjected to environmental insult. In addition, genetic engineering and multi-organoid fusion enable the assessment of a broader array of disease mechanisms, such as abnormal interregional development. Various methods can be used to evaluate the developmental changes that underlie the disparate phenotypes observed between normal and diseased organoids.

Applications of Brain Organoids as Neurodevelopmental Disease Models

Perhaps the greatest application of brain organoid technology thus far, *in vitro* modeling of neurodevelopmental disease enables observation of disease progression throughout neurodevelopment and—in conjunction with novel genetic techniques—the opportunity to interrogate underlying pathologic mechanisms with previously precluded precision. The versatility of brain organoids permits modeling diseases of either intrinsic (i.e., genetic) or extrinsic (i.e., environmentally mediated) etiology (Figure 8). However, despite recent characterization of functional network development (Trujillo et al., 2018),

developmental disorders in which gross structural abnormalities predominate remain the more accessible for *in vitro* modeling.

Autosomal Recessive Primary Microcephaly. Autosomal recessive primary microcephaly (MCPH)—a genetic form of microcephaly, itself a clinical entity of heterogeneous etiology—has been linked to genetic mutations in neurodevelopmental pathways (Morris-Rosendahl & Kaindl, 2015). Individuals with MCPH clinically portray nonprogressive intellectual disability and neuropathologically exhibit microcephalic brains with reduction concentrated in the cerebral cortex (Woods et al., 2005). MCPH has been modeled with organoids generated from patient-derived iPSCs carrying mutation(s) in either *ASPM*—the gene, which codes for a protein involved with mitotic spindle function, accounting for a plurality of MCPH cases (Francis et al., 2006)—or *CDK5RAP2*, a gene whose product localizes to the mitotic spindle pole during neurogenesis (Lancaster et al., 2013; R. Li et al., 2017; Woods et al., 2005). Those iPSCs in which *ASPM* expression was downregulated, predicted to impede neural progenitor proliferation, yielded hypoplastic organoids with fewer proliferative cells, decreased neocortex-like morphology, and diminished neuroepithelial structural integrity (R. Li et al., 2017). Functional analysis revealed calcium activity in fewer cells than the controls—implicating neuronal maturation impediment—and decreased synchrony (R. Li et al., 2017). *CDK5RAP2*-mutant organoids likewise portrayed hypoplasticity with sparse progenitor and neuroepithelial regions (Lancaster et al., 2013). Coincident findings of premature neural differentiation and increased neuron quantity were supported by observation of increased neuronal differentiation upon *CDK5RAP2* RNAi-knockdown (Lancaster et al.,

2013). Successful phenotypic rescue upon electroporated expression of CDK5RAP2 protein confirmed viable *in vitro* recapitulation of MCPH (Lancaster et al., 2013).

Microcephaly in Seckel Syndrome. Seckel syndrome—a disorder argued to be on a clinical spectrum with primary microcephaly and whose clinical features include severe pre and postnatal growth restriction, microcephaly, and intellectual disability (Majewski & Goecke, 1982; Marakhonov et al., 2018)—is observed in individuals with mutated centrosomal-P4.1-associated protein (CPAP). Concordant with other microcephalies, organoids of Seckel syndrome patient-derivation featured diminished size with reduced neuroepithelium and disordered progenitor regions (Gabriel et al., 2016). In argument for organoids' biologically intrinsic mechanistic value, Gabriel et al. (2016) identified a ciliary role in NPC sustenance and a regulatory role of ciliary length by CPAP. Indeed, detailed interrogation of Seckel organoids revealed more numerous and longer apical progenitor cilia compared to controls (Gabriel et al., 2016). Their work thus demonstrated that in addition to modeling structural deficits, brain organoids enable investigation—*in vitro*—of molecular mechanisms underlying neurodevelopmental disease.

Macrocephaly. Just as some mutations confer a microcephalic phenotype, others—*PTEN* loss-of-function, for example—have macrocephalic consequence (Butler et al., 2005). Cortical organoids generated from *PTEN*-knockout hESCs exhibit increased neuroepithelial outgrowth, surface area, and volume (Y. Li et al., 2017). Most striking, however, is the enhanced gyrification evident in *PTEN*-mutant organoids. At the cellular level, *PTEN*-mutants displayed more proliferative cells throughout development, an increase reflected in expanded

neural progenitor pools in the ventricular and subventricular zones. It was over these pools of increased proliferative cellularity that the neuroepithelial curvature was more pronounced, an observation later supported biophysically (Karzbrun et al., 2018). Viral reintroduction of *PTEN* offered successful phenotypic rescue, with normal neural differentiation and proliferation and the generation of smooth organoids. Indeed, manipulating AKT signaling effected a phenotypic dose-response: Less AKT signaling yielded smaller, smoother cortical organoids, and increased AKT signaling generated larger organoids with increased fold density (Y. Li et al., 2017).

Congenital Lissencephaly. Lissencephaly is a clinical entity characterized by decreased or absent gyration resulting from deficient neuronal migration during development (Icenogle & Kaplan, 1981). Heterozygous chromosome 17p13.3 deletion results in Miller-Dieker syndrome (MDS), a neurodevelopmental lissencephalic disorder whose clinical characteristics include intellectual disability and seizures (Blazejewski et al., 2018). This deletion often involves *LIS1* and *YWHAE*, the gene products of which are components of a multiprotein complex that has regulatory function of cytoskeletal protein dynamics (Wynshaw-Boris, 2007). Because the LIS1 multiprotein complex is involved with the mitotic spindle and radial glia proliferation, protein defects within the complex yield structural defects during development (Yingling et al., 2008). Organoids developed from MDS patient–derived iPSCs exhibited smaller size and slower expansion compared to controls and likewise featured structural aberrancies in neuroepithelial loops, including reduced apical and basal membrane length, loop diameter, and overall size of a ventricle-like space (Iefremova et al., 2017). Interrogation of MDS organoids at finer resolution revealed disrupted radial glia cytoskeletal

networks with diminished projection of truncated microtubules towards the basal membrane (Iefremova et al., 2017). Moreover, mitotic spindle cleavage in MDS organoids exhibited a non-random planar switch (from vertical to horizontal and asymmetric) and disrupted adhesion molecules in the ventricular zone. Reduced β-catenin expression in organoids and influential N-cadherin signaling in MDS patient rosettes implicated Wnt pathway disruption in MDS; pharmacological β-catenin activation via CHIR99021 inhibition of GSK3β rescued division plane orientation, cortical loop structure, and apical membrane length (Iefremova et al., 2017). Notably, expressing LIS1 or 14-3-3ε (the protein product of *YWHAE*) in MDS patient cells offered partial restoration of a control phenotype (Iefremova et al., 2017).

Individuals with MDS exhibit pronouncedly disrupted cortical cellular distribution: Immature neurons appear in the deepest cortical layer, and cell proliferation markers imply disruption of neural progenitor proliferation (Sheen et al., 2006). Organoids from MDS patients—developed to investigate neural progenitor defects *in vitro*—revealed a disrupted ventricular zone surface, disproportionately frequent horizontal cleavage angles, and outer radial glia with longer mitotic delay prior to cytokinesis (Bershteyn et al., 2017). Despite intact migratory processes, MDS organoids exhibited impaired neural migration such that migration was initiated but not sustained and was observed to be slower and less linear. Remarkably, restoration of the LIS1 and 14-3-3ε proteins completely rescued phenotypic aberrancy to wild-type (Bershteyn et al., 2017).

Karzbrun et al. (2018) sought to define the physical forces that regulate cortical folding and then apply that understanding to a lissencephalic organoid model. Physically, organoid surface wrinkling appeared to be subject to the mechanical instability instigated by compression such that wrinkling starkly emerged when the nuclear density reached a

threshold (Karzbrun et al., 2018). Application to a heterozygous *LIS1* mutant organoid model revealed a wider range of cortical thicknesses than control organoids and the longer wavelengths (i.e., distance from one wrinkle crest to another) and decreased curvature expected of lissencephaly (Karzbrun et al., 2018). *LIS1* mutants exhibited decreased expression of cytoskeletal genes, and assessment of ESCs and NPCs with atomic force microscopy indicated the *LIS1* mutant cells were twice as elastic as their control counterparts (Karzbrun et al., 2018). Increased elasticity would be expected to confer resistance against a compressive force inducing folding and might partially explain the decreased gyrification of lissencephaly. Such a model would likewise be consistent with a separate group's observation of increased neuroepithelial curvature in areas with more proliferating cells (Y. Li et al., 2017).

Sandhoff Disease. Sandhoff disease is an autosomal recessive lysosomal storage disorder in which mutant-*HEXB* insufficiency of β-hexosaminidase causes lysosomal accumulation of GM2 ganglioside (Sandhoff, 1969; Sandhoff et al., 1971). The GM2 gangliosidoses clinically feature developmental delay or regression, seizures, macrocephaly, hypotonia, and progressive decline in motor and cognitive functioning (Allende et al., 2018; Tavasoli et al., 2018). Allende et al. (2018) developed organoids from a Sandhoff disease patient and from CRISPR/Cas9-corrected *HEXB* mutant isogenic iPSCs. In comparison to *HEXB*-corrected organoids, Sandhoff disease patient organoids appeared macrocephalic with increased proliferation and dysfunctional differentiation (Allende et al., 2018). By the fourth week of growth, immunostaining revealed GM2 ganglioside accumulation and even inclusion body development in Sandhoff disease organoids; *HEXB*-corrected organoids accumulated

significantly less GM2 ganglioside (Allende et al., 2018). In evidence of phenotypic rescue, restoration of β-hexosaminidase via AAV-*HEXA/B* injection decreased Sandhoff disease organoid size and lessened GM2 accumulation (Allende et al., 2018).

Tuberous Sclerosis Complex. Tuberous sclerosis complex (TSC) is a multisystem developmental disorder in which heterozygous germline mutations in *TSC1* or *TSC2*—encoding hamartin and tuberin, respectively—cause constitutive activation of mechanistic target of rapamycin complex 1 (mTORC1; Peron & Northrup, 2018). The wide-ranging clinical features of TSC include seizures, autism, and intellectual disability; facial angiofibromas; cardiac rhabomyomas; and, most characteristically, cortical tubers (Crino et al., 2006). Blair et al. (2018) sought to investigate the underlying genetic mechanisms of cortical tuber development—the proposed of which include "second hit" loss of heterozygosity, abnormal retrotransposition, and haploinsufficiency (Jacob-Hirsch et al., 2018; Martin et al., 2017)—using cortical spheroids generated from CRISPR/Cas9-mutated (both hetero and homozygously) *TSC1* or *TSC2* hESCs. Homozygous *TSC2*-knockout spheroids exhibited persistently upregulated mTORC1 during neuronal differentiation, a period customarily of quiescent mTORC1 signaling (Blair et al., 2018). Homozygous *TSC1* or *TSC2* knockouts additionally featured enhanced mTOR-dependent, gliogenic JAK-STAT signaling: Treatment with the mTOR inhibitor rapamycin reduced pathway activation, decreased astrocytic GFAP expression, and increased expression of neuronal markers (Blair et al., 2018). Blair et al. (2018) then engineered hESCs with a Cre-inducible *TSC2* mutation to assess the verity of the second-hit hypothesis. Homozygous, but not heterozygous, spheroids exhibited enlarged, misshapen neurons; increased glial cells; and hypertrophic, filamentous

"giant cells" resembling those characteristic of cortical tubers. Spheroids developed from a heterozygous TSC patient, reprogrammed from fibroblasts and engineered to receive a second hit, subsequently confirmed the necessity of biallelic inactivation to develop the dysmorphic cells characteristic of TSC. Just as rapamycin earlier reduced JAK-STAT signaling to combat mTORC1 overactivation, so, too, could it reduce cellular enlargement and recover neuronal—rather than glial—differentiation. A developmental time dependency constrained treatment efficacy, however, such that rapamycin administered too late offered insufficient phenotypic rescue (Blair et al., 2018).

Rett Syndrome. Rett syndrome is a neurodevelopmental disorder almost universally caused by X-linked mutations in *MECP2*, the gene encoding methyl-CpG binding protein 2. Clinically, females with Rett syndrome typically experience normally appearing development for 12-18 months followed by regression—in domains such as hand movement and language—and the onset of gait abnormalities (Ip et al., 2018; Neul et al., 2010); males experience severe congenital encephalopathy and early death (Schüle et al., 2008). Rett patient-derived cells exhibit structural and connectivity defects (M. C. N. Marchetto et al., 2010), and a suppressive role of MeCP2 has been implicated in posttranscriptional microRNA processing essential for neural development (Cheng et al., 2014). Brain organoids generated from Rett syndrome patients revealed upregulated miR-199 and miR-214, two microRNAs that are involved in ERK and AKT signaling pathways for neurogenesis and neural differentiation (Mellios et al., 2018). Moreover, Rett mutant organoids displayed increased ventricular area with decreased ventricular wall thickness, consistent with increased neural progenitors and proliferation with concomitantly impaired neurogenesis (Mellios et al., 2018).

Autism Spectrum Disorder. The term autism spectrum disorder (ASD) describes a set of clinically heterogeneous disorders whose core characteristics include behavioral stereotypies and impairments in social interaction and language (Abrahams & Geschwind, 2008). ASD is thought to be of both genetic and environmental etiologic derivation (Ramaswami & Geschwind, 2018), and despite the wide-ranging concordance estimates observed for twins, the estimated heritability of ASD is 0.7-0.8 (Colvert et al., 2015; Spence, 2004). Perhaps underlying the broad clinical heterogeneity, ASD is associated with a broad array of genetic profiles and aberrancies—from widely varying allelic frequencies (e.g., common, rare, etc.) to disparate inheritance patterns (e.g., dominant, x-linked, etc.) to variant type (e.g., insertion/deletion, copy number variant, etc.; Ramaswami & Geschwind, 2018). Despite this genetic heterogeneity, autism may represent a convergence phenotype of several common pathways (Geschwind, 2008); *in vitro* cellular modeling may offer a versatile modality by which to interrogate these underlying mechanisms (Griesi-Oliveira et al., 2015; Lullo & Kriegstein, 2017; M. C. Marchetto et al., 2017).

ASD may be attributable to heterogeneous intercellular transcriptomic changes with convergent cellular and molecular pathways (Quesnel-Vallières et al., 2018), one of which may be excitatory/inhibitory imbalance (Rubenstein, 2010; Tang et al., 2016). Cortical organoids using iPSCs drawn from macrocephalic ASD individuals revealed—compared to unaffected family members—transcriptomic differences in cell fate and proliferation; cytoskeletal regulation of dynamic cytological growth, guidance, and maintenance; synaptic assembly and channel functioning, such as potassium ion channel upregulation and ligand-receptor interactions; and upregulated GABAergic enzyme synthesis (Mariani et al., 2015). Despite the low number of individuals tested, the similar findings observed in an independent

cohort of ASD individuals increase confidence in the data (M. C. Marchetto et al., 2017). Cytological analysis exhibited increased VGAT+ inhibitory synapse formation with concomitantly increased GABAergic neural fate, a finding subsequently confirmed electrophysiologically (Mariani et al., 2015). Transcriptomic upregulation correlated with autism symptom severity, and one of the principal genes upregulated throughout development was *FOXG1*, the product of which is a developmental transcription factor for the telencephalon and mutations in which confer neurodevelopmental dysfunction (Ariani et al., 2008; Butler et al., 2005; Jacob et al., 2009; Mariani et al., 2015; Mitter et al., 2018; Powers et al., 2004). Remarkably, interference with *FOXG1* expression could revert the GABAergic neural production in ASD organoids to normal (Mariani et al., 2015). Evaluation of another gene frequently involved in autism, the chromatin-remodeling factor *CHD8* (chromodomain helicase DNA-binding protein 8), likewise revealed upregulation of transcripts used for GABAergic interneuronal development (P. Wang et al., 2017). Although ASD is associated with an excitatory/inhibitory imbalance, the concordant findings of GABAergic increase in these models contrasts with evidence indicating GABAergic reduction in ASD (Chao et al., 2010; Fatemi et al., 2010).

Microglia in Organoids

Concomitantly with imbalanced excitation and inhibition, individuals with ASD and other neuropsychiatric disorders are proposed to have aberrant synaptic structure and connectivity (Belmonte, 2004; Hutsler & Zhang, 2010; M. C. N. Marchetto et al., 2010; Penzes et al., 2011; Toro et al., 2010). Microglia function in synaptic remodeling during development (McKenzie et al., 2018; Schafer et al., 2012; Sominsky et al., 2018; Stevens et

al., 2007) and may be involved in ASD and other neurodevelopmental disorders (Filipello et al., 2018; Koyama & Ikegaya, 2015; Pardo et al., 2005; Schafer et al., 2016). For example, ASD patients exhibit increased microglia density and microglial morphology indicative of activation (Morgan et al., 2010; Suzuki et al., 2013; Tetreault et al., 2012), and wild-type microglial engraftment could impede disease progression and improve phenotype in a Rett syndrome mouse model (Derecki et al., 2012). Indeed, rodents have, to date, been the primary model for studying microglia (Bilimoria & Stevens, 2015; Sominsky et al., 2018); however, murine and human microglia are thought to differ markedly (A. M. Smith et al., 1953). Recent derivation of microglia from hiPSCs offers a novel opportunity by which to study microglial function in neurologic disease (Abud et al., 2017; Muffat et al., 2016). Two groups separately derived microglia-like cells from human iPS cells that could, in organoid co-culture, integrate and respond to either laser- or needle-induced traumatic injury (Abud et al., 2017; Muffat et al., 2016), and a third group induced an inflammatory response by exposing neurospheres co-cultured with human microglia to bacterial lipopolysaccharide and flaviviral infection (Monteiro Abreu et al., 2018). Whereas it had been thought that microglia—of primitive myeloid progenitor yolk-sac derivation (Ginhoux et al., 2010)—must be introduced to neuroectodermally derived organoids, recent modification of an undirected-differentiation brain organoid protocol, in which all three primitive germ layers are present in early organoidogenesis, revealed intrinsic development of Iba-1-positive microglia from mesodermal precursors (Ormel et al., 2018). Such inclusion of microglia in organoids promises expanded opportunities for disease modeling.

Teratogens Modeling

In addition to genetically based neurodevelopmental disease modeling, the *in vitro* accessibility and manipulability of brain organoids has also facilitated their use in studying CNS teratogens. Alcohol consumption during pregnancy, perhaps the foremost CNS teratogen, is a major public health concern (Sebastiani et al., 2018). Clinically, fetal alcohol spectrum disorder features developmental delay, behavioral impairment, and cognitive dysfunction (Riley et al., 2011). The neuropathological consequences of prenatal alcohol exposure include decreased brain volume and thinning of the corpus callosum (reviewed in (Lebel et al., 2011)). Exposure of brain organoids to alcohol impaired neural maturation, reduced neurite outgrowth, and increased cell death (Zhu et al., 2017). Nicotine is another common teratogen, fetal exposure to which can disrupt development and increase long-lasting health risks for the offspring even into adulthood (Bruin et al., 2010). Brain organoids exposed to nicotine showed impaired neuronal migration and differentiation (Y. Wang et al., 2018).

In addition to toxin exposure, viral insult presents a separate external mechanism by which neural development can be impaired (Bale, 2009). Exposure to Zika virus *in utero* has been associated with an increased frequency of congenital microcephaly (Oliveira et al., 2016). A causal mechanism underlying this association was established by infecting brain organoids and a mouse model with a Brazilian strain of Zika virus (Cugola et al., 2016). In addition to the microcephaly observed in mice, the virus depleted the neural progenitor cell pool of organoids by preferentially infecting NPCs, causing cell death, and disrupting the cortical plate (Cugola et al., 2016).

Fusion, Genome Engineering, and the Next Generation of Organoid Technology

Modeling neurological disorders in the past has often required animal or other model systems, and neurodevelopmental disorders present a particular challenge due to limited accessibility. The enhanced breadth and depth of organoid technology using human cells, however, has facilitated the modeling of an ever-increasing array of disorders with both unprecedented recapitulative accuracy and genetic manipulative capacity. Multi-organoid fusion, genomic engineering, and methods of vascularization promise further advancement in disease modeling and pharmacological development.

Multi-Organoid Fusion. Development of the nervous system is a complex yet synchronous dance of multi-modal events, including neuronal migration and the establishment of synaptic interconnectivity. Although organoid modeling methods to date recapitulate neural development remarkably well (Lancaster et al., 2013; Qian et al., 2016), the disrupted neuronal migration and regional interconnectivity underlying some neurological disorders argues for methods that can model these actions. Fusing together organoids of different pre-specified brain regions offers a modality by which to model such interregional interaction (Bagley et al., 2017; Birey et al., 2017; Xiang et al., 2017, 2019). Birey et al. (2017) pre-patterned and fused pallium and subpallium spheroids using patient-derived cells to identify GABAergic interneuronal migration deficits present in Timothy syndrome. Timothy syndrome—a multisystem neurodevelopmental disorder resulting from defective L-type calcium channels (LTCC) secondary to mutations in their encoding gene, *CACNA1C* ($Ca_V1.2$)—clinically includes features such as cognitive impairment and autism, cardiac defects, syndactyly, and immune deficiency (Splawski et al., 2004). Assessment of interneuronal migration in fused spheroids revealed increased neuronal saltation frequency

but decreased length and speed (Birey et al., 2017). Because Timothy syndrome results from gain-of-function mutation, adding the LTCC blocker nimodipine to patient-derived cells rescued the defective saltatory phenotype (Birey et al., 2017). Multi-organoid fusion thus offers a viable means by which to model interregional developmental dynamics as well as phenotypic defects associated with disease.

Genome Engineering. Novel techniques in genomic engineering—including zinc-finger nucleases, transcription activator-like effector nucleases (TALEN), and the CRISPR/Cas9 system (Chiba & Hockemeyer, 2015; Cong et al., 2015; Hockemeyer et al., 2009, 2011; Joung & Sander, 2013; Mali et al., 2013)—have enhanced our ability to manipulate the human cellular genome with unprecedented precision (Byrne et al., 2014; Komor et al., 2017). The considerable genetic heterogeneity underlying neurologic disease demands techniques by which to more efficiently define the effects of genetic variants on neurodevelopmental pathways and phenotypic change (McClellan & King, 2010). These new techniques have enhanced the utility of *in vitro* disease modeling by enabling pathogenic mutations to be introduced into wild-type stem cells or mutations to be corrected in patient-derived stem cells (Shi et al., 2017; Trujillo & Muotri, 2018). Despite concern of off-target effects and inefficiency (Fu et al., 2013; Lin et al., 2014; Mali et al., 2013; X. H. Zhang et al., 2015), whole-genome sequencing suggests these effects may be less prevalent in iPSCs than feared (C. Smith et al., 2014; Veres et al., 2014), and updated genome editing strategies—such as target selection and guide protein modification—have sought to minimize these effects (C. F. Cho et al., 2017; S. W. Cho et al., 2014; Cong et al., 2015; Hsu et al., 2013; Kleinstiver et al., 2016; Mali et al., 2013; P. Wang et al., 2017; X. H. Zhang et al., 2015). *In vitro* organoid

modeling of several of the diseases featured in this review has only been successful because of genomic manipulability, and further genomic innovation promises disease modeling with even greater complexity—sporadic diseases, for example (Hockemeyer & Jaenisch, 2016)—and portends enhanced clinical translatability (Schwank et al., 2013).

Transplantation, Vascularization, and Pharmaceutical Development. One of the primary factors limiting further development of organoid technology has been size restriction imposed by insufficient nutrient delivery to the organoid interior due to the absence of vascularization (Giandomenico & Lancaster, 2017; Yin et al., 2016). One solution is to appropriate *in vivo* nutrient distribution machinery (Daviaud et al., 2018; Mansour et al., 2018). Brain organoids engrafted into the retrosplenial cortex of immunodeficient mice successfully vascularized, yielding coincidently increasing graft surface area with minimal or absent apoptosis (Mansour et al., 2018). The engrafted organoids retained differentiability, underwent astrocytic and oligodendrocytic gliogenesis, and functionally integrated (Mansour et al., 2018). Another solution—separate differentiation of patient-derived iPSCs into cortical organoids and endothelial cells with subsequent co-culture—likewise exhibited organoid vascularization (Pham et al., 2018).

Much of the immediate clinical utility expected of the cortical organoid system is its pharmaceutical potential; the true efficacy of such a model, however, demands vasculature and a blood-brain barrier (BBB). To that end, a vascularized 3D model has been used for multi-disciplinary interrogation of neurotoxicity (Schwartz et al., 2015), and dynamic BBB spheroids have been employed to model drug transport and neurotoxicity (C. F. Cho et al., 2017; Nzou et al., 2018). Following co-culture of endothelial cells, astrocytes, and pericytes,

the spheroid exhibited an interior with preponderant astrocytes and an exterior surface of pericytes and endothelial cells (Bergmann et al., 2018). Critically, this external surface appeared dynamic, with regulated permeability, expression and activity of a P-glycoprotein efflux pump, and peptide receptor-mediated transcytosis (C. F. Cho et al., 2017). Successful development of these early BBB models suggests organoid technology—irrespective of BBB inclusion—may relieve dependence on imperfect animal models for pharmaceutical development and toxin interrogation and may well confer future opportunity for personalized therapeutics (Lou & Leung, 2018; Schwartz et al., 2015).

Future Challenges

Brain organoid technology has greatly enhanced neurodevelopmental disease research, but despite its potential, many challenges and technical limitations remain. Organoid protocols may exhibit significant batch variability and can give rise to different compositions of brain regions (Lancaster & Knoblich, 2014); however, improvements aiming to reduce organoid heterogeneity and improve reproducibility are being developed (Qian et al., 2016; Sloan et al., 2018; Trujillo & Muotri, 2018; Yoon et al., 2019). Organoids are also limited by their minimal or lack of relevant cellular subtypes (e.g., microglia and endothelial cells), which restricts their resemblance of *in vivo* development to only early gestation (Pasca et al., 2015; Qian et al., 2016). Later neocortical development requires vascularization for nutrient diffusion, the absence of which results in interior necrosis (Lancaster & Knoblich, 2014). As was previously mentioned, however, novel vascularization techniques are initial steps to resolving this challenge (Mansour et al., 2018; Pham et al., 2018). Moreover, because most differentiation protocols favor ectodermal fate, microglia, of mesodermal origination, are

usually absent. Improved methods of co-culturing or introducing these cells into brain organoids is necessary for accurate disease modeling. Lastly, to advance the translation of pathophysiologic findings from organoids to the human brain, it is imperative to understand if brain organoids create the neural circuitry observed in the human brain and address any ensuing ethical concerns.

REFERENCES

Abrahams, B. S., & Geschwind, D. H. (2008). Advances in autism genetics: On the threshold of a new neurobiology. *Nature Reviews Genetics*, *9*(5), 341–355. https://doi.org/10.1038/nrg2346

Abud, E. M., Ramirez, R. N., Martinez, E. S., Healy, L. M., Nguyen, C. H. H., Newman, S. A., Yeromin, A. V., Scarfone, V. M., Marsh, S. E., Fimbres, C., Caraway, C. A., Fote, G. M., Madany, A. M., Agrawal, A., Kayed, R., Gylys, K. H., Cahalan, M. D., Cummings, B. J., Antel, J. P., Mortazavi, A., Carson, M. J., Poon, W. W., & Blurton-Jones, M. (2017). iPSC-Derived Human Microglia-like Cells to Study Neurological Diseases. *Neuron*, *94*(2), 278-293.e9. https://doi.org/10.1016/j.neuron.2017.03.042

Allende, M. L., Cook, E. K., Larman, B. C., Nugent, A., Brady, J. M., Golebiowski, D., Sena-Esteves, M., Tifft, C. J., & Proia, R. L. (2018). Cerebral organoids derived from Sandhoff disease-induced pluripotent stem cells exhibit impaired neurodifferentiation. *Journal of Lipid Research*, *59*(3), 550–563. https://doi.org/10.1194/jlr.M081323

Ariani, F., Hayek, G., Rondinella, D., Artuso, R., Mencarelli, M. A., Spanhol-Rosseto, A., Pollazzon, M., Buoni, S., Spiga, O., Ricciardi, S., Meloni, I., Longo, I., Mari, F., Broccoli, V., Zappella, M., & Renieri, A. (2008). FOXG1 Is Responsible for the Congenital Variant of Rett Syndrome. *American Journal of Human Genetics*, *83*(1), 89–93. https://doi.org/10.1016/j.ajhg.2008.05.015

Bagley, J. A., Reumann, D., Bian, S., Lévi-Strauss, J., & Knoblich, J. A. (2017). Fused cerebral organoids model interactions between brain regions. *Nature Methods*, *14*(7), 743–751. https://doi.org/10.1038/nmeth.4304

Bale, J. F. (2009). Fetal Infections and Brain Development. *Clinics in Perinatology*, *36*(3), 639–653. https://doi.org/10.1016/j.clp.2009.06.005

Belmonte, M. K. (2004). Autism and Abnormal Development of Brain Connectivity. *Journal of Neuroscience*, *24*(42), 9228–9231. https://doi.org/10.1523/JNEUROSCI.3340-04.2004

Bergmann, S., Lawler, S. E., Qu, Y., Fadzen, C. M., Wolfe, J. M., Regan, M. S., Pentelute, B. L., Agar, N. Y. R., & Cho, C. F. (2018). Blood–brain-barrier organoids for investigating the permeability of CNS therapeutics. *Nature Protocols*, *13*(December). https://doi.org/10.1038/s41596-018-0066-x

Bershteyn, M., Nowakowski, T. J., Pollen, A. A., Di Lullo, E., Nene, A., Wynshaw-Boris, A., & Kriegstein, A. R. (2017). Human iPSC-Derived Cerebral Organoids Model Cellular Features of Lissencephaly and Reveal Prolonged Mitosis of Outer Radial Glia. *Cell Stem Cell*, *20*(4), 435-449.e4. https://doi.org/10.1016/j.stem.2016.12.007

Bilimoria, P. M., & Stevens, B. (2015). Microglia function during brain development: New insights from animal models. *Brain Research*, *1617*, 7–17. https://doi.org/10.1016/j.brainres.2014.11.032

Birey, F., Andersen, J., Makinson, C. D., Islam, S., Wei, W., Huber, N., Fan, H. C., Metzler, K. R. C., Panagiotakos, G., Thom, N., O'Rourke, N. A., Steinmetz, L. M., Bernstein, J. A., Hallmayer, J., Huguenard, J. R., & Pasca, S. P. (2017). Assembly of functionally integrated human forebrain spheroids. *Nature*, *545*(7652), 54–59. https://doi.org/10.1038/nature22330

Blair, J. D., Hockemeyer, D., & Bateup, H. S. (2018). Genetically engineered human cortical spheroid models of tuberous sclerosis. *Nature Medicine*, *24*(10), 1568–1578. https://doi.org/10.1038/s41591-018-0139-y

Blazejewski, S. M., Bennison, S. A., Smith, T. H., & Toyo-oka, K. (2018). Neurodevelopmental genetic diseases associated with microdeletions and microduplications of chromosome 17p13.3. *Frontiers in Genetics*, *9*(MAR), 1–18. https://doi.org/10.3389/fgene.2018.00080

Bruin, J. E., Gerstein, H. C., & Holloway, A. C. (2010). *Long-Term Consequences of Fetal and Neonatal Nicotine Exposure : A Critical Review*. *116*(2), 364–374. https://doi.org/10.1093/toxsci/kfq103

Butler, M. G., Dazouki, M. J., Zhou, X. P., Talebizadeh, Z., Brown, M., Takahashi, T. N., Miles, J. H., Wang, C. H., Stratton, R., Pilarski, R., & Eng, C. (2005). Subset of individuals with autism spectrum disorders and extreme macrocephaly associated with germline PTEN tumour suppressor gene mutations. *Journal of Medical Genetics*, *42*(4), 318–321. https://doi.org/10.1136/jmg.2004.024646

Byrne, S. M., Mali, P., & Church, G. M. (2014). Genome editing in human stem cells. In *Methods in Enzymology* (1st ed., Vol. 546, Issue C). Elsevier Inc. https://doi.org/10.1016/B978-0-12-801185-0.00006-4

Caiazzo, M., Teresa, M., Anno, D., Dvoretskova, E., Lazarevic, D., Taverna, S., Leo, D., Sotnikova, T. D., Menegon, A., Roncaglia, P., Colciago, G., Russo, G., Carninci, P., Pezzoli, G., Gainetdinov, R. R., Gustincich, S., Dityatev, A., & Broccoli, V. (2011). neurons from mouse and human fibroblasts. *Nature*, 10–15. https://doi.org/10.1038/nature10284

Camp, J. G., Badsha, F., Florio, M., Kanton, S., Gerber, T., Wilsch-Bräuninger, M., Lewitus, E., Sykes, A., Hevers, W., Lancaster, M., Knoblich, J. A., Lachmann, R., Pääbo, S., Huttner, W. B., & Treutlein, B. (2015). Human cerebral organoids recapitulate gene expression programs of fetal neocortex development. *Proceedings of the National Academy of Sciences*, *112*(51), 201520760. https://doi.org/10.1073/pnas.1520760112

Cederquist, G. Y., Asciolla, J. J., Tchieu, J., Walsh, R. M., Cornacchia, D., Resh, M. D., & Studer, L. (2019). Specification of positional identity in forebrain organoids. *Nature Biotechnology*, *37*(April). https://doi.org/10.1038/s41587-019-0085-3

Chambers, S. M., Fasano, C. A., Papapetrou, E. P., Tomishima, M., Sadelain, M., & Studer, L. (2009). Highly efficient neural conversion of human ES and iPS cells by dual inhibition of SMAD signaling. *Nature Biotechnology*, *27*(3), 275–280. https://doi.org/10.1038/nbt.1529

Chao, H. T., Chen, H., Samaco, R. C., Xue, M., Chahrour, M., Yoo, J., Neul, J. L., Gong, S., Lu, H. C., Heintz, N., Ekker, M., Rubenstein, J. L. R., Noebels, J. L., Rosenmund, C., & Zoghbi, H. Y. (2010). Dysfunction in GABA signalling mediates autism-like stereotypies and Rett syndrome phenotypes. *Nature*, *468*(7321), 263–269. https://doi.org/10.1038/nature09582

Cheng, T.-L., Wang, Z., Liao, Q., Zhu, Y., Zhou, W.-H., Xu, W., & Qiu, Z. (2014). MeCP2 suppresses nuclear microRNA processing and dendritic growth by regulating the DGCR8/Drosha complex. *Developmental Cell*, *28*(5), 547–560. https://doi.org/10.1016/j.devcel.2014.01.032

Chiba, K., & Hockemeyer, D. (2015). *Genome Editing in Human Pluripotent Stem Cells Using Site-Specific Nucleases* (pp. 267–280). Humana Press, New York, NY. https://doi.org/10.1007/978-1-4939-1862-1_15

Cho, C. F., Wolfe, J. M., Fadzen, C. M., Calligaris, D., Hornburg, K., Chiocca, E. A., Agar, N. Y. R., Pentelute, B. L., & Lawler, S. E. (2017). Blood-brain-barrier spheroids as an in vitro screening platform for brain-penetrating agents. *Nature Communications*, *8*, 1–14. https://doi.org/10.1038/ncomms15623

Cho, S. W., Kim, S., Kim, Y., Kweon, J., Kim, H. S., Bae, S., & Kim, J. S. (2014). Analysis of off-target effects of CRISPR/Cas-derived RNA-guided endonucleases and nickases. *Genome Research*. https://doi.org/10.1101/gr.162339.113

Colvert, E., Tick, B., McEwen, F., Stewart, C., Curran, S. R., Woodhouse, E., Gillan, N., Hallett, V., Lietz, S., Garnett, T., Ronald, A., Plomin, R., Rijsdijk, F., Happé, F., & Bolton, P. (2015). Heritability of autism spectrum disorder in a UK population-based twin sample. *JAMA Psychiatry*, *72*(5), 415–423. https://doi.org/10.1001/jamapsychiatry.2014.3028

Cong, L., Ran, F. A., Cox, D., Lin, S., Barretto, R., Habib, N., Hsu, P. D., Wu, X., Jiang, W., Marraffini, L. A., & Zhang, F. (2015). Rationally engineered Cas9 nucleases with improved specificity. *Science*, *339*(6121), 819–823.

https://doi.org/10.1126/science.aad5227

Crino, P. B., Nathanson, K. L., & Henske, E. P. (2006). The Tuberous Sclerosis Complex. *New England Journal of Medicine*, *355*(13), 1345–1356. https://doi.org/10.1056/NEJMra055323

Cugola, F. R., Fernandes, I. R., Russo, F. B., Freitas, B. C., Dias, J. L. M., Guimarães, K. P., Benazzato, C., Almeida, N., Pignatari, G. C., Romero, S., Polonio, C. M., Cunha, I., Freitas, C. L., Brandaõ, W. N., Rossato, C., Andrade, D. G., Faria, D. D. P., Garcez, A. T., Buchpigel, C. A., Braconi, C. T., Mendes, E., Sall, A. A., Zanotto, P. M. D. A., Peron, J. P. S., Muotri, A. R., & Beltrao-Braga, P. C. B. B. (2016). The Brazilian Zika virus strain causes birth defects in experimental models. *Nature*. https://doi.org/10.1038/nature18296

Daviaud, N., Friedel, R. H., & Zou, H. (2018). *Vascularization and Engraftment of Transplanted Human Cerebral Organoids in Mouse Cortex*. *5*(December), 1–18. https://doi.org/10.1523/ENEURO.0219-18.2018

Derecki, N. C., Cronk, J. C., Lu, Z., Xu, E., Abbott, S. B. G., Guyenet, P. G., & Kipnis, J. (2012). Wild-type microglia arrest pathology in a mouse model of Rett syndrome. *Nature*, *484*(7392), 105–109. https://doi.org/10.1038/nature10907

Eiraku, M., Takata, N., Ishibashi, H., Kawada, M., Sakakura, E., & Okuda, S. (2011). Self-organizing optic-cup morphogenesis in three-dimensional culture. *Nature*, *472*(7341), 51–56. https://doi.org/10.1038/nature09941

Fatemi, S. H., Reutiman, T. J., Folsom, T. D., Rooney, R. J., Patel, D. H., & Thuras, P. D. (2010). mRNA and protein levels for GABAAα4, α5, β1 and GABABR1 receptors are altered in brains from subjects with autism. *Journal of Autism and Developmental Disorders*, *40*(6), 743–750. https://doi.org/10.1007/s10803-009-0924-z

Filipello, F., Morini, R., Corradini, I., Zerbi, V., Canzi, A., Michalski, B., Erreni, M., Markicevic, M., Starvaggi-Cucuzza, C., Otero, K., Piccio, L., Cignarella, F., Perrucci, F., Tamborini, M., Genua, M., Rajendran, L., Menna, E., Vetrano, S., Fahnestock, M., Paolicelli, R. C., & Matteoli, M. (2018). The Microglial Innate Immune Receptor TREM2 Is Required for Synapse Elimination and Normal Brain Connectivity. *Immunity*, *48*(5), 979-991.e8. https://doi.org/10.1016/j.immuni.2018.04.016

Francis, F., Meyer, G., Fallet-Bianco, C., Moreno, S., Kappeler, C., Socorro, A. C., Tuy, F. P. D., Beldjord, C., & Chelly, J. (2006). Human disorders of cortical development: From past to present. *European Journal of Neuroscience*, *23*(4), 877–893. https://doi.org/10.1111/j.1460-9568.2006.04649.x

Fu, Y., Foden, J. A., Khayter, C., Maeder, M. L., Reyon, D., Joung, J. K., & Sander, J. D. (2013). High-frequency off-target mutagenesis induced by CRISPR-Cas nucleases in human cells. *Nature Biotechnology*, *31*(9), 822–826. https://doi.org/10.1038/nbt.2623

Gabriel, E., Wason, A., Ramani, A., Gooi, L. M., Keller, P., Pozniakovsky, A., Poser, I.,

Noack, F., Telugu, N. S., Calegari, F., Šarić, T., Hescheler, J., Hyman, A. A., Gottardo, M., Callaini, G., Alkuraya, F. S., & Gopalakrishnan, J. (2016). CPAP promotes timely cilium disassembly to maintain neural progenitor pool. *The EMBO Journal*, *35*(8), 803–819. https://doi.org/10.15252/embj.201593679

Geschwind, D. H. (2008). Autism: Many Genes, Common Pathways? *Cell*, *135*(3), 391–395. https://doi.org/10.1016/j.cell.2008.10.016

Geschwind, D. H., & Flint, J. (2015). *Psychiatric Disease*. *349*(6255), 719–724.

Giandomenico, S. L., & Lancaster, M. A. (2017). Probing human brain evolution and development in organoids. *Current Opinion in Cell Biology*, *44*, 36–43. https://doi.org/10.1016/j.ceb.2017.01.001

Ginhoux, F., Greter, M., Leboeuf, M., Nandi, S., See, P., Gokhan, S., Mehler, M. F., Conway, S. J., Ng, L. G., Stanley, E. R., Samokhvalov, I. M., & Merad, M. (2010). Microglia Derive from Primitive Macrophages. *Science*, *701*, 841–845. https://doi.org/10.1126/science.1194637

Griesi-Oliveira, K., Acab, A., Gupta, A. R., Sunaga, D. Y., Chailangkarn, T., Nicol, X., Nunez, Y., Walker, M. F., Murdoch, J. D., Sanders, S. J., Fernandez, T. V., Ji, W., Lifton, R. P., Vadasz, E., Dietrich, A., Pradhan, D., Song, H., Ming, G. L., Gu, X., Haddad, G., Marchetto, M. C. N., Spitzer, N., Passos-Bueno, M. R., State, M. W., & Muotri, A. R. (2015). Modeling non-syndromic autism and the impact of TRPC6 disruption in human neurons. *Molecular Psychiatry*, *20*(11), 1350–1365. https://doi.org/10.1038/mp.2014.141

Hockemeyer, D., & Jaenisch, R. (2016). Induced pluripotent stem cells meet genome editing. *Cell Stem Cell*, *18*(5), 573–586. https://doi.org/10.1016/j.stem.2016.04.013

Hockemeyer, D., Soldner, F., Beard, C., Gao, Q., Mitalipova, M., DeKelver, R. C., Katibah, G. E., Amora, R., Boydston, E. A., Zeitler, B., Meng, X., Miller, J. C., Zhang, L., Rebar, E. J., Gregory, P. D., Urnov, F. D., & Jaenisch, R. (2009). Efficient targeting of expressed and silent genes in human ESCs and iPSCs using zinc-finger nucleases. *Nature Biotechnology*, *27*(9), 851–857. https://doi.org/10.1038/nbt.1562

Hockemeyer, D., Wang, H., Kiani, S., Lai, C. S., Gao, Q., Cassady, J. P., Cost, G. J., Zhang, L., Santiago, Y., Miller, J. C., Zeitler, B., Cherone, J. M., Meng, X., Hinkley, S. J., Rebar, E. J., Gregory, P. D., Urnov, F. D., & Jaenisch, R. (2011). Genetic engineering of human pluripotent cells using TALE nucleases. *Nature Biotechnology*, *29*(8), 731–734. https://doi.org/10.1038/nbt.1927

Hsu, P. D., Scott, D. A., Weinstein, J. A., Ran, F. A., Konermann, S., Agarwala, V., Li, Y., Fine, E. J., Wu, X., Shalem, O., Cradick, T. J., Marraffini, L. A., Bao, G., & Zhang, F. (2013). DNA targeting specificity of RNA-guided Cas9 nucleases. *Nature Biotechnology*, *31*(9), 827–832. https://doi.org/10.1038/nbt.2647

Hutsler, J. J., & Zhang, H. (2010). Increased dendritic spine densities on cortical projection

neurons in autism spectrum disorders. *Brain Research*, *1309*, 83–94. https://doi.org/10.1016/j.brainres.2009.09.120

Icenogle, D. A., & Kaplan, A. M. (1981). A Review of Congenital Neurologic Malformations. *Clinical Pediatrics*, *20*(9), 565–576. https://doi.org/10.1177/000992288102000903

Iefremova, V., Manikakis, G., Krefft, O., Jabali, A., Weynans, K., Wilkens, R., Marsoner, F., Brändl, B., Müller, F. J., Koch, P., & Ladewig, J. (2017). An Organoid-Based Model of Cortical Development Identifies Non-Cell-Autonomous Defects in Wnt Signaling Contributing to Miller-Dieker Syndrome. *Cell Reports*, *19*(1), 50–59. https://doi.org/10.1016/j.celrep.2017.03.047

Ip, J. P. K., Mellios, N., & Sur, M. (2018). Rett syndrome: Insights into genetic, molecular and circuit mechanisms. *Nature Reviews Neuroscience*, *19*(6), 368–382. https://doi.org/10.1038/s41583-018-0006-3

Jacob-Hirsch, J., Eyal, E., Knisbacher, B. A., Roth, J., Cesarkas, K., Dor, C., Farage-Barhom, S., Kunik, V., Simon, A. J., Gal, M., Yalon, M., Moshitch-Moshkovitz, S., Tearle, R., Constantini, S., Levanon, E. Y., Amariglio, N., & Rechavi, G. (2018). Whole-genome sequencing reveals principles of brain retrotransposition in neurodevelopmental disorders. *Cell Research*, *28*(2), 187–203. https://doi.org/10.1038/cr.2018.8

Jacob, F. D., Ramaswamy, V., Andersen, J., & Bolduc, F. V. (2009). Atypical Rett syndrome with selective FOXG1 deletion detected by comparative genomic hybridization: Case report and review of literature. *European Journal of Human Genetics*, *17*(12), 1577–1581. https://doi.org/10.1038/ejhg.2009.95

Joung, J. K., & Sander, J. D. (2013). TALENs: A widely applicable technology for targeted genome editing. *Nature Reviews Molecular Cell Biology*, *14*(1), 49–55. https://doi.org/10.1038/nrm3486

Karzbrun, E., Kshirsagar, A., Cohen, S. R., Hanna, J. H., & Reiner, O. (2018). Human brain organoids on a chip reveal the physics of folding. *Nature Physics*, *14*(5), 515–522. https://doi.org/10.1038/s41567-018-0046-7

Kirwan, P., Turner-Bridger, B., Peter, M., Momoh, A., Arambepola, D., Robinson, H. P. C., & Livesey, F. J. (2015). Development and function of human cerebral cortex neural networks from pluripotent stem cells in vitro. *Development*, *142*(18), 3178–3187. https://doi.org/10.1242/dev.123851

Kleinstiver, B. P., Pattanayak, V., Prew, M. S., Tsai, S. Q., Nguyen, N. T., Zheng, Z., & Joung, J. K. (2016). High-fidelity CRISPR-Cas9 nucleases with no detectable genome-wide off-target effects. *Nature*, *529*(7587), 490–495. https://doi.org/10.1038/nature16526

Komor, A. C., Badran, A. H., & Liu, D. R. (2017). CRISPR-Based Technologies for the Manipulation of Eukaryotic Genomes. *Cell*, *168*(1–2), 20–36. https://doi.org/10.1016/j.cell.2016.10.044

Koyama, R., & Ikegaya, Y. (2015). Microglia in the pathogenesis of autism spectrum disorders. *Neuroscience Research*, *100*, 1–5.https://doi.org/10.1016/j.neures.2015.06.005

Lancaster, M. A., & Knoblich, J. A. (2014). Organogenesis in a dish: Modeling development and disease using organoid technologies. *Science*, *345*(6194), 1247125–1247125. https://doi.org/10.1126/science.1247125

Lancaster, M. A., Renner, M., Martin, C. A., Wenzel, D., Bicknell, L. S., Hurles, M. E., Homfray, T., Penninger, J. M., Jackson, A. P., & Knoblich, J. A. (2013). Cerebral organoids model human brain development and microcephaly. *Nature*, *501*(7467), 373–379. https://doi.org/10.1038/nature12517

Lebel, C., Roussotte, F., & Sowell, E. R. (2011). Imaging the impact of prenatal alcohol exposure on the structure of the developing human brain. *Neuropsychology Review*, *21*(2), 102–118. https://doi.org/10.1007/s11065-011-9163-0

Li, R., Sun, L., Fang, A., Li, P., Wu, Q., & Wang, X. (2017). Recapitulating cortical development with organoid culture in vitro and modeling abnormal spindle-like (ASPM related primary) microcephaly disease. *Protein and Cell*, *8*(11), 823–833.

Li, Y., Muffat, J., Omer, A., Bosch, I., Lancaster, M. A., Sur, M., Gehrke, L., Knoblich, J. A., & Jaenisch, R. (2017). Induction of Expansion and Folding in Human Cerebral Organoids. *Cell Stem Cell*, *20*(3), 385-396.e3. https://doi.org/10.1016/j.stem.2016.11.017

Lin, Y., Cradick, T. J., Brown, M. T., Deshmukh, H., Ranjan, P., Sarode, N., Wile, B. M., Vertino, P. M., Stewart, F. J., & Bao, G. (2014). CRISPR/Cas9 systems have off-target activity with insertions or deletions between target DNA and guide RNA sequences. *Nucleic Acids Research*, *42*(11), 7473–7485. https://doi.org/10.1093/nar/gku402

Lou, Y. R., & Leung, A. W. (2018). Next generation organoids for biomedical research and applications. *Biotechnology Advances*, *36*(1), 132–149.

Lullo, E. Di, & Kriegstein, A. R. (2017). The use of brain organoids to. *Nature Publishing Group*, *18*(10), 573–584. https://doi.org/10.1038/nrn.2017.107

Luo, C., Lancaster, M. A., Castanon, R., Nery, J. R., Knoblich, J. A., & Ecker, J. R. (2016). Cerebral Organoids Recapitulate Epigenomic Signatures of the Human Fetal Brain. *Cell Reports*, *17*(12), 3369–3384. https://doi.org/10.1016/j.celrep.2016.12.001

Majewski, F., & Goecke, T. (1982). Studies of microcephalic primordial dwarfism I: Approach to a delineation of the Seckel syndrome. *American Journal of Medical Genetics*, *12*(1), 7–21. https://doi.org/10.1002/ajmg.1320120103

Mali, P., Aach, J., Stranges, P. B., Esvelt, K. M., Moosburner, M., Kosuri, S., Yang, L., & Church, G. M. (2013). CAS9 transcriptional activators for target specificity screening and paired nickases for cooperative genome engineering. *Nature Biotechnology*, *31*(9), 833–838. https://doi.org/10.1038/nbt.2675

Mansour, A. A., Gonçalves, J. T., Bloyd, C. W., Li, H., Fernandes, S., Quang, D., Johnston, S., Parylak, S. L., Jin, X., & Gage, F. H. (2018). An in vivo model of functional and vascularized human brain organoids. *Nature Biotechnology*, *36*(5), 432–441. https://doi.org/10.1038/nbt.4127

Marakhonov, A. V., Konovalov, F. A., Makaov, A. K., Vasilyeva, T. A., Kadyshev, V. V., Galkina, V. A., Dadali, E. L., Kutsev, S. I., & Zinchenko, R. A. (2018). Primary microcephaly case from the Karachay-Cherkess Republic poses an additional support for microcephaly and Seckel syndrome spectrum disorders. *BMC Medical Genomics*, *11*(Suppl 1). https://doi.org/10.1186/s12920-018-0326-1

Marchetto, M. C., Belinson, H., Tian, Y., Freitas, B. C., Fu, C., Vadodaria, K. C., Beltrao-Braga, P. C., Trujillo, C. A., Mendes, A. P. D., Padmanabhan, K., Nunez, Y., Ou, J., Ghosh, H., Wright, R., Brennand, K. J., Pierce, K., Eichenfield, L., Pramparo, T., Eyler, L. T., Barnes, C. C., Courchesne, E., Geschwind, D. H., Gage, F. H., Wynshaw-Boris, A., & Muotri, A. R. (2017). Altered proliferation and networks in neural cells derived from idiopathic autistic individuals. *Molecular Psychiatry*, *22*(6), 820–835. https://doi.org/10.1038/mp.2016.95

Marchetto, M. C. N., Carromeu, C., Acab, A., Yu, D., Yeo, G. W., Mu, Y., Chen, G., Gage, F. H., & Muotri, A. R. (2010). A model for neural development and treatment of rett syndrome using human induced pluripotent stem cells. *Cell*, *143*(4), 527–539. https://doi.org/10.1016/j.cell.2010.10.016

Mariani, J., Coppola, G., Zhang, P., Abyzov, A., Provini, L., Tomasini, L., Amenduni, M., Szekely, A., Palejev, D., Wilson, M., Gerstein, M., Grigorenko, E. L., Chawarska, K., Pelphrey, K. A., Howe, J. R., & Vaccarino, F. M. (2015). FOXG1-Dependent Dysregulation of GABA/Glutamate Neuron Differentiation in Autism Spectrum Disorders. *Cell*, *162*(2), 375–390. https://doi.org/10.1016/j.cell.2015.06.034

Martin, K. R., Zhou, W., Bowman, M. J., Shih, J., Au, K. S., Dittenhafer-Reed, K. E., Sisson, K. A., Koeman, J., Weisenberger, D. J., Cottingham, S. L., Deroos, S. T., Devinsky, O., Winn, M. E., Cherniack, A. D., Shen, H., Northrup, H., Krueger, D. A., & Mackeigan, J. P. (2017). The genomic landscape of tuberous sclerosis complex. *Nature Communications*, *8*(May), 1–13. https://doi.org/10.1038/ncomms15816

McClellan, J., & King, M. C. (2010). Genetic heterogeneity in human disease. *Cell*, *141*(2), 210–217. https://doi.org/10.1016/j.cell.2010.03.032

McKenzie, A. T., Wang, M., Hauberg, M. E., Fullard, J. F., Kozlenkov, A., Keenan, A., Hurd, Y. L., Dracheva, S., Casaccia, P., Roussos, P., & Zhang, B. (2018). Synaptic Pruning by Microglia Is Necessary for Normal Brain Development. *Scientific Reports*, *8*(1), 8868.

Mellios, N., Feldman, D. A., Sheridan, S. D., Ip, J. P. K., Kwok, S., Amoah, S. K., Rosen, B., Rodriguez, B. A., Crawford, B., Swaminathan, R., Chou, S., Li, Y., Ziats, M., Ernst, C., Jaenisch, R., Haggarty, S. J., & Sur, M. (2018). MeCP2-regulated miRNAs control early human neurogenesis through differential effects on ERK and AKT signaling. *Molecular Psychiatry*, *23*(4), 1051–1065. https://doi.org/10.1038/mp.2017.86

Mitter, D., Pringsheim, M., Kaulisch, M., Plümacher, K. S., Schröder, S., Warthemann, R., Abou Jamra, R., Baethmann, M., Bast, T., Büttel, H. M., Cohen, J. S., Conover, E., Courage, C., Eger, A., Fatemi, A., Grebe, T. A., Hauser, N. S., Heinritz, W., Helbig, K. L., Heruth, M., Huhle, D., Höft, K., Karch, S., Kluger, G., Korenke, G. C., Lemke, J. R., Lutz, R. E., Patzer, S., Prehl, I., Hoertnagel, K., Ramsey, K., Rating, T., Rieß, A., Rohena, L., Schimmel, M., Westman, R., Zech, F. M., Zoll, B., Malzahn, D., Zirn, B., & Brockmann, K. (2018). FOXG1 syndrome: Genotype-phenotype association in 83 patients with FOXG1 variants. *Genetics in Medicine*, *20*(1), 98–108. https://doi.org/10.1038/gim.2017.75

Monteiro Abreu, C., Gama, L., Krasemann, S., Chesnut, M., Odwin-Dacosta, S., Hogberg, H., Hartung, T., & Pamies, D. (2018). Microglia Increase Inflammatory Responses in iPSC-dervied Human BrainSpheres. *Frontiers in Microbiology*, *9*(December), 2766.

Morgan, J. T., Chana, G., Pardo, C. A., Achim, C., Semendeferi, K., Buckwalter, J., Courchesne, E., & Everall, I. P. (2010). Microglial activation and increased microglial density observed in the dorsolateral prefrontal cortex in autism. *Biological Psychiatry*, *68*(4), 368–376. https://doi.org/10.1016/j.biopsych.2010.05.024

Morris-Rosendahl, D. J., & Kaindl, A. M. (2015). What next-generation sequencing (NGS) technology has enabled us to learn about primary autosomal recessive microcephaly (MCPH). *Molecular and Cellular Probes*, *29*(5), 271–281. https://doi.org/10.1016/j.mcp.2015.05.015

Muffat, J., Li, Y., Yuan, B., Mitalipova, M., Omer, A., Corcoran, S., Bakiasi, G., Tsai, L. H., Aubourg, P., Ransohoff, R. M., & Jaenisch, R. (2016). Efficient derivation of microglia-like cells from human pluripotent stem cells. *Nature Medicine*, *22*(11), 1358–1367. https://doi.org/10.1038/nm.4189

Muotri, A. R. (2016). The human model: Changing focus on autism research. *Biological Psychiatry*, *79*(8), 642–649. https://doi.org/10.1016/j.biopsych.2015.03.012

Nakano, T., Ando, S., Takata, N., Kawada, M., Muguruma, K., Sekiguchi, K., Saito, K., Yonemura, S., Eiraku, M., & Sasai, Y. (2012). Article Self-Formation of Optic Cups and Storable Stratified Neural Retina from Human ESCs. *STEM*, *10*(6), 771–785. https://doi.org/10.1016/j.stem.2012.05.009

Neul, J. L., Kaufmann, W. E., Glaze, D. G., Christodoulou, J., Clarke, A. J., Bahi-Buisson, N., Leonard, H., Bailey, M. E. S., Schanen, N. C., Zappella, M., Renieri, A., Huppke, P., & Percy, A. K. (2010). Rett syndrome: Revised diagnostic criteria and nomenclature. *Annals of Neurology*, *68*(6), 944–950. https://doi.org/10.1002/ana.22124

Nzou, G., Wicks, R. T., Wicks, E. E., Seale, S. A., Sane, C. H., Chen, A., Murphy, S. V., Jackson, J. D., & Atala, A. J. (2018). Human cortex spheroid with a functional blood brain barrier for high-throughput neurotoxicity screening and disease modeling. *Scientific Reports*, *8*(1), 1–10. https://doi.org/10.1038/s41598-018-25603-5

Oliveira, W. K. De, Cortez-escalante, J., Tenório, W., Holanda, G., & Madeleine, G. (2016).

Increase in Reported Prevalence of Microcephaly in Infants Born to Women Living in Areas with Confirmed Zika Virus Transmission During the First Trimester of Pregnancy — Brazil , 2015. *65*(9), 242–247.

Ormel, P. R., Vieira de Sá, R., van Bodegraven, E. J., Karst, H., Harschnitz, O., Sneeboer, M. A. M., Johansen, L. E., van Dijk, R. E., Scheefhals, N., Berdenis van Berlekom, A., Ribes Martínez, E., Kling, S., MacGillavry, H. D., van den Berg, L. H., Kahn, R. S., Hol, E. M., de Witte, L. D., & Pasterkamp, R. J. (2018). Microglia innately develop within cerebral organoids. *Nature Communications*, *9*(1). https://doi.org/10.1038/s41467-018-06684-2

Pang, Z. P., Yang, N., Vierbuchen, T., Ostermeier, A., Fuentes, D. R., Yang, T. Q., Citri, A., Sebastiano, V., Marro, S., Sudhof, T. C., & Wernig, M. (2011). Induction of human neuronal cells by defined transcription factors. *Nature*, *476*, 220-223.

Pardo, C. A., Vargas, D. L., & Zimmerman, A. W. (2005). Immunity, neuroglia and neuroinflammation in autism. *International Review of Psychiatry*, *17*(6), 485–495. https://doi.org/10.1080/02646830500381930

Pasca, A. M., Sloan, S. A., Clarke, L. E., Tian, Y., Makinson, C. D., Huber, N., Kim, C. H., Park, J. Y., O'Rourke, N. A., Nguyen, K. D., Smith, S. J., Huguenard, J. R., Geschwind, D. H., Barres, B. A., & Pasca, S. P. (2015). Functional cortical neurons and astrocytes from human pluripotent stem cells in 3D culture. *Nature Methods*, *12*(7), 671–678. https://doi.org/10.1038/nmeth.3415

Paşca, S. P., Panagiotakos, G., & Dolmetsch, R. E. (2014). Generating Human Neurons In Vitro and Using Them to Understand Neuropsychiatric Disease. *Annual Review of Neuroscience*, *37*(1), 479–501. https://doi.org/10.1146/annurev-neuro-062012-170328

Penzes, P., Cahill, M. E., Jones, K. A., Vanleeuwen, J. E., & Woolfrey, K. M. (2011). Dendritic spine pathology in neuropsychiatric disorders. *Nature Neuroscience*, *14*(3), 285–293. https://doi.org/10.1038/nn.2741

Peron, A., & Northrup, H. (2018). Tuberous sclerosis complex. *American Journal of Medical Genetics Part C: Seminars in Medical Genetics*, *178*(3), 274–277. https://doi.org/10.1002/ajmg.c.31657

Pham, M. T., Pollock, K. M., Rose, M. D., Cary, W. A., Stewart, H. R., Zhou, P., Nolta, J. A., & Waldau, B. (2018). Generation of human vascularized brain organoids. *NeuroReport*, *29*(7), 588–593. https://doi.org/10.1097/WNR.0000000000001014

Powers, W. R., Goebel, T., Drozdov, N. I., Elias, S. A., Fedoseeva, S., Eliseev, E., Culturali, B., Webb, S., Cring, D., Sorg, M., Romanenko, F., Lozhkin, A. V, Waters, M. R., Dikova, M., & Re-, A. (2004). Foxg1 Suppresses Early Cortical. *Science (New York, N.Y.)*, *303*(January), 56–59. https://doi.org/10.1126/science.1090674

Qian, X., Nguyen, H. N., Song, M. M., Hadiono, C., Ogden, S. C., Hammack, C., Yao, B., Hamersky, G. R., Jacob, F., Zhong, C., Yoon, K. J., Jeang, W., Lin, L., Li, Y., Thakor,

J., Berg, D. A., Zhang, C., Kang, E., Chickering, M., Nauen, D., Ho, C. Y., Wen, Z., Christian, K. M., Shi, P. Y., Maher, B. J., Wu, H., Jin, P., Tang, H., Song, H., & Ming, G. L. (2016). Brain-Region-Specific Organoids Using Mini-bioreactors for Modeling ZIKV Exposure. *Cell*, *165*(5), 1238–1254. https://doi.org/10.1016/j.cell.2016.04.032

Quesnel-Vallières, M., Weatheritt, R. J., Cordes, S. P., & Blencowe, B. J. (2018). Autism spectrum disorder: insights into convergent mechanisms from transcriptomics. *Nature Reviews Genetics*. https://doi.org/10.1038/s41576-018-0066-2

Ramaswami, G., & Geschwind, D. H. (2018). Genetics of autism spectrum disorder. In *Handbook of Clinical Neurology* (1st ed., Vol. 147). Elsevier B.V. https://doi.org/10.1016/B978-0-444-63233-3.00021-X

Renner, M., Lancaster, M. A., Bian, S., Choi, H., Ku, T., Peer, A., Chung, K., & Knoblich, J. A. (2017). Self-organized developmental patterning and differentiation in cerebral organoids. *The EMBO Journal*, *36*(10), 1316–1329.

Riley, E. P., Infante, M. A., & Warren, K. R. (2011). Fetal Alcohol Spectrum Disorders : An Overview. *Neuropsychology Review*, *21*, 73–80. https://doi.org/10.1007/s11065-011-9166-x

Rubenstein, J. L. R. (2010). Three hypotheses for developmental defects that may underlie some forms of autism spectrum disorder. *Current Opinion in Neurology*, *23*(2), 118–123. https://doi.org/10.1097/WCO.0b013e328336eb13

Sandhoff, K. (1969). /3-N-acetylhexosaminidases and their separation by isoelectric focusing. *FEBS Letters*, *4*(4), 351–354.

Sandhoff, K., Harzer, K., Wässle, W., & Jatzkewitz, H. (1971). Enzyme Alterations and Lipid Storage in Three Variants of Tay-Sachs Disease. *Journal of Neurochemistry*, *18*(12), 2469–2489. https://doi.org/10.1111/j.1471-4159.1971.tb00204.x

Schafer, D. P., Heller, C. T., Gunner, G., Heller, M., Gordon, C., Hammond, T., Wolf, Y., Jung, S., & Stevens, B. (2016). Microglia contribute to circuit defects in Mecp2 null mice independent of microglia-specific loss of Mecp2 expression. *ELife*, *5*(2016JULY), 1–19. https://doi.org/10.7554/eLife.15224

Schafer, D. P., Lehrman, E. K., Kautzman, A. G., Koyama, R., Mardinly, A. R., Yamasaki, R., Ransohoff, R. M., Greenberg, M. E., Barres, B. A., & Stevens, B. (2012). Microglia Sculpt Postnatal Neural Circuits in an Activity and Complement-Dependent Manner. *Neuron*, *74*(4), 691–705. https://doi.org/10.1016/j.neuron.2012.03.026

Schüle, B., Armstrong, D. D., Vogel, H., Oviedo, A., & Francke, U. (2008). Severe congenital encephalopathy caused by MECP2 null mutations in males: Central hypoxia and reduced neuronal dendritic structure. *Clinical Genetics*, *74*(2), 116–126. https://doi.org/10.1111/j.1399-0004.2008.01005.x

Schwank, G., Koo, B. K., Sasselli, V., Dekkers, J. F., Heo, I., Demircan, T., Sasaki, N.,

Boymans, S., Cuppen, E., Van Der Ent, C. K., Nieuwenhuis, E. E. S., Beekman, J. M., & Clevers, H. (2013). Functional repair of CFTR by CRISPR/Cas9 in intestinal stem cell organoids of cystic fibrosis patients. *Cell Stem Cell*, *13*(6), 653–658. https://doi.org/10.1016/j.stem.2013.11.002

Schwartz, M. P., Hou, Z., Propson, N. E., Zhang, J., Engstrom, C. J., Costa, V. S., Jiang, P., Nguyen, B. K., Bolin, J. M., Daly, W., Wang, Y., Stewart, R., Page, C. D., Murphy, W. L., & Thomson, J. A. (2015). Human pluripotent stem cell-derived neural constructs for predicting neural toxicity. *Proceedings of the National Academy of Sciences*, *112*(40), 12516–12521. https://doi.org/10.1073/pnas.1516645112

Sebastiani, G., Borr, C., Casanova, M. A., Tutusaus, M. P., & Ferrero, S. (2018). *The Effects of Alcohol and Drugs of Abuse on Maternal Nutritional Profile during Pregnancy*. 1–17.

Sheen, V. L., Ferland, R. J., Neal, J., Harney, M., Hill, R. S., Banham, A., Brown, P., Chenn, A., Corbo, J., Hecht, J., Folkerth, R., & Walsh, C. A. (2006). Neocortical neuronal arrangement in Miller Dieker syndrome. *Acta Neuropathologica*, *111*(5), 489–496. https://doi.org/10.1007/s00401-005-0010-3

Shi, Y., Inoue, H., Wu, J. C., & Yamanaka, S. (2017). Induced pluripotent stem cell technology: A decade of progress. *Nature Reviews Drug Discovery*, *16*(2), 115–130. https://doi.org/10.1038/nrd.2016.245

Sloan, S. A., Andersen, J., Paşca, A. M., Birey, F., & Paşca, S. P. (2018). Generation and assembly of human brain region–specific three-dimensional cultures. *Nature Protocols*, *13*(9), 2062–2085. https://doi.org/10.1038/s41596-018-0032-7

Smith, A. M., Gibbons, H. M., Lill, C., Faull, R. L. M., & Dragunow, M. (1953). SHAME of the slums. *American Journal of Public Health*, *43*, 621–623. https://doi.org/10.1007/978-1-62703-520-0

Smith, C., Gore, A., Yan, W., Abalde-Atristain, L., Li, Z., He, C., Wang, Y., Brodsky, R. A., Zhang, K., Cheng, L., & Ye, Z. (2014). Whole-genome sequencing analysis reveals high specificity of CRISPR/Cas9 and TALEN-based genome editing in human iPSCs. *Cell Stem Cell*, *15*(1), 12–13. https://doi.org/10.1016/j.stem.2014.06.011

Sominsky, L., De Luca, S., & Spencer, S. J. (2018). Microglia: Key players in neurodevelopment and neuronal plasticity. *International Journal of Biochemistry and Cell Biology*, *94*(September 2017), 56–60. https://doi.org/10.1016/j.biocel.2017.11.012

Spence, S. J. (2004). The genetics of autism. *Seminars in Pediatric Neurology*, *11*(3), 196–204. https://doi.org/10.1016/j.spen.2004.07.003

Splawski, I., Timothy, K. W., Sharpe, L. M., Decher, N., Kumar, P., Bloise, R., Napolitano, C., Schwartz, P. J., Joseph, R. M., Condouris, K., Tager-Flusberg, H., Priori, S. G., & Sanguinetti, M. C. (2004). Ca V 1.2 Calcium Channel Dysfunction Causes a Multisystem Disorder Including Arrhythmia and Autism ultimate signaling molecule for organisms ranging from prokaryotes to humans. In higher organisms, Ca2 mediates

processes as diverse as synaptic transmiss. *Cell*, *119*, 19–31.

Stevens, B., Allen, N. J., Vazquez, L. E., Howell, G. R., Christopherson, K. S., Nouri, N., Micheva, K. D., Mehalow, A. K., Huberman, A. D., Stafford, B., Sher, A., Litke, A. M. M., Lambris, J. D., Smith, S. J., John, S. W. M., & Barres, B. A. (2007). The Classical Complement Cascade Mediates CNS Synapse Elimination. *Cell*, *131*(6), 1164–1178. https://doi.org/10.1016/j.cell.2007.10.036

Suzuki, K., Sugihara, G., Ouchi, Y., Nakamura, K., Futatsubashi, M., Takebayashi, K., Yoshihara, Y., Omata, K., Matsumoto, K., Tsuchiya, K. J., Iwata, Y., Tsujii, M., Sugiyama, T., & Mori, N. (2013). Microglial activation in young adults with autism spectrum disorder. *Archives of General Psychiatry*, *70*(1), 49–58. https://doi.org/10.1001/jamapsychiatry.2013.272

Takahashi, K., Tanabe, K., Ohnuki, M., Narita, M., Ichisaka, T., Tomoda, K., & Yamanaka, S. (2007). Induction of Pluripotent Stem Cells from Adult Human Fibroblasts by Defined Factors. *Cell*, *131*(5), 861–872. https://doi.org/10.1016/j.cell.2007.11.019

Tang, X., Kim, J., Zhou, L., Wengert, E., Zhang, L., Wu, Z., Carromeu, C., Muotri, A. R., Marchetto, M. C. N., Gage, F. H., & Chen, G. (2016). KCC2 rescues functional deficits in human neurons derived from patients with Rett syndrome. *Proceedings of the National Academy of Sciences*, *113*(3), 751–756.

Tavasoli, A. R., Parvaneh, N., Ashrafi, M. R., Rezaei, Z., & Zschocke, J. (2018). *Clinical presentation and outcome in infantile Sandhoff disease : a case series of 25 patients from Iranian neurometabolic bioregistry with five novel mutations*. 1–8.

Tetreault, N. A., Hakeem, A. Y., Jiang, S., Williams, B. A., Allman, E., Wold, B. J., & Allman, J. M. (2012). Microglia in the cerebral cortex in autism. *Journal of Autism and Developmental Disorders*, *42*(12), 2569–2584. https://doi.org/10.1007/s10803-012-1513-0

Toro, R., Konyukh, M., Delorme, R., Leblond, C., Chaste, P., Fauchereau, F., Coleman, M., Leboyer, M., Gillberg, C., & Bourgeron, T. (2010). Key role for gene dosage and synaptic homeostasis in autism spectrum disorders. *Trends in Genetics*, *26*(8), 363–372. https://doi.org/10.1016/j.tig.2010.05.007

Trujillo, C. A., Gao, R., Negraes, P. D., Chaim, I. A., Domissy, A., Vandenberghe, M., Devor, A., Yeo, G. W., Voytek, B., & Muotri, A. R. (2018). Nested oscillatory dynamics in cortical organoids model early human brain network development. *BioRxiv*, 358622. https://doi.org/10.1101/358622

Trujillo, C. A., & Muotri, A. R. (2018). Brain Organoids and the Study of Neurodevelopment. *Trends in Molecular Medicine*, *24*(12), 982–990. https://doi.org/10.1016/j.molmed.2018.09.005

Veres, A., Gosis, B. S., Ding, Q., Collins, R., Ragavendran, A., Brand, H., Erdin, S., Talkowski, M. E., & Musunuru, K. (2014). Low incidence of Off-target mutations in

individual CRISPR-Cas9 and TALEN targeted human stem cell clones detected by whole-genome sequencing. *Cell Stem Cell*, *15*(1), 27–30. https://doi.org/10.1016/j.stem.2014.04.020

Wang, P., Mokhtari, R., Pedrosa, E., Kirschenbaum, M., Bayrak, C., Zheng, D., & Lachman, H. M. (2017). CRISPR/Cas9-mediated heterozygous knockout of the autism gene CHD8 and characterization of its transcriptional networks in cerebral organoids derived from iPS cells. *Molecular Autism*, *8*(1), 1–17. https://doi.org/10.1186/s13229-017-0124-1

Wang, Y., Wang, L., Zhu, Y., & Qin, J. (2018). Human brain organoid-on-a-chip to model prenatal nicotine exposure. *Lab on a Chip*, *18*(6), 851–860. https://doi.org/10.1039/c7lc01084b

Woods, C. G., Bond, J., & Enard, W. (2005). Autosomal Recessive Primary Microcephaly (MCPH): A Review of Clinical, Molecular, and Evolutionary Findings. *The American Journal of Human Genetics*, *76*(5), 717–728. https://doi.org/10.1086/429930

Wynshaw-Boris, A. (2007). Lissencephaly and LIS1: Insights into the molecular mechanisms of neuronal migration and development. *Clinical Genetics*, *72*(4), 296–304. https://doi.org/10.1111/j.1399-0004.2007.00888.x

Xiang, Y., Tanaka, Y., Cakir, B., Lee, S., Weissman, S. M., Park, I., Xiang, Y., Tanaka, Y., Cakir, B., Patterson, B., Kim, K., Sun, P., & Kang, Y. (2019). Short Article hESC-Derived Thalamic Organoids Form Reciprocal Projections When Fused with Cortical Organoids Short Article hESC-Derived Thalamic Organoids Form Reciprocal Projections When Fused with Cortical Organoids. *Stem Cell*, *24*(3), 487-497.e7. https://doi.org/10.1016/j.stem.2018.12.015

Xiang, Y., Tanaka, Y., Patterson, B., Kang, Y. J., Govindaiah, G., Roselaar, N., Cakir, B., Kim, K. Y., Lombroso, A. P., Hwang, S. M., Zhong, M., Stanley, E. G., Elefanty, A. G., Naegele, J. R., Lee, S. H., Weissman, S. M., & Park, I. H. (2017). Fusion of Regionally Specified hPSC-Derived Organoids Models Human Brain Development and Interneuron Migration. *Cell Stem Cell*, *21*(3), 383-398.e7. https://doi.org/10.1016/j.stem.2017.07.007

Yin, X., Mead, B. E., Safaee, H., Langer, R., Karp, J. M., & Levy, O. (2016). Engineering Stem Cell Organoids. *Cell Stem Cell*, *18*(1), 25–38. https://doi.org/10.1016/j.stem.2015.12.005

Yingling, J., Youn, Y. H., Darling, D., Toyo-oka, K., Pramparo, T., Hirotsune, S., & Wynshaw-Boris, A. (2008). Neuroepithelial Stem Cell Proliferation Requires LIS1 for Precise Spindle Orientation and Symmetric Division. *Cell*, *132*(3), 474–486. https://doi.org/10.1016/j.cell.2008.01.026

Yoon, S., Elahi, L. S., Pașca, A. M., Marton, R. M., Gordon, A., Revah, O., Miura, Y., Walczak, E. M., Holdgate, G. M., Fan, H. C., Huguenard, J. R., Geschwind, D. H., & Pașca, S. P. (2019). Reliability of human cortical organoid generation. *Nature Methods*, *16*(January). https://doi.org/10.1038/s41592-018-0255-0

Zhang, X. H., Tee, L. Y., Wang, X. G., Huang, Q. S., & Yang, S. H. (2015). Off-target effects in CRISPR/Cas9-mediated genome engineering. *Molecular Therapy - Nucleic Acids*, *4*(11), e264. https://doi.org/10.1038/mtna.2015.37

Zhang, Y., Pak, C., Han, Y., Ahlenius, H., Zhang, Z., Chanda, S., Marro, S., Patzke, C., Acuna, C., Covy, J., Xu, W., Yang, N., Danko, T., Chen, L., Wernig, M., & Su, T. C. (2013). *NeuroResource Rapid Single-Step Induction of Functional Neurons from Human Pluripotent Stem Cells*. 785–798. https://doi.org/10.1016/j.neuron.2013.05.029

Zhu, Y., Wang, L., Yin, F., Yu, Y., & Wang, Y. (2017). *Integrative Biology Probing impaired neurogenesis in human brain organoids exposed to alcohol †*. 968–978. https://doi.org/10.1039/C7IB00105C

Acknowledgements

Appendix 1, in full, is a reprint of the material as it appears in the following manuscript, published in *Physiology*: Adams, J. W., Cugola, F. R., & Muotri, A. R. (2019). **Brain Organoids as Tools for Modeling Human Neurodevelopmental Disorders**. The dissertation author was the primary author of this paper.

APPENDIX 2 Pharmacological rescue of synaptic and network pathology in human *MECP2*-KO neurons and cortical organoids

Abstract

Duplication or deficiency of the X-linked *MECP2* gene reliably produces profound neurodevelopmental impairment. *MECP2* mutations are almost universally responsible for Rett syndrome (RTT), and particular mutations and cellular mosaicism of *MECP2* may underlie the spectrum of RTT symptomatic severity. No clinically approved treatments for RTT are currently available, but human pluripotent stem cell technology offers a platform to identify neuropathology and test candidate therapeutics. Using a strategic series of increasingly complex human stem cell-derived technologies, including human neurons, *MECP2*-mosaic neurospheres to model RTT female brain mosaicism, and cortical organoids, we identified synaptic dysregulation downstream from knockout of *MECP2* and screened select pharmacological compounds for their ability to treat this dysfunction. Two lead compounds, Nefiracetam and PHA 543613, specifically reversed *MECP2*-knockout cytologic neuropathology. The capacity of these compounds to reverse neuropathologic phenotypes and networks in human models supports clinical studies for neurodevelopmental disorders in which MeCP2 deficiency is the predominant etiology.

Introduction

MECP2 is an X-linked gene that encodes an epigenetic regulatory protein, methyl CpG binding protein-2 (MeCP2), that is critical for typical human brain development (Chahrour et al., 2008; Gonzales & LaSalle, 2010). In addition to an array of other neurodevelopmental disorders (Samaco et al., 2005; Shibayama et al., 2004; Watson et al., 2001), *MECP2* loss-of-function mutations are the most common etiology of RTT (Amir et al., 1999), a severe neurodevelopmental disorder clinically characterized by head growth deceleration, profound cognitive decline, regression of acquired abilities, and stereotypies in early infancy (Hagberg et al., 2002). Critically, these syndromic clinical features appear following a brief period of normal development (Hagberg et al., 2002). Although the precise neurobiological changes linking *MECP2* mutations to the RTT phenotype are unclear, human postmortem tissue from RTT females portrays reduced brain size, decreased dendritic arborization and spine formation, and reduced synapse numbers (Gonzales & LaSalle, 2010; Johnston et al., 2003). Moreover, studies in murine models of *Mecp2*-deficiency implicate an accordant deficit in synaptic function, including decreased synaptic transmission and plasticity (Dani & Nelson, 2009; Moretti et al., 2006; Z. Zhou et al., 2006). The findings suggest that synaptic dysfunction is a central pathology of MeCP2 deficiency and may be a viable treatment target (Gonzales & LaSalle, 2010; Johnston et al., 2003).

Therapeutically targeting pathways downstream from *MECP2* has been proposed as a RTT treatment strategy (Benke & Möhler, 2018; Braat & Kooy, 2015; Katz et al., 2016; Pozzo-Miller et al., 2015), and the narrow window of typical development suggests intervention during this period to bolster synaptic function may be opportune to preserve clinical function and ameliorate subsequent decline. Development and discovery of

therapeutics for RTT and other neurodevelopmental disorders have been challenged by limited opportunity to investigate disease pathogenesis in a human model. Advances in pluripotent stem cell (PSC) technology, including three-dimensional neural differentiation, offer a promising human-based platform to evaluate candidate therapeutics for neurodevelopmental disorders and hasten clinical translatability (Adams et al., 2019).

Here, we employed a series of increasingly complex human stem cell-derived models as a screening platform to identify pharmacological compounds capable of specifically improving the neurocytological deficits caused by knockout of *MECP2* (*MECP2*-KO) without affecting control neurons. Using our strategic pipeline, we demonstrated *MECP2*-KO-attributable synaptic pathology in genetic expression, morphology, and physiology and screened a series of drugs with synapse-relevant mechanisms of action for their ability to improve these alterations. Two currently available lead compounds, Nefiracetam and PHA 543613, exhibited potential to partially rescue the synaptic defects caused by MeCP2 deficiency and are viable candidates for clinical trial.

Results

MECP2-KO produces synaptic pathology in human neurons

To develop our human models of MeCP2 deficiency, human PSCs with *MECP2* exonic loss-of-function mutations (Q83X nonsense or K82 frameshift with familial and isogenic PSC controls, respectively), were differentiated into cortical neurons as previously described (Figure 9A and B, Figure 14 A-I, Figure 15A-C; Espuny-Camacho et al., 2013; Nageshappa et al., 2016). We first compared the morphologies between control and *MECP2*-KO neurons. Compared to controls, *MECP2*-KO neurons transfected with Syn1::GFP

lentiviral vectors had decreased soma areas and spine density ($P < 0.0001$). The spine-like protrusions in *MECP2*-KO neurons were less stable ($P < 0.01$), but there was no observable difference in its formation ($P = 0.26$), length ($P = 0.28$), or motility ($P = 0.17$; Figure 15D and E), supporting previous descriptions of RTT neuronal pathology (Marchetto et al., 2010; Nguyen et al., 2012).

Because MeCP2 is an epigenetic regulator, we sought to identify changes in gene expression resulting from its deficiency. RT-PCR array (Figure 9C and D, Figure 16A and B) and single-cell RT-qPCR (Figure 9E-G, Figure 16C-K) analyses at timepoints throughout neuronal differentiation from neural progenitor cells (NPCs; day 0) revealed differences in genetic expression between *MECP2*-KO and control neurons. Concordant with the prominent roles of MeCP2 in synaptic function and neuronal maturation (Gonzales & LaSalle, 2010), many of the implicated genes appeared relevant to synaptic function and showed differences in expression during differentiation (Figure 9C-G). In further agreement with previous findings of RTT pathology (Stuss et al., 2012), our quantitation of cellular markers of neuronal fate and function in cells positive for the neuronal marker MAP2 revealed a decreased proportion of layer V and VI cortical neurons (CTIP2+ and FOXP2+) in *MECP2*-KO ($P = 0.04$; Figure 9H, top) and altered neurotransmitter identity. Transcriptional analysis of genes related to neurotransmission in *MECP2*-KO populations showed changes in glutamatergic, GABAergic, and cholinergic systems ($P < 0.0001$; Figure 9H, bottom, Figure 16G-K). A summary gene ontology analysis confirmed these findings, showing that alterations in gene expression due to *MECP2*-KO primarily concentrated in neurotransmitter synthesis and receptor pathways in overlapping alignment with the results of our quantitative analysis (Figure 9I).

Figure 9: Human *MECP2*-KO neurons exhibit alterations in synapse-relevant genes and pathways. A Pluripotent stem cells (PSCs) with one of two distinct exonic loss-of-function mutations (Q83X nonsense or K82 frameshift (K82fs)) at the *MECP2* locus were generated and differentiated into neurons via a neural progenitor cell (NPC) intermediate. **B** Immunofluorescent staining confirmed the absence of MeCP2 in *MECP2*-KO PSCs, NPCs, and neurons. Scale bar = 10 μm. **C** RT-qPCR array revealed differential gene expression between control and *MECP2*-KO 28-day neurons. The *P* values are calculated based on a Student's *t*-test of the replicate $2^{-\Delta\Delta Ct}$ values for each gene in the control group and KO groups (WT83/Q83X cell lines were used; $N = 3$ clones from each genotype). **D** Overtime quantitative gene expression profile of many of the involved genes relevant to synaptic function (days 14 and 28 post differentiation; normalized by control NPC expression). **E** Single-cell RT-qPCR analysis distinguished populations of control and KO 28-day neurons. Principal Component Analysis (PCA) of 441 cells projected onto the first two components. Overlaid populations of WT83/Q83X and WT82/K82fs neurons are shown. **F** Violin plots of selected genes showing the comparison between control and *MECP2*-KO neurons from the single-cell analyses (log2(expression) values) that overlapped with the results obtained via RT-PCR array. **G** Volcano plot illustrates differences in expression patterns of target genes of neurons from the qPCR single-cell analyses. The dotted lines represent differentially expressed genes between the groups at $P < 0.05$ (unpaired Student's *t*-test). **H** Left: Schematic of laminar cortical markers. Right: Top: Quantitation of laminar cell markers based on the single-cell RT-qPCR analysis (two-way analysis of variance (ANOVA), $N = 3$ replicates per genotype, $F_{3,24} = 3.31$, $^*P = 0.04$, with difference in the proportion of cortical layers V and VI, 95% confidence interval (CI) [8.31, 42.41]); Bottom: altered proportions of neurotransmitter markers (two-way ANOVA, $N = 3$ replicates per genotype, $F_{5,24} = 27.33$, $^*P < 0.0001$, with differences in the proportions of glutamatergic, 95% CI [22.33, 33.60], and cholinergic, 95% CI [0.166, 11.43], neurons). **I** Gene ontology (GO) analysis of targeted genes relevant to synaptic function displaying the differences between *MECP2*-KO and control neurons. Data information: Note that * signifies a statistically significant difference from *MECP2*-KO. Data are presented as mean ± standard error of the mean (s.e.m.).

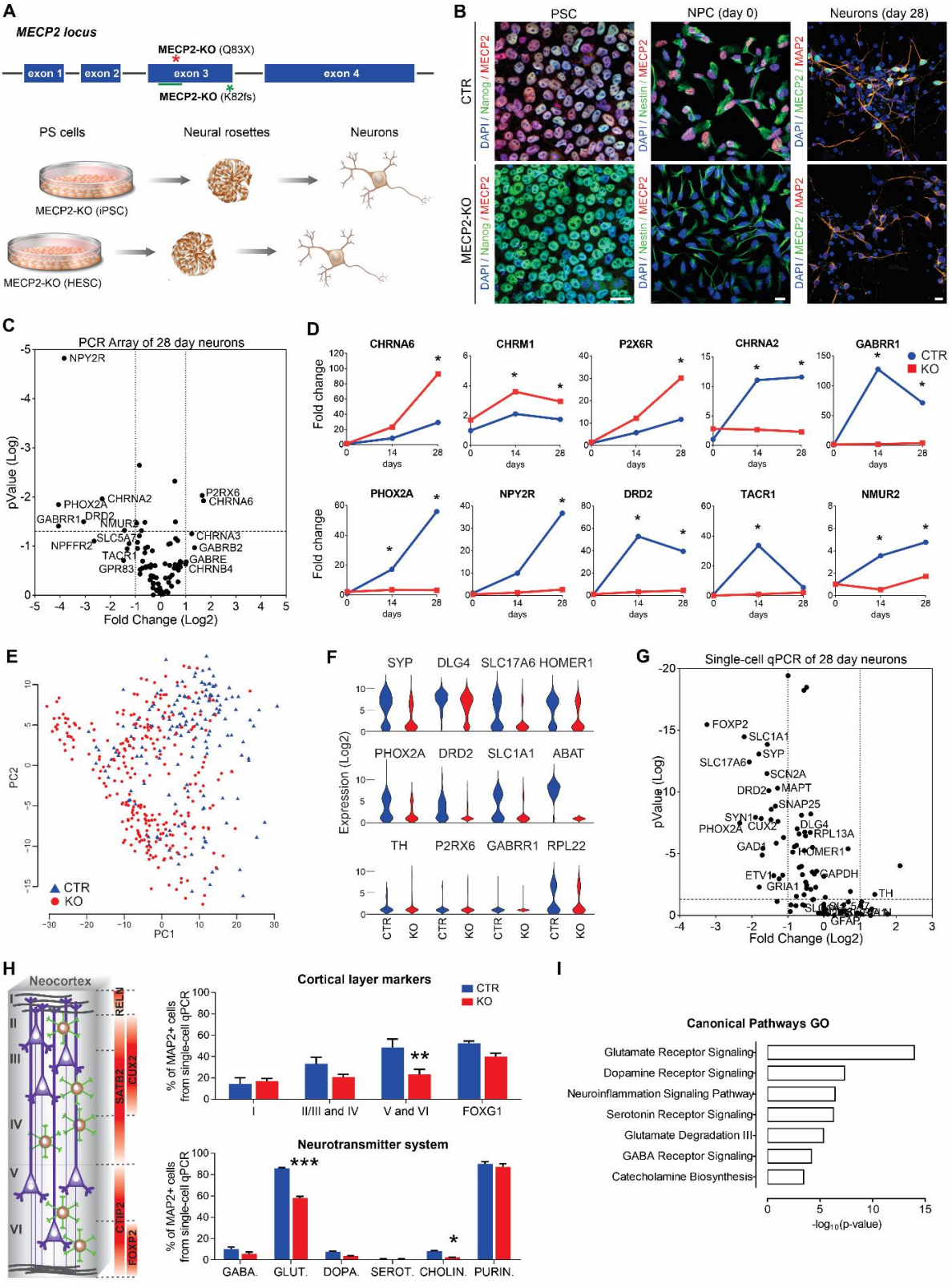
A
MECP2 locus
MECP2-KO (Q83X)
exon 1
exon 2
exon 3
exon 4
MECP2-KO (K82fs)
PS cells
Neural rosettes
Neurons
MECP2-KO (iPSC)
MECP2-KO (HESC)
B
PSC
NPC (day 0)
Neurons (day 28)
CTR
MECP2-KO
DAPI / Nanog / MECP2
DAPI / Nestin / MECP2
DAPI / MECP2 / MAP2
C
PCR Array of 28 day neurons
pValue (Log)
Fold Change (Log2)
NPY2R
PHOX2A
CHRNA2
P2RX6
CHRNA6
GABRR1
DRD2
NMUR1
SLC5A7
CHRNA3
NPFFR2
GABRB2
TACR1
GABRE
GPR83
CHRNB4
D
CHRNA6
CHRM1
P2X6R
CHRNA2
GABRR1
PHOX2A
NPY2R
DRD2
TACR1
NMUR2
Fold change
days
CTR
KO
E
PC2
PC1
CTR
KO
F
SYP
DLG4
SLC17A6
HOMER1
PHOX2A
DRD2
SLC1A1
ABAT
TH
P2RX6
GABRR1
RPL22
Expression (Log2)
CTR
KO
G
Single-cell qPCR of 28 day neurons
pValue (Log)
Fold Change (Log2)
FOXP2
SLC1A1
SYP
SLC17A6
SCN2A
DRD2
MAPT
SNAP25
SYN1
PHOX2A
CUX2
DLG4
RPL13A
GAD1
HOMER1
ETV1
GAPDH
GRIA1
TH
GFAP
H
Neocortex
I
II
III
IV
V
VI
RELN
SATB2
CUX2
CTIP2
FOXP2
Cortical layer markers
% of MAP2+ cells from single-cell qPCR
CTR
KO
I
II/III and IV
V and VI
FOXG1
Neurotransmitter system
GABA.
GLUT.
DOPA.
SEROT.
CHOLIN.
PURIN.
I
Canonical Pathways GO
Glutamate Receptor Signaling
Dopamine Receptor Signaling
Neuroinflammation Signaling Pathway
Serotonin Receptor Signaling
Glutamate Degradation III
GABA Receptor Signaling
Catecholamine Biosynthesis
-log10(p-value)

Artificial neural network modeling supports targeting synaptic dysfunction for treatment

Although synaptic pathology is a prominent consequence of MeCP2 deficiency (Gonzales & LaSalle, 2010; Johnston et al., 2003; Nguyen et al., 2012), many compensatory factors may influence network function, and it is unclear that targeted treatment of synaptic dysfunction will yield measurably linked improvement in neuronal population activity. The variation between individuals in network connectivity patterns or the proportions of excitatory and inhibitory neurons, for example, may modulate the link between synaptic phenotype and altered neural activity (Pena et al., 2018; Van Vreeswijk & Sompolinsky, 1996). Artificial neural networks offer a biologically plausible framework to explore how parameterized manipulation affects network activity (Kim et al., 2019; Miconi, 2017). We generated a neural network *in silico* to predict the change in neuronal spiking activity expected to result from isolated rescue of synaptic structure. We used co-localized synaptic puncta values from a previously published study (Marchetto et al., 2010) as a proxy for synaptic knockdown. Considering the full range of possible excitatory-inhibitory ratios (E-I balance) and connection sparsity, we simulated neural activity in networks using synaptic levels commensurate with untreated and rescued *MECP2*-KO. Holding all other parameters equivalent, rescuing the synaptic defect in isolation sufficiently increased neuronal network activity across the parameter space (pairwise delta mean = 0.877, range [-0.002, 7.981]; Figure 10A). The model supports the use of synaptic and neurotransmission phenotypes as actionable targets to improve network function.

Pharmacological screening identifies two lead compounds that specifically reverse *MECP2*-KO phenotypes

We selected 14 pharmacological compounds with mechanisms of action that counteract the synapse and neurotransmitter pathologies that we identified in Figure 9 (Figure 10B). For instance, because *MECP2*-KO neurons exhibit cholinergic deficiency (Oginsky et al., 2014; Y. Zhang et al., 2016; H. Zhou et al., 2017), we included compounds that are predicted to specifically promote this action (e.g., Tacrine, Carbamoylcholine). We treated *MECP2*-KO and control neurons with each of the 14 compounds and employed a tiered series of assays to identify those that could specifically rescue *MECP2*-KO pathology without affecting controls (Figure 10C). Compounds that either did not treat pathology or significantly altered controls were excluded from use in subsequent assays. In initial assays of synaptogenesis, nine of the 14 compounds increased the quantity of either the presynaptic protein Synapsin1 or the postsynaptic protein PSD-95, the primary treatment endpoints (Figure 10D and E, Figure 17A and B). We evaluated the capacity of these nine compounds to increase the quantity of pre and post co-localized synaptic puncta in *MECP2*-KO neurons, eliminating the drugs that affected control neurons (Figure 10F and G, Figure 17C and D).

Our initial screening isolated three drugs (Nefiracetam, Carbamoylcholine, and Acamprosate) that specifically increased synaptogenesis in human *MECP2*-KO neurons (Figure 10D-G). However, the large Carbamoylcholine metabolite has limited gastrointestinal bioavailability and cannot traverse the blood-brain barrier. We elected to instead retain PHA 543613, another direct cholinergic agonist that increased co-localized synaptic puncta with effect nearly identical to that of Carbamoylcholine (PHA 543613, 95% confidence interval

(CI) [-8.994, 0.4944] vs Carbamoylcholine, 95% CI [-9.619, -0.1306]), but which has high oral bioavailability and rapid brain penetration *in vivo* (Wishka et al., 2006).

Following the successful increase of protein markers of synaptogenesis and synaptic puncta, we tested the surviving compounds' (Nefiracetam, PHA 543613, and Acamprosate) effects on synaptic function and network activity via calcium imaging and multi-electrode array (MEA) electrophysiology (Nageshappa et al., 2016). *MECP2*-KO neurons exhibit less frequent calcium transients that are tractable to manipulators of synaptic function ($P < 0.001$), a decreased percentage of active neurons ($P < 0.001$), and decreased MEA spike frequency (Figure 10H and I, Figure 17E-G), corroborating the predictions of our *in silico* network simulations. Nefiracetam and PHA 543613 significantly increased the frequency of calcium transients and the percentage of neurons that are active (Figure 10H) and restored the MEA spike frequency in *MECP2*-KO neurons (Figure 10I, Figure 17E-G). Because Nefiracetam and PHA 543613 specifically rescued synaptic activity in *MECP2*-KO neurons without appreciably affecting controls, these compounds emerged as the most efficacious candidates for further testing in human 3D models.

Figure 10: Screening selected drugs with synaptic action in human neurons identifies Nefiracetam and PHA 543613 as top treatment candidates for MeCP2 deficiency. A *In silico* neural network modeling using our previous synaptic puncta values for untreated (top, knockdown (KD) [6/16] = 0.375*control) and treated (bottom, KD [24/16] = 1.5*control) RTT neurons (Marchetto et al., 2010a) suggested that isolated increase of synaptic knockdown sufficiently increases neural activity (untreated, mean = 0.665, range = [0.050,1.002]; treated, mean = 1.542, range = [0.997,8.395]). For excitatory-inhibitory (E-I) balance, "0" is fully excitatory, "1" is fully inhibitory. **B** List of compounds for the phenotypic screening. The compounds were selected for mechanisms of action that counteracted the neurotransmitter deficiencies observed in Figure 1. The final concentration was determined based on previous studies. **C** Schematic of drug treatment workflow. Briefly, 28-day-old *MECP2*-KO neurons were treated for 2 more weeks prior to performing phenotypic reversal experiments. **D, E** Western blot quantification showed decreased presynaptic Synapsin1 (D) and postsynaptic PSD-95 (E) in untreated 6-week *MECP2*-KO neurons that can be increased by drug treatment (* $P < 0.05$; full Western blot, Fig EV4A) (WT83/Q83X cell lines were used; $N = 3$ clones from each genotype). **F, G** 6-week *MECP2*-KO neurons (F) showed a pharmacologically rescuable reduction of co-localized synaptic puncta (G; one-way ANOVA, $F_{16,118} = 9.148$, *$P < 0.05$; Dunnet's multiple comparisons test vs untreated KO (WT83/Q83X cell lines were used; N = 7-8 neurons/condition). Z scores relative to KO untreated: Control = 3.903; Nefiracetam = 3.560; Carbamoylcholine = 2.705; Pirenzepine = 0.0448; PHA543613 = 2.121; Acamprosate = 3.339; Baclofen = 0.5672; GR73632 = 2.237; Hyperforin = 3.016, and IGF-1 = 3.791. Scale bar = 5 μm. **H** Drug treatment increased calcium transient frequency in 6-week neurons. Fluorescence intensity changes reflecting intracellular calcium transients in neurons in different regions of interest (one-way ANOVA, $F_{4,52} = 20.28$, Dunnett's multiple comparisons test vs untreated KO: Nefiracetam, $P < 0.01$ and $Z = 2.364$; PHA 543613, $P < 0.001$ and $Z = 3.391$; Acamprosate, $P < 0.001$ and $Z = 3.153$; WT83/Q83X cell lines were used; N = 10-14 neurons/condition) and the percentage of active neurons (one-way ANOVA, $F_{4,52} = 23.11$; Dunnett's multiple comparison test vs untreated KO: Nefiracetam, $P < 0.001$ and $Z = 3.144$; PHA 543613, $P < 0.01$ and $Z = 2.567$; Acamprosate, $P < 0.01$ and $Z = 2.285$; N = 10-14 neurons/condition). **I** Treatment with either Nefiracetam or PHA 543613 increased network spiking activity in *MECP2*-KO neurons on MEA (two-sided unpaired Student's *t*-test compared to KO untreated: Nefiracetam, $P = 0.016$ and $Z = 2.418$; PHA 543613, $P = 0.027$ and $Z = 2.147$; Acamprosate, $P = 0.39$ and $Z = 0.477$; WT83/Q83X and WT82/K82fs cell lines were used; N = 4-11 MEA wells/condition). Data information: Note that * signifies a statistically significant difference from *MECP2*-KO untreated. Data are presented as mean ± s.e.m.

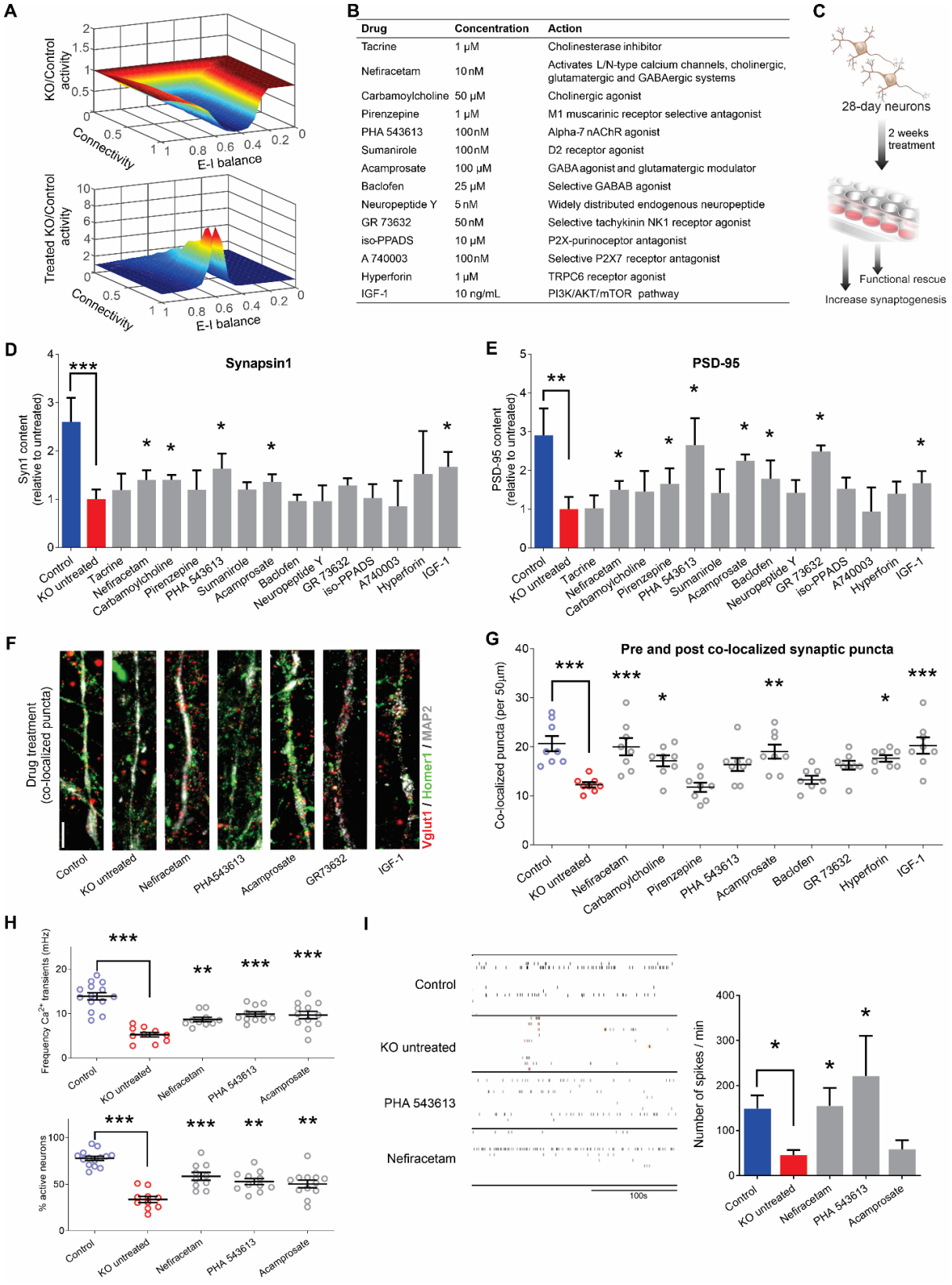
A
KO/Control activity
Connectivity
E-I balance
Treated KO/Control activity
B
Drug | Concentration | Action
Tacrine | 1 µM | Cholinesterase inhibitor
Nefiracetam | 10 nM | Activates L/N-type calcium channels, cholinergic, glutamatergic and GABAergic systems
Carbamoylcholine | 50 µM | Cholinergic agonist
Pirenzepine | 1 µM | M1 muscarinic receptor selective antagonist
PHA 543613 | 100 nM | Alpha-7 nAChR agonist
Sumanirole | 100 nM | D2 receptor agonist
Acamprosate | 100 µM | GABA agonist and glutamatergic modulator
Baclofen | 25 µM | Selective GABAB agonist
Neuropeptide Y | 5 nM | Widely distributed endogenous neuropeptide
GR 73632 | 50 nM | Selective tachykinin NK1 receptor agonist
iso-PPADS | 10 µM | P2X-purinoceptor antagonist
A 740003 | 100 nM | Selective P2X7 receptor antagonist
Hyperforin | 1 µM | TRPC6 receptor agonist
IGF-1 | 10 ng/mL | PI3K/AKT/mTOR pathway
C
28-day neurons
2 weeks treatment
Functional rescue
Increase synaptogenesis
D
Synapsin1
Syn1 content (relative to untreated)
Control
KO untreated
Tacrine
Nefiracetam
Carbamoylcholine
Pirenzepine
PHA 543613
Sumanirole
Acamprosate
Baclofen
Neuropeptide Y
GR 73632
iso-PPADS
A740003
Hyperforin
IGF-1
E
PSD-95
PSD-95 content (relative to untreated)
F
Drug treatment (co-localized puncta)
Vglut1 / Homer1 / MAP2
G
Pre and post co-localized synaptic puncta
Co-localized puncta (per 50µm)
H
Frequency Ca2+ transients (mHz)
% active neurons
I
Control
KO untreated
PHA 543613
Nefiracetam
100s
Number of spikes / min

Treatment of *MECP2*-mosaic neurospheres increases cell viability and calcium activity

Because *MECP2* resides on the X chromosome, random X-inactivation in females can produce a pattern of cellular genetic mosaicism, with consequent phenotypic gradation, in which some cells express the normal allele and others are mutant (Amir et al., 1999; Renthal et al., 2018). Therefore, as the next stage to evaluate the two drug candidates, we developed a model of *MECP2* cellular mosaicism (*MECP2*-mosaic) to mimic the female RTT brain by combining control and *MECP2*-KO NPCs in a 50/50 mixture (Figure 11A-C; Sirenko et al., 2019). We detected no difference in size (diameter) between untreated *MECP2*-mosaic (CTR/KO) neurospheres and controls (Figure 11D), but both *MECP2*-KO ($P < 0.001$) and *MECP2*-mosaic ($P < 0.001$) neurospheres showed decreased calcium transient amplitude compared to controls (Figure 11E).

Treating *MECP2*-mosaic neurospheres with either Nefiracetam or PHA 543613 did not alter the diameter ($P = 0.79$; Figure 11F). Post-treatment cell viability (representing the inverse of drug-induced cytotoxicity) in the *MECP2*-mosaic neurospheres was improved in a dose-dependent manner by combined treatment with Nefiracetam and PHA 543613 (0.1 µM, 95% CI [-25.94, 0.10], $P > 0.05$; 1 µM, 95% CI [-29.89, -3.85], $P < 0.01$; 10 µM, 95% CI [-39.47, -13.44], $P < 0.001$; Figure 11G). Calcium transient frequency in *MECP2*-mosaic neurospheres was increased by treatment with Nefiracetam in isolation (1 µM, $P < 0.05$) and when combined with PHA 543613 (10 µM, $P < 0.001$; Figure 11H), but calcium transient amplitude was unaffected by either compound ($P = 0.255$; Figure 11I).

To investigate the impact of the drug treatments on the electrophysiological properties of the *MECP2*-mosaic model, neurospheres treated with 1 µM Nefiracetam, 1 µM PHA 543613, or both Nefiracetam and PHA 543613 were plated to perform MEA analysis. Despite

variability in the recordings, we observed an inverse relationship of decreasing spike frequency with an increasing percentage of *MECP2*-KO cells in the neurospheres, but this association did not reach significance (P = 0.20). PHA 543613 and Nefiracetam each increased the overall spike count of *MECP2*-mosaic (CTR/KO) neurospheres after 5 weeks of treatment, but because *MECP2*-mosaic neurospheres exhibit similar spiking frequency as control neurospheres (P = 0.65), these increases were likewise not significant (PHA 543613 vs CTR/KO, P = 0.65; Nefiracetam vs CTR/KO, P = 0.98; PHA + Nefi vs CTR/KO, P = 0.86; Figure 11J and K). Because each drug conferred a benefit to *MECP2*-mosaic neurospheres, we retained both Nefiracetam and PHA 543613 for further evaluation in a more complex human neurodevelopmental model.

Figure 11: Treatment of *MECP2*-mosaic neurospheres with Nefiracetam and PHA 543613. A Schematic showing the formation of control, *MECP2*-KO, and mosaic *MECP2*-KO/control neurospheres (WT83/Q83X cell lines were used). **B, C** Immunofluorescent staining (B) and quantitation (C) confirmed the graded decrease in MeCP2 expression from control to 50% *MECP2* mosaic to full *MECP2*-KO neurospheres. **D** 8-week *MECP2*-KO neurospheres exhibited decreased size (diameter; $*P < 0.01$), but 50% *MECP2*-mosaic (CTR/KO) neurospheres were unchanged from controls (one-way ANOVA, $F_{2,150} = 6.03$, $P = 0.003$; Dunnett's multiple comparisons test). Scale bar = 200 µm. **E** Calcium imaging analysis showing calcium transients normalized by control (one-way ANOVA, $F_{2,72} = 15.62$, $P < 0.0001$; Dunnett's multiple comparisons test vs control: *MECP2*-mosaic, $P < 0.001$; *MECP2*-KO, $P < 0.001$). WT83/Q83X cell lines were used; $N = 44$ Q83X neurospheres and 65 WT83 neurospheres. **F** 8-week neurosphere size (diameter) remained unchanged by treatment with either drug (one-way ANOVA, $F_{6,344} = 0.52$, $P = 0.79$; $N = 44$ Q83X neurospheres and 65 WT83 neurospheres). **G** Cell viability was improved or unharmed in treated 8-week neurospheres (one-way ANOVA, $F_{9,104} = 6.81$; Dunnett's multiple comparisons test vs CTR/KO untreated: Nefi + PHA 1 µM, $P < 0.01$ and $Z = 2.974$; Nefi + PHA 10 µM, $P < 0.001$ and $Z = 3.733$; N = 8-24 neurospheres per condition). **H, I** Calcium transient frequency (number of peaks in 10 mins recording) normalized by CTR/KO untreated (H; one-way ANOVA, $F_{9,239} = 6.18$; Dunnett's multiple comparisons test vs CTR/KO untreated: Nefi 1 µM, $P < 0.05$ and $Z = 0.780$; Nefi + PHA 10 µM, $P < 0.001$ and $Z = 1.972$; N = 15-61 neurospheres per condition) and calcium transient amplitude normalized by CTR/KO untreated (I; one-way ANOVA, $F_{9,241} = 1.27$, $P = 0.255$; N = 16-62 neurospheres per condition). **J, K** MEA spike frequency heatmap (J) and quantification (K) normalized by CTR/KO untreated (one-way ANOVA, $F_{5,38} = 1.21$, $P = 0.321$; Dunnett's multiple comparisons test vs CTR/KO untreated: PHA, $P = 0.65$ and $Z = 1.134$; Nefi, $P = 0.98$ and $Z = 0.06$; PHA + Nefi, $P = 0.86$ and $Z = 0.94$; N = 7-8 wells per condition). 'X' on activity heatmap signifies absence of a neurosphere in that position. Data information: Nefi: Nefiracetam; PHA: PHA 543613. Note that * in F-K signifies a statistically significant difference in treated *MECP2*-mosaic (CTR/KO) neurospheres compared to untreated CTR/KO neurospheres. Data are presented as mean ± s.e.m.

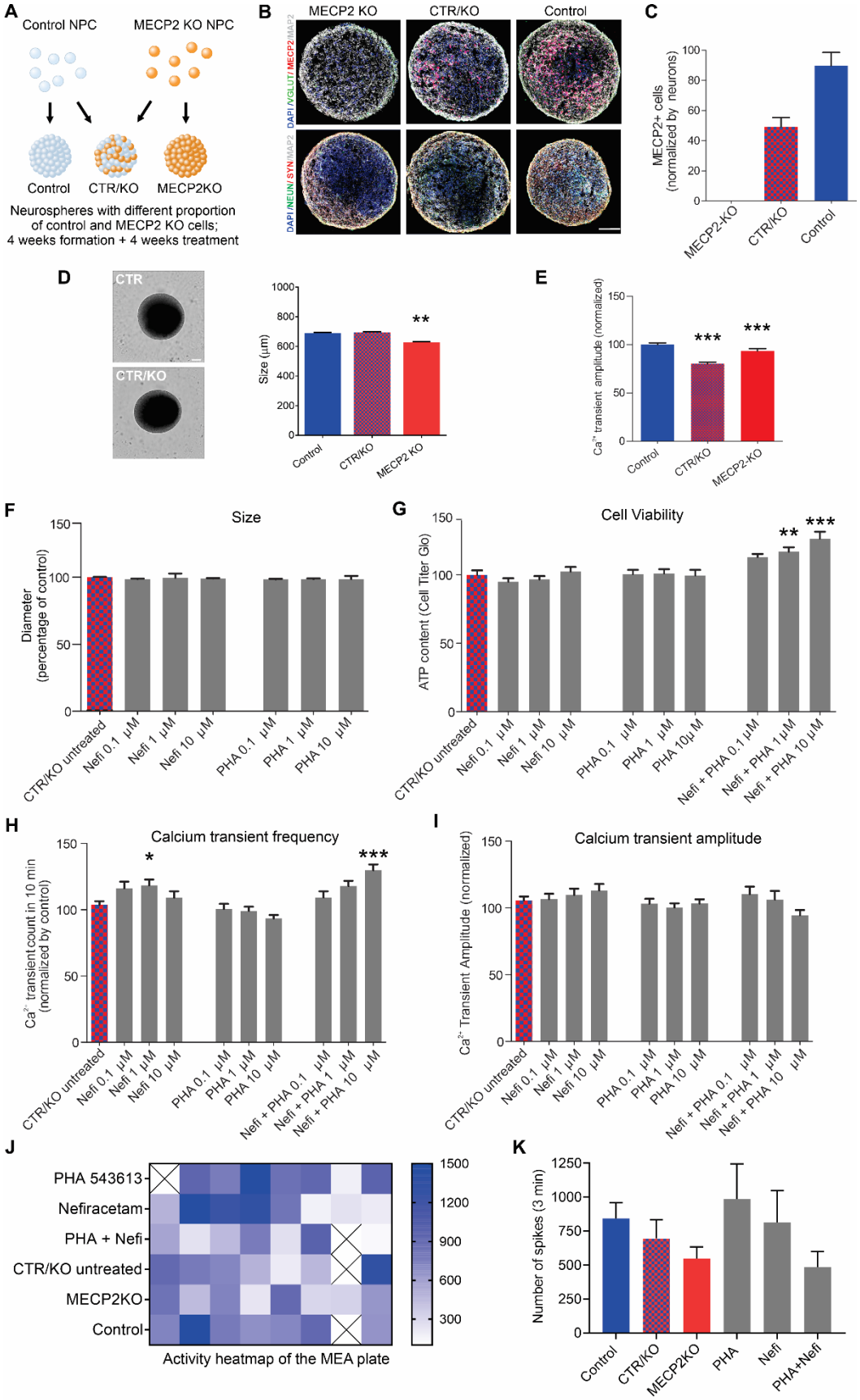
A
Control NPC
MECP2 KO NPC
Control
CTR/KO
MECP2KO
Neurospheres with different proportion of control and MECP2 KO cells; 4 weeks formation + 4 weeks treatment
B
MECP2 KO
CTR/KO
Control
DAPI /VGLUT/ MECP2/MAP2
DAPI /NEUN/ SYN/MAP2
C
MECP2+ cells (normalized by neurons)
MECP2-KO
CTR/KO
Control
D
CTR
CTR/KO
Size (µm)
Control
CTR/KO
MECP2 KO
E
Ca2+ transient amplitude (normalized)
Control
CTR/KO
MECP2-KO
F
Size
Diameter (percentage of control)
CTR/KO untreated
Nefi 0.1 µM
Nefi 1 µM
Nefi 10 µM
PHA 0.1 µM
PHA 1 µM
PHA 10 µM
G
Cell Viability
ATP content (Cell Titer Glo)
CTR/KO untreated
Nefi 0.1 µM
Nefi 1 µM
Nefi 10 µM
PHA 0.1 µM
PHA 1 µM
PHA 10µ M
Nefi + PHA 0.1 µM
Nefi + PHA 1 µM
Nefi + PHA 10 µM
H
Calcium transient frequency
Ca2+ transient count in 10 min (normalized by control)
CTR/KO untreated
Nefi 0.1 µM
Nefi 1 µM
Nefi 10 µM
PHA 0.1 µM
PHA 1 µM
PHA 10 µM
Nefi + PHA 0.1 µM
Nefi + PHA 1 µM
Nefi + PHA 10 µM
I
Calcium transient amplitude
Ca2+ Transient Amplitude (normalized)
CTR/KO untreated
Nefi 0.1 µM
Nefi 1 µM
Nefi 10 µM
PHA 0.1 µM
PHA 1 µM
PHA 10 µM
Nefi + PHA 0.1 µM
Nefi + PHA 1 µM
Nefi + PHA 10 µM
J
PHA 543613
Nefiracetam
PHA + Nefi
CTR/KO untreated
MECP2KO
Control
Activity heatmap of the MEA plate
K
Number of spikes (3 min)
Control
CTR/KO
MECP2KO
PHA
Nefi
PHA+Nefi

Nefiracetam and PHA 543613 reverse network activity in *MECP2*-KO cortical organoids

Our final approach to evaluate the therapeutic efficacy of Nefiracetam and PHA 543613 was using cortical organoids, a three-dimensional human neurodevelopmental model that closely recapitulates aspects of human fetal neurodevelopment (Camp et al., 2015; Luo et al., 2016; Trujillo et al., 2019). We generated *MECP2*-KO and control cortical organoids as previously described (Figure 12A, Figure 18A and B; Trujillo et al., 2019). One-month old cortical organoids were treated for another month with either Nefiracetam (1 μM) or PHA 543613 (1 μM), and experiments and analyses were performed using organoids at 2-3 months of age. Both Nefiracetam ($P < 0.001$) and PHA 543613 ($P < 0.001$) increased the diameter of *MECP2*-KO organoids (Figure 12B), which is reduced despite their equivalent areas of Ki67+ proliferation ($P = 0.73$; Figure 12C).

RNA sequencing and gene ontology analyses in two-month-old organoids revealed that both Nefiracetam and PHA 543613 promoted expression of genes involved in pathways relevant to synaptic function (Figure 12D-G, Figure 18C and D). The compounds were able to increase gene expression of specific neurotransmitter markers including cholinergic, GABAergic, and glutamatergic signaling. These findings were supported by the capacity of Nefiracetam ($P < 0.01$), albeit not PHA 543613, to increase synaptic puncta (Figure 12H, Figure 18E and F). In 2-3-month-old *MECP2*-KO and control organoids, an equivalent percentage of cells immunostained positive for the neuronal marker NeuN ($P = 0.80$; Figure 12I), and the cortical layer V and VI marker CTIP2 was unaffected by drug treatment ($P = 0.07$; Figure 12J). Although the primary aim of the drug screening pipeline was to increase synaptogenesis and activity in *MECP2*-KO neurons, morphological features were also

investigated. Nefiracetam and PHA 543613 did not increase the number or length of neurites and did not rescue nuclei size. However, we observed an increase in neuronal spine-like protrusions due to the treatments (Figure 18G).

To further evaluate network activity, we use cortical organoids to perform MEA electrophysiology, as we previously demonstrated (Trujillo et al., 2019). *MECP2*-KO organoids exhibited decreased population spiking compared to the controls ($P < 0.01$), but treating the *MECP2*-KO organoids with Nefiracetam and PHA 543613 each increased population spiking to a level not significantly different from that of control organoids (Nefiracetam, $P = 0.98$ in comparison to control organoids; PHA 543613, $P = 0.12$ in comparison to control organoids; Figure 12K-M).

Figure 12: Treatment increases synapse-related gene expression and network activity in *MECP2*-KO cortical organoids. A Schematic of PSC aggregation and development into cortical organoids. **B** 2-month-old cortical organoid diameter (one-way ANOVA, $F_{2,173} = 91.07$; Dunnett's multiple comparisons test vs untreated: Nefiracetam, $^*P < 0.001$ and $Z = 5.414$; PHA 543613, $^*P < 0.001$ and $Z = 5.351$; WT83/Q83X and WT82/K82fs cell lines were used; N = 28-90 organoids per condition). Scale bar = 200 µm. **C** Ki67+ proliferative area (Student's t-test, $t10 = 0.36$, $P = 0.73$, N = 6 each). Scale bar = 50 µm. **D, E** RNA sequencing and GO analysis of untreated *MECP2*-KO organoids vs Nefiracetam indicated that treatment upregulated genetic expression in synapse-relevant pathways. **F, G** RNA sequencing and GO analysis of untreated *MECP2*-KO organoids vs PHA 543613 indicated that treatment upregulated expression of genes in synapse-relevant pathways. **H** Synapsin1+ puncta quantitation (one-way ANOVA, $F_{3,34} = 10.07$; Dunnett's multiple comparisons test vs untreated: Nefiracetam, $^*P < 0.01$ and $Z = 2.998$; PHA 543613, $P > 0.05$ and $Z = 1.266$; WT83/Q83X cell lines were used; N = 8-10 each). Scale bar = 20 µm. **I, J** *MECP2*-KO and control organoids had similar proportions of cells positive for the neuronal marker NeuN (G; Student's t-test, $t14 = 0.26$, $P = 0.80$, N = 8 each) and cortical layer V and VI neuronal marker CTIP2 (H; one-way ANOVA, $F_{3,40} = 2.489$, $P = 0.074$ and $Z < 1$, WT83/Q83X and WT82/K82fs cell lines were used; N = 8-14 organoids each). Scale bar = 50 µm. **K-M** *MECP2*-KO cortical organoids plated on MEA (**K**) showed decreased population spiking (Scale bar = 200 µm). (**L, M**) Drug treatment increased spiking network activity of MECP2-KO cortical organoids to a level not significantly different from that of control organoids (M; one-way ANOVA, $F_{3,31} = 3.775$, Dunnett's multiple comparisons test vs control: untreated KO, $^*P < 0.01$ and $Z = 3.192$; Nefiracetam, $P = 0.98$ and $Z = 2.117$; PHA 543613, $P = 0.12$ and $Z = 1.101$, WT83/Q83X cell lines were used; N = 7-10 MEA wells per condition). Data information: Note that * signifies a statistically significant difference from untreated *MECP2*-KO cortical organoids. Data are presented as mean ± s.e.m.

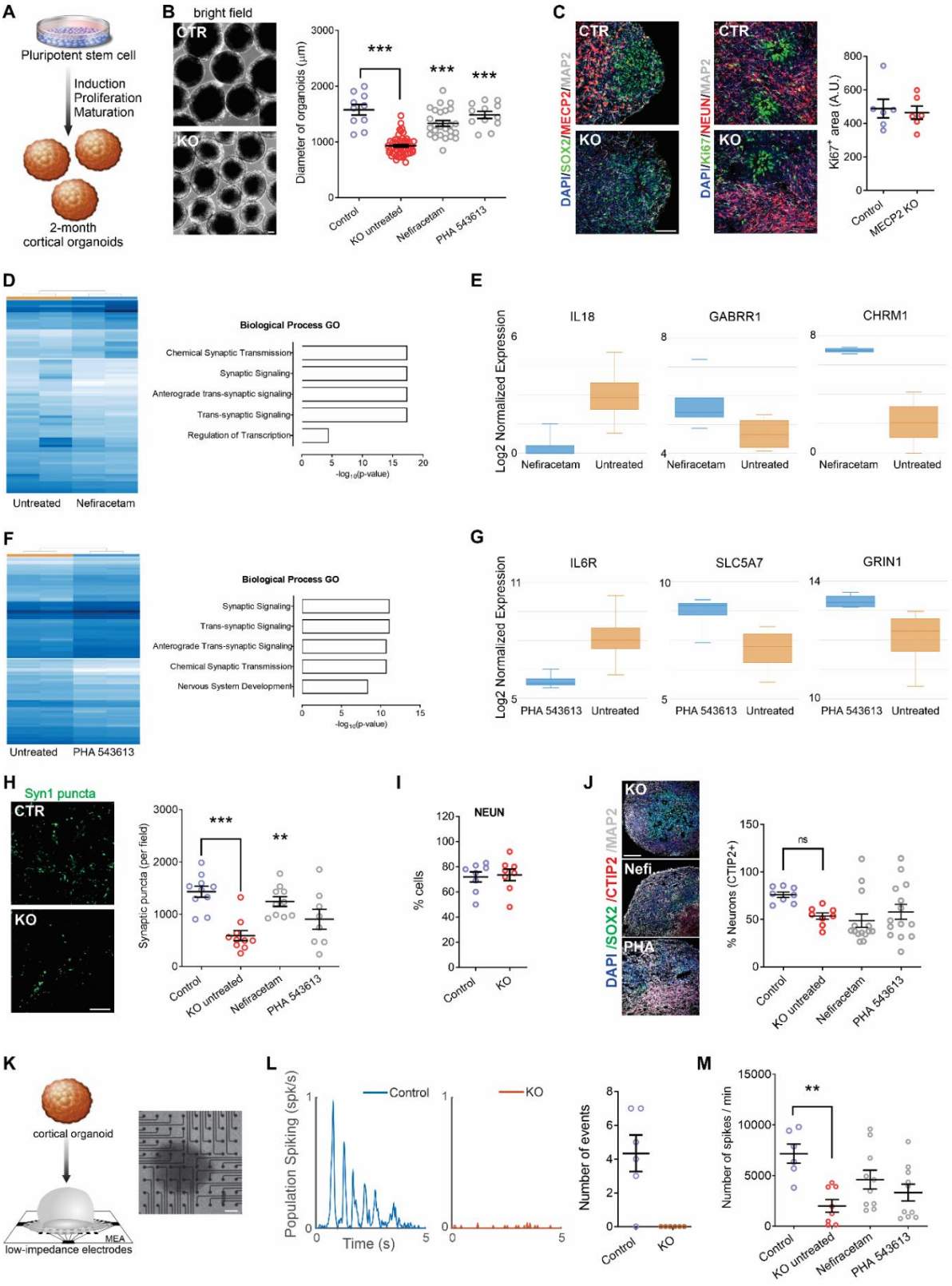
A
Pluripotent stem cell
Induction
Proliferation
Maturation
2-month
cortical organoids
B
bright field
CTR
KO
Diameter of organoids (µm)
Control
KO untreated
Nefiracetam
PHA 543613
C
CTR
KO
DAPI/SOX2/MECP2/MAP2
DAPI/Ki67/NEUN/MAP2
Ki67+ area (A.U.)
Control
MECP2 KO
D
Untreated
Nefiracetam
Biological Process GO
Chemical Synaptic Transmission
Synaptic Signaling
Anterograde trans-synaptic signaling
Trans-synaptic Signaling
Regulation of Transcription
E
IL18
GABRR1
CHRM1
Log2 Normalized Expression
Nefiracetam
Untreated
F
Untreated
PHA 543613
Biological Process GO
Synaptic Signaling
Trans-synaptic Signaling
Anterograde Trans-synaptic Signaling
Chemical Synaptic Transmission
Nervous System Development
G
IL6R
SLC5A7
GRIN1
Log2 Normalized Expression
PHA 543613
Untreated
H
Syn1 puncta
CTR
KO
Synaptic puncta (per field)
Control
KO untreated
Nefiracetam
PHA 543613
I
NEUN
% cells
Control
KO
J
KO
Nefi
PHA
DAPI /SOX2 /CTIP2 /MAP2
% Neurons (CTIP2+)
ns
Control
KO untreated
Nefiracetam
PHA 543613
K
cortical organoid
MEA
low-impedance electrodes
L
Control
KO
Population Spiking (spk/s)
Time (s)
Number of events
Control
KO
M
Number of spikes / min
Control
KO untreated
Nefiracetam
PHA 543613

Discussion

In the present study, we used human *MECP2*-KO PSCs to undertake the goals of identifying gene-specific pathology and therapeutically targeting pathways downstream from *MECP2* loss-of-function (Benke & Möhler, 2018; Braat & Kooy, 2015; Katz et al., 2016; Pozzo-Miller et al., 2015). Our analyses of *MECP2*-KO neurons revealed altered expression of synapse-relevant genes, findings that corroborate the contribution of synaptic impairment to RTT pathology (Banerjee et al., 2019; Chao et al., 2007, 2010; C. Y. Chen et al., 2018; Dani & Nelson, 2009; Krishnan et al., 2017). After identifying targetable neuropathology, supported by computational simulations of network behavior, we developed a human-based drug screening platform comprised of increasingly complex models that closely mimic human fetal neurodevelopment, thereby facilitating clinical translatability. We strategically employed a tiered series of assays and models (monolayer neurons, *MECP2*-mosaic neurospheres, and cortical organoids) to screen 14 targeted pharmacological compounds. Two of these, Nefiracetam and PHA 543613, specifically treated *MECP2*-KO pathophysiology while leaving controls unaffected (Figure 13).

Figure 13: Drug screening pipeline overview. Top: Left: *MECP2*-KO neurons exhibit aberrant synaptic transcriptomics and synaptic morphology as well as decreased calcium transients and neural network activities. Right: Pharmacological compounds were selected for screening based on the expected ability of their mechanisms of action to counteract the synaptic and neurotransmitter pathologies we identified. Center: With step-wise progression through a pipeline of assays (shown as dark-to-light shades of blue), drugs were eliminated either if they did not reverse the *MECP2*-KO pathology identified in the assay or if they affected controls. Nefiracetam and PHA 543613 emerged as the two compounds that could reverse *MECP2*-KO neurocytopathology without affecting controls. Middle: The effects of Nefiracetam and PHA 543613 were validated in two 3D human cell models, *MECP2*-mosaic neurospheres (Left) and *MECP2*-KO cortical organoids (Right). Left: One or both drugs reversed calcium transient frequency and amplitude as well as MEA spike frequency in *MECP2*-mosaic neurospheres, but not their size. Right: One or both drugs reversed organoid size, SYN1 puncta, and MEA spike frequency in *MECP2*-KO cortical organoids. Bottom: A schematic proposing a hypothetical mechanism by which Nefiracetam and PHA 543613 might influence synaptic function.

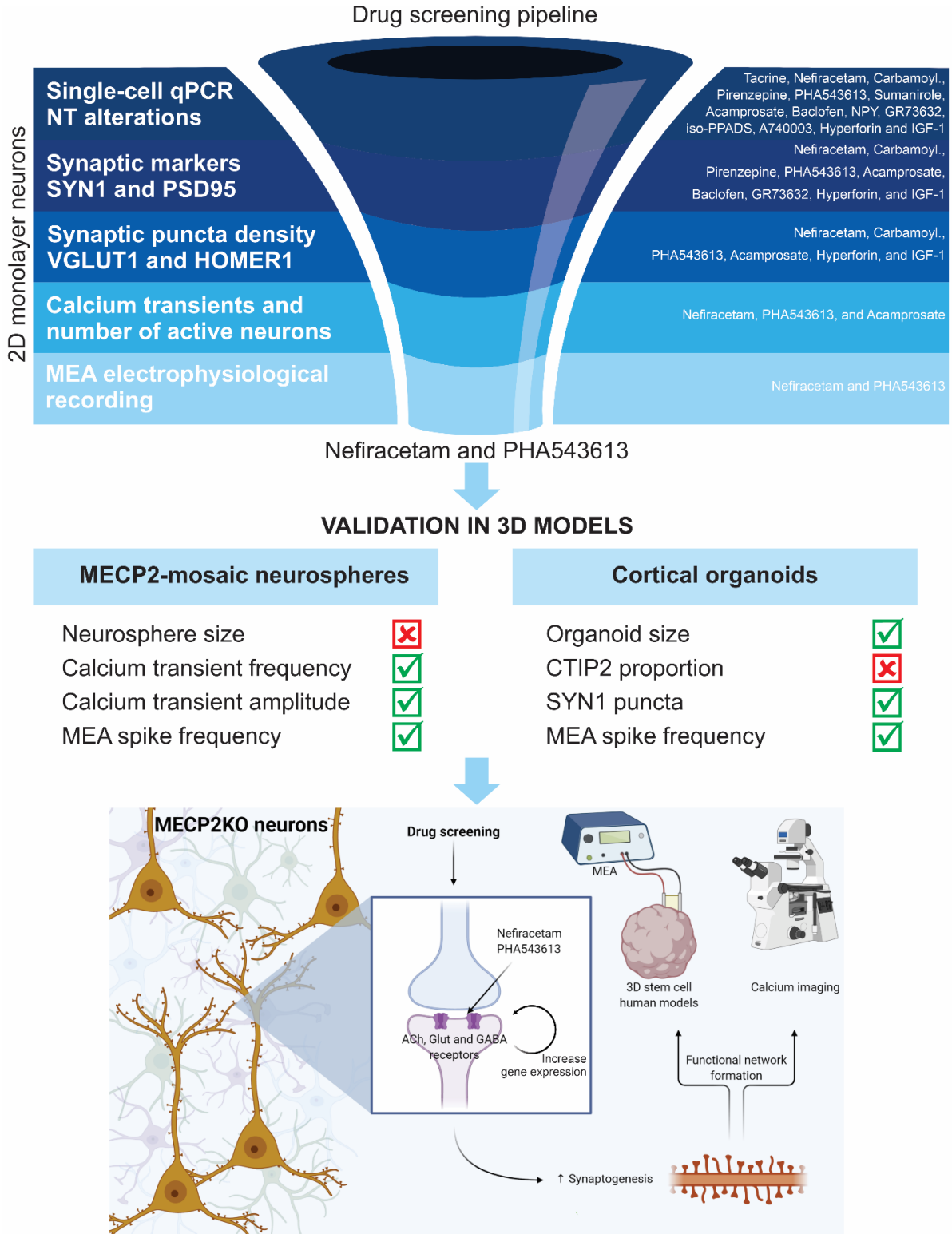
Drug screening pipeline
2D monolayer neurons
Single-cell qPCR NT alterations
Synaptic markers SYN1 and PSD95
Synaptic puncta density VGLUT1 and HOMER1
Calcium transients and number of active neurons
MEA electrophysiological recording
Tacrine, Nefiracetam, Carbamoyl., Pirenzepine, PHA543613, Sumanirole, Acamprosate, Baclofen, NPY, GR73632, iso-PPADS, A740003, Hyperforin and IGF-1
Nefiracetam, Carbamoyl., Pirenzepine, PHA543613, Acamprosate, Baclofen, GR73632, Hyperforin, and IGF-1
Nefiracetam, Carbamoyl., PHA543613, Acamprosate, Hyperforin, and IGF-1
Nefiracetam, PHA543613, and Acamprosate
Nefiracetam and PHA543613
Nefiracetam and PHA543613
VALIDATION IN 3D MODELS
MECP2-mosaic neurospheres
Neurosphere size
Calcium transient frequency
Calcium transient amplitude
MEA spike frequency
Cortical organoids
Organoid size
CTIP2 proportion
SYN1 puncta
MEA spike frequency
MECP2KO neurons
Drug screening
MEA
Nefiracetam
PHA543613
ACh, Glut and GABA receptors
Increase gene expression
3D stem cell human models
Calcium imaging
Functional network formation
↑ Synaptogenesis

Our *MECP2*-KO neuronal cultures showed that synaptic and neurotransmitter pathophysiology principally concentrated in glutamatergic and cholinergic dysregulation. Clinically, the lead compounds Nefiracetam and PHA 543613, both of which are orally administered, have invaluable mechanisms of action to treat these deficiencies. Nefiracetam is a cholinergic, GABAergic, and glutamatergic agonist developed to enhance cognitive functioning (Malykh & Sadaie, 2010; Moriguchi, 2011), and PHA 543613 is an α7-nAChR agonist with proven neuroprotective effects in a neurodevelopmental disease model (Foucault-Fruchard et al., 2018). Cholinergic modulatory effects within the nervous system are many because nAChRs are widely dispersed across the neuronal and synaptic architecture, and acetylcholine additionally affects the release of other neurotransmitters (Picciotto et al., 2012). Although pronounced GABAergic pathology has been observed in mice (Chao et al., 2010), we observed lesser GABAergic contribution in our human-based neuronal cultures, and compounds that mainly modulate GABA failed our drug-screening pipeline. We do not observe high proportions of GABAergic neurons in our 3D systems (organoids and neurospheres), so the compounds' effects that we observed here are presumably via their cholinergic and, for Nefiracetam, glutamatergic actions. Nevertheless, inhibitory dysregulation likely contributes to *MECP2*-KO pathophysiology, and future studies of RTT that employ human-based cell models with high GABAergic representation could explore this aspect of the pathology.

Several completed and ongoing clinical trials have explored therapeutic safety or efficacy in RTT patients, mainly of IGF-1 or modulators of BDNF, the encoding gene of which is a target of MeCP2 (W. G. Chen et al., 2003). Although formulations of IGF-1 are expected to be promising candidates (Pozzo-Miller et al., 2015), results thus far have been

mixed. Recombinant human IGF-1 (mescarmin) was safe and mildly efficacious in a phase 1 trial of RTT patients (clinicaltrials.gov NCT01253317; Khwaja et al., 2014), but a double-blind, placebo-controlled follow-up study of mescarmin did not show significant phenotypic improvements (clinicaltrials.gov identifier NCT01777542; O'Leary et al., 2018). In contrast, the trial of a synthetic form of IGF-1 (trofinetide; NCT02715115; Glaze et al., 2017) demonstrated sufficient safety and efficacy to warrant initiation of a phase 3 trial (NCT04279314). Meanwhile, clinical trials that have preliminarily investigated modulators of BDNF have shown efficacy of glatiramer acetate (NCT02153723; Djukic et al., 2016) and led to further trial of fingolimod (NCT02061137). Of the two compounds we identified in the present study, Nefiracetam has previously entered clinical trials for other disorders involving cholinergic deficiency, including dementia, post-stroke apathy, and major depressive disorder (Fujimaki et al., 1993; Robinson et al., 2009). Thus, the ready availability of Nefiracetam and PHA 543613 and their capacity to specifically improve the neurocytopathology identified in our human *MECP2*-KO models encourages suggestion of clinical efficacy and therapeutic trial for patients with neurodevelopmental disorders.

Past research has investigated the capacity of pharmacological compounds to rescue RTT pathophysiology using *in vivo* mouse models (Tang et al., 2019). Several recent studies highlight that despite general conservation, homologous human and mouse cell types exhibit extensive differences, including alterations in proportion, distribution, gene expression, and neurotransmission. Notably, the most different systems are glutamatergic, serotoninergic, and cholinergic (Hodge et al., 2019; Sjostedt et al., 2020). These species-specific features emphasize the lack of clinical translatability and the importance of directly studying human brain models. In addition, as was alluded to above, the safety of Nefiracetam and PHA

543613 have already been evaluated in animal models, and the safety of Nefiracetam has been demonstrated in human populations, being commercially available for human use (Foucault-Fruchard et al., 2018; Fujimaki et al., 1993; Robinson et al., 2009). We directly demonstrated the effects of these compounds in a human context with a variety of *MECP2*-KO human cell models. Our lab has shown that the most sophisticated of these models, cortical organoids, develop oscillatory activity similar to that observed during human fetal neurodevelopment (Trujillo et al., 2019). Due to the synaptic and network impairment resulting from MeCP2 deficiency, development of similar oscillatory activity likely occurs much later in *MECP2*-KO organoids, but documentation and characterization of such activity in future studies may reveal itself to be a useful biomarker in a clinical setting.

Previous research in human RTT neurons associated MeCP2 deficiency with a reduction in total RNA (Li et al., 2013), suggesting that increased synaptic expression following treatment may be secondary to increased total RNA. However, our transcriptional analyses showed reduced expression of genes concentrated in pathways relevant to synaptic function, and our process of screening synaptically targeted compounds retained only those that increased these deficient pathways in KO cells without affecting controls, suggesting that increased expression of synaptic genes is a primary effect of the targeted therapeutics. Regardless, MeCP2 deficiency causes a spectrum of severity of synaptic phenotypes, both between and within individuals, and it is this fact that encouraged our development of a cellular model of *MECP2* mosaicism. Our innovative human-based neural model of cellular mosaicism has clear utility for *MECP2* and other X-linked genetic disorders, and the concept can likewise be expanded to include other aspects of pharmacogenomic precision medicine, such as characterizing pharmacological response or variation in cytotoxicity for patients with

novel mutations. Furthermore, the impact of somatic mosaicism on clinical and neurodevelopmental phenotypes is becoming increasingly appreciated, so this human model will offer further utility for the study of somatic neuronal mosaicism in other neuropsychiatric diseases and human neurodevelopment in general (Lodato et al., 2015; McConnell et al., 2017).

Our study has several intrinsic limitations. One limitation is that, as a proof-of-concept study for our drug-screening platform, we tested only a restricted number of compounds. Because we selected candidate drugs such that their mechanisms of action were directed against the pathological alterations we had identified, any compounds not explicitly mentioning a desired action would have gone unconsidered. A future study employing a platform with similar complexity as ours but with high-throughput screening capability may identify additional efficacious compounds. A second limitation is that the drugs were administered during an early neurodevelopmental period, even in the cortical organoids (Camp et al., 2015; Luo et al., 2016; Trujillo et al., 2019), which may be challenging to assess in a clinical setting. Trial of these compounds in an expanded age range may help optimize their clinical utilization, aided by the fact that the control models were not significantly affected by treatment with these drugs.

As would be expected in any pharmacological context, the selected compounds were unable to fully reverse all MeCP2-deficient phenotypes. Although Nefiracetam and PHA 543613 increased the MEA network activity of *MECP2*-KO cortical organoids, they did not fully restore activity, suggesting other deficiencies also contribute to *MECP2*-KO network pathology, synaptic and otherwise, that must be investigated and targeted with other compounds. In addition, neither compound significantly increased calcium transient

amplitude in *MECP2*-mosaic neurospheres, but the compounds did increase their calcium transient frequency, a finding that aligns with our observation that Nefiracetam and PHA 543613 increased calcium transient frequency and activity in *MECP2*-KO neurons. The clinical implication of calcium frequency vs amplitude in *MECP2*-mosaic neurospheres is unclear and presents an important direction for future study, but the concordance of our findings between assays and models affirms our confidence in the compounds' effects. Neither compound, moreover, increased the proportion of CTIP2+ cells, a not unexpected result considering the drugs were selected to counteract synaptic pathology, not neuronal fate. It is unclear why populations of *MECP2*-KO monolayer neurons contained a smaller proportion of layer V/VI neurons. However, previous research has noted that these neurons are profoundly heterogeneous in their morphology, gene expression, axonal projection, and electrophysiological function and that *MECP2* may affect any of these parameters in a context- and region-specific manner (Stuss et al., 2012). It would be reasonable to expect that a smaller proportion of these neurons would reduce synaptic maturation and connectivity, but correcting the mechanism responsible for this deficit requires compounds whose function is not restricted to the synapse and may require intervention at an earlier timepoint. Treatment of diseases incident to MeCP2 deficiency may thus be improved with a combination of drugs, another reason to explore a more comprehensive array of compounds.

Despite the limitations, we believe the findings of our study warrant a pilot trial of Nefiracetam and/or PHA 543613 in a clinical setting of RTT or another disorder of MeCP2 deficiency. Our drug-screening platform was developed to facilitate clinical translatability. We used a series of increasingly complex human models with the final, cortical organoids, closely recapitulating *in vivo* human fetal neurodevelopment, and we eliminated drugs that

significantly affected controls to limit either clinical error or adverse clinical effects. Nefiracetam is already available for human use commercially, and it has undergone extensive safety testing in human populations (Fujimaki et al., 1993). Neurodevelopmental disorders caused by MeCP2 deficiency are severe and treatment options are limited or altogether unavailable, so our findings that Nefiracetam and PHA 543613 improve synaptic morphology, genetic expression, and network activity suggest that, for some patients, these pharmacological compounds may offer a meaningful clinical impact.

Materials and Methods

Generation of *MECP2*-KO cell lines and cell culture. Control PSCs were generated and characterized as previously described (Gore et al., 2011; Nageshappa et al., 2016; Trujillo et al., 2019). Of the two MeCP2-deficient PSC lines, one was generated via pluripotent induction of male patient-derived fibroblasts as described (Marchetto et al., 2010), and the other was created via CRISPR/Cas9 introduction of a frameshift mutation into the *MECP2* locus of H9 hESCs (Thomas et al., 2017), creating an early stop codon and non-functional MeCP2. We used exome sequencing to confirm mutagenesis and analyze off-target effects. PSC colonies were maintained on Matrigel-coated dishes (BD-Biosciences, San Jose, CA, USA) and fed daily with mTeSR1 (StemCell Technologies, Vancouver, Canada) as we have previously described (Chailangkarn et al., 2016); only mycoplasma-negative cell cultures were used. Cells were evaluated by karyotype and CNV arrays to detect genomic alteration. Informed consent was obtained from all human subjects, and experiments conformed to the principles set forth in the WMA Declaration of Helsinki and the Department of Health and

Human Services Belmont Report. The study was approved by the UCSD IRB/ESCRO committee (protocol 141223ZF).

Karyotyping. Molecular Diagnostics Service (San Diego, CA, USA) performed G-banding karyotyping analyses.

Teratoma assay. PSC colonies were dissociated, centrifuged, resuspended in 1:1 Matrigel:PBS, and subcutaneously injected into nude mice. Teratomas were excised, fixed, and sliced after 1-2 months, and sections were stained with H&E. Protocols were previously approved by the UCSD Institutional Animal Care and Use Committee.

Neuronal differentiation of PSCs. Differentiation was performed as previously described (Chailangkarn et al., 2016). After seven days, mTeSR1 used to feed PSCs was replaced with N2 medium [DMEM/F12 (Life Technologies, Carlsbad, CA, USA), 0.5x N2 (Life Technologies), 1% penicillin/streptomycin (P/S; Life Technologies), 1μM Dorsomorphin (Dorso; R&D Systems, Minneapolis, MN, USA), and 10μM SB431542 (SB; Stemgent, Cambridge, MA, USA)] for 1-2 days, after which embryoid bodies (EBs) were formed by scraping PSC colonies and culturing them in shaker suspension (95 rpm at 37°C) for eight days. EBs were dissociated and plated on a Matrigel-coated dish in N2B27 medium [N2 medium with 0.5x B27-Supplement (Life Technologies) and 20 ng/mL FGF-2]. Emerging rosettes were picked manually, dissociated in Accutase (Life Technologies), and seeded on poly-L-ornithine/laminin plates. Emergent NPCs were expanded and maintained in N2B27 medium with feeding on alternate days; all NPCs used for neurons were passage 5-20. FGF-2

was withdrawn from the medium to induce neuronal differentiation, considered Day 0 of differentiation.

Calcium imaging in monolayer neurons. Calcium imaging was performed as described (Chailangkarn et al., 2016). Briefly, PSC-derived neuronal networks were transduced a lentivirus Syn::RFP reporter construct. Cultures were washed with Krebs HEPES buffer and incubated with Fluo-4AM (Molecular Probes/Invitrogen, Carlsbad, CA, USA). A Hamamatsu ORCA-ER digital camera (Hamamatsu Photonics, Japan) with 488 nm filter on an Olympus IX81 inverted fluorescence confocal microscope (Olympus Optical, Tokyo, Japan) acquired 5000 frames at 28Hz in a 256 x 256-pixel region (100x magnification). Images were acquired with MetaMorph7.7 (MDS Analytical Technologies, Sunnyvale, CA, USA) and analyzed using ImageJ and Matlab7.2 (Mathworks, Natick, MA, USA) using *PeakCaller* script. A 95^{th}-percentile threshold of amplitude for calcium spikes was set for event detection; signal amplitude is presented as fluorescence change ($\Delta F/F$) following background subtraction.

***MECP2*-mosaic neurospheres.** StemoniX, Inc. provided human *MECP2*-mosaic cortical neural spheroids as customized microBrain®3D Assay Ready 384-Plates (Sirenko et al., 2019). Briefly, each well of a 384-well plate contained a single, free-floating human PSC-derived neurosphere, comprised of a balanced culture of cortical neurons and astrocytes generated from a 50/50 mixture of NPCs obtained from a male patient with Rett syndrome (Q83X mutation in the *MECP2* gene) and its sex-matched parental control. Four-week-old neurospheres were treated with Nefiracetam (0.1, 1, or 10μM), PHA 543613 (0.1, 1, or 10μM), or a combination of both, for an additional four weeks. Bright-field images of the

neurospheres were taken using an Image Xpress Micro Confocal High-Content Imaging System (Molecular Devices LLC, San Jose, CA, USA) and the size measured using an automated plug-in in the MetaMorph Microscopy Automation and Imaging Analysis Software (Molecular Devices LLC).

Calcium transients assay in neurospheres. Intracellular Ca^{2+} transients of *MECP2*-KO, *MECP2*-mosaic, and control neurospheres were measured using a fluorescence-based assay, as previously described (Sirenko et al., 2019). Briefly, eight weeks after differentiation, neurospheres were incubated with FLIPR Calcium-6 dye for two hours at 37°C, 5% CO_2. Next, the cultures were transferred to a FLIPR Tetra High-Throughput Cellular Screening System (Molecular Devices LLC) to determine the kinetics of intracellular Ca^{2+} transients. With the instrument at 37°C, the recording was performed for 10 minutes at a frequency of 2Hz, exposure time per read of 0.4s, excitation intensity of 40%, and with the gain set to 30. The analysis was performed using ScreenWorks Peak Pro (4.2) software package (Molecular Devices LLC) and included the quantitative evaluation of transient peak count and average transient peak amplitude (Sirenko et al., 2019). A 95^{th}-percentile threshold of amplitude for calcium spikes was set for event detection; signal amplitude is presented as fluorescence change ($\Delta F/F$) following background subtraction.

Cell viability assay in neurospheres. The viability of neurospheres after eight weeks of differentiation, untreated and treated with Nefiracetam and/or PHA 543613, was established using the CellTiter-Glo 3D Viability Assay (Promega, Madison, WI, USA), according to the manufacturer instructions. Briefly, a CellTiter-Glo 3D Reagent volume equal to the volume of

media present in each well was added to the neurospheres. After mixing vigorously for five minutes to promote cell lysis, the plate was incubated for 25 additional minutes at room temperature. The luminescence signal was recorded using a PHERAstar FSX plate reader (BMG Labtech Inc., Cary, NC, USA).

Generation of cortical organoids. Cortical organoids were generated as previously described (Trujillo et al., 2019). Briefly, PSCs cultured for approximately seven days were dissociated with 1:1 Accutase (Life Technologies):PBS, and cells were plated into a 6-well plate ($4x10^6$ cells/well) in mTeSR1 supplemented with 10 μM SB (Stemgent), 1 μM Dorso (R&D Systems), and 5μM Y-27632 (EMD-Millipore, Burlington, MA, USA) and cultured hereafter in shaker suspension (95 rpm at 37°C). Formed spheres were fed mTeSR1 (with 10 μM SB and 1 μM Dorso) for three days followed by Media1 [Neurobasal (Life Technologies), 1x Glutamax (Life Technologies), 2% Gem21-NeuroPlex (Gemini Bio-Products, Sacramento, CA, USA), 1% N2-NeuroPlex (Gemini Bio-Products), 1% non-essential amino acids (NEAA; Life Technologies), 1% P/S (Life Technologies), 10 μM SB, and 1 μM Dorso] for six days, every other day; Media2 (Neurobasal, 1x Glutamax, 2% Gem21, 1% NEAA, and 1% P/S) with 20 ng/mL FGF-2 (Life Technologies) for seven days, daily; Media2 with 20 ng/mL each of FGF-2 and EGF (PeproTech, Rocky Hill, NJ, USA) for six days, every other day; and Media2 with 10 ng/mL each of BDNF, GDNF, and NT-3 (all PeproTech), 200 μM L-ascorbic acid (Sigma-Aldrich, St. Louis, MO, USA), and 1 mM dibutyryl-cAMP (Sigma-Aldrich) for six days, every other day. Cortical organoids were subsequently maintained indefinitely in Media2 without supplementation.

Pharmacological treatment. One-month old neurons were treated for two weeks at the drug concentrations listed in Fig 2B. Neurospheres were treated as detailed above. One-month old cortical organoids were treated for one month with either Nefiracetam (1 µM) or PHA 543613 (1 µM) during every-other-day media changes. The concentration of the drugs was selected based on the specific K_d reported for each drug and from previous work on animal models and human neurons. The time points were strategically selected after we observed a cellular or functional phenotype in *MECP2*-KO neurons. Based on published work from our group, *MECP2*-KO neurons and neurospheres already show a distinct deficit after 4 weeks.

RNA extraction and RT-PCR array. RNA was extracted using a RNeasy Mini Kit (Qiagen, Hilden, Germany) according to the manufacturer's instructions. DNase-treated RNA was assessed with a NanoDrop1000 (ThermoScientific, Waltham, MA, USA). Total RNA was converted to cDNA and evaluated for RT-PCR array per the manufacturer's instructions (Qiagen, Hilden, Germany).

Single-cell qRT–PCR. Single-Cell and BioMark HD Systems (Fluidigm, San Francisco, CA, USA) were used for specific target amplification in NPCs, neurons, and organoids as described (Chailangkarn et al., 2016; Trujillo et al., 2019). Briefly, single cells were captured on a C1 chip, and a LIVE/DEAD Cell Viability/Cytotoxicity kit (Life Technologies) was used to assess viability. DELTAgene primer pairs (96.96 Dynamic Array IFC chip) were used for single-cell qPCR; results analysis was performed using Fluidigm Real-time PCR Analysis Software and Singular Analysis Toolset 3.0.

RNA sequencing analyses. A RNeasy Mini kit (Qiagen) was used to isolate RNA for library preparation (Illumina TruSeq RNA Sample Preparation Kit; San Diego, CA, USA) and sequencing (Illumina HiSeq2000, 50bp paired-end reads, 50 million high-quality sequencing fragments per sample, on average). Data was analyzed by Rosalind (https://rosalind.onramp.bio/), with a HyperScale architecture (OnRamp BioInformatics, Inc., San Diego, CA). Reads were trimmed using cutadapt, quality scores were assessed using FastQC, and reads were aligned to the *Homo sapiens* genome build hg19 using STAR. Individual sample reads were quantified using HTseq and normalized via Relative Log Expression using DESeq2 R library. DEseq2 was also used to calculate fold changes and p-values and perform optional covariate correction. Gene clustering of differentially expressed genes was done using the Partitioning Around Medoids method using the fpc R library. Functional enrichment analysis of pathways, gene ontology, domain structure, and other ontologies was performed using several databases (HOMER, Interpro, NCBI, MSigDB, REACTOME, WikiPathways).

Gene ontology (GO). RNA sequencing enrichment was performed with the WebGestalt (B. Zhang et al., 2005) and Cytoscape (Shannon et al., 2003) plug-ins utilizing statistically significant categories ($P < 0.05$). Genes evaluated for differential expression set the background for GO annotation and enrichment analysis.

Immunofluorescence of cells and cortical organoids. Immunofluorescence was performed as previously described (Chailangkarn et al., 2016; Trujillo et al., 2019). Cells were fixed in 4% paraformaldehyde, washed three times with PBS (5min each), and permeabilized/blocked (0.1% Triton X-100 and 2% BSA in PBS). Cortical organoids were fixed overnight in 4% paraformaldehyde and then transferred to 30% sucrose, sunken, embedded in O.C.T. (Sakura,

Tokyo, Japan), and cryostat-sectioned at 20 µm. Slides with organoid sections were air-dried and then permeabilized/blocked (0.1% Triton X-100 and 3% FBS in PBS). Primary antibodies (goat anti-Nanog, Abcam (Cambridge, UK) ab77095, 1:500; rabbit anti-Lin28, Abcam ab46020, 1:500; mouse anti-MeCP2, Sigma-Aldrich M7443, 1:500; rabbit anti-Oct4, Abcam ab19857, 1:500; mouse anti-Nestin, Abcam ab22035, 1:200 (organoid: 1:250); rat anti-CTIP2, Abcam ab18465, 1:250 (organoid: 1:500); rabbit anti-SATB2, Abcam ab34735, 1:200; chicken anti-MAP2, Abcam ab5392, 1:1000 (organoid: 1:2000); rabbit anti-Synapsin1, EMD-Millipore AB1543P, 1:500; mouse anti-Vglut1, Synaptic Systems (Goettingen, Germany) 135311, 1:500; rabbit anti-Homer1, Synaptic Systems 160003, 1:500; mouse anti-NeuN, EMD-Millipore MAB377, 1:500; rabbit anti-Ki67, Abcam ab15580, 1:1000; rabbit anti-SOX2, Cell Signaling Technology (Danvers, MA, USA) 2748, 1:500; rabbit anti-GFAP, DAKO (Carpinteria, CA, USA) Z033429, 1:1000; rabbit anti-TBR1, Abcam ab31940, 1:500; rabbit anti-TBR2, Abcam ab23345, 1:500; rabbit anti-beta-catenin, Abcam E247, 1:200; mouse anti-GABA, Abcam ab86186, 1:200; rabbit anti-PROX1, Abcam ab101651, 1:250) in blocking buffer incubated overnight at 4°C. Slides were washed three times with PBS (5min each) and incubated with secondary antibodies (Alexa Fluor 488, 555, and 647, Life Technologies, 1:1000 in blocking buffer). Nuclei were stained with DAPI (1:10,000). Slides were mounted with ProLong Gold anti-fade mountant (Life Technologies) and analyzed with a Z1 Axio Observer Apotome fluorescence microscope (Zeiss, Oberkochen, Germany).

Artificial neural network simulations. Simulations of neural network activity were done with artificial recurrent neural networks using biologically plausible parameter choices, defined by five free parameters: number of neurons in the network (N), connection sparsity or

percent connectivity (p_{con}), percentage of inhibitory vs excitatory neurons (p_{inh}), synaptic weights (W), and synaptic decay time constants of the neurons (τ). A network size of $N = 512$ neurons was used; simulations performed with larger and smaller network sizes yielded qualitatively similar results. Percent connectivity (p_{con}) refers to the percentage of all possible pairwise connections in the network for which a connection was present (non-zero entry in W). Our networks followed Dale's Law, which states that any given neuron is either excitatory or inhibitory. For each simulation, an excitatory-inhibitory balance was chosen determining the percent of inhibitory neurons (p_{inh}).

Our artificial neural network implementation was similar to the continuous rate networks outlined in Kim et al. (2019). Briefly, each simulated network consisted of a pool of neurons that could be connected to any other neuron in the pool. Each neuron received weighted input from other neurons and integrated these inputs to produce a firing rate. The network dynamics are governed by the equation:

$$\boldsymbol{\tau}\frac{d\boldsymbol{x}}{dt} = -\boldsymbol{x} + W\boldsymbol{r} \qquad (1)$$

where $\boldsymbol{\tau} \in \mathbb{R}^{1\times N}$ is the synaptic decay time constant for the N neurons in the network, $\boldsymbol{x} \in \mathbb{R}^{1\times N}$ is the synaptic current variable, $W \in \mathbb{R}^{N\times N}$ is the matrix of synaptic weights between all N neurons, and $\boldsymbol{r} \in \mathbb{R}^{1\times N}$ is the output firing rates. The output firing rate is given by an element-wise nonlinear transformation of the synaptic current variable. We used the standard logistic sigmoid function per Kim et al. (2019):

$$\boldsymbol{r} = \frac{1}{1+\exp(-x)} \qquad (2)$$

The synaptic connectivity matrix W was randomly initialized from a normal distribution with mean of zero and standard deviation of $g/\sqrt{N \cdot p_{con}}$, where g is the gain term. We set $g = 15$ because previous studies have shown that networks operating in a high gain regime ($g \geq 1.5$)

support rich dynamics analogous to those of biological networks (Kim et al., 2019; Laje & Buonomano, 2013). Synaptic decay time constants were randomly initialized to a value in the biologically plausible range of 20-100ms. As in Kim et al. (2019), we used the first-order Euler approximation method to discretize equation (1) for the simulations.

To vary synaptic knockdown or strengthening, we introduced a synaptic weight scaling factor, p_{KD}. Based on Marchetto et al. (2010), synaptic strength was decreased in a PSC model of RTT, particularly for excitatory neurons, so we perturbed the synaptic strength of excitatory synaptic connections only. To model synaptic knockdown or strengthening we multiplied the excitatory synaptic weights by p_{KD}. Each network simulation was generated with randomly initialized synaptic weights and synaptic time constants, as described above, and then run for 200-time steps (one time step simulates 5ms). For each parameter combination, $[p_{con}, p_{inh}, p_{KD}]$, 100 independent simulations were run, and the average of all neurons' firing rates on the last time step was taken from each simulation as a measure of network activity. We then took the average network activity across all 100 simulations as an estimate for the network activity for the given set of parameters. For every $[p_{con}, p_{inh}]$ pair we ran simulations for the p_{KD} values of interest as well as a "control" network for which $p_{KD} = 1$ (i.e., no synaptic scaling was applied). All measures of network activity were normalized to that of the corresponding control network to obtain the relative network activity.

To create the relative activity surface plots we ran the simulations described above for all networks with $p_{con} \in \{1e-5, 0.05, 0.1, 0.15, \ldots, 0.95, 1.0\}$ and $p_{inh} \in \{0.0, 0.05, 0.1, \ldots, 0.95, 1.0\}$, representing 441 $[p_{con}, p_{inh}]$ pairs tiling the possible space of network connectivity and excitatory-inhibitory balance. Simulations across this space

were run for each of the synaptic perturbation conditions taken from Marchetto et al. (2010): RTT-like synaptic knockdown ($p_{KD} = 0.375$), IGF-1-like synaptic improvement ($p_{KD} = 1.5$), and control ($p_{KD} = 1$). A minimum value of $p_{con} = 1e-5$ was used because p_{con} must be greater than zero to calculate the standard deviation of the random initialization distribution for the synaptic weights, as described above.

Western blotting. Cells were lysed in RIPA buffer with protease inhibitor and total protein was extracted and quantified (Pierce BCA Protein Assay Kit, ThermoScientific). Total protein (20µg) was separated using a Bolt 4–12% Bis-Tris Plus Gel (Life Technologies) and transferred to a nitrocellulose membrane using an iBlot2 dry blotting system (ThermoScientific). Membranes were blocked for 1-4 hours (Rockland Immunochemicals, VWR International, Arlington Heights, IL, USA); primary antibodies (rabbit anti-Synapsin1, EMD-Millipore AB1543P, 1:1500; mouse anti-PSD-95, Neuromab, 1:1500; chicken anti-MAP2, Abcam ab5392, 1:2000; rabbit anti-GFAP, DAKO Z033429, 1:2000) in blocking buffer incubated, shaking, overnight at 4°C and secondary antibodies (IRDye 680RD and IRDye 800CW, 1:5000 in blocking buffer) for one hour at room temperature. Proteins were detected by an Odyssey CLx infrared imaging system (LiCOR Biosciences, Lincoln, NE, USA), and semi-quantitative analysis of signal intensity was corrected to the relative quantification of β-actin.

Synaptic puncta quantification. Co-localized Vglut1 (presynaptic) and Homer1 (postsynaptic) immunostained puncta along MAP2-positive processes were quantified as described (Nageshappa et al., 2016). Primary antibodies incubated two hours, secondary antibodies incubated one hour, and coverslips were mounted; see above for complete

immunofluorescence methodology. The slides were imaged using a Z1 Axio Observer Apotome fluorescence microscope (Zeiss), and a blinded investigator manually quantified co-localized synaptic puncta along 50 μm segments of randomly selected MAP2-positive processes (7-8 per condition); for quantification, no distinction was made between proximal and distal segments.

Analysis of spine density, stability, and motility. pHIV7/Syn-EGFP lentivirus was prepared by transfecting HEK cells using the transfection agent polyethylenimine (Polysciences, Inc., Warrington, PA, USA), Syn-EGFP, and packaging plasmids pMDL, Rev RSV, and VSVG. Control and *MECP2*-KO neurons were transduced with pHIV7/Syn-EGFP on day 40 of differentiation and allowed to further differentiate until day 70, after which they were fixed with 4% paraformaldehyde, and processed for imaging. Confocal images were obtained using a confocal laser-scanning microscope (Nikon, 60x oil) and sequential acquisition setting at a resolution of 4096 × 4096 pixels. Each image is a Z-series projection of ~7 to 15 images, averaged twice and taken at 0.5μm depth intervals. GFP-labeled differentiated neurons were chosen randomly for quantification. Dendrites on primary branches were selected randomly, and two to three segments of 10μm were analyzed for each neuron. Morphometric measurements were performed manually using the ImageJ software, and dendritic spines were manually traced by a blinded investigator. Nuclei size was manually measured using ImageJ.

Analysis of neuronal morphology. PSC-derived neuronal morphometry was performed as previously described (Chailangkarn et al., 2016). Neurons with branching neurites featuring dendritic spine-like protrusions were randomly selected, and neuronal morphology was quantified using Neurolucida v9 (MBF Bioscience, Williston, VT) via Nikon Eclipse E600 microscope (40x oil). Measurements were as follows: spine number: number of spines

protruding from neurites; soma size: soma area on cross-section; spine length: summed length of all spines per neuron. The rater traced the same neuron after to ensure intra-rater reliability.

Multi-electrode array (MEA) analysis. MEA analyses of neurons and cortical organoids were performed as described (Nageshappa et al., 2016; Trujillo et al., 2019). Briefly, neurospheres were plated on dual-chamber MEA; spontaneous spike activity was evaluated with the MED64 System (Panasonic). Glutamatergic (AP5, NBQX), GABAergic (Gabazine), and gap channel (Mefloquine) antagonism were used to verify neuronal activity. Recorded spikes were analyzed using the Neuroexplorer software (Nex Technologies, Madison, AL, USA). For cortical organoids, one-month old organoids were plated on MEA plates and recordings were collected with a Maestro MEA system and AxIS Software Spontaneous Neural Configuration (Axion Biosystems, Atlanta, GA, USA). The plate was incubated in the machine for three minutes before five minutes of recording. Axion Biosystems's Neural Metrics Tool classified as "active" those electrodes with at least five spikes/minute. Bursts were identified using an inter-spike interval (ISI) threshold requiring a 5-spike minimum and 100ms maximum ISI. Network bursts required a minimum of 10 spikes under the same ISI and at least 25% active electrodes.

Statistical analysis. Statistical analyses were performed using GraphPad Prism (GraphPad Software, La Jolla, CA), except the *in silico* neural network model, the procedure for which is detailed above. Sample sizes were determined based on previous publications from this lab and others. Experiments were performed in at least three independent replicates and different cell lines; experiment-specific information is detailed in the figure legends. Samples were

allocated and evaluated according to genotype; no randomization was applied. Analyses of synaptic puncta and dendritic spine tracing were made blinded. Data exclusion in MEA datasets (outliers) was carried out automatically using pre-established criteria as described above. Outliers in other experiments were determined using GraphPad criteria and excluded. Results for continuous variables were expressed as mean ± standard error of the mean and 95% confidence intervals were normal-based. Normality was assessed visually, and variance was accounted for in all analyses. Means for continuous variables were compared between groups using, where appropriate, unpaired Student's *t*-test, one-way, or two-way analyses of variance, and nonparametric distributions were compared using Kruskal-Wallis test. Tests were performed two-sided with α throughout set as 0.05.

Data availability. All data, computational coding, and/or analyses generated during the current study are available from the corresponding authors upon reasonable request.

The paper explained

Problem

The X-linked gene *MECP2* encodes an epigenetic regulatory protein that is critical for typical human brain development. *MECP2* deficiency causes severe neurodevelopmental impairment that clinically presents most commonly as Rett syndrome. However, despite pinpointing the genetic disruption and the eminent treatability of the disease, no clinically approved treatments for Rett syndrome are currently available.

Results

By establishing an innovative drug-screening pipeline using human pluripotent stem cells differentiated into neurons, *MECP2*-mosaic neurospheres, and cortical organoids, we

isolated two lead compounds that specifically reversed synaptic and network pathology resulting from *MECP2* deficiency while leaving controls unaffected. The two compounds, Nefiracetam and PHA 543613, improved synaptic morphology and function in *MECP2*-KO human neurons, increased calcium activity in *MECP2*-mosaic neurospheres, and reversed synaptic transcriptomic pathways and neural network function in *MECP2*-KO cortical organoids.

Impact

MECP2 deficiency causes profound neurodevelopmental impairment that urgently demands treatment. This study identified two pharmacological lead compounds, one of which has already been approved for human use commercially, that could specifically reverse *MECP2*-KO neurocytopathology in human cell models. These compounds may offer meaningful clinical impact for some patients with severe neurodevelopmental impairment resulting from *MECP2* deficiency, and trial in a clinical setting is warranted following regulatory approval.

Extended View Figures

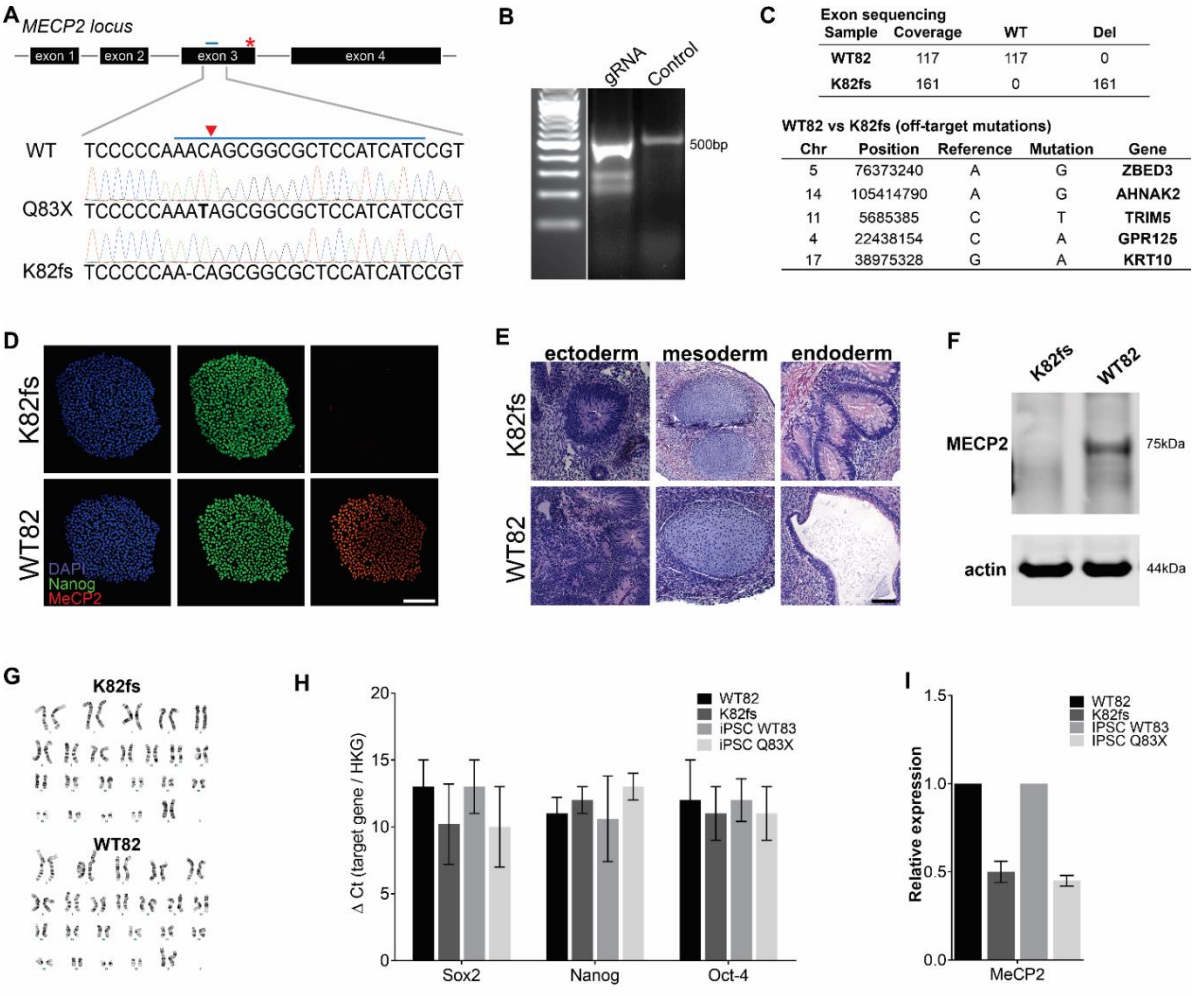

Figure 14: Generation of *MECP2*-KO pluripotent stem cells. A Mutations resulting in loss of functional MeCP2 protein shown by Sanger sequencing. CRISPR guide RNA is depicted as a blue bar over WT sequence and the cut site as a red triangle. **B** CRISPR guide RNA to generate K82 frameshift mutation. **C** Identification of off-target mutations by exome sequencing. **D-I** *MECP2*-KO was successfully generated and did not affect pluripotency, as confirmed by immunochemistry (**D**), teratoma assay (**E**), Western blot (**F**), karyotype (**G**), and RT-qPCR (**H, I**). Scale bar = 200 µm.

Figure 15: *MECP2*-KO neurons exhibit defects in spine-like morphology. A Schematic showing neuronal differentiation from human PSCs. Scale bar = 200 µm. **B** Neuronal markers immunostaining of 28-days *MECP2*-KO and control neurons. **C** No difference in the resultant proportions of neurons or glia was observed between 28-days *MECP2*-KO and control neural differentiations. Similar results were observed for the proportions of glutamatergic and GABAergic neurons. **D** 28-days *MECP2*-KO neurons had decreased soma area and spine number (WT83/Q83X cell lines were used*; N* = 13 neurons per genotype, t_{24} = 5.03, **P* < 0.05). Scale bar = 20 µm. **E** Observation over time showed decreased spine stability (**P* < 0.01), but spine motility (**P* = 0.17), spine formation (*P* = 0.26), and spine length (*P* = 0.28) were unchanged in *MECP2*-KO neurons. Scale bar = 5 µm. WT83/Q83X cell lines were used. Analyses were two-sided Student's *t*-tests. Data information: Data are presented as mean ± s.e.m.

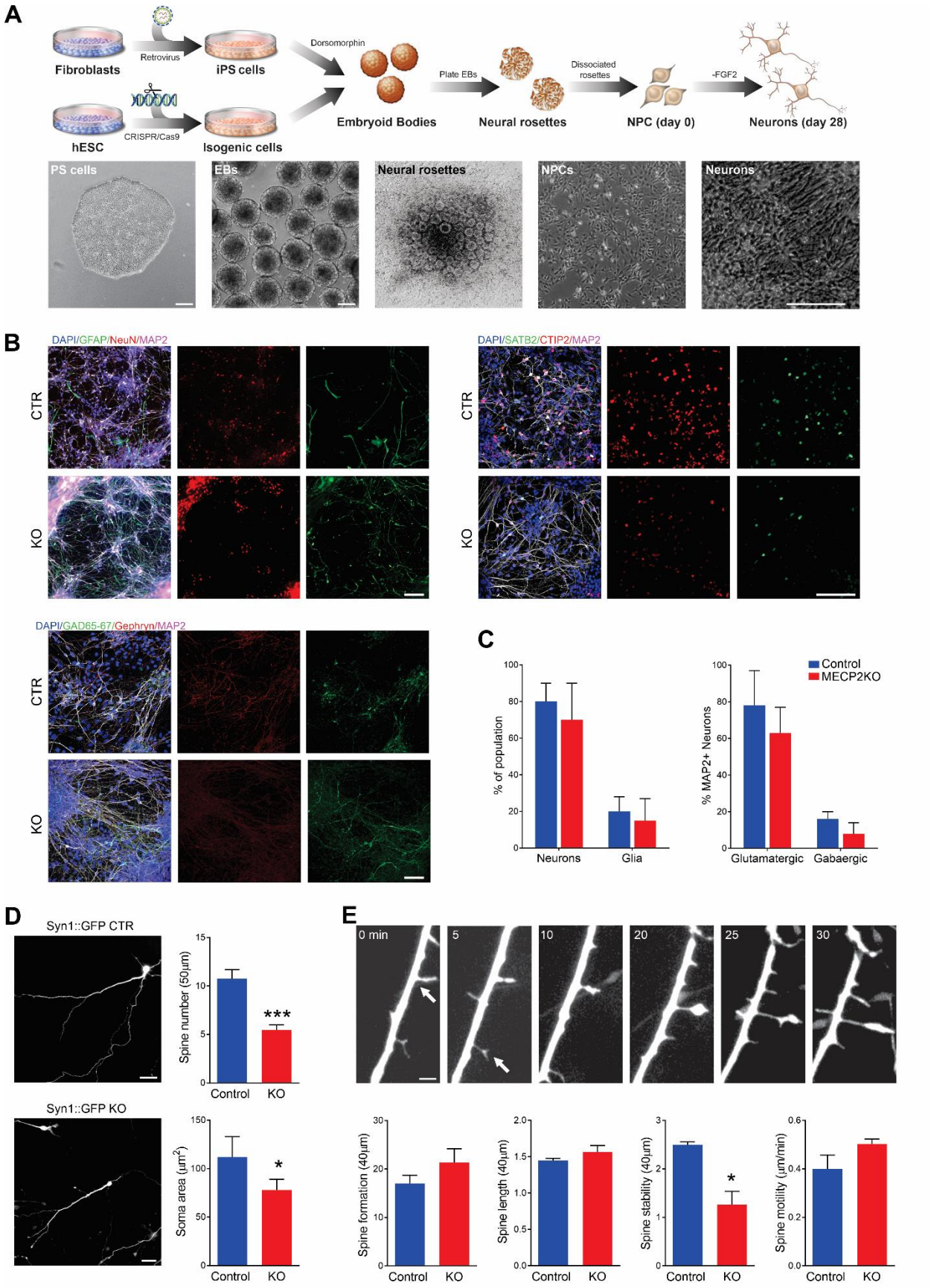
A
Fibroblasts
Retrovirus
iPS cells
hESC
CRISPR/Cas9
Isogenic cells
Dorsomorphin
Embryoid Bodies
Plate EBs
Neural rosettes
Dissociated rosettes
NPC (day 0)
-FGF2
Neurons (day 28)
PS cells
EBs
Neural rosettes
NPCs
Neurons
B
DAPI/GFAP/NeuN/MAP2
DAPI/SATB2/CTIP2/MAP2
DAPI/GAD65-67/Gephryn/MAP2
CTR
KO
C
% of population
Neurons
Glia
% MAP2+ Neurons
Control
MECP2KO
Glutamatergic
Gabaergic
D
Syn1::GFP CTR
Syn1::GFP KO
Spine number (50µm)
Soma area (µm²)
Control
KO
E
0 min
5
10
20
25
30
Spine formation (40µm)
Spine length (40µm)
Spine stability (40µm)
Spine motility (µm/min)

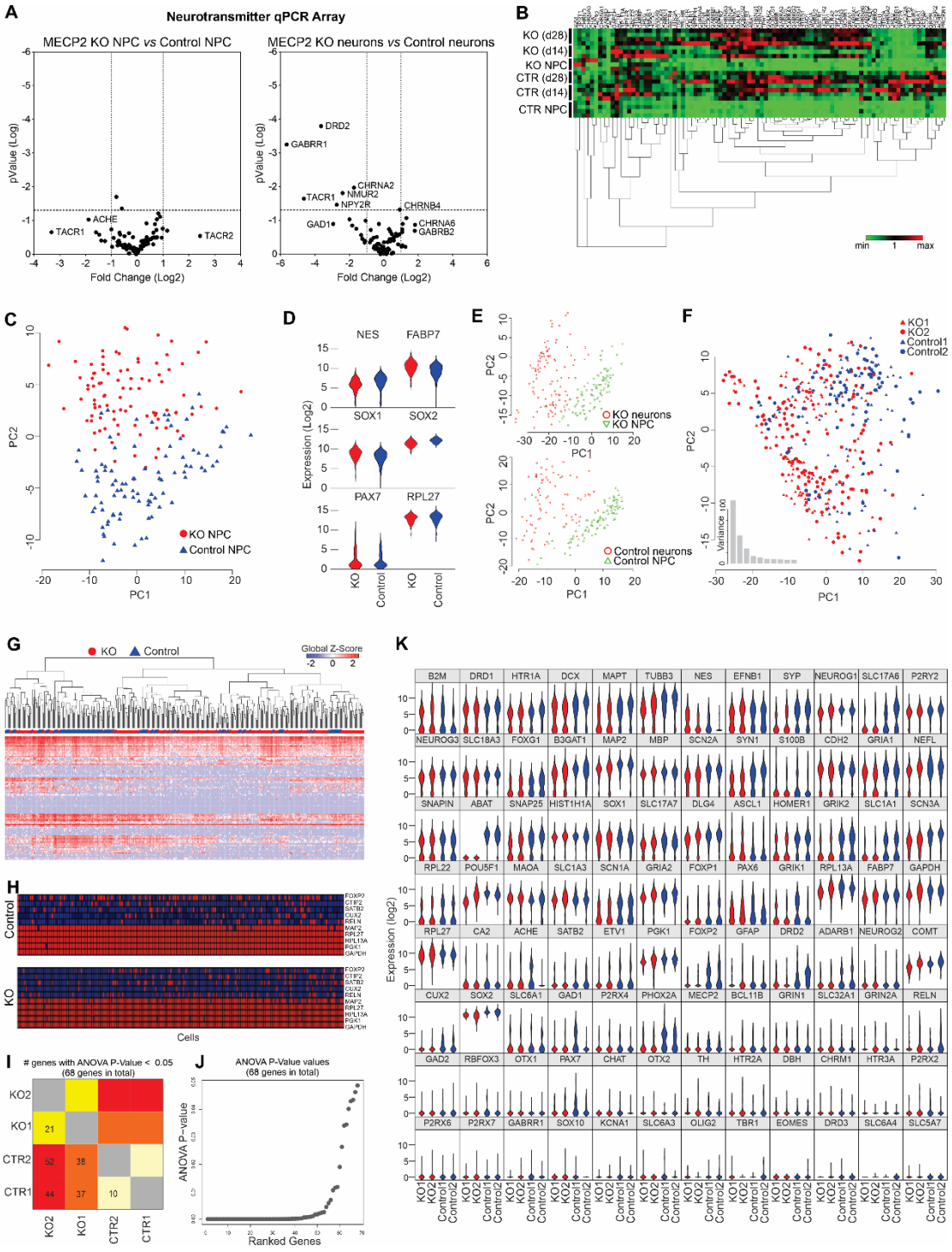

Figure 16: RT-PCR array and single-cell RT-qPCR analyses. A, B RT-PCR array revealed that differences in genetic expression showed variation between control and *MECP2*-KO NPCs and neurons, as depicted on volcano plots (**A**) and heatmap (**B**). **C-K** Single-cell RT-qPCR analysis likewise showed differences in gene expression throughout neuronal differentiation due to *MECP2*-KO that appear to involve synaptic function. 28-days WT83/Q83X and WT82/K82fs neurons were used.

Figure 17: Drug treatment of *MECP2*-KO and control neurons. A Representative Western blot images after *MECP2*-KO drug treatment. Samples run at the same time in different gels. **B** Analysis of treatment effect on quantities of the astrocytic marker GFAP and neuronal marker MAP2. **C** Full depiction of synaptic puncta following drug treatment. Scale bar = 5 µm. **D** Synaptic puncta co-localization following drug treatment of 6-week control neurons (WT83/Q83X cell lines were used; N = 8 neurons per condition; one-way ANOVA, $F_{6,49}$ = 10.94, *P < 0.05). Z scores of control untreated vs compound: Nefiracetam = 1.010; PHA 543613 = 0.282; Acamprosate = 0.175; GR73632 = 1.010; IGF-1 = 3.231; Hyperforin = 2.639). **E, F** Calcium imaging showed increasing spike frequency with time (**E**) that was tractable to manipulators of synaptic function (**F**). **G** Representative image of MEA activity of control and *MECP2*-KO neurons. Data information: Data are presented as mean ± s.e.m.

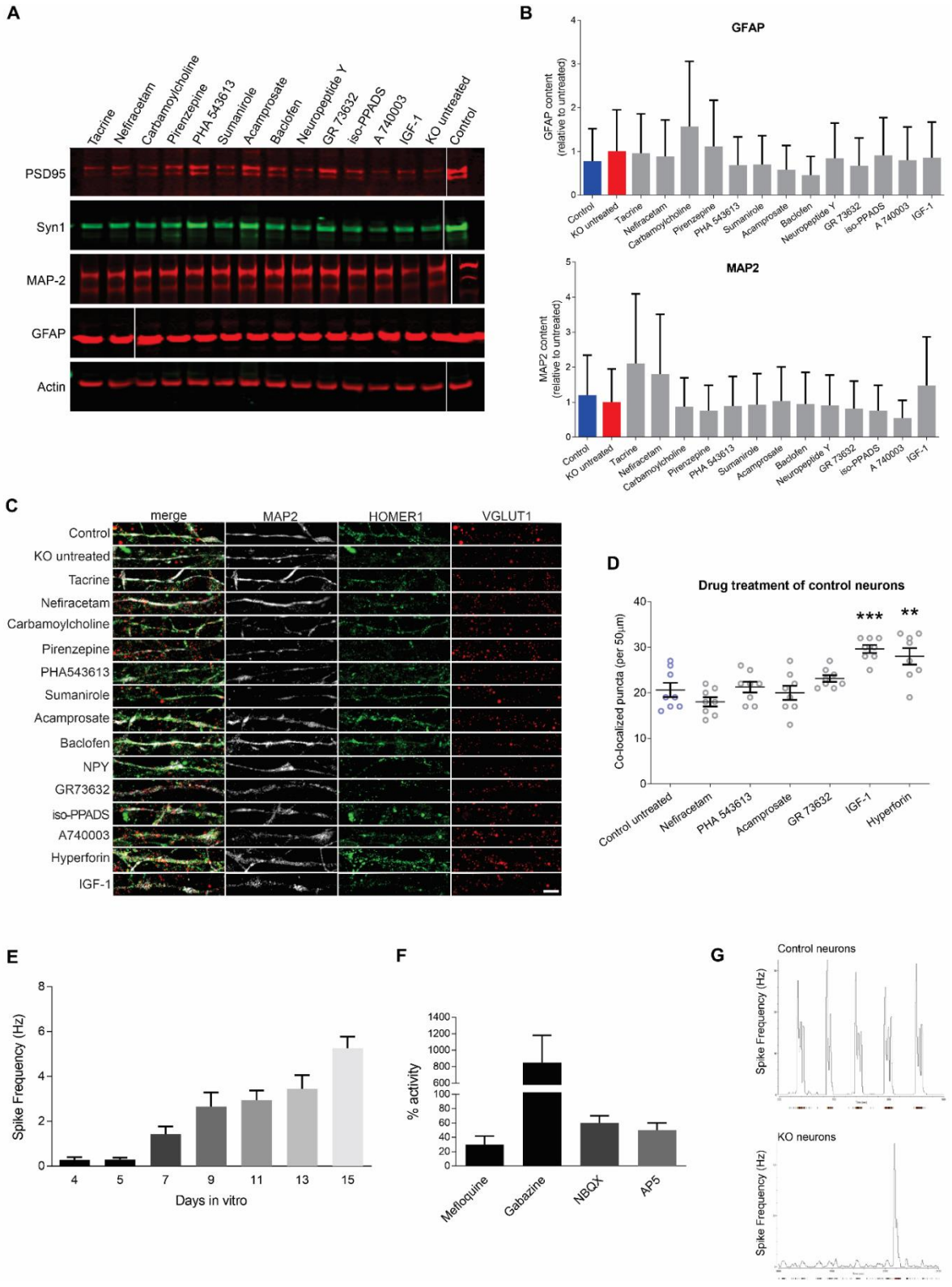
A
Tacrine
Nefiracetam
Carbamoylcholine
Pirenzepine
PHA 543613
Sumanirole
Acamprosate
Baclofen
Neuropeptide Y
GR 73632
iso-PPADS
A 740003
IGF-1
KO untreated
Control
PSD95
Syn1
MAP-2
GFAP
Actin
B
GFAP
GFAP content (relative to untreated)
MAP2
MAP2 content (relative to untreated)
C
merge
MAP2
HOMER1
VGLUT1
Control
KO untreated
Tacrine
Nefiracetam
Carbamoylcholine
Pirenzepine
PHA543613
Sumanirole
Acamprosate
Baclofen
NPY
GR73632
iso-PPADS
A740003
Hyperforin
IGF-1
D
Drug treatment of control neurons
Co-localized puncta (per 50µm)
***
**
Control untreated
Nefiracetam
PHA 543613
Acamprosate
GR 73632
IGF-1
Hyperforin
E
Spike Frequency (Hz)
Days in vitro
F
% activity
Mefloquine
Gabazine
NBQX
AP5
G
Control neurons
KO neurons
Spike Frequency (Hz)

Figure 18: Cellular and molecular characterization of human cortical organoids. A Schematic of the protocol used to generate cortical organoids. Scale bar = 200 μm. **B** Reproducibility of organoid size at 3 weeks of maturation (*N = 20* independent experiment, 7 different cell lines). **C, D** Gene expression of specific neurotransmission markers of treated vs untreated cortical organoids. **E, F** Representative images of quantification of Synapsin1 puncta. Scale bar = 50 μm. SYN1 puncta mask was made using ImageJ to access the number and area of the puncta**. G** Nefiracetam and PHA 543613 treatment did not rescue *MECP2*-KO neuronal morphology, for either the number of neurites (Kruskall-Wallis test, $P = 0.011$; Dunn's multiple comparisons test vs KO untreated: control, $P = 0.01$ and $Z = 3.13$; Nefiracetam, $P = 0.49$ and $Z = 1.74$; PHA 543613, $P > 0.99$ and $Z = 0.87$; WT83/Q83X and WT82/K82fs cell lines; N = 5-10 neurons per condition) or the total neurite length (one-way ANOVA, $F_{3,21} = 9.62$, $P = 0.0003$; Dunnett's multiple comparisons test vs KO untreated: control, $P = 0.002$ and $Z = 3.08$; Nefiracetam, $P = 0.89$ and $Z = 0.64$; PHA 543613, $P = 0.99$ and $Z = 0.17$; WT83/Q83X and WT82/K82fs cell lines; N = 5-10 neurons per condition) and, nearly uniformly, did not rescue nuclei size in neurons (one-way ANOVA, $F_{3,221} = 26.04$, $P < 0.0001$; Dunnett's multiple comparisons test vs KO untreated: control, $P < 0.0001$ and $Z = 6.37$; Nefiracetam, $P = 0.91$ and $Z = 0.39$; PHA 543613, $P = 0.19$ and $Z = 1.74$; WT83/Q83X and WT82/K82fs cell lines; N = 45 nuclei per condition), neurospheres (one-way ANOVA, $F_{5,264} = 5.579$, $P < 0.0001$; Dunnett's multiple comparisons test vs CTR/KO untreated: control, $P < 0.0001$ and $Z = 3.782$; KO untreated, $P = 0.51$ and $Z = 1.066$; Nefiracetam, $P = 0.23$ and $Z = 1.35$; PHA 543613, $P = 0.99$ and $Z = 0.05$; Nefi + PHA, $P = 0.24$ and $Z = 1.012$; WT83/Q83X cell lines; N = 45 nuclei per condition), or cortical organoids (one-way ANOVA, $F_{3,281} = 6.594$, $P = 0.0003$; Dunnett's multiple comparisons test vs KO untreated: control, $P = 0.009$ and $Z = 2.38$; Nefiracetam, $P = 0.01$ and $Z = 3.05$; PHA 543613, $P = 0.98$ and $Z = 0.30$; WT83/Q83X and WT82/K82fs cell lines; N = 45-90 nuclei per condition). Spine density was rescued or partially rescued by the compounds (one-way ANOVA, $F_{3,63} = 8.449$, $P < 0.0001$; Dunnett's multiple comparisons test vs KO untreated: control, $P < 0.0001$ and $Z = 4.35$; Nefiracetam, $P = 0.16$ and $Z = 2.01$; PHA 543613, $P = 0.001$ and $Z = 3.24$; WT83/Q83X and WT82/K82fs cell lines; N = 11-28 neurons per condition). Note that statistical comparisons are presented relative to KO untreated or, for mosaic neurospheres, CTR/KO untreated. Data information: Data are presented as mean ± s.e.m.

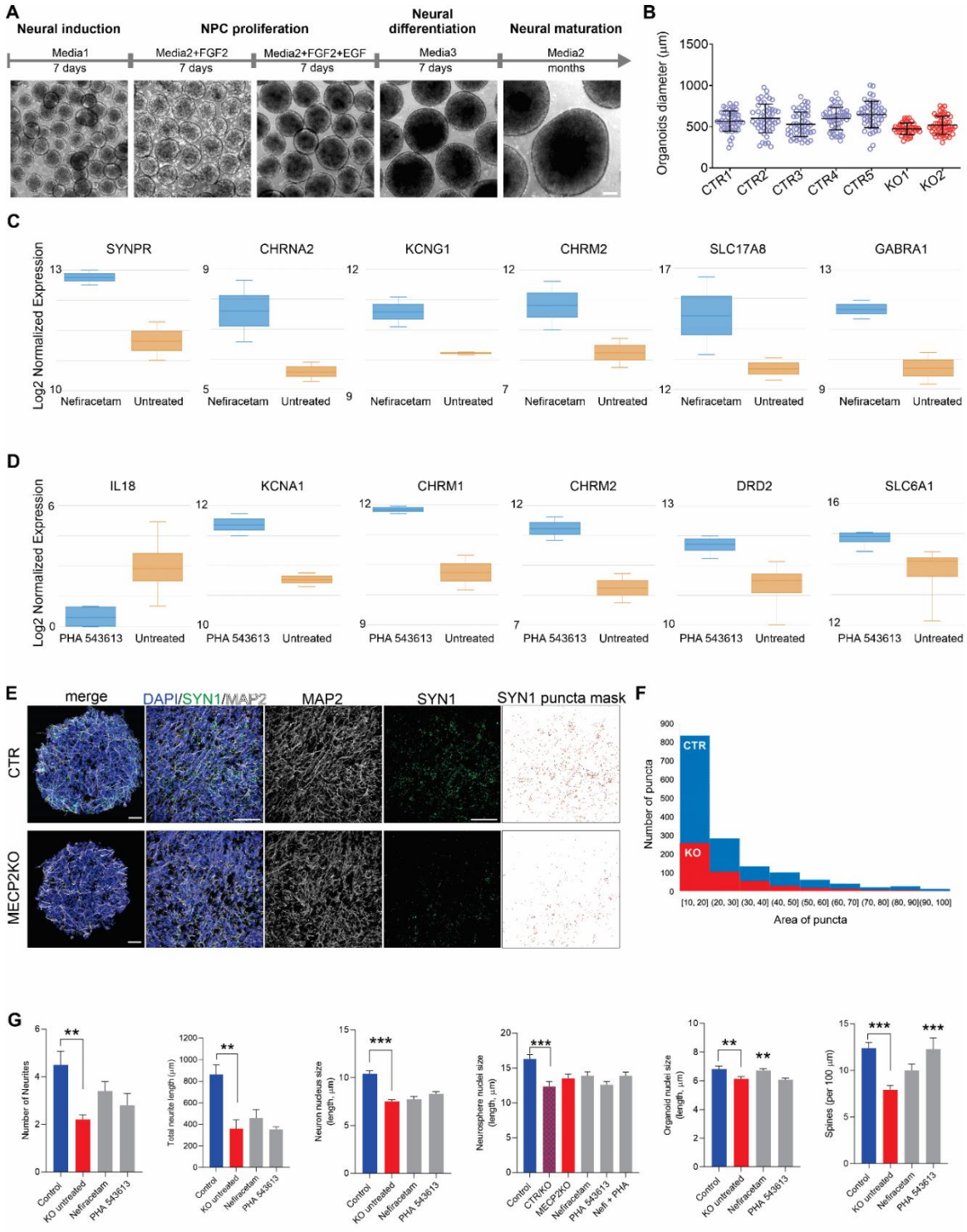
A
Neural induction
NPC proliferation
Neural differentiation
Neural maturation
Media1
7 days
Media2+FGF2
7 days
Media2+FGF2+EGF
7 days
Media3
7 days
Media2
months
B
Organoids diameter (µm)
1500
1000
500
0
CTR1'
CTR2'
CTR3'
CTR4'
CTR5'
KO1'
KO2'
C
Log2 Normalized Expression
SYNPR
CHRNA2
KCNG1
CHRM2
SLC17A8
GABRA1
Nefiracetam
Untreated
D
Log2 Normalized Expression
IL18
KCNA1
CHRM1
CHRM2
DRD2
SLC6A1
PHA 543613
Untreated
E
merge
DAPI/SYN1/MAP2
MAP2
SYN1
SYN1 puncta mask
CTR
MECP2KO
F
Number of puncta
CTR
KO
[10, 20] (20, 30] (30, 40] (40, 50] (50, 60] (60, 70] (70, 80] (80, 90](90, 100]
Area of puncta
G
Number of Neurites
Total neurite length (µm)
Neuron nucleus size (length, µm)
Neurosphere nuclei size (length, µm)
Organoid nuclei size (length, µm)
Spines (per 100 µm)
Control
KO untreated
Nefiracetam
PHA 543613
CTR/KO
MECP2KO
Nefi + PHA

References

Adams, J. W., Cugola, F. R., & Muotri, A. R. (2019). Brain organoids as tools for modeling human neurodevelopmental disorders. *Physiology*, *34*(5), 365–375. https://doi.org/10.1152/physiol.00005.2019

Amir, R. E., Van Den Veyver, I. B., Wan, M., Tran, C. Q., Francke, U., & Zoghbi, H. Y. (1999). Rett syndrome is caused by mutations in X-linked MECP2, encoding methyl-CpG-binding protein 2. *Nature Genetics*, *23*(2), 185–188. https://doi.org/10.1038/13810

Banerjee, A., Miller, M. T., Li, K., Sur, M., & Kaufmann, W. E. (2019). Towards a better diagnosis and treatment of Rett syndrome: A model synaptic disorder. *Brain*, *142*(2), 239–248. https://doi.org/10.1093/brain/awy323

Benke, D., & Möhler, H. (2018). Impact on GABA systems in monogenetic developmental CNS disorders: Clues to symptomatic treatment. *Neuropharmacology*, *136*, 46–55. https://doi.org/10.1016/j.neuropharm.2017.07.030

Braat, S., & Kooy, R. F. (2015). The GABAA Receptor as a Therapeutic Target for Neurodevelopmental Disorders. *Neuron*, *86*(5), 1119–1130. https://doi.org/10.1016/j.neuron.2015.03.042

Camp, J. G., Badsha, F., Florio, M., Kanton, S., Gerber, T., Wilsch-Bräuninger, M., Lewitus, E., Sykes, A., Hevers, W., Lancaster, M., Knoblich, J. A., Lachmann, R., Pääbo, S., Huttner, W. B., & Treutlein, B. (2015). Human cerebral organoids recapitulate gene expression programs of fetal neocortex development. *Proceedings of the National Academy of Sciences*, *112*(51), 201520760. https://doi.org/10.1073/pnas.1520760112

Chahrour, M., Yun Jung, S., Shaw, C., Zhou, X., Wong, S. T., Qin, J., & Zoghbi, H. Y. (2008). MeCP2, a key contributor to neurological disease, activates and represses transcription. *Science*, *320*, 1224–1229.

Chailangkarn, T., Trujillo, C. A., Freitas, B. C., Hrvoj-Mihic, B., Herai, R. H., Yu, D. X., Brown, T. T., Marchetto, M. C., Bardy, C., McHenry, L., Stefanacci, L., Järvinen, A., Searcy, Y. M., Dewitt, M., Wong, W., Lai, P., Ard, M. C., Hanson, K. L., Romero, S., Jacobs, B., Dale, A. M., Dai, L., Korenberg, J. R., Gage, F. H., Bellugi, U., Halgren, E., Semendeferi, K., & Muotri, A. R. (2016). A human neurodevelopmental model for Williams syndrome. *Nature*, *536*(7616), 338–343. https://doi.org/10.1038/nature19067

Chao, H. T., Chen, H., Samaco, R. C., Xue, M., Chahrour, M., Yoo, J., Neul, J. L., Gong, S., Lu, H. C., Heintz, N., Ekker, M., Rubenstein, J. L. R., Noebels, J. L., Rosenmund, C., & Zoghbi, H. Y. (2010). Dysfunction in GABA signalling mediates autism-like stereotypies and Rett syndrome phenotypes. *Nature*, *468*(7321), 263–269. https://doi.org/10.1038/nature09582

Chao, H. T., Zoghbi, H. Y., & Rosenmund, C. (2007). MeCP2 Controls Excitatory Synaptic

Strength by Regulating Glutamatergic Synapse Number. *Neuron*, *56*(1), 58–65. https://doi.org/10.1016/j.neuron.2007.08.018

Chen, C. Y., Di Lucente, J., Lin, Y. C., Lien, C. C., Rogawski, M. A., Maezawa, I., & Jin, L. W. (2018). Defective GABAergic neurotransmission in the nucleus tractus solitarius in Mecp2-null mice, a model of Rett syndrome. *Neurobiology of Disease*, *109*(August 2017), 25–32. https://doi.org/10.1016/j.nbd.2017.09.006

Chen, W. G., Chang, Q., Lin, Y., Meissner, A., West, A. E., Griffith, E. C., Jaenisch, R., & Greenberg, M. E. (2003). Derepression of BDNF Transcription Involves Calcium-Dependent Phosphorylation of MeCP2. *Science*, *302*(5646), 885–889. https://doi.org/10.1126/science.1086446

Dani, V. S., & Nelson, S. B. (2009). Intact long-term potentiation but reduced connectivity between neocortical layer 5 pyramidal neurons in a mouse model of Rett syndrome. *Journal of Neuroscience*, *29*(36), 11263–11270. https://doi.org/10.1523/JNEUROSCI.1019-09.2009

Djukic, A., Holtzer, R., Shinnar, S., Muzumdar, H., Rose, S. A., Mowrey, W., Galanopoulou, A. S., Shinnar, R., Jankowski, J. J., Feldman, J. F., Pillai, S., & Moshé, S. L. (2016). Pharmacologic Treatment of Rett Syndrome With Glatiramer Acetate. *Pediatric Neurology*, *61*, 51–57. https://doi.org/10.1016/j.pediatrneurol.2016.05.010

Espuny-Camacho, I., Michelsen, K. A., Gall, D., Linaro, D., Hasche, A., Bonnefont, J., Bali, C., Orduz, D., Bilheu, A., Herpoel, A., Lambert, N., Gaspard, N., Péron, S., Schiffmann, S. N., Giugliano, M., Gaillard, A., & Vanderhaeghen, P. (2013). Pyramidal Neurons Derived from Human Pluripotent Stem Cells Integrate Efficiently into Mouse Brain Circuits In Vivo. *Neuron*, *77*(3), 440–456. https://doi.org/10.1016/j.neuron.2012.12.011

Foucault-Fruchard, L., Tronel, C., Bodard, S., Gulhan, Z., Busson, J., Chalon, S., & Antier, D. (2018). Alpha-7 nicotinic acetylcholine receptor agonist treatment in a rat model of Huntington's disease and involvement of heme oxygenase-1. *Neural Regeneration Research*, *13*(4), 737–741. https://doi.org/10.4103/1673-5374.230301

Fujimaki, Y., Sudo, K., & Hakusui, H. (1993). Pharmacokinetics of nefiracetam and three metabolites in humans and stereoselective hydroxylation of its pyrrolidine ring. *Xenobiotica*, *23*(1), 61–70. https://doi.org/10.3109/00498259309059362

Glaze, D. G., Neul, J. L., Percy, A., Feyma, T., Beisang, A., Yaroshinsky, A., Stoms, G., Zuchero, D., Horrigan, J., Glass, L., & Jones, N. E. (2017). A Double-Blind, Randomized, Placebo-Controlled Clinical Study of Trofinetide in the Treatment of Rett Syndrome. *Pediatric Neurology*, *76*, 37–46. https://doi.org/10.1016/j.pediatrneurol.2017.07.002

Gonzales, M. L., & LaSalle, J. M. (2010). The role of MeCP2 in brain development and neurodevelopmental disorders. *Current Psychiatry Reports*, *12*(2), 127–134.

Gore, A., Li, Z., Fung, H. L., Young, J. E., Agarwal, S., Antosiewicz-Bourget, J., Canto, I., Giorgetti, A., Israel, M. A., Kiskinis, E., Lee, J. H., Loh, Y. H., Manos, P. D., Montserrat, N., Panopoulos, A. D., Ruiz, S., Wilbert, M. L., Yu, J., Kirkness, E. F., Belmonte, J. C. I., Rossi, D. J., Thomson, J. A., Eggan, K., Daley, G. Q., Goldstein, L. S. B., & Zhang, K. (2011). Somatic coding mutations in human induced pluripotent stem cells. *Nature*, *471*(7336), 63–67. https://doi.org/10.1038/nature09805

Hagberg, B., Hanefeld, F., Percy, A., & Skjeldal, O. (2002). An update on clinically applicable diagnostic criteria in Rett syndrome: Comments to Rett syndrome clinical criteria consensus panel satellite to European Paediatric Neurology Society Meeting Baden Baden, Germany, 11 September 2001. *European Journal of Paediatric Neurology*, *6*(5), 293–297. https://doi.org/10.1053/ejpn.2002.0612

Hodge, R. D., Bakken, T. E., Miller, J. A., Smith, K. A., Barkan, E. R., Graybuck, L. T., Close, J. L., Long, B., Johansen, N., Penn, O., Yao, Z., Eggermont, J., Höllt, T., Levi, B. P., Shehata, S. I., Aevermann, B., Beller, A., Bertagnolli, D., Brouner, K., Casper, T., Cobbs, C., Dalley, R., Dee, N., Ding, S. L., Ellenbogen, R. G., Fong, O., Garren, E., Goldy, J., Gwinn, R. P., Hirschstein, D., Keene, C. D., Keshk, M., Ko, A. L., Lathia, K., Mahfouz, A., Maltzer, Z., McGraw, M., Nguyen, T. N., Nyhus, J., Ojemann, J. G., Oldre, A., Parry, S., Reynolds, S., Rimorin, C., Shapovalova, N. V., Somasundaram, S., Szafer, A., Thomsen, E. R., Tieu, M., Quon, G., Scheuermann, R. H., Yuste, R., Sunkin, S. M., Lelieveldt, B., Feng, D., Ng, L., Bernard, A., Hawrylycz, M., Phillips, J. W., Tasic, B., Zeng, H., Jones, A. R., Koch, C., & Lein, E. S. (2019). Conserved cell types with divergent features in human versus mouse cortex. *Nature*, *573*(7772), 61–68. https://doi.org/10.1038/s41586-019-1506-7

Johnston, M. V., Mullaney, B., & Blue, M. E. (2003). Neurobiology of Rett syndrome. *Journal of Child Neurology*, *18*(10), 688–692. https://doi.org/10.1177/08830738030180100501

Katz, D. M., Bird, A., Coenraads, M., Gray, S. J., Menon, D. U., Philpot, B. D., & Tarquinio, D. C. (2016). Rett Syndrome: Crossing the Threshold to Clinical Translation. *Trends in Neurosciences*, *39*(2), 100–113. https://doi.org/10.1016/j.tins.2015.12.008

Khwaja, O. S., Ho, E., Barnes, K. V., O'Leary, H. M., Pereira, L. M., Finkelstein, Y., Nelson, C. A., Vogel-Farley, V., DeGregorio, G., Holm, I. A., Khatwa, U., Kapur, K., Alexander, M. E., Finnegan, D. M., Cantwell, N. G., Walco, A. C., Rappaport, L., Gregas, M., Fichorova, R. N., Shannon, M. W., Sur, M., & Kaufmann, W. E. (2014). Safety, pharmacokinetics, and preliminary assessment of efficacy of mecasermin (recombinant human IGF-1) for the treatment of Rett syndrome. *Proceedings of the National Academy of Sciences of the United States of America*, *111*(12), 4596–4601. https://doi.org/10.1073/pnas.1311141111

Kim, R., Li, Y., & Sejnowski, T. J. (2019). Simple framework for constructing functional spiking recurrent neural networks. *Proceedings of the National Academy of Sciences of the United States of America*, *116*(45), 22811–22820.

Krishnan, K., Lau, B. Y. B., Ewall, G., Huang, Z. J., & Shea, S. D. (2017). MECP2 regulates cortical plasticity underlying a learned behaviour in adult female mice. *Nature Communications*, *8*, 1–13. https://doi.org/10.1038/ncomms14077

Laje, R., & Buonomano, D. V. (2013). Robust timing and motor patterns by taming chaos in recurrent neural networks. *Nature Neuroscience*, *16*(7), 925–933. https://doi.org/10.1038/nn.3405

Li, Y., Wang, H., Muffat, J., Cheng, A. W., Orlando, D. A., Lovén, J., Kwok, S. M., Feldman, D. A., Bateup, H. S., Gao, Q., Hockemeyer, D., Mitalipova, M., Lewis, C. A., Vander Heiden, M. G., Sur, M., Young, R. A., & Jaenisch, R. (2013). Global transcriptional and translational repression in human-embryonic- stem-cell-derived rett syndrome neurons. *Cell Stem Cell*, *13*(4), 446–458. https://doi.org/10.1016/j.stem.2013.09.001

Lodato, M. A., Woodworth, M. B., Lee, S., Evrony, G. D., Mehta, B. K., Karger, A., Lee, S., Chittenden, T. W., D'Gama, A. M., Cai, X., Luquette, L. J., Lee, E., Park, P. J., & Walsh, C. A. (2015). Somatic mutation in single human neurons tracks developmental and transcriptional history. *Science*, *350*(6256), 94–98. https://doi.org/10.1126/science.aab1785

Luo, C., Lancaster, M. A., Castanon, R., Nery, J. R., Knoblich, J. A., & Ecker, J. R. (2016). Cerebral Organoids Recapitulate Epigenomic Signatures of the Human Fetal Brain. *Cell Reports*, *17*(12), 3369–3384. https://doi.org/10.1016/j.celrep.2016.12.001

Malykh, A. G., & Sadaie, M. R. (2010). Piracetam and piracetam-like drugs: From basic science to novel clinical applications to CNS disorders. *Drugs*, *70*(3), 287–312. https://doi.org/10.2165/11319230-000000000-00000

Marchetto, M. C. N., Carromeu, C., Acab, A., Yu, D., Yeo, G. W., Mu, Y., Chen, G., Gage, F. H., & Muotri, A. R. (2010). A model for neural development and treatment of rett syndrome using human induced pluripotent stem cells. *Cell*, *143*(4), 527–539. https://doi.org/10.1016/j.cell.2010.10.016

McConnell, M. J., Moran, J. V., Abyzov, A., Akbarian, S., Bae, T., Cortes-Ciriano, I., Erwin, J. A., Fasching, L., Flasch, D. A., Freed, D., Ganz, J., Jaffe, A. E., Kwan, K. Y., Kwon, M., Lodato, M. A., Mills, R. E., Paquola, A. C. M., Rodin, R. E., Rosenbluh, C., Sestan, N., Sherman, M. A., Shin, J. H., Song, S., Straub, R. E., Thorpe, J., Weinberger, D. R., Urban, A. E., Zhou, B., Gage, F. H., Lehner, T., Senthil, G., Walsh, C. A., Chess, A., Courchesne, E., Gleeson, J. G., Kidd, J. M., Park, P. J., Pevsner, J., & Vaccarino, F. M. (2017). Intersection of diverse neuronal genomes and neuropsychiatric disease: The Brain Somatic Mosaicism Network. *Science*, *356*(6336). https://doi.org/10.1126/science.aal1641

Miconi, T. (2017). Biologically plausible learning in recurrent neural networks reproduces neural dynamics observed during cognitive tasks. *ELife*, *6*, 1–24. https://doi.org/10.7554/eLife.20899

Moretti, P., Levenson, J. M., Battaglia, F., Atkinson, R., Teague, R., Antalffy, B., Armstrong, D., Arancio, O., Sweatt, J. D., & Zoghbi, H. Y. (2006). Learning and memory and synaptic plasticity are impaired in a mouse model of Rett syndrome. *Journal of Neuroscience*, *26*(1), 319–327. https://doi.org/10.1523/JNEUROSCI.2623-05.2006

Moriguchi, S. (2011). Pharmacological study on Alzheimer's drugs targeting calcium/calmodulin- dependent protein kinase II. *Journal of Pharmacological Sciences*, *117*(1), 6–11. https://doi.org/10.1254/jphs.11R06CP

Nageshappa, S., Carromeu, C., Trujillo, C. A., Mesci, P., Espuny-Camacho, I., Pasciuto, E., Vanderhaeghen, P., Verfaillie, C. M., Raitano, S., Kumar, A., Carvalho, C. M. B., Bagni, C., Ramocki, M. B., Araujo, B. H. S., Torres, L. B., Lupski, J. R., Van Esch, H., & Muotri, A. R. (2016). Altered neuronal network and rescue in a human MECP2 duplication model. *Molecular Psychiatry*, *21*(2), 178–188. https://doi.org/10.1038/mp.2015.128

Nguyen, M. V. C., Du, F., Felice, C. A., Shan, X., Nigam, A., Mandel, G., Robinson, J. K., & Ballas, N. (2012). MeCP2 is critical for maintaining mature neuronal networks and global brain anatomy during late stages of postnatal brain development and in the mature adult brain. *Journal of Neuroscience*, *32*(29), 10021–10034. https://doi.org/10.1523/JNEUROSCI.1316-12.2012

O'Leary, H. M., Kaufmann, W. E., Barnes, K. V., Rakesh, K., Kapur, K., Tarquinio, D. C., Cantwell, N. G., Roche, K. J., Rose, S. A., Walco, A. C., Bruck, N. M., Bazin, G. A., Holm, I. A., Alexander, M. E., Swanson, L. C., Baczewski, L. M., Mayor Torres, J. M., Nelson, C. A., & Sahin, M. (2018). Placebo-controlled crossover assessment of mecasermin for the treatment of Rett syndrome. *Annals of Clinical and Translational Neurology*, *5*(3), 323–332. https://doi.org/10.1002/acn3.533

Oginsky, M. F., Cui, N., Zhong, W., Johnson, C. M., & Jiang, C. (2014). Alterations in the cholinergic system of brain stem neurons in a mouse model of Rett syndrome. *American Journal of Physiology - Cell Physiology*, *307*(6), C508–C520. https://doi.org/10.1152/ajpcell.00035.2014

Pena, R. F. O., Zaks, M. A., & Roque, A. C. (2018). Dynamics of spontaneous activity in random networks with multiple neuron subtypes and synaptic noise: Spontaneous activity in networks with synaptic noise. *Journal of Computational Neuroscience*, *45*(1), 1–28. https://doi.org/10.1007/s10827-018-0688-6

Picciotto, M. R., Higley, M. J., & Mineur, Y. S. (2012). Acetylcholine as a Neuromodulator: Cholinergic Signaling Shapes Nervous System Function and Behavior. *Neuron*, *76*(1), 116–129. https://doi.org/10.1016/j.neuron.2012.08.036

Pozzo-Miller, L., Pati, S., & Percy, A. K. (2015). Rett Syndrome: Reaching for Clinical Trials. *Neurotherapeutics*, *12*(3), 631–640. https://doi.org/10.1007/s13311-015-0353-y

Renthal, W., Boxer, L. D., Hrvatin, S., Li, E., Silberfeld, A., Nagy, M. A., Griffith, E. C., Vierbuchen, T., & Greenberg, M. E. (2018). Characterization of human mosaic Rett syndrome brain tissue by single-nucleus RNA sequencing. *Nature Neuroscience*, *21*(12), 1670–1679. https://doi.org/10.1038/s41593-018-0270-6

Robinson, R. G., Jorge, R. E., Clarence-Smith, K., & Starkstein, S. (2009). Double-blind treatment of apathy in patients with poststroke depression using nefiracetam. *Journal of Neuropsychiatry and Clinical Neurosciences*, *21*(2), 144–151. https://doi.org/10.1176/jnp.2009.21.2.144

Samaco, R. C., Hogart, A., & LaSalle, J. M. (2005). Epigenetic overlap in autism-spectrum neurodevelopmental disorders: MECP2 deficiency causes reduced expression of UBE3A and GABRB3. *Human Molecular Genetics*, *14*(4), 483–492. https://doi.org/10.1093/hmg/ddi045

Shannon, P., Markiel, A., Ozier, O., Baliga, N. S., Wang, J. T., Ramage, D., Amin, N., Schwikowski, B., & Ideker, T. (2003). Cytoscape: A Software Environment for Integrated Models of Biomolecular Interaction Networks. *Genome Research*, *13*, 2498–2504. https://doi.org/10.1101/gr.1239303.metabolite

Shibayama, A., Cook, E. H., Feng, J., Glanzmann, C., Yan, J., Craddock, N., Jones, I. R., Goldman, D., Heston, L. L., & Sommer, S. S. (2004). MECP2 structural and 3'-UTR variants in schizophrenia, autism and other psychiatric diseases: A possible association with autism. *American Journal of Medical Genetics*, *128B*(1), 50–53. https://doi.org/10.1002/ajmg.b.30016

Sirenko, O., Parham, F., Dea, S., Sodhi, N., Biesmans, S., Mora-Castilla, S., Ryan, K., Behl, M., Chandy, G., Crittenden, C., Vargas-Hurlston, S., Guicherit, O., Gordon, R., Zanella, F., & Carromeu, C. (2019). Functional and mechanistic neurotoxicity profiling using human iPSC-Derived neural 3D cultures. *Toxicological Sciences*, *167*(1), 249–257. https://doi.org/10.1093/toxsci/kfy218

Sjostedt, E., Zhong, W., Fagerberg, L., Karlsson, M., Mitsios, N., Adori, C., Oksvold, P., Edfors, F., Limiszewska, A., Hikmet, F., Huang, J., Du, Y., Lin, L., Dong, Z., Yang, L., Liu, X., Jiang, H., Xu, X., Wang, J., Yang, H., Bolund, L., Mardinoglu, A., Zhang, C., von Feilitzen, K., Lindskog, C., Ponten, F., Luo, Y., Hokfelt, T., Uhlen, M., & Mulder, J. (2020). An atlas of the protein-coding genes in the human, pig, and mouse brain. *Science*, *367*(6482). https://doi.org/10.1126/science.aay5947

Stuss, D. P., Boyd, J. D., Levin, D. B., & Delaney, K. R. (2012). MeCP2 mutation results in compartment-specific reductions in dendritic branching and spine density in layer 5 motor cortical neurons of YFP-H mice. *PLoS ONE*, *7*(3), 1–11. https://doi.org/10.1371/journal.pone.0031896

Tang, X., Drotar, J., Li, K., Clairmont, C. D., Brumm, A. S., Sullins, A. J., Wu, H., Liu, X. S., Wang, J., Gray, N. S., Sur, M., & Jaenisch, R. (2019). Pharmacological enhancement of

KCC2 gene expression exerts therapeutic effects on human Rett syndrome neurons and Mecp2 mutant mice. *Science Translational Medicine*, *11*(503), 1–14. https://doi.org/10.1126/scitranslmed.aau0164

Thomas, C. A., Tejwani, L., Trujillo, C. A., Negraes, P. D., Herai, R. H., Mesci, P., Macia, A., Crow, Y. J., & Muotri, A. R. (2017). Modeling of TREX1-Dependent Autoimmune Disease using Human Stem Cells Highlights L1 Accumulation as a Source of Neuroinflammation. *Cell Stem Cell*, *21*(3), 319-331.e8. https://doi.org/10.1016/j.stem.2017.07.009

Trujillo, C. A., Gao, R., Negraes, P. D., Gu, J., Buchanan, J., Preissl, S., Wang, A., Wu, W., Haddad, G. G., Chaim, I. A., Domissy, A., Vandenberghe, M., Devor, A., Yeo, G. W., Voytek, B., & Muotri, A. R. (2019). Complex Oscillatory Waves Emerging from Cortical Organoids Model Early Human Brain Network Development. *Cell Stem Cell*, *25*(4), 558-569.e7. https://doi.org/10.1016/j.stem.2019.08.002

Van Vreeswijk, C., & Sompolinsky, H. (1996). Chaos in neuronal networks with balanced excitatory and inhibitory activity. *Science*, *274*(5293), 1724–1726. https://doi.org/10.1126/science.274.5293.1724

Watson, P., Black, G., Ramsden, S., Barrow, M., Super, M., Kerr, B., & Clayton-Smith, J. (2001). Angelman syndrome phenotype associated with mutations in *MECP2*, a gene encoding a methyl CpG binding protein. *Journal of Medical Genetics*, *38*(4), 224–228. https://doi.org/10.1136/jmg.38.4.224

Wishka, D. G., Walker, D. P., Yates, K. M., Reitz, S. C., Jia, S., Myers, J. K., Olson, K. L., Jacobsen, E. J., Wolfe, M. L., Groppi, V. E., Hanchar, A. J., Thornburgh, B. A., Cortes-Burgos, L. A., Wong, E. H. F., Staton, B. A., Raub, T. J., Higdon, N. R., Wall, T. M., Hurst, R. S., Walters, R. R., Hoffmann, W. E., Hajos, M., Franklin, S., Carey, G., Gold, L. H., Cook, K. K., Sands, S. B., Zhao, S. X., Soglia, J. R., Kalgutkar, A. S., Arneric, S. P., & Rogers, B. N. (2006). Discovery of N-[(3R)-1-azabicyclo[2.2.2]oct-3-yl]furo[2,3-c]pyridine-5- carboxamide, an agonist of the α7 nicotinic acetylcholine receptor, for the potential treatment of cognitive deficits in schizophrenia: Synthesis and structure-activity relationship. *Journal of Medicinal Chemistry*, *49*(14), 4425–4436. https://doi.org/10.1021/jm0602413

Zhang, B., Kirov, S., & Snoddy, J. (2005). WebGestalt: An integrated system for exploring gene sets in various biological contexts. *Nucleic Acids Research*, *33*(SUPPL. 2), 741–748. https://doi.org/10.1093/nar/gki475

Zhang, Y., Cao, S. X., Sun, P., He, H. Y., Yang, C. H., Chen, X. J., Shen, C. J., Wang, X. D., Chen, Z., Berg, D. K., Duan, S., & Li, X. M. (2016). Loss of MeCP2 in cholinergic neurons causes part of RTT-like phenotypes via α7 receptor in hippocampus. *Cell Research*, *26*(6), 728–742. https://doi.org/10.1038/cr.2016.48

Zhou, H., Wu, W., Zhang, Y., He, H., Yuan, Z., Zhu, Z., & Zhao, Z. (2017). Selective

preservation of cholinergic MeCP2 rescues specific Rett-syndrome-like phenotypes in MeCP2stop mice. *Behavioural Brain Research*, *322*, 51–59. https://doi.org/10.1016/j.bbr.2017.01.023

Zhou, Z., Hong, E. J., Cohen, S., Zhao, W. ning, Ho, H. yi H., Schmidt, L., Chen, W. G., Lin, Y., Savner, E., Griffith, E. C., Hu, L., Steen, J. A. J., Weitz, C. J., & Greenberg, M. E. (2006). Brain-Specific Phosphorylation of MeCP2 Regulates Activity-Dependent Bdnf Transcription, Dendritic Growth, and Spine Maturation. *Neuron*, *52*(2), 255–269. https://doi.org/10.1016/j.neuron.2006.09.037

Acknowledgements

Appendix 2, in full, is a reprint of the material as it appears in the following manuscript, published in *EMBO Molecular Medicine*: Trujillo, C. A.*, Adams, J. W.*, Negraes, P. D., Carromeu, C., Tejwani, L., Acab, A., Tsuda, B., Thomas, C. A., Sodhi, N., Fichter, K. M., Romero, S., Zanella, F., Sejnowski, T. J., Ulrich, H., & Muotri, A. R. (2021). **Pharmacological reversal of synaptic and network pathology in human *MECP2*-KO neurons and cortical organoids.** The dissertation author was one of the primary investigators and co-first authors of this paper.

APPENDIX 3 Impact of alcohol exposure on neural development and network formation in human cortical organoids

Abstract

Prenatal alcohol exposure is the foremost preventable etiology of intellectual disability and leads to a collection of diagnoses known as Fetal Alcohol Spectrum Disorders (FASD). Alcohol (EtOH) impacts diverse neural cell types and activity, but the precise functional pathophysiological effects on the human fetal cerebral cortex are unclear. Here, we used human cortical organoids to study the effects of EtOH on neurogenesis and validated our findings in primary human fetal neurons. EtOH exposure produced temporally dependent cellular effects on proliferation, cell cycle, and apoptosis. In addition, we identified EtOH-induced alterations in post-translational histone modifications and chromatin accessibility, leading to impairment of cAMP and calcium signaling, glutamatergic synaptic development, and astrocytic function. Proteomic spatial profiling of cortical organoids showed region-specific, EtOH-induced alterations linked to changes in cytoskeleton, gliogenesis, and impaired synaptogenesis. Finally, multi-electrode array electrophysiology recordings confirmed the deleterious impact of EtOH on neural network formation and activity in cortical organoids, which was validated in primary human fetal tissues. Our findings demonstrate progress in defining the human molecular and cellular phenotypic signatures of prenatal alcohol exposure on functional neurodevelopment, increasing our knowledge for potential therapeutic interventions targeting FASD symptoms.

Introduction

Despite public health efforts, prenatal alcohol exposure (PAE) remains the leading preventable cause of neurodevelopmental disorders (Roozen et al., 2016). Alcohol (EtOH) exposure during pregnancy can result in Fetal Alcohol Spectrum Disorders (FASD; Lange et al., 2017; May et al., 2018; Popova et al., 2018), which together have a prevalence of approximately 2-5% in the United States alone (May et al., 2009, 2018). FASD can present with a wide range of symptomatic severity, from neurobehavioral abnormalities to embryonic lethality. Primary cognitive and behavioral deficits can underpin secondary disabilities, such as mental health problems, disrupted school experience, addiction, sexually deviant behavior, and dependent living (Burd et al., 2008; Hoyme et al., 2016; Jones & Smith, 1973; Popova et al., 2018; Rasmussen et al., 2008). The resultant clinical profile appears to be influenced by the fetal brain's stage of development at the time of exposure and pattern of maternal EtOH consumption (De Filippis et al., 2016; Guizzetti et al., 2010; Halder et al., 2015; Mews et al., 2019; Sánchez-Alvarez et al., 2013; Valenzuela et al., 2011; Veazey et al., 2013).

Although the public burden of FASD is recognized, the precise molecular pathophysiology and neurodevelopmental consequences of EtOH exposure *in utero* remain understudied in humans. Previous investigations using *in vitro* and animal models have identified a broad impact of EtOH on neural functioning, with effects dependent upon cell type and the severity of exposure (De Filippis et al., 2016; Guizzetti et al., 2010; Halder et al., 2015; Mews et al., 2019; Rasmussen et al., 2008; Sánchez-Alvarez et al., 2013; Valenzuela et al., 2011; Veazey et al., 2013). However, translating these findings to clinical application in humans has been challenged by the suboptimal recapitulation of human cortical development by animal models (Zhao & Bhattacharyya, 2018). Human induced pluripotent stem cells

(hiPSCs) provide an experimental model that supports interrogation of the pathophysiological effects of EtOH exposure in a dynamic neurodevelopmental context (Arzua et al., 2020). Most valuably, hiPSCs can be aggregated and differentiated into three-dimensional cortical organoids that develop closely to human fetal corticogenesis and can be used to study mechanisms of neurodevelopmental disease (Adams et al., 2019; Camp et al., 2015; Lancaster et al., 2013, 2017; Luo et al., 2016; Pașca et al., 2019; Quadrato et al., 2017; Trujillo et al., 2019; Trujillo, Adams, et al., 2021).

Here, we identified EtOH-induced, temporally specific alterations at neurodevelopmental time points in hiPSC-derived cortical organoids and astrocytes, and we validated these findings in primary human fetal tissue. EtOH exposure alters the accessibility of the chromatin regulatory landscape in a pattern that is proposed to overlie transcriptomic alterations, cellular phenotypic changes, and impairment of functional network formation. Our findings suggest that this cortex-specific neurodevelopmental model can be a valuable platform to study the vulnerability of the early human brain to environmental damage and offers urgently needed insights into the pathophysiology of PAE.

Materials and Methods

Human cell source (hiPSC and primary fetal tissues)

Three hiPSC lines, WT83C6 (male), CVB (male), and 4C1 (female), were derived from control individuals and have been previously characterized elsewhere (Chailangkarn et al., 2016; Nageshappa et al., 2016; Negraes et al., 2021). The hiPSC colonies were expanded on Matrigel-coated dishes (BD Biosciences, San Jose, CA, USA) with mTeSR1 medium (StemCell Technologies, Vancouver, Canada). The cells were routinely checked by karyotype

and CNV arrays to avoid genomic alterations in the culture. Embryonic samples were obtained from fetal brains (10-11 weeks post-conception (PCW)) and cultured in Neurobasal (Life Technologies, Carlsbad, CA, USA) supplemented with 1X GlutaMAX (Life Technologies), 1% Gem21 NeuroPlex (Gemini Bio-Products, West Sacramento, CA, USA), 1% MEM nonessential amino acids (NEAA; Life Technologies), and 1% penicillin/streptomycin (Pen/Strep; Life Technologies). All cellular cultures were routinely tested for mycoplasma by PCR. The study was approved by the University of California San Diego IRB/ESCRO committee (protocol 141223ZF).

Generation of cortical organoids

Cortical organoids were generated as previously described (Negraes et al., 2021; Trujillo et al., 2019; Trujillo, Rice, et al., 2021). The newly formed cortical organoids were maintained in defined culture media transitioning through factors to promote proliferation, maturation, gliogenesis, and electrophysiological activity. Briefly, hiPSC colonies were dissociated with Accutase (Life Technologies) and resuspended in mTeSR1 supplemented with 10 μM SB431542 (SB; Stemgent, Cambridge, MA, USA), 1 μM Dorsomorphin (Dorso; R&D Systems, Minneapolis, MN, USA), and 5 μM ROCK inhibitor (Y-27632; Calbiochem, Sigma-Aldrich, St. Louis, MO, USA). After three days, media was switched to Media1 [Neurobasal (Life Technologies) supplemented with 1X GlutaMAX (Life Technologies), 1X Gem21 (Gemini Bio-Products), 1X N2 NeuroPlex (Gemini Bio-Products), 1X NEAA (Life Technologies), 1X Pen/Strep (Life Technologies), 10 μM SB, and 1 μM Dorso] for six days. Media2 [Neurobasal with 1X GlutaMAX, 1X Gem21, 1X NEAA, and 1X Pen/Strep] supplemented with 20 ng/mL FGF2 (Life Technologies) was used for seven days and then

further supplemented with 20 ng/mL EGF (PeproTech, Rocky Hill, NJ, USA) with 20 ng/mL FGF2 every other day for another six days. Next, cells were maintained for six days in Media3 [Media2 supplemented with 10 ng/mL BDNF, 10 ng/mL GDNF, 10 ng/mL NT-3 (all from PeproTech), 200 μM L-ascorbic acid, and 1 mM dibutyryl-cAMP (Sigma-Aldrich)]. Cortical organoids were subsequently kept in Media2 alone with media changes every 2-3 days.

Generation of astrocytes

Astrocytes were generated according to protocols published elsewhere (Santos et al., 2017). Briefly, neural progenitor cells were dissociated with Accutase, transferred to a 6-well plate, and kept in suspension under rotation in neural media [DMEM/F12 (Life Technologies) supplemented with 1X GlutaMAX, 1X Gem21 (Gemini Bio-products), and 1X Pen/Strep (Life Technologies)] containing 20 ng/mL FGF2 (PeproTech). Approximately 5 x 10^6 cells were plated into each well. ROCK inhibitor (Y-27632; Calbiochem) was added to a final concentration of 5 μM for 48 hours. After the removal of ROCK inhibitor, neural media without FGF2 was used for one week. Next, the media was switched to astrocyte growth medium (AGM; Lonza Group, Basel, Switzerland) for two weeks, when the spheres were plated onto poly-L-ornithine/laminin pre-coated dishes. The spheres continued to be cultured in AGM as astrocytes projected outward to populate the plate.

Alcohol (EtOH) exposure strategy

Cortical organoids were exposed to EtOH by supplementing the culture media with 200-proof EtOH (100 mM, Sigma-Aldrich) for seven days, with media changes every other

day. After this period, cells were maintained in media without EtOH for as long as needed. The same EtOH exposure approach was performed in mature primary fetal neurons and hiPSC-derived astrocytes. Although cortical organoids, fetal neurons, and astrocytes were initially exposed to 100 mM EtOH, the final EtOH concentration in the media stabilized around 20 mM after a couple of hours, as demonstrated by over-time measurements using the DensitoPro Handheld Density Meter (Mettler Toledo, Columbus, OH, USA). Cells were incubated at 37°C throughout treatment. Control and treated cell types were kept separately in distinct and covered conditions with no cross-contamination or EtOH leakage. In order to maintain a stable environmental concentration close to 20 mM and avoid evaporation of EtOH, cells were always kept in an EtOH-saturated atmosphere.

Immunofluorescence staining

Cells were fixed with 4% paraformaldehyde, permeabilized and blocked with 0.1% Triton X-100 and 3% FBS in PBS, and incubated with primary antibodies overnight at 4ºC. Primary antibodies used in this study were: rat anti-CTIP2, ab18465 (Abcam, Cambridge, United Kingdom), 1:500; rabbit anti-cleaved-caspase-3, #9661 (Cell Signaling, Danvers, MA, USA), 1:400; chicken anti-MAP2, ab5392 (Abcam), 1:2000; mouse anti-NeuN, MAB377 (EMD-Millipore, Burlington, MA, USA), 1:500; rabbit anti-Ki67, ab15580 (Abcam), 1:1000; rabbit anti-GFAP, Z033429 (DAKO A/S, Glostrup, Denmark), 1:1000; mouse anti-Vglut1, 135311 (Synaptic Systems, Goettingen, Germany), 1:500; rabbit anti-Homer1, 160003 (Synaptic Systems), 1:500. After being washed with PBS, samples were incubated with secondary antibodies (Alexa Fluor 488-, 555-, and 647-conjugated antibodies, Life Technologies, 1:1000) for two hours at room temperature. The slides were mounted using

ProLong Gold antifade reagent (Thermo Fisher Scientific, Waltham, MA, USA) and analyzed under a fluorescence microscope.

Gene expression profile (RNA sequencing)

Total polyA-based RNA was extracted from treated and non-treated cells using an RNeasy Kit (Qiagen, Hilden, Germany). Extracted RNA was prepared as stranded RNAseq libraries using Truseq Stranded mRNA LT Kit (Illumina, San Diego, CA, USA) and was multiplexed and sequenced on Illumina HiSeq 2500 to generate 100 bases paired-end reads, considering a minimum of 40 million of sequenced fragments per sample. Data were analyzed by Rosalind (https://rosalind.onramp.bio/), with a HyperScale architecture developed by OnRamp BioInformatics, Inc. (San Diego, CA, USA). Reads were trimmed using cutadapt, and quality scores were assessed using FastQC. Reads were aligned to the *Homo sapiens* genome build hg19 using STAR. Individual sample reads were quantified using HTseq and normalized via Relative Log Expression (RLE) using DESeq2 R library. Functional enrichment analysis of pathways, gene ontology, domain structure, and other ontologies were performed using HOMER (Heinz et al., 2010). Several database sources were referenced for enrichment analysis, including Interpro (Mitchell et al., 2019), NCBI, MSigDB (Liberzon et al., 2011; Subramanian et al., 2005), REACTOME (Fabregat et al., 2018), WikiPathways (Slenter et al., 2018), and Advaita (Draghici et al., 2007). Enrichment was calculated relative to a set of background genes relevant to the experiment (Camp et al., 2015; Fietz et al., 2012; Kang et al., 2011; Patro et al., 2017; R Core Team, 2020; Stein et al., 2014).

Epigenetic profile (Assay for Transposase Accessible Chromatin Sequencing; ATAC-Seq)

Samples were cryopreserved in a solution containing 50% FBS/40% maintenance media/10% DMSO and transferred to Active Motif (Carlsbad, CA, USA), where the assay was performed according to their optimized protocol. Data was analyzed by Rosalind (https://rosalind.onramp.bio/) using a HyperScale architecture developed by OnRamp BioInformatics, Inc. (San Diego, CA, USA). Peaks were called using MACS2 (Zhang et al., 2008). Peak overlaps and differential accessibility were calculated using the DiffBind R library. Differential accessibility was calculated at gene promoter sites. Read distribution percentages, identity heatmaps, and FRiP plots were generated as part of the QC step using ChIPQC R library and HOMER (Heinz et al., 2010). HOMER was also used to generate known and *de novo* motifs and perform functional enrichment analysis of pathways, gene ontology, domain structure, and other ontologies.

Histone extraction and mass spectrometry

Bulk histones were acid-extracted from cell pellets, propionylated, and subjected to trypsin digestion as previously described (Garcia et al., 2007). Briefly, histones were extracted by incubation and intermittent vortexing. Histones were then precipitated, recovered, washed twice with PBS, and air-dried. While adjusting the pH to 7-8, the pelleted histones were resuspended and digested with trypsin before resuspension in 100 mM ammonium bicarbonate overnight at 37°C and dried again. For mass spectrometry analysis, histone peptides were resuspended in 0.1% TFA in water.

Samples were analyzed in a triple quadrupole (QqQ) mass spectrometer (TSQ Quantiva, Thermo Fisher Scientific) directly coupled with an UltiMate 3000 nano-liquid chromatography system (Dionex, Sunnyvale, CA, USA). Peptides were first loaded onto a

packed trapping column and then separated on a New Objectives PicoChip analytical column. Both columns were packed with New Objectives ProntoSIL C18-AQ, 3μm, 200Å resin. The chromatography gradient was achieved by increasing the percentage of buffer B from 0 to 35% at a flow rate of 0.30 μL/min over 45 minutes. Solvent A: 0.1% formic acid in the water, and B: 0.1% formic acid in 95% acetonitrile. The QqQ settings were as follows: collision gas pressure of 1.5 mTorr; Q1 peak width of 0.7 (FWHM); cycle time of two seconds; skimmer offset of 10V; electrospray voltage of 2.5kV. In addition, targeted analysis of unmodified and various modified histone peptides was performed. This entire process was repeated three separate times for each sample.

Raw MS files were imported and analyzed in Skyline with Savitzky-Golay smoothing (MacLean et al., 2010). All Skyline peak area assignments for monitored peptide transitions were manually confirmed. A minimum of three peptide transitions was quantified for each modification. For each monitored amino acid residue, each modified (and unmodified) form was quantified by first calculating the sum of peak areas of corresponding peptide transitions. Finally, each modification is represented as a percentage of the total pool of modifications.

Cell cycle analysis

Cortical organoids, primary fetal neurons, and astrocytes were manually dissociated and counted using a Via1-Cassette with the NucleoCounter NC-3000 (Chemometec, Allerod, Denmark). Dissociated cells were fixed with 70% EtOH for two hours, resuspended in 0.5 μg/ml DAPI with 0.1% Triton X-100 in PBS, and incubated at 37ºC for five minutes. Cells were subsequently loaded into an NC-Slide A2 chamber (Chemometec), and cellular

fluorescence was quantified with the NucleoCounter NC-3000 using the manufacturer's protocol.

Annexin and cell death

Cortical organoids, primary fetal neurons, and astrocytes were manually dissociated and resuspended in Annexin V binding buffer (Invitrogen). Next, Annexin V-CF488A conjugate (Biotium, Inc., Hayward, CA, USA) was added, followed by Hoechst 33342 (Chemometec). After a PBS wash, the cells were resuspended in Annexin V binding buffer (Invitrogen) containing 10 μg/mL propidium iodide (Chemometec). Cells were loaded into NC-Slide A2 chambers, and the "Annexin V Assay" was run with the NucleoCounter NC-3000.

Synaptic puncta quantification

Pre (Vglut1+) and postsynaptic (PSD-95+) puncta were quantified along MAP2+ neuronal processes, as previously described (Chailangkarn et al., 2016). The primary antibodies (Vglut1, 1:1000, Synaptic Systems; PSD-95, 1:1000, NeuroMab; and MAP2, 1:2000, Sigma-Aldrich) were incubated for two hours at room temperature. After PBS wash, secondary antibodies (Alexa Fluor 488-, 555-, and 647-conjugated antibodies, 1:1000, Life Technologies) were incubated for one hour. Coverslips were mounted, and slides were analyzed under a fluorescence microscope (Z1 Axio Observer Apotome, Zeiss).

Western blotting

Western blotting was performed as previously described (Thomas et al., 2017). Total protein was extracted from cortical organoids and quantified with the BCA Protein Assay Kit (Pierce Biotechnology, Rockford, IL, USA). After separation, membrane transfer, and blocking of 20 μg of protein, membranes were incubated with primary antibodies overnight at 4ºC [rabbit anti-Synapsin1, AB1543P (EMD-Millipore), 1:500; rabbit anti-GFAP, Z033429 (DAKO A/S), 1:1000; mouse anti-PSD-95 (NeuroMab), 1:1000; rabbit anti-cleaved-caspase-3, #9661 (Cell Signaling), 1:400; mouse anti-β-III-tubulin, MMS-435P (Covance, Princeton, NJ, USA), 1:1000; rat anti-CTIP2, ab18465 (Abcam), 1:500; mouse anti-β-Actin, ab8226 (Abcam), 1:7000], followed by two-hour incubation with secondary antibodies before imaging and quantification using the Odyssey CLx imaging system (Li-Cor, Lincoln, NE, USA).

Nanostring Technologies GeoMx Digital Spatial Profiling

The Nanostring Technologies GeoMx Digital Spatial Profiling (DSP) quantifies protein abundance by counting indexing oligonucleotides specific to the desired targets (Merritt et al., 2020). EtOH-exposed and control organoid sections were stained with fluorescently labeled imaging reagents and select protein markers as described (Merritt et al., 2020). Cellular markers used included Ki-67, GFAP, MAP2, and nuclear stain. Proteins focused upon were based on choosing the protein panels Neural Cell Profiling, Alzheimer's Pathology, and Glial Cell Subtyping. In addition, specific regions or areas of interest were chosen for profiling (Merritt et al., 2020). Regions selected were rosettes and non-rosettes containing areas within each condition. (Merritt et al., 2020)

Multi-electrode array (MEA) recording

Multi-electrode array recordings were achieved as previously described (Negraes et al., 2021; Trujillo et al., 2019). Six-week-old cortical organoids were plated in 12-well MEA plates (Axion Biosystems, Atlanta, GA, USA) pre-coated with 100 µg/mL poly-L-ornithine and 10 µg/mL laminin. Cellular cultures were fed twice a week and, 14 days after plating, weekly measurements were performed. Recordings were conducted in a Maestro MEA system with AxIS Software Spontaneous Neural Configuration (Axion Biosystems). Using Axion Biosystems' Neural Metrics Tool, active electrodes required at least five spikes/min. Bursts/electrode used an inter-spike interval (ISI) threshold requiring minimally five spikes with a maximum ISI of 100 ms. Network bursts required at least 10 spikes under the same ISI. The synchrony index utilized a cross-correlogram window of 20 ms.

Statistical analysis

Statistical analysis was performed using GraphPad Prism versions 8 and 9 (GraphPad Software, La Jolla, CA, USA). Results from continuous variables are presented as mean ± standard error of the mean (s.e.m.), and 95% confidence intervals were normal-based. Means were compared between groups using, where appropriate, unpaired Student's *t*-test, one-way, or two-way analyses of variance (ANOVA). Whenever possible, the investigator was blind to the sample conditions. Tests were performed two-sided with α throughout set as 0.05.

Results

Cortical organoids resemble early stages of human corticogenesis in vitro

To investigate the neurodevelopmental consequences of EtOH exposure, human cell platforms encompassing diverse neural cell types were employed. We derived functional cortical organoids and astrocytes from three hiPSC lines (Figure 24a-g) and prepared primary neuron cultures from human fetal tissue at 10-11 PCW (Figure 24h-j). Each cell type underwent moderate-high physiological concentration of EtOH exposure for one week (organoids, fetal neurons, and astrocytes), followed by continued maintenance in the absence of EtOH (Figure 19a). Although the choice to administer 100 mM of EtOH is high, the concentration to which the cells were kept corresponds to around 20 mM or 90 mg/dL (Figure 24l,m). This treatment dosage was selected considering EtOH cytotoxicity and its concentration in amniotic fluid (Burd et al., 2012; Dolganiuc & Szado, 2009; Tateno et al., 2005; Vangipuram et al., 2008).

Immunocytochemistry in cortical organoid cryosections indicated close fidelity to the cytoarchitectural complexity and temporal progression of fetal cortical development. The expected SOX2+ progenitor regions enriched for proliferation (Ki67+) organized in the ventricular zone (VZ)-like areas around a lumen. These regions were surrounded by intermediate progenitors resembling the sub-ventricular zone (SVZ), giving rise to a cortical plate displaying mature neurons (NeuN+, MAP2+) that express cortical layer-specific markers (CTIP2+ or *BLC11B*; Figure 19b and Figure 24b,c). Because glia cells emerge later during neurodevelopment and are thus absent or sparse in early cortical organoids (Figure 24b; Trujillo et al., 2019), we differentiated astrocytes independently to capture alteration due to EtOH exposure.

EtOH exposure alters cell cycle, proliferation, and survival

EtOH-exposed cortical organoids showed reduced diameter at two months compared to controls ($P < 0.0001$; Figure 19c). Ki67+ staining was used to delineate the proliferative VZ-like region from the cortical plate-like domain, as previously described in a cortical organoid system (Bershteyn et al., 2017). At two months of age, a stage in organoid development with considerable cell proliferation, we observed a smaller population of Ki67+ proliferative cells in EtOH-exposed cultures compared to controls ($P < 0.0001$); however, at three months, this difference had narrowed ($P = 0.12$; Figure 19d). The overall amount of cells (DAPI+) remained constant, independent of treatment. Next, cell cycle analysis showed that cells from EtOH-exposed organoids were less likely to be in the proliferative S and G2/M phases ($P = 0.002$; Figure 19e). Similar alterations in cell cycle were also observed in EtOH-exposed astrocytes ($P < 0.0001$; Figure 19f and Figure 24g) and fetal neurons ($P < 0.0001$; Figure 19g and Figure 24k).

After identifying alterations in proliferation and cell cycle progression, we investigated the effect of EtOH exposure on cell survival and found a higher frequency of apoptotic cells (CC3+) in two-month EtOH-exposed organoids compared to controls ($P < 0.0001$; Figure 19h). Analogous to the proliferative impairment, we observed that by three months the increased frequency of apoptosis in EtOH-exposed organoids had comparatively stabilized ($P = 0.076$; Figure 19h). To evaluate cell death in astrocytes and fetal neurons, we assessed the frequency of Annexin+ cells, which was also increased in both astrocytes ($P < 0.0001$; Figure 19i and Figure 19f) and fetal neurons ($P = 0.0002$; Figure 19j and Figure 24j) exposed to EtOH.

Figure 19: Ethanol (EtOH) exposure alters proliferation and survival dynamics in human cellular models. a EtOH was applied to human iPSC-derived cortical organoids, human iPSC-derived astrocytes, and human fetal primary neurons. **b** Immunohistochemistry in cortical organoids shows SOX2+ progenitor regions, Ki67+ proliferation, and mature neurons (NeuN+, MAP2+) with laminar specificity (CTIP2+). **c** Cortical organoid diameter is decreased by EtOH exposure (Student's *t*-test, t_{541} = 17.05, P<0.0001; n=210-333 organoids/condition). **d** Immunohistochemistry portrays layers of Ki67+ proliferation (two months, Student's *t*-test, t_{64} = 4.518, P<0.0001; three months, Student's *t*-test, t_{18} = 1.63, P=0.12; n=10-33 organoids/condition). **e-g** EtOH exposure produces cell cycle alterations in cortical organoids (two-way analysis of variance (ANOVA), $F_{3,16}$ = 8.14, P=0.002) (**e**), iPSC-derived astrocytes (two-way ANOVA, $F_{2,42}$ = 17.06, P<0.0001) (**f**), and fetal neurons (two-way ANOVA, $F_{2,42}$ = 41.92, P<0.0001) (**g**). **h-j** EtOH exposure promotes cell death, shown by CC3+ immunohistochemistry in cortical organoids (two months, Student's *t*-test, t_{28} = 5.785, P<0.0001; three months, Student's *t*-test, t_{18} = 1.886, P=0.076; n=10-15 organoids/condition) (**h**) and Annexin+ in astrocytes (Student's *t*-test, t_{14} = 15.03, P<0.0001; n=8 replicates/condition) (**i**) and fetal neurons (Student's *t*-test, t_{6} = 7.872, P=0.0002; n=4 replicates/condition) (**j**). Data are presented as mean ± standard error of the mean (s.e.m.). Scale bar = 100 µm

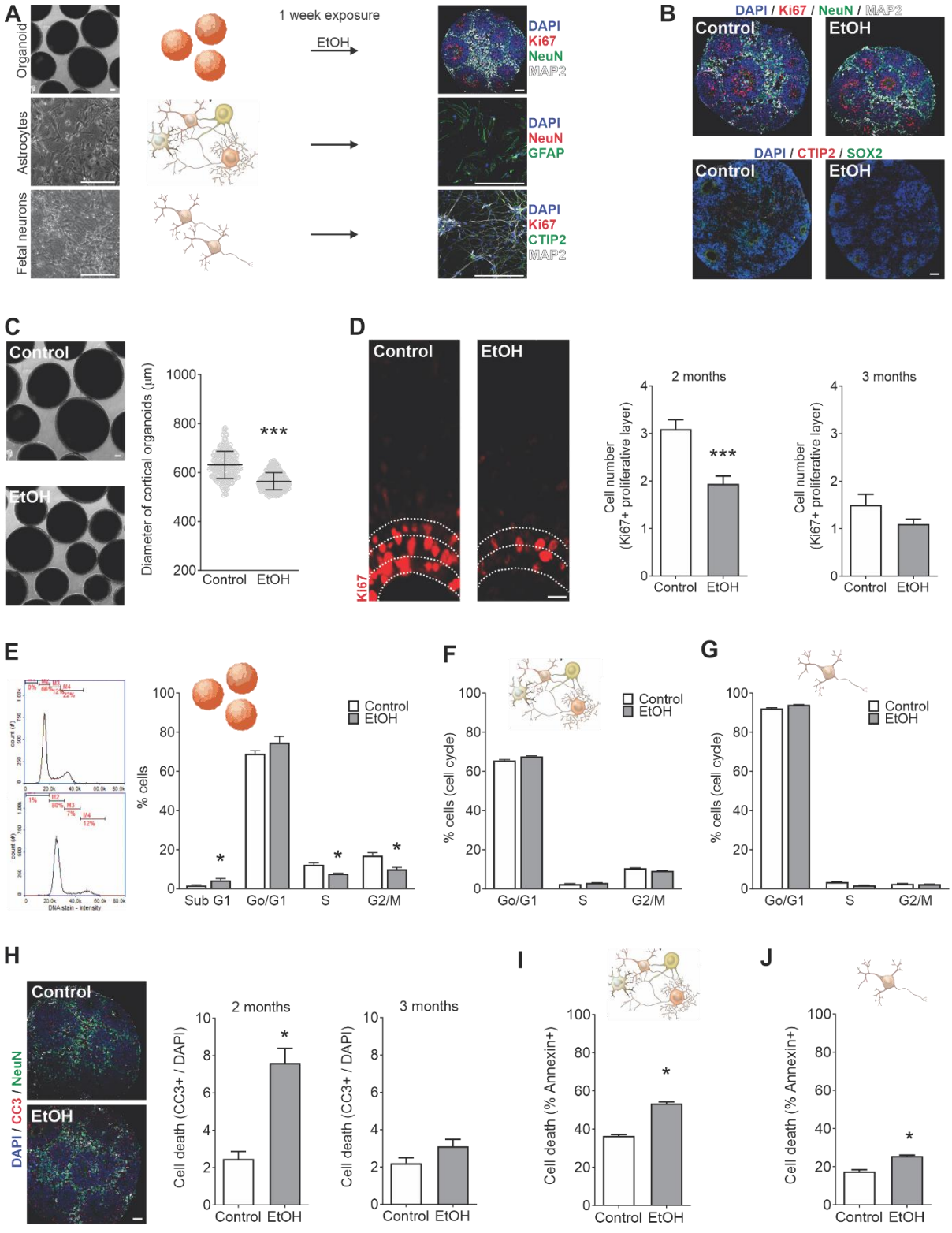
A
Organoid
Astrocytes
Fetal neurons
1 week exposure
EtOH
DAPI
Ki67
NeuN
MAP2
DAPI
NeuN
GFAP
DAPI
Ki67
CTIP2
MAP2
B
DAPI / Ki67 / NeuN / MAP2
Control
EtOH
DAPI / CTIP2 / SOX2
Control
EtOH
C
Control
EtOH
Diameter of cortical organoids (µm)
1000
800
600
400
200
***
Control
EtOH
D
Control
EtOH
Ki67
2 months
Cell number (Ki67+ proliferative layer)
***
Control
EtOH
3 months
Cell number (Ki67+ proliferative layer)
Control
EtOH
E
DNA stain - Intensity
% cells
Control
EtOH
Sub G1
Go/G1
S
G2/M
F
% cells (cell cycle)
Control
EtOH
Go/G1
S
G2/M
G
% cells (cell cycle)
Control
EtOH
Go/G1
S
G2/M
H
DAPI / CC3 / NeuN
Control
EtOH
2 months
Cell death (CC3+ / DAPI)
Control
EtOH
3 months
Cell death (CC3+ / DAPI)
Control
EtOH
I
Cell death (% Annexin+)
Control
EtOH
J
Cell death (% Annexin+)
Control
EtOH

Epigenetic landscape during neurodevelopment is altered by EtOH exposure

Epigenetic signaling is the principal mediator of the transcriptional response to environmental stimuli, a dynamic process in which stimulus-induced shifts in chromatin accessibility modulate differential gene expression. To define alterations in the chromatin human neurodevelopmental regulatory landscape due to EtOH exposure, we performed ATAC-seq in control and EtOH-exposed cortical organoids (Trevino et al., 2020). A high-quality library (Q30>90) was generated for each sample, and we detected a total of 604,998 peaks; EtOH-exposed organoids exhibited 20,731 peaks that were both common between replicates and distinct from controls. Annotating the peaks by genomic region suggested preferential enrichment of intergenic regions expected to have a regulatory function (Figure 20a,b, and Figure 25a-e). Analysis of chromatin motifs showed an association of EtOH exposure with enrichment of different sequences linked with proliferation and neurogenesis, including *NF1*, *NeuroD1,* and *Ascl1* (Figure 20c,d). For instance, *ARHGEF10* and *ARHGAP23* are linked with rho GTPases, and *NRXN1* and *NRXN3* produce synaptic cell adhesion molecules to promote synaptic structural integrity (Figure 20e,f). A summary Reactome analysis confirmed the prominent neurodevelopmental consequences of EtOH, with affected functions including axon guidance, cellular adhesion, and synaptic communication (Figure 20g).

In order to extend our ATAC-seq findings, we performed mass spectrometry to characterize EtOH-induced histone modifications in astrocytes, cortical organoids, and primary fetal neurons. Compared to controls, EtOH exposure was associated with specific enrichment of H3K9ac, H3K27me2,3, and H3K9me2, but we also observed a broader epigenetic shift: Histone methylation and acetylation were often decreased and increased,

respectively, in EtOH-exposed cells (Figure 20h,I). Histone deacetylase and methyltransferase expression were concordantly increased between all cell types in association with EtOH exposure. Moreover, EtOH appeared to induce a systematic decrease in the methylation of promoter regions (Figure 20h,i and Figure 25f,g). Together, these findings suggest that EtOH exposure resulted in an epigenetic shift affecting chromatin accessibility and histone post-translational modifications.

Figure 20: EtOH affects chromatin accessibility in regions critical for neurodevelopment. a-g, ATAC-seq analysis of two-month-old control and EtOH-exposed cortical organoids. **a** Transcription start site (TSS) enrichment plot showing TSS±1.0Kb for each sample. **b** Venn diagram depicts peaks in EtOH-exposed and control organoids. **c,d** Motif enrichment in control (**c**) and EtOH-exposed (**d**) organoids. **e** Plotting enrichment P values identifies prominent regions of altered accessibility. **f** Tracks plot of select prominent genes. **g** Reactome analysis predicts that the effects of altered chromatin accessibility concentrate in physiological processes central to neurodevelopment. **h,i** Mass spectrometry analysis shows histone modifications in astrocytes, cortical organoids, and fetal neurons attributable to EtOH-exposure. Heatmap shows EtOH exposure modifies histone methylation (ME) and acetylation (AC) patterns in diverse neural cell types (**h**), and a recurrent pattern of modifications is observed between astrocytes, organoids, and fetal neurons (**i**).

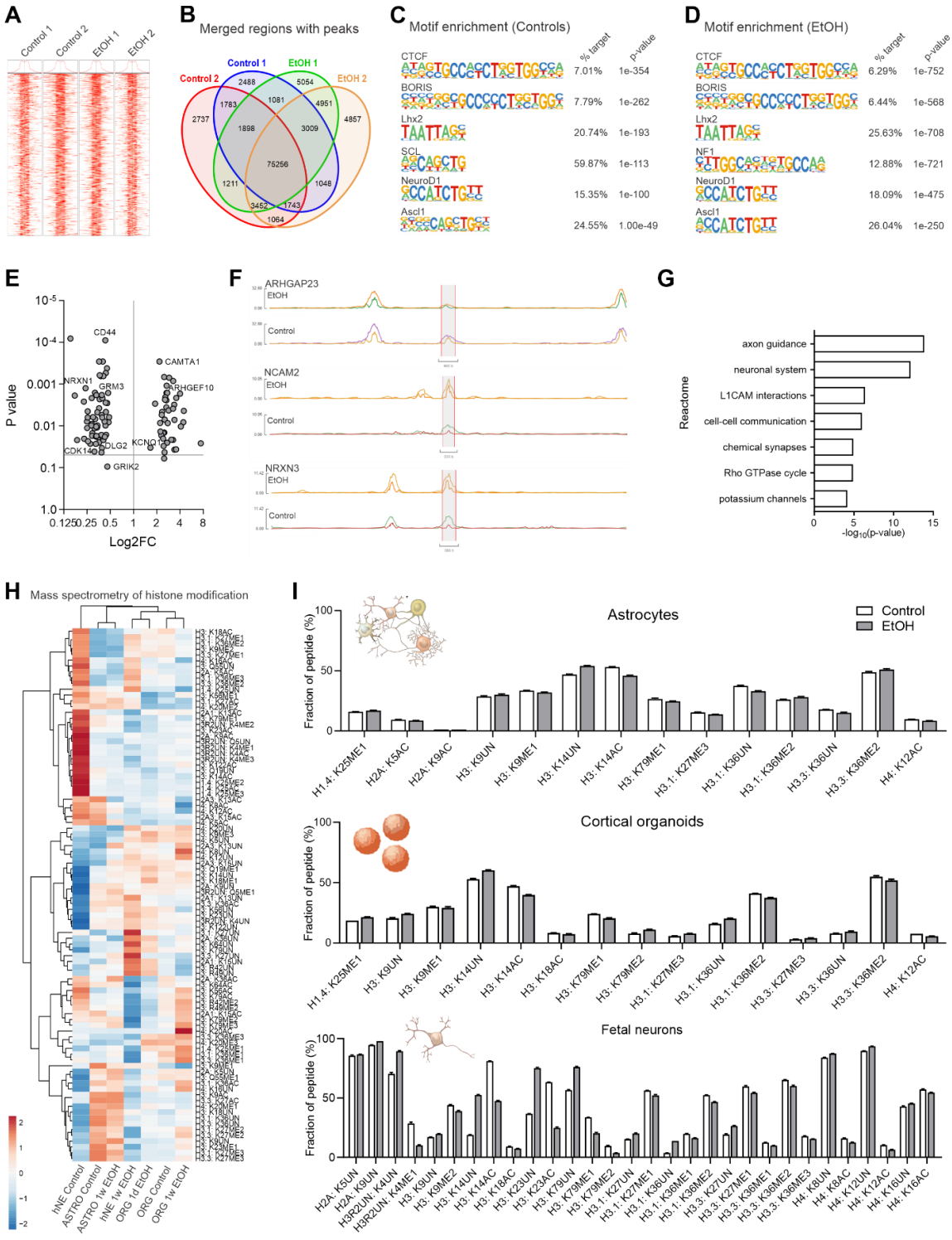
A
Control 1
Control 2
EtOH 1
EtOH 2
B
Merged regions with peaks
Control 1
Control 2
EtOH 1
EtOH 2
2488
5054
1783
1081
4951
2737
4857
1898
3009
75256
1211
1048
3452
1743
1054
C
Motif enrichment (Controls)
% target
p-value
CTCF
7.01%
1e-354
BORIS
7.79%
1e-262
Lhx2
20.74%
1e-193
SCL
59.87%
1e-113
NeuroD1
15.35%
1e-100
Ascl1
24.55%
1.00e-49
D
Motif enrichment (EtOH)
% target
p-value
CTCF
6.29%
1e-752
BORIS
6.44%
1e-568
Lhx2
25.63%
1e-708
NF1
12.88%
1e-721
NeuroD1
18.09%
1e-475
Ascl1
26.04%
1e-250
E
P value
Log2FC
CD44
CAMTA1
NRXN1
GRM3
ARHGEF10
DLG2
KCNQ5
CDK14
GRIK2
F
ARHGAP23
EtOH
Control
NCAM2
EtOH
Control
NRXN3
EtOH
Control
G
Reactome
axon guidance
neuronal system
L1CAM interactions
cell-cell communication
chemical synapses
Rho GTPase cycle
potassium channels
-log10(p-value)
H
Mass spectrometry of histone modification
hNE Control
ASTRO Control
ASTRO 1w EtOH
hNE 1w EtOH
ORG 1d EtOH
ORG Control
ORG 1w EtOH
I
Astrocytes
Control
EtOH
Fraction of peptide (%)
H1.4: K25ME1
H2A: K5AC
H2A: K9AC
H3: K9UN
H3: K9ME1
H3: K14UN
H3: K14AC
H3: K79ME1
H3.1: K27ME3
H3.1: K36UN
H3.1: K36ME2
H3.3: K36UN
H3.3: K36ME2
H4: K12AC
Cortical organoids
Fetal neurons

EtOH exposure is associated with transcriptomic alteration in neurodevelopmental pathways

EtOH-induced alterations in chromatin accessibility are expected to contribute to transcriptomic changes that underlie PAE neural cytopathology. We compared gene expression profiles between control and EtOH-exposed organoids and fetal neurons. Broadly, EtOH-exposed cortical organoids and fetal neurons exhibited differential global gene expression and clustered distinctly from controls (Figure 21a and Figure 26a,b). The affected transcriptomic pathways in cortical organoids include protein processing and cell cycle regulation (Figure 21b and Figure 26c), also identified by ATAC-seq analysis. Many of the altered processes appeared to interact (Figure 21c), underscoring the breadth of cellular impairment by EtOH. Summary gene ontology analysis in fetal neurons likewise implicated the effects of EtOH on cell cycle and cytoskeletal structure (Figure 21d and Figure 26d). EtOH induces alterations in cellular signaling pathways, ligand-receptor interaction, and neurotransmission at a later stage in cortical organoids, including excitatory and GABAergic signaling and astrocytic function (Figure 21e-h and Figure 26e). In addition, cAMP, PI3K-Akt, and Hedgehog signaling were impaired, leading to alterations in cell viability, calcium homeostasis, synaptic vesicle cycling, and long-term potentiation (Figure 21i,j and Figure 27).

Figure 21: EtOH alters neurodevelopmental transcriptional pathways in cortical organoids and fetal neurons. a RNAseq heatmap within cortical organoid and fetal neuron subgroups shows differential gene expression clustering by EtOH exposure. **b** Visualization of prominently altered cell processes in two-month-old EtOH-exposed organoids. Pathway enrichment analysis of genes altered by EtOH exposure is displayed according to total perturbation accumulation (pACC) and gene overrepresentation within pathways (pORA). Red dots represent pathways modified with a significant P value, proportional to the size of the dots. **c** Interactome depicting the interrelatedness of these processes. **d** Cross-comparative gene ontology analysis of EtOH-exposed fetal neurons shows overlapping pathway alterations with organoids. **e** Plot of P values for gene expression in three-month old organoids portrays range of alteration severity. **f** Visualization of prominently altered cell processes in three-month old EtOH-exposed organoids. **g** Gene ontology analysis of three-month old organoids shows gene expression alterations prominently affect neurotransmission and biochemical signaling pathways. **h** Interactome highlights involvement of key processes including excitatory and GABAergic signaling and astrocytic expression. **i,j** EtOH exposure impacts gene expression in prominent pathways with multifactorial downstream consequences. Shown are EtOH-induced changes in the cAMP signaling pathway (**I**) and glutamatergic synaptic function (**j**).

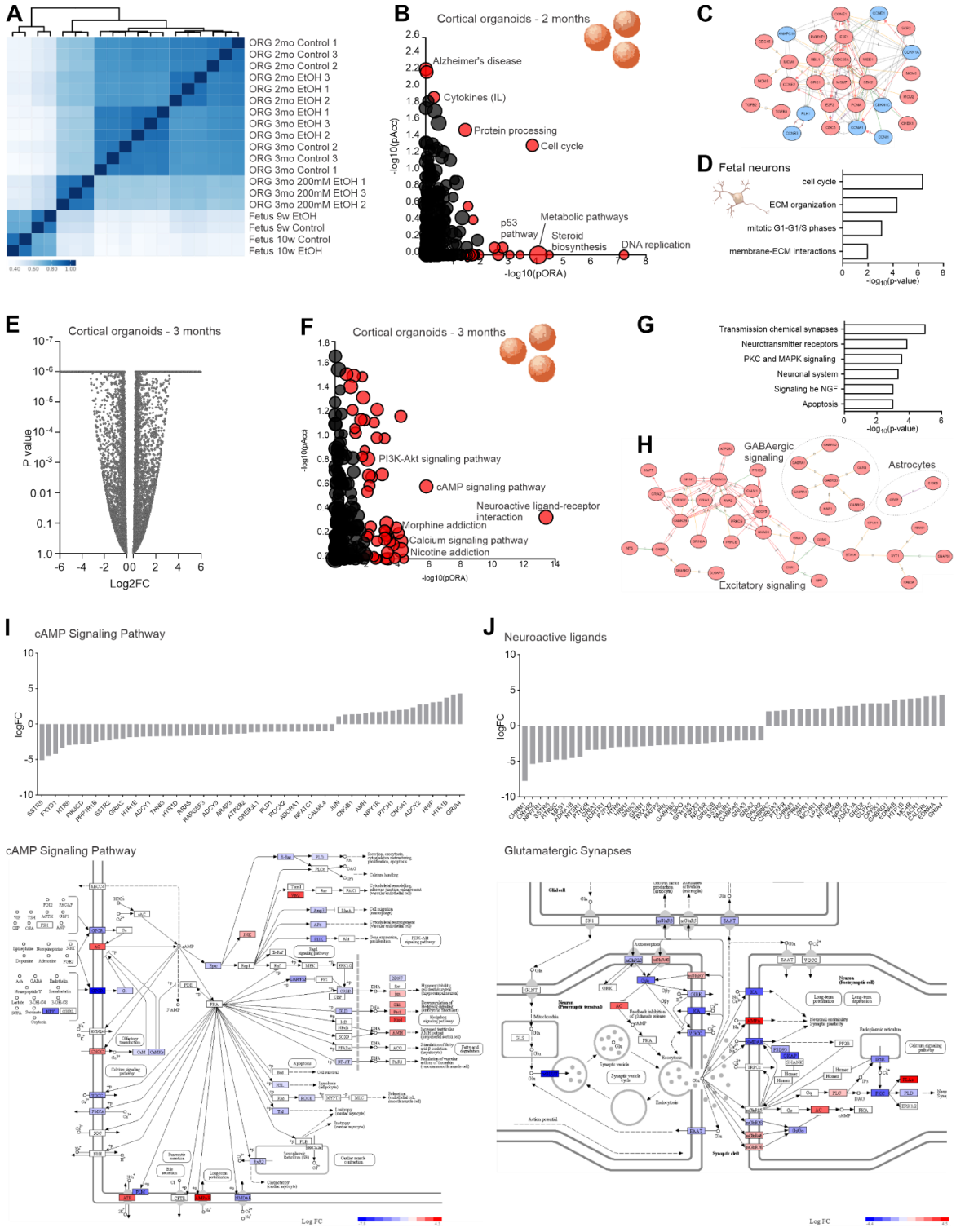
A
ORG 2mo Control 1
ORG 2mo Control 3
ORG 2mo Control 2
ORG 2mo EtOH 3
ORG 2mo EtOH 1
ORG 2mo EtOH 2
ORG 3mo EtOH 1
ORG 3mo EtOH 3
ORG 3mo EtOH 2
ORG 3mo Control 2
ORG 3mo Control 3
ORG 3mo Control 1
ORG 3mo 200mM EtOH 1
ORG 3mo 200mM EtOH 3
ORG 3mo 200mM EtOH 2
Fetus 9w EtOH
Fetus 9w Control
Fetus 10w Control
Fetus 10w EtOH
B
Cortical organoids - 2 months
Alzheimer's disease
Cytokines (IL)
Protein processing
Cell cycle
p53 pathway
Metabolic pathways
Steroid biosynthesis
DNA replication
-log10(pAcc)
-log10(pORA)
C
D
Fetal neurons
cell cycle
ECM organization
mitotic G1-G1/S phases
membrane-ECM interactions
-log10(p-value)
E
Cortical organoids - 3 months
P value
Log2FC
F
Cortical organoids - 3 months
PI3K-Akt signaling pathway
cAMP signaling pathway
Neuroactive ligand-receptor interaction
Morphine addiction
Calcium signaling pathway
Nicotine addiction
-log10(pAcc)
-log10(pORA)
G
Transmission chemical synapses
Neurotransmitter receptors
PKC and MAPK signaling
Neuronal system
Signaling be NGF
Apoptosis
-log10(p-value)
H
GABAergic signaling
Astrocytes
Excitatory signaling
I
cAMP Signaling Pathway
logFC
J
Neuroactive ligands
logFC
cAMP Signaling Pathway
Log FC
Glutamatergic Synapses
Log FC

Digital Spatial Profiling portrays differential proteomics of EtOH-exposed cortical organoids

The transcriptomic and gene expression alterations observed prompted us to explore protein expression patterns after EtOH exposure. (Merritt et al., 2020) Proliferative rosette-like and non-proliferative regions within cortical organoids exhibited distinct clusters of protein abundance variation (Figure 22c). Cortical organoid samples, EtOH-exposed or untreated, and cells within different regions, rosette or non-rosette, are distinct from one another (Figure 22d). Proliferative cells within EtOH-exposed rosettes showed expression changes for proteins such as Neurofilament light, Phospho-Tau (S396), HLA-DR, CD-45, CD-68, TMEM119, and TDP-43. phospho-Tau (S199) was upregulated in EtOH-exposed proliferative rosette regions (Figure 22e).

EtOH exposure increases astroglia cluster content and impairs synaptogenesis and connectivity

The combined analysis of epigenetic and transcriptomic profiles implicated synaptic connectivity and astrocytic alteration defects due to EtOH exposure, leading us to target these properties for further investigation. Western blot analysis showed EtOH-exposed cortical organoids exhibited altered content of hallmark neural proteins, including SYN1, PSD95, and GFAP (Figure 22a,b and Figure 28). To gain insights into a potential cellular vulnerability, we quantitated cell type in cortical organoids. EtOH exposure was associated with higher percentages of cells in clusters expressing the astrocytic GFAP marker at two ($P = 0.007$) and three months of age ($P = 0.04$; Figure 23a). Despite the astrocytic increase, the neuronal fate seemed unaffected because quantities of the cortical layer V/VI neuronal marker CTIP2 remained equivalent (Figure 23a). Impairment of synaptogenesis was evaluated by

quantifying synaptic puncta density, characterized by co-localization of the presynaptic Vglut1 and postsynaptic Homer1 proteins. Reduced synaptic puncta density was observed after two months of EtOH exposure (P = 0.01; Figure 23b), suggesting that early exposure can impact neuronal connectivity for an extended period.

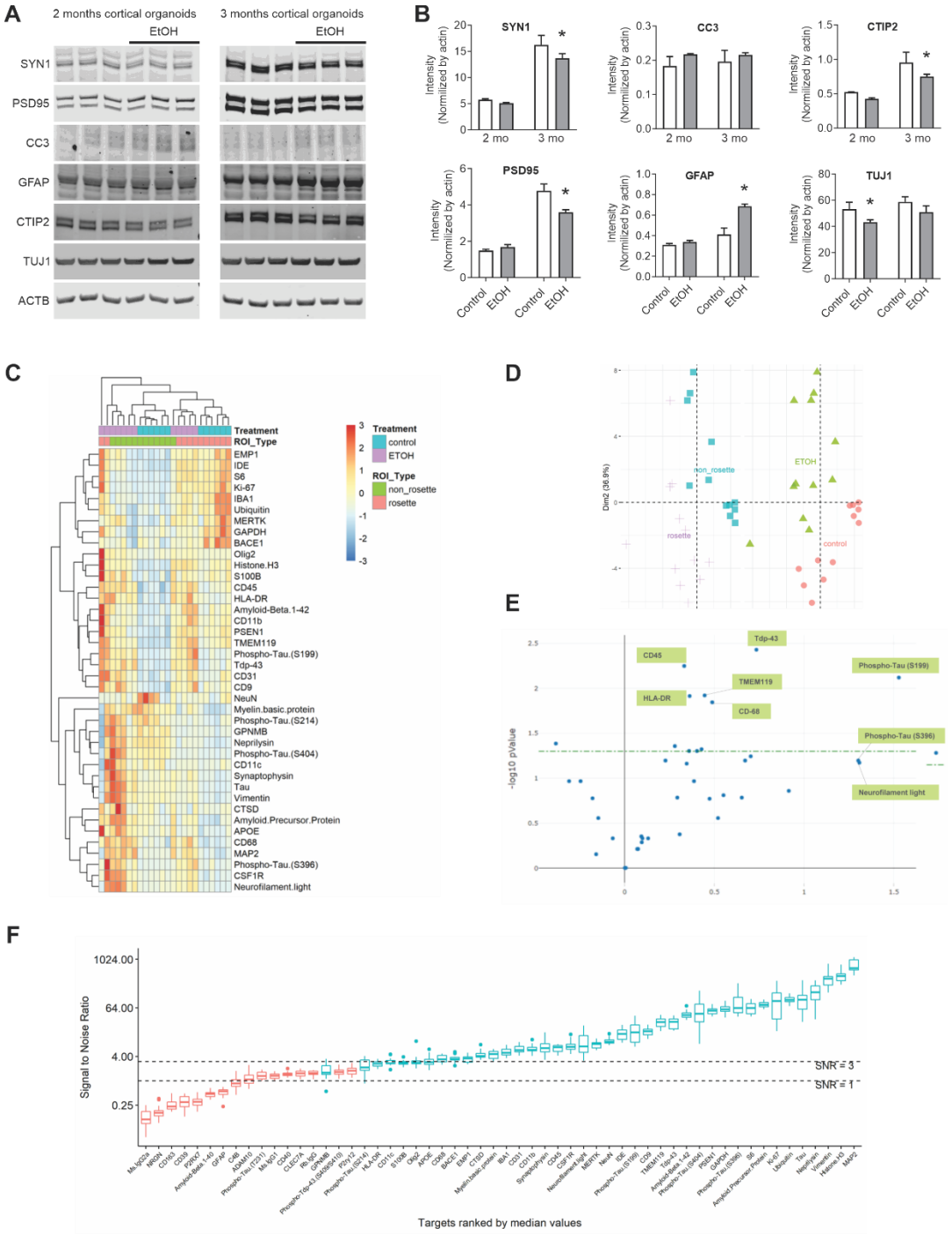

Figure 22: EtOH alters astrocytic and synaptic protein quantities and promotes differential protein abundance in cortical organoids. a,b Western blot and quantification of astrocytic and synaptic protein markers in cortical organoids during development (two-way ANOVA for each protein; **P*<0.05, ***P*<0.01, ****P*<0.001). **c** Heatmap protein abundance. **e** Volcano plot of proliferative (rosette) regions highlights various proteins. Protein values below SNR < 1 may be attributed to background noise while proteins with values between 1 and 3 may need further validation.

Multi-electrode array electrophysiology recordings enable dynamic interrogation of how human neurons behave in circuits, a valuable approach given that connectivity cannot be assessed during the early stages of human corticogenesis *in utero*. We plated one-month-old paired control and EtOH-exposed organoids to mature in MEA plates and recorded their activity (Figure 23c,e). Compared to controls, EtOH-exposed cortical organoids spiked fewer times per minute ($P = 0.01$) and had fewer bursts ($P = 0.047$), although synchronous network bursts remained unchanged ($P = 0.93$; Figure 23d). Finally, we used primary human fetal neural tissues to validate our results. Fetal neurons exhibited a similar MEA profile with fewer spikes ($P = 0.01$) and fewer bursts ($P = 0.01$) per minute, but the decrease in synchronous network bursts did not reach significance ($P = 0.08$; Figure 23f). These findings showed that EtOH-induced alterations in neuronal network formation persist despite cessation of the exposure (Trujillo, Adams, et al., 2021).

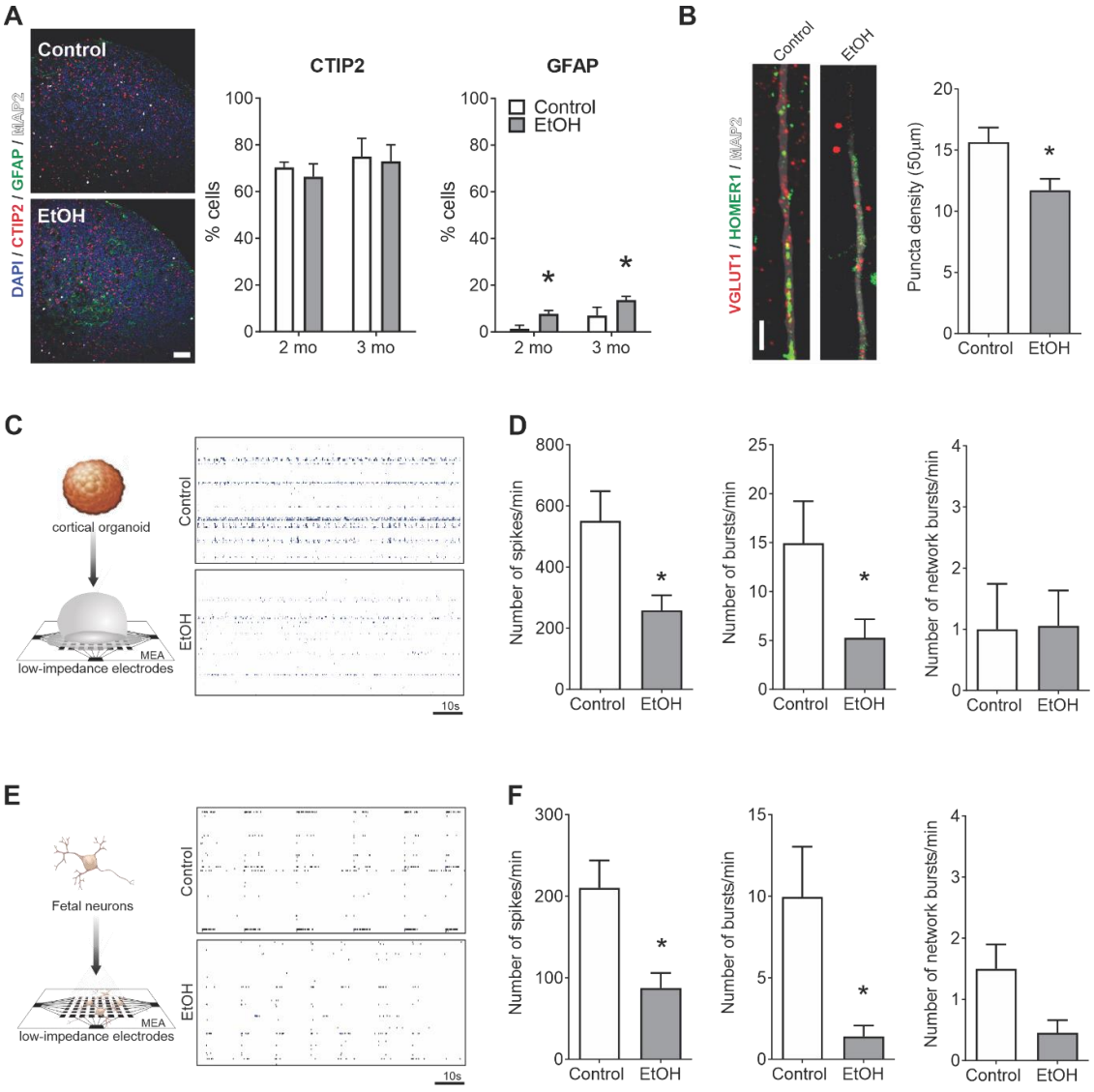

Figure 23: EtOH exposure increases astrocytic content and impairs network connectivity. a Immunohistochemistry reveals no difference in the proportion of CTIP2+ cells (left graph; two months, P=0.88; three months, P>0.99) but shows EtOH increases GFAP expression (right graph; two months, P=0.017; three months, P=0.013; two-way ANOVAs). **b** EtOH exposure decreases co-localized synaptic puncta density (Student's t-test, t_{32} = 2.59, P=0.01; n=17 neurons/condition). **c-e** Multi-electrode array (MEA) analysis in cortical organoids (**c,d**, n=18 MEA wells/condition) and fetal neurons (**e,f**, n=11-22 MEA wells/condition). **c** Representative cortical organoid MEA raster plot. **d** EtOH-exposed cortical organoids showed fewer spikes per minute (Student's t-test, t_{34} = 2.68, P=0.011) and fewer bursts (Student's t-test, P=0.047), although not network bursts (Student's t-test, t_{34} = 0.06, P=0.95). **e** Representative fetal neuron MEA raster plot. **f** EtOH-exposed fetal neurons showed fewer spikes per minute (Student's t-test, t_{30} = 2.68, P=0.012) and fewer bursts per minute (Student's t-test, t_{40} = 2.60, P=0.013), but not network bursts (Student's t-test, t_{31} = 1.78, P=0.085). Data are presented as mean ± s.e.m

Discussion

In the present study, hiPSC-derived cortical organoids were exposed to EtOH and then comprehensively assayed to investigate the neurodevelopmental impact of EtOH on neural proliferation and viability, chromatin alteration and histone modification, transcriptomic and proteomic shifts, and neuronal electrophysiology and network formation. We validated our findings and further explored cell-type specific defects in hiPSC-derived astrocytes and human fetal primary neurons. EtOH-exposed cortical organoids showed impaired proliferation and increased cell death, and we observed shifts in their epigenomic and transcriptomic profiles resulting from the exposure that paralleled the particular cell-type-specific defects that we had detected. In particular, the regions of altered chromatin accessibility were most prominently related to neurodevelopment, neurotransmission, cell-cell interaction, and Rho GTPase signaling. Concordantly, electrophysiological analysis demonstrated that EtOH exposure caused prolonged functional impairment and decreased network connectivity in the organoids that was validated by findings in human fetal primary neurons.

Prenatal exposure to EtOH is associated with microcephaly during all stages of brain growth (Hendrickson et al., 2017; Jones et al., 1973; Sawada Feldman et al., 2012), and magnetic resonance imaging (MRI) in FASD patients portrays volumetric reductions in the cortex, corpus callosum, cerebellum, and other subcortical structures (Astley et al., 2009; Lebel et al., 2011; Riley et al., 2004, 2011). Similarly, we observed that the size of EtOH-exposed cortical organoids was reduced compared to control organoids. In agreement, EtOH-exposed organoids had fewer dividing cells during proliferative stages and increased cell death, a phenotype that aligns with effects reported in other model systems (Anthony et al.,

2008; Santillano et al., 2005). However, despite this convergence, it is unlikely that these acute neurotoxic effects are the only pathologies underlying the long-lasting effects of PAE.

Epigenetic signaling mediates the transcriptional response to environmental stimuli, and EtOH has previously been shown to induce epigenetic alterations (Kaminen-Ahola et al., 2010). ATAC-seq of organoids showed that EtOH exposure was associated with widespread changes in chromatin accessibility that was most prominently related to neurodevelopment, neurotransmission, and Rho GTPase signaling. Rho GTPases have been linked with gene expression, cell-cell interaction, neuronal morphology, and cell cycle progression (Amin et al., 2016; Stankiewicz & Linseman, 2014), and they also contribute to the regulation of neuronal survival via MAPK pathway activation. Additionally, a decreased accessibility of chromatin sites related to cell interaction was observed, such as the neurexin genes. The neurexins are involved in early cortical synaptogenesis, axon guidance, and intercellular communication, and mutations in *NRXN3* have been identified in patients with autism spectrum disorders (Joshi et al., 2006; Lindsley et al., 2011; Vaags et al., 2012; Zhou, 2015). Furthermore, we used the GeoMx DSP platform to investigate the spacial profile of proteins in specific regions of the organoids. Interestingly, EtOH exposure affected numerous proteins that are salient in other neurological diseases, including inflammatory and degenerative proteins (Neurofilament light, Phospho-Tau (S396), HLA-DR, CD-45, CD-68, TMEM119, and TDP-43). The cell models used in this study lack neuroinflammatory cells and are thus sub-optimal to more deeply study the cell-type specific aspects of these pathologies, so further investigation of these findings using other models will be an important direction for future research.

DNA methylation and histone modifications regulate the accessibility of DNA for transcriptional proteins and are thought to be central mediators of the lifelong clinical effects of FASD (Renthal & Nestler, 2009). Using mass spectrometry, we quantified the relative abundance of >80 different post-translational histone modifications (e.g., acetylation, methylation, ubiquitination, and unmodified peptides). EtOH exposure induced a unique profile of histone modifications among cortical organoids, hiPSC-derived astrocytes, and human fetal neurons. Notably, EtOH exposure produced parallel duration-dependent gradients in the modification patterns in cortical organoids and human fetal neurons (e.g., acetylation and H3K14UN, H3K79ME1 and H4K12AC and H3K23). These findings align with previously reported EtOH-induced changes in post-translational modifications in FASD patients and other model systems (Laufer et al., 2015; Mandal et al., 2017), further underscoring their involvement in its pathophysiology.

Aligning epigenetic information with transcriptomic data may indicate how EtOH affects early brain formation. Exposed samples showed differences in gene expression and clustered distinctly from controls. In early cortical organoids, the main processes affected by EtOH exposure were related to normal cellular function, such as protein processing and cell cycle. However, later in their development, transcriptional alterations were related to cAMP signaling, neuroactive ligand pathways, RAP1, and Hippo signaling pathways. The Hippo signaling pathway regulates growth via proliferation and apoptosis, which may partially explain the EtOH-induced cellular phenotypes we observed.

Beyond its neuronal effects, PAE may also impair neurodevelopment via astrocytic disruption. EtOH increased cell death, altered the histone modification pattern, and produced shifts in the astrocytic cell cycle and proliferation in parallel with the findings of other studies

(Adermark & Bowers, 2016; Guerri et al., 1990). Interestingly, the amount of astrocytic protein GFAP was increased in EtOH-exposed organoids, suggesting that astrocytes may be more involved with PAE pathogenesis than was previously appreciated. Indeed, consistent with our findings, a previous study by Boronat and coworkers (2017) detected abundant gliosis in MRIs of 72 pediatric FASD patients. Further investigation of astrocytic involvement in the setting of PAE will be an important direction for future studies.

We performed MEA electrophysiological analysis of neuronal network circuitry and validated our findings using human primary neurons. EtOH exposure impaired synaptogenesis, concordant with gross and microscopic neuropathology described in FASD patients (Kroener et al., 2012). These findings contrast with the propensity for seizures in these patients and murine models, which is thought to result from neuronal hyperexcitability. However, comparing these differences may be inequitable because these observations are drawn from hippocampal regions, whereas our models are cortical (Bell et al., 2010; Krawczyk et al., 2016). Nevertheless, the induced network changes persisted for months despite halting the exposure, supporting the prevailing understanding that even acute EtOH exposure is sufficient to produce lasting neurodevelopmental effects.

Although this study is a step towards understanding PAE, it was unavoidably subject to several limitations. Despite advancements in technology, cortical organoids are only a cellular model rather than a bonafide human brain, so making a direct judgment about the full effects of *in utero* EtOH exposure remains limited. We have sought to minimize this limitation by including analyses in human primary fetal neurons, which appear to validate the findings in the cortical organoids. Another limitation is that EtOH metabolites were not assessed. Thus, although EtOH exposure is associated with specific cellular alterations, it is

unclear whether particular metabolites or variations in the rate of EtOH metabolism, for example, can alter the severity of the effects of the exposure. However, our results were consistent between cell lines and exposures, minimizing any concern about individual metabolite variation. A third limitation is that the EtOH concentration and exposure are unavoidably different from those experienced during fetal development, particularly considering fetal recycling of amniotic fluid and the consequent risk of prolonged EtOH exposure *in utero* (Heller & Burd, 2014).

hiPSC-derived cortical organoids are a valuable model to assess the effects of EtOH exposure on human neurodevelopment and will facilitate further study of the pathophysiology underlying the clinical symptoms associated with PAE. Supported by validation in human primary fetal neurons, EtOH-exposed cortical organoids portrayed impaired cell growth and viability, featured alterations in their epigenomic and transcriptomic profiles in regions critical to neurodevelopment, and experienced dysfunctional neuronal network formation. EtOH exposure disrupted several prominent growth and signaling pathways, and future research efforts may discover that these are opportune targets to therapeutically impede the developmental neuropathology of PAE.

Figure 24: Generation and characterization of iPSC-derived cortical organoids and astrocytes and characterization of fetal human primary neurons. a Schematic depicting generation of cortical organoids by aggregation and differentiation of iPSCs. **b** Cell type as a percentage changes as cortical organoid development progresses. **c** Immunohistochemical characterization of neural markers in young cortical organoids. **d** Schematic depicting derivation of astrocytes from iPSCs. **e** Quantification of astrocytic population purity. **f,g** Representative plots for annexin (**f**) and cell cycle (**g**) between control and EtOH-exposed astrocytes. **h** Schematic depicting acquisition of fetal human primary neurons. **i** Quantification of neuronal population purity. **j,k** Representative plots for annexin (**j**) and cell cycle (**k**) between control and EtOH-exposed fetal neurons. **l** EtOH exposure scheme showing method of containment to promote EtOH-saturated environment. **m** EtOH concentration in media sharply decreases in the first two hours and stabilizes around 20 mM with time. EtOH was added every other day.

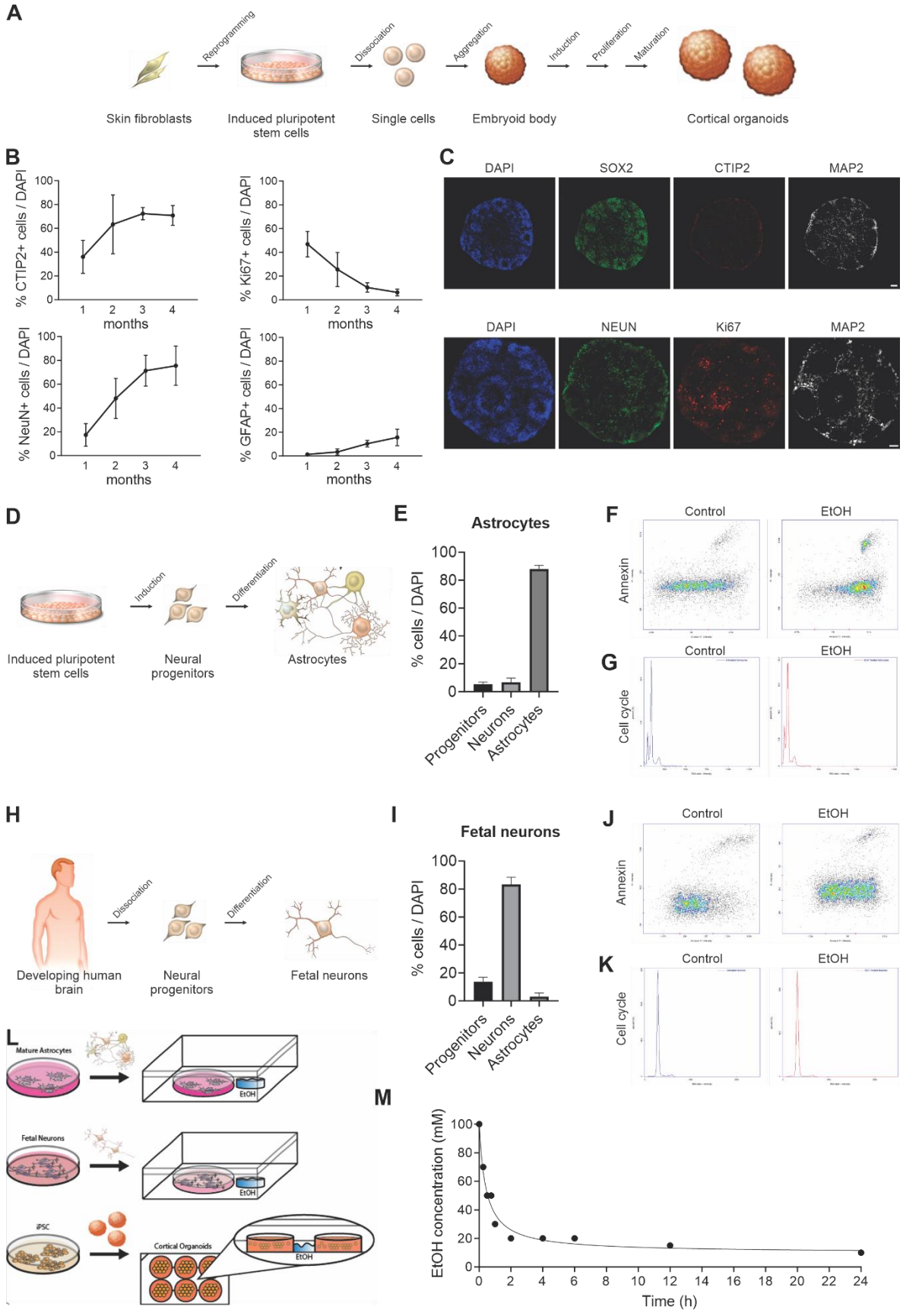
A
Reprogramming
Dissociation
Aggregation
Induction
Proliferation
Maturation
Skin fibroblasts
Induced pluripotent stem cells
Single cells
Embryoid body
Cortical organoids
B
% CTIP2+ cells / DAPI
% Ki67+ cells / DAPI
% NeuN+ cells / DAPI
% GFAP+ cells / DAPI
months
C
DAPI
SOX2
CTIP2
MAP2
DAPI
NEUN
Ki67
MAP2
D
Induction
Differentiation
Induced pluripotent stem cells
Neural progenitors
Astrocytes
E
Astrocytes
% cells / DAPI
Progenitors
Neurons
Astrocytes
F
Control
EtOH
Annexin
G
Control
EtOH
Cell cycle
H
Dissociation
Differentiation
Developing human brain
Neural progenitors
Fetal neurons
I
Fetal neurons
% cells / DAPI
Progenitors
Neurons
Astrocytes
J
Control
EtOH
Annexin
K
Control
EtOH
Cell cycle
L
Mature Astrocytes
Fetal Neurons
iPSC
Cortical Organoids
EtOH
M
EtOH concentration (mM)
Time (h)

Figure 25: ATAC-seq peak distribution and mass spectrometry analysis of histone modification in cortical organoids due to one day of EtOH exposure. a,b ATAC-seq plots show the fraction of reads within peaks of enrichment (**a**) and how peaks distribute by genomic region (**b**). **c** Autocorrelation plots for samples. **d,e** Plots showing peak regions (**d**) and TS sites concentrated around promoters (**e**). Mass spectrometry analysis of EtOH-induced histone modifications shows sample distinction upon principal component analysis (**f**). EtOH exposure for one day is sufficient to alter the epigenetic pattern of histone methylation (ME) and acetylation (AC) in cortical organoids akin to that of longer durations of exposure (**g**).

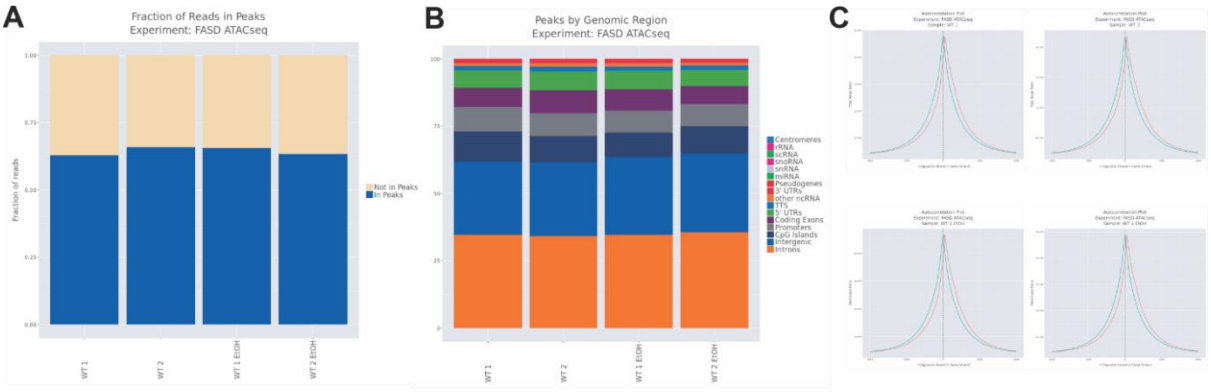
A
Fraction of Reads in Peaks
Experiment: FASD ATACseq
Fraction of reads
Not in Peaks
In Peaks
WT 1
WT 2
WT 1 EtOH
WT 2 EtOH
B
Peaks by Genomic Region
Experiment: FASD ATACseq
Centromeres
rRNA
scRNA
snoRNA
snRNA
miRNA
Pseudogenes
3' UTRs
other ncRNA
TTS
5' UTRs
Coding Exons
Promoters
CpG Islands
Intergenic
Introns
C

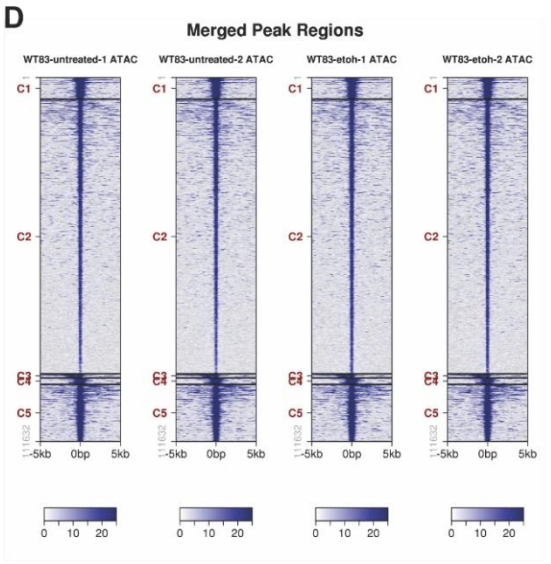
D
Merged Peak Regions
WT83-untreated-1 ATAC
WT83-untreated-2 ATAC
WT83-etoh-1 ATAC
WT83-etoh-2 ATAC
C1
C2
C3
C4
C5
-5kb
0bp
5kb
0
10
20

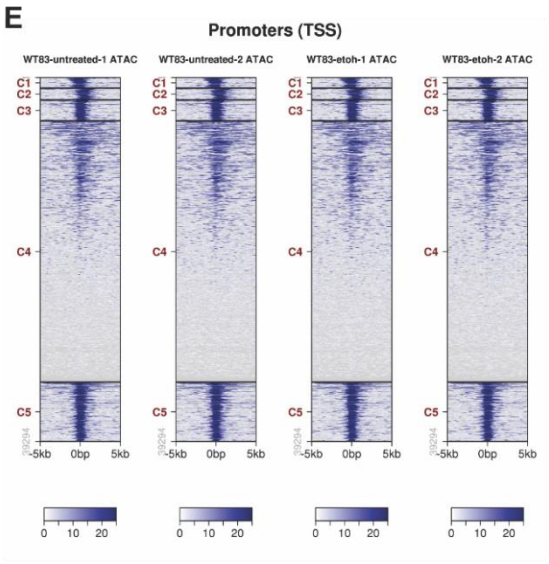
E
Promoters (TSS)
WT83-untreated-1 ATAC
WT83-untreated-2 ATAC
WT83-etoh-1 ATAC
WT83-etoh-2 ATAC
C1
C2
C3
C4
C5
-5kb
0bp
5kb
0
10
20

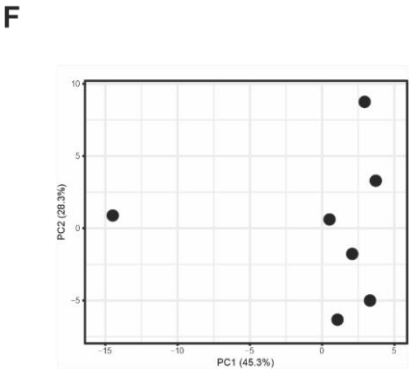
F
PC2 (28.3%)
PC1 (45.3%)

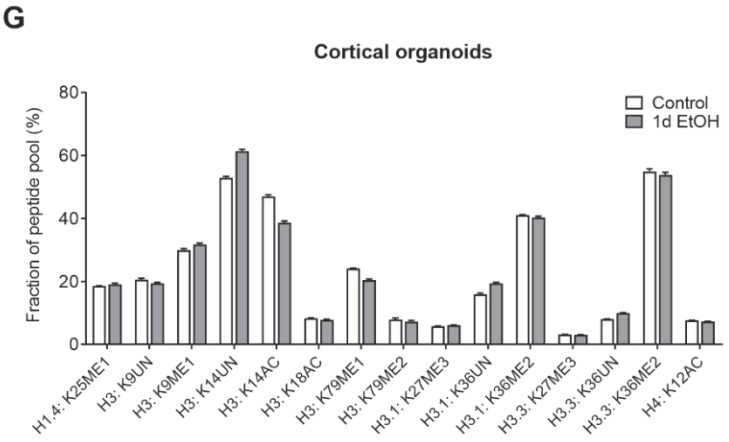
G
Cortical organoids
Control
1d EtOH
Fraction of peptide pool (%)
H1.4: K25ME1
H3: K9UN
H3: K9ME1
H3: K14UN
H3: K14AC
H3: K18AC
H3: K79ME1
H3: K79ME2
H3.1: K27ME3
H3.1: K36UN
H3.1: K36ME2
H3.3: K27ME3
H3.3: K36UN
H3.3: K36ME2
H4: K12AC

Figure 26: RNA-seq analysis of control and EtOH-exposed cortical organoids and fetal neurons. a Samples segregate with distinct gene expression signatures. **b** Visualization of the genomic distribution of reads. **c** Gene expression comparison between EtOH-exposed and control two-month-old cortical organoids. **d** Gene expression comparison between three-month-old [200 mM] EtOH-exposed and control cortical organoids. **e** Gene expression comparison between EtOH-exposed and control fetal neurons.

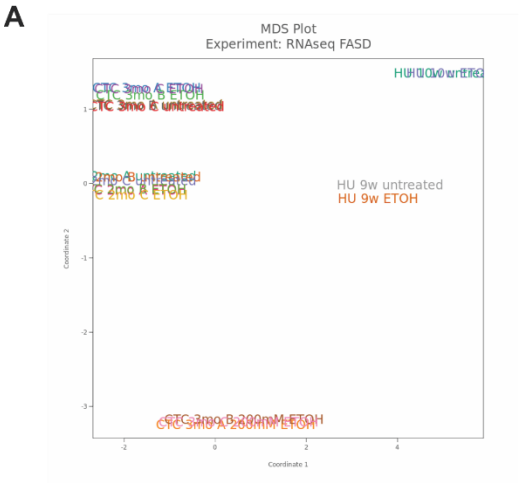
A
MDS Plot
Experiment: RNAseq FASD
CTC 3mo A ETOH
CTC 3mo B ETOH
CTC 3mo C untreated
CTC 2mo A untreated
CTC 2mo B untreated
CTC 2mo C ETOH
HU 9w untreated
HU 9w ETOH
CTC 2mo B 200mM ETOH
CTC 3mo A 200mM ETOH
Coordinate 1
Coordinate 2

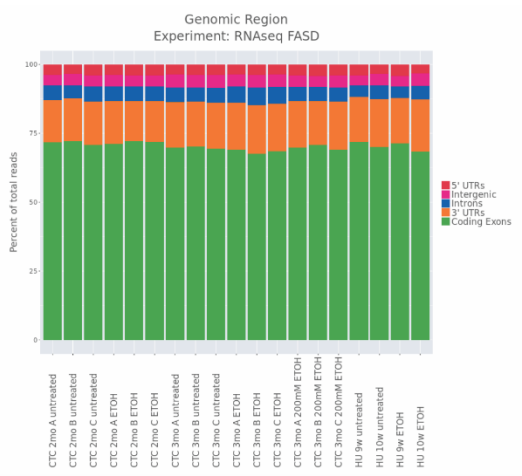
B
Genomic Region
Experiment: RNAseq FASD
Percent of total reads
5' UTRs
Intergenic
Introns
3' UTRs
Coding Exons
CTC 2mo A untreated
CTC 2mo B untreated
CTC 2mo C untreated
CTC 2mo A ETOH
CTC 2mo B ETOH
CTC 2mo C ETOH
CTC 3mo A untreated
CTC 3mo B untreated
CTC 3mo C untreated
CTC 3mo A ETOH
CTC 3mo B ETOH
CTC 3mo C ETOH
CTC 3mo A 200mM ETOH
CTC 3mo B 200mM ETOH
CTC 3mo C 200mM ETOH
HU 9w untreated
HU 10w untreated
HU 9w ETOH
HU 10w ETOH

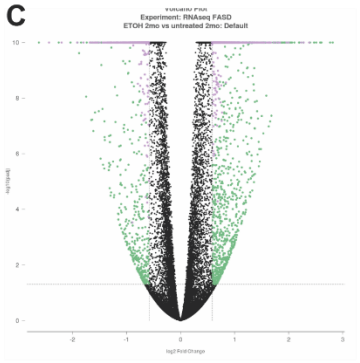
C
Experiment: RNAseq FASD
ETOH 2mo vs untreated 2mo: Default

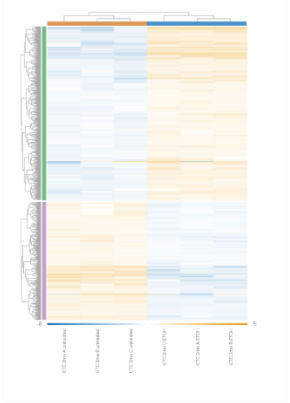

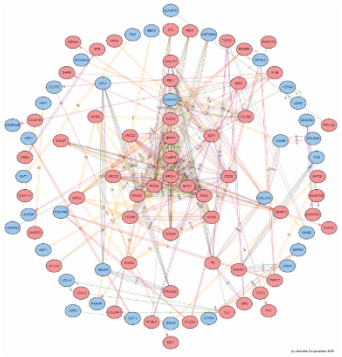

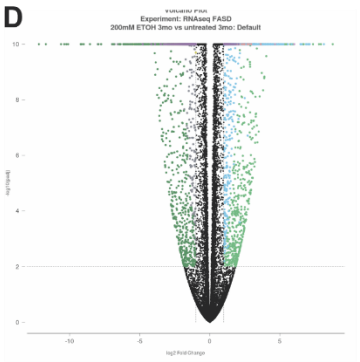
D
Experiment: RNAseq FASD
200mM ETOH 3mo vs untreated 3mo: Default

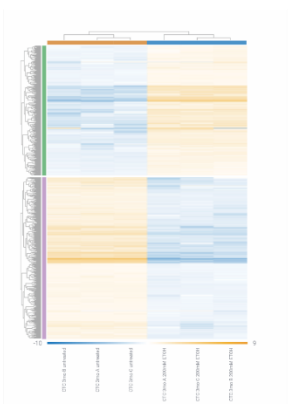

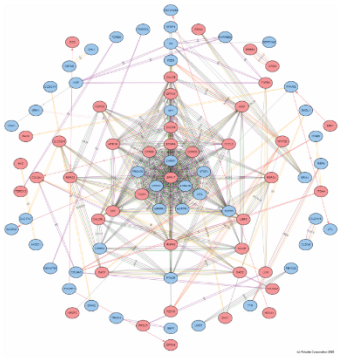

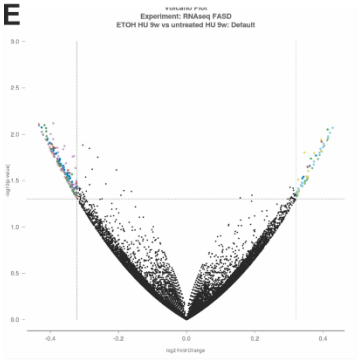
E
Experiment: RNAseq FASD
ETOH HU 9w vs untreated HU 9w: Default

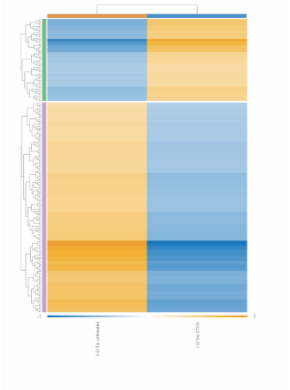

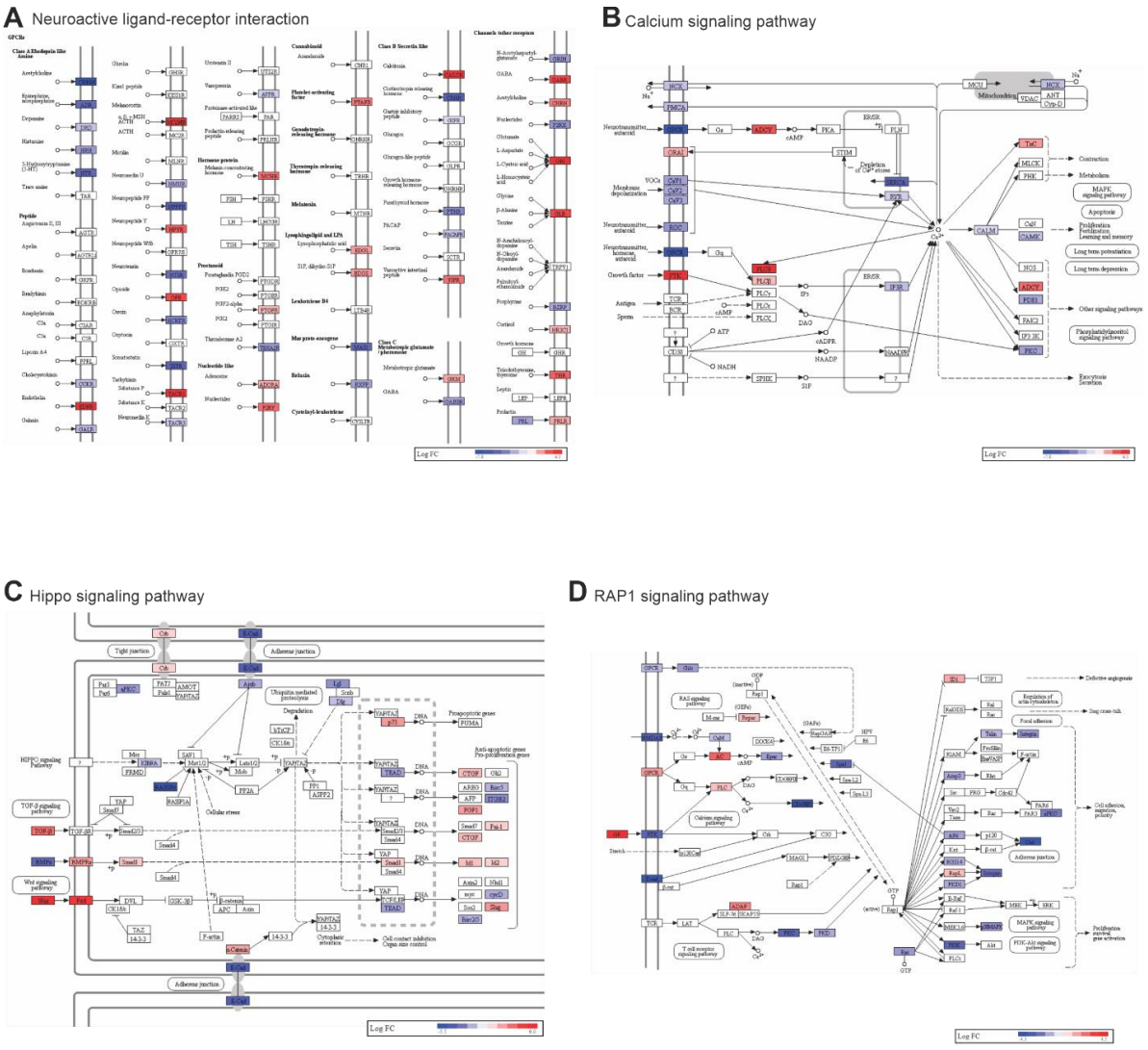

Figure 27: Pathway analyses of EtOH-induced differential gene expression in cortical organoids. a Broad involvement of pathways relevant to neural development and function. **b** Prominent involvement of calcium signaling pathways, with central consequences in MAPK signaling, long-term potentiation and depression, apoptosis, and the phosphatidylinositol signaling pathway. **c** EtOH-induced changes in gene expression include effects on the TGF-β and Wnt signaling pathways as well as cell-cell interactions via adherens junctions. **d** EtOH-induced changes in the RAP1 signaling pathway are likewise consequential for calcium signaling, cell-cell adhesion, and MAPK signaling.

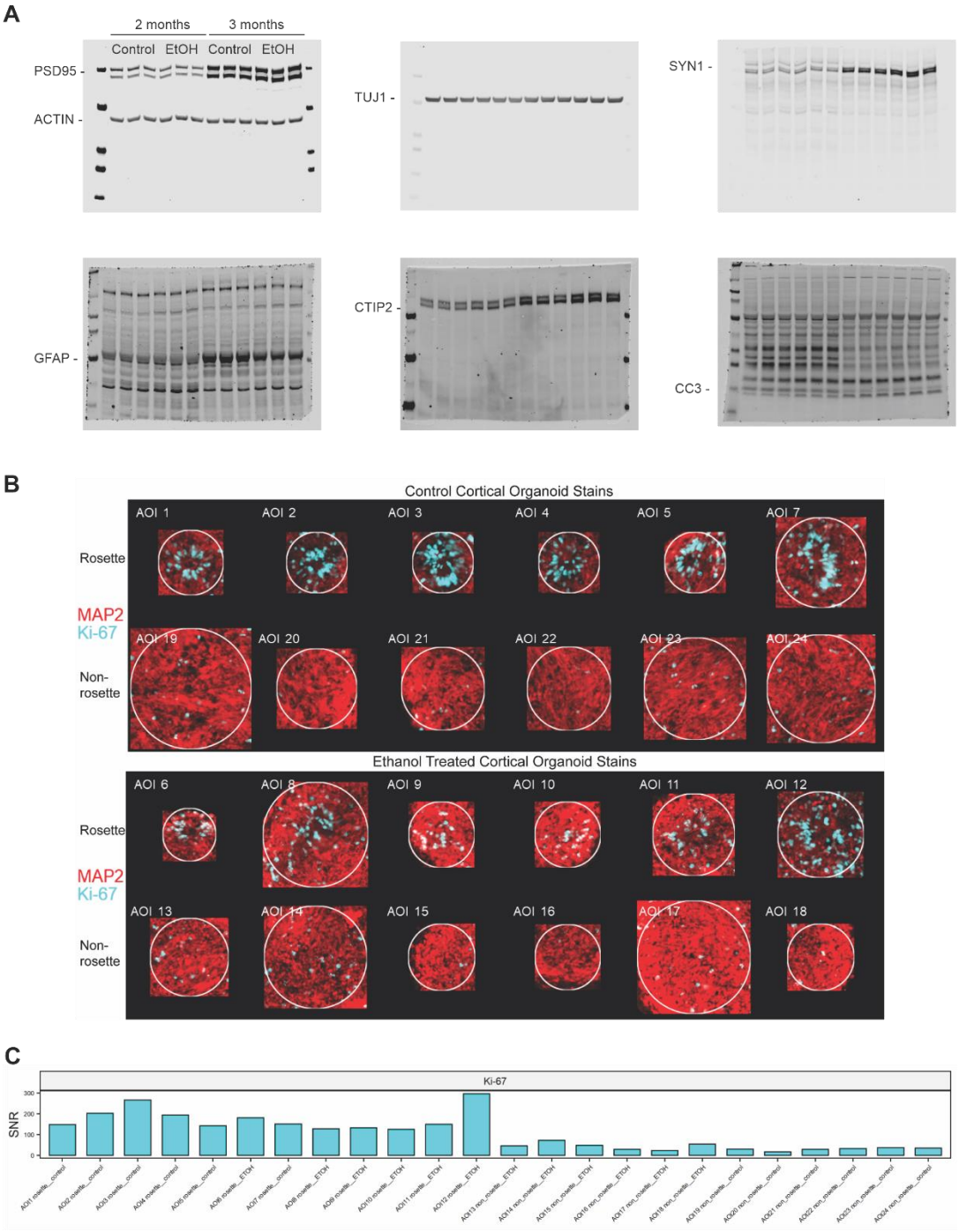

Figure 28: Protein level analysis in different developmental time points and regions in cortical organoids. a Full Western blots shown for two-month and three-month-old control and EtOH-exposed cortical organoids. **b** Spatial proteomic profile of Ki67 and MAP2 staining of selected proliferative (rosette) and differentiated (non-rosette) regions within each cortical organoid condition. **c** Plot showing Ki67 expression for all selected areas of interest (AOIs) corresponding to stain images in (**b**).

References

Adams, J. W., Cugola, F. R., & Muotri, A. R. (2019). Brain organoids as tools for modeling human neurodevelopmental disorders. *Physiology*, *34*(5), 365–375. https://doi.org/10.1152/physiol.00005.2019

Adermark, L., & Bowers, M. S. (2016). Disentangling the Role of Astrocytes in Alcohol Use Disorder. *Alcoholism: Clinical and Experimental Research*, *40*(9), 1802–1816. https://doi.org/10.1111/acer.13168

Amin, E., Jaiswal, M., Derewenda, U., Reis, K., Nouri, K., Koessmeier, K. T., Aspenström, P., Somlyo, A. V., Dvorsky, R., & Ahmadian, M. R. (2016). Deciphering the molecular and functional basis of RHOGAP family proteins: A systematic approach toward selective inactivation of RHO family proteins. *Journal of Biological Chemistry*, *291*(39), 20353–20371. https://doi.org/10.1074/jbc.M116.736967

Anthony, B., Zhou, F. C., Ogawa, T., Goodlett, C. R., & Ruiz, J. (2008). Alcohol exposure alters cell cycle and apoptotic events during early neurulation. *Alcohol and Alcoholism*, *43*(3), 261–273. https://doi.org/10.1093/alcalc/agm166

Arzua, T., Yan, Y., Jiang, C., Logan, S., Allison, R. L., Wells, C., Kumar, S. N., Schäfer, R., & Bai, X. (2020). Modeling alcohol-induced neurotoxicity using human induced pluripotent stem cell-derived three-dimensional cerebral organoids. *Translational Psychiatry*, *10*(347). https://doi.org/10.1038/s41398-020-01029-4

Astley, S. J., Aylward, E. H., Olson, H. C., Kerns, K., Brooks, A., Coggins, T. E., Davies, J., Dorn, S., Gendler, B., Jirikowic, T., Kraegel, P., Maravilla, K., & Richards, T. (2009). Magnetic resonance imaging outcomes from a comprehensive magnetic resonance study of children with fetal alcohol spectrum disorders. *Alcoholism: Clinical and Experimental Research*, *33*(10), 1671–1689. https://doi.org/10.1111/j.1530-0277.2009.01004.x

Bell, S. H., Stade, B., Reynolds, J. N., Rasmussen, C., Andrew, G., Hwang, P. A., & Carlen, P. L. (2010). The remarkably high prevalence of epilepsy and seizure history in fetal alcohol spectrum disorders. *Alcoholism: Clinical and Experimental Research*, *34*(6), 1084–1089. https://doi.org/10.1111/j.1530-0277.2010.01184.x

Bershteyn, M., Nowakowski, T. J., Pollen, A. A., Di Lullo, E., Nene, A., Wynshaw-Boris, A., & Kriegstein, A. R. (2017). Human iPSC-Derived Cerebral Organoids Model Cellular Features of Lissencephaly and Reveal Prolonged Mitosis of Outer Radial Glia. *Cell Stem Cell*, *20*(4), 435-449.e4. https://doi.org/10.1016/j.stem.2016.12.007

Boronat, S., Sánchez-Montañez, A., Gómez-Barros, N., Jacas, C., Martínez-Ribot, L., Vázquez, E., & del Campo, M. (2017). Correlation between morphological MRI findings and specific diagnostic categories in fetal alcohol spectrum disorders. *European Journal of Medical Genetics*, *60*(1), 65–71. https://doi.org/10.1016/j.ejmg.2016.09.003

Burd, L., Blair, J., & Dropps, K. (2012). Prenatal alcohol exposure, blood alcohol concentrations and alcohol elimination rates for the mother, fetus and newborn. *Journal of Perinatology*, *32*(9), 652–659. https://doi.org/10.1038/jp.2012.57

Burd, L., Klug, M. G., Bueling, R., Martsolf, J., Olson, M., & Kerbeshian, J. (2008). Mortality rates in subjects with fetal alcohol spectrum disorders and their siblings. *Birth Defects Research Part A - Clinical and Molecular Teratology*, *82*(4), 217–223. https://doi.org/10.1002/bdra.20445

Camp, J. G., Badsha, F., Florio, M., Kanton, S., Gerber, T., Wilsch-Bräuninger, M., Lewitus, E., Sykes, A., Hevers, W., Lancaster, M., Knoblich, J. A., Lachmann, R., Pääbo, S., Huttner, W. B., & Treutlein, B. (2015). Human cerebral organoids recapitulate gene expression programs of fetal neocortex development. *Proceedings of the National Academy of Sciences*, *112*(51), 201520760. https://doi.org/10.1073/pnas.1520760112

Chailangkarn, T., Trujillo, C. A., Freitas, B. C., Hrvoj-Mihic, B., Herai, R. H., Yu, D. X., Brown, T. T., Marchetto, M. C., Bardy, C., McHenry, L., Stefanacci, L., Järvinen, A., Searcy, Y. M., Dewitt, M., Wong, W., Lai, P., Ard, M. C., Hanson, K. L., Romero, S., Jacobs, B., Dale, A. M., Dai, L., Korenberg, J. R., Gage, F. H., Bellugi, U., Halgren, E., Semendeferi, K., & Muotri, A. R. (2016). A human neurodevelopmental model for Williams syndrome. *Nature*, *536*(7616), 338–343. https://doi.org/10.1038/nature19067

De Filippis, L., Halikere, A., McGowan, H., Moore, J. C., Tischfield, J. A., Hart, R. P., & Pang, Z. P. (2016). Ethanol-mediated activation of the NLRP3 inflammasome in iPS cells and iPS cells-derived neural progenitor cells. *Molecular Brain*, *9*(51). https://doi.org/10.1186/s13041-016-0221-7

Dolganiuc, A., & Szado, G. (2009). In vitro and in vivo models of acute alcohol exposure. *World Journal of Gastroenterology*, *15*(10), 1168–1177. https://doi.org/10.3748/wjg.15.1168

Draghici, S., Khatri, P., Tarca, A. L., Amin, K., Done, A., Voichita, C., Georgescu, C., & Romero, R. (2007). A systems biology approach for pathway level analysis. *Genome Research*, *17*(10), 1537–1545. https://doi.org/10.1101/gr.6202607

Fabregat, A., Jupe, S., Matthews, L., Sidiropoulos, K., Gillespie, M., Garapati, P., Haw, R., Jassal, B., Korninger, F., May, B., Milacic, M., Roca, C. D., Rothfels, K., Sevilla, C., Shamovsky, V., Shorser, S., Varusai, T., Viteri, G., Weiser, J., Wu, G., Stein, L., Hermjakob, H., & D'Eustachio, P. (2018). The Reactome Pathway Knowledgebase. *Nucleic Acids Research*, *46*, D649–D655. https://doi.org/10.1093/nar/gkx1132

Fietz, S. A., Lachmann, R., Brandl, H., Kircher, M., Samusik, N., Schröder, R., Lakshmanaperumal, N., Henry, I., Vogt, J., Riehn, A., Distler, W., Nitsch, R., Enard, W., Pääbo, S., & Huttner, W. B. (2012). Transcriptomes of germinal zones of human and mouse fetal neocortex suggest a role of extracellular matrix in progenitor self-renewal. *Proceedings of the National Academy of Sciences of the United States of America*,

109(29), 11836–11841. https://doi.org/10.1073/pnas.1209647109

Garcia, B. A., Mollah, S., Ueberheide, B. M., Busby, S. A., Muratore, T. L., Shabanowitz, J., & Hunt, D. F. (2007). Chemical derivatization of histones for facilitated analysis by mass spectrometry. *Nature Protocols*, *2*(4), 933–938. https://doi.org/10.1038/nprot.2007.106

Guerri, C., Sáez, R., Sancho-Tello, M., Martin de Aquilera, E., & Renau-Piqueras, J. (1990). Ethanol alters astrocyte development: A study of critical periods using primary cultures. *Neurochemical Research*, *15*(5), 559–565. https://doi.org/10.1007/BF00966217

Guizzetti, M., Moore, N. H., Giordano, G., VanDeMark, K. L., & Costa, L. G. (2010). Ethanol inhibits neuritogenesis induced by astrocyte muscarinic receptors. *Glia*, *58*(12), 1395–1406. https://doi.org/10.1002/glia.21015

Halder, D., Mandal, C., Lee, B. H., Lee, J. S., Choi, M. R., Chai, J. C., Lee, Y. S., Jung, K. H., & Chai, Y. G. (2015). PCDHB14 - And GABRB1 -like nervous system developmental genes are altered during early neuronal differentiation of NCCIT cells treated with ethanol. *Human and Experimental Toxicology*, *34*(10), 1017–1027. https://doi.org/10.1177/0960327114566827

Heinz, S., Benner, C., Spann, N., Bertolino, E., Lin, Y. C., Laslo, P., Cheng, J. X., Murre, C., Singh, H., & Glass, C. K. (2010). Simple Combinations of Lineage-Determining Transcription Factors Prime cis-Regulatory Elements Required for Macrophage and B Cell Identities. *Molecular Cell*, *38*(4), 576–589. https://doi.org/10.1016/j.molcel.2010.05.004

Heller, M., & Burd, L. (2014). Review of ethanol dispersion, distribution, and elimination from the fetal compartment. *Birth Defects Research Part A - Clinical and Molecular Teratology*, *100*(4), 277–283. https://doi.org/10.1002/bdra.23232

Hendrickson, T. J., Mueller, B. A., Sowell, E. R., Mattson, S. N., Coles, C. D., Kable, J. A., Jones, K. L., Boys, C. J., Lim, K. O., Riley, E. P., & Wozniak, J. R. (2017). Cortical gyrification is abnormal in children with prenatal alcohol exposure. *NeuroImage: Clinical*, *15*, 391–400. https://doi.org/10.1016/j.nicl.2017.05.015

Hoyme, H. E., Kalberg, W. O., Elliott, A. J., Blankenship, J., Buckley, D., Marais, A. S., Manning, M. A., Robinson, L. K., Adam, M. P., Abdul-Rahman, O., Jewett, T., Coles, C. D., Chambers, C., Jones, K. L., Adnams, C. M., Shah, P. E., Riley, E. P., Charness, M. E., Warren, K. R., & May, P. A. (2016). Updated clinical guidelines for diagnosing fetal alcohol spectrum disorders. *Pediatrics*, *138*(2). https://doi.org/10.1542/peds.2015-4256

Jones, K. L., & Smith, D. W. (1973). Recognition of the Fetal Alcohol Syndrome in Early Infancy. *The Lancet*, *302*(7836), 999–1001. https://doi.org/10.1016/S0140-6736(73)91092-1

Jones, K. L., Smith, D. W., Ulleland, C. N., & Streissguth, A. P. (1973). Pattern of

Malformation in Offspring of Chronic Alcoholic Mothers. *The Lancet*, *1*(7815), 1267–1271.

Joshi, S., Guleria, R. S., Pan, J., Bayless, K. J., Davis, G. E., DiPette, D., & Singh, U. S. (2006). Ethanol impairs Rho GTPase signaling and differentiation of cerebellar granule neurons in a rodent model of fetal alcohol syndrome. *Cellular and Molecular Life Sciences*, *63*(23), 2859–2870. https://doi.org/10.1007/s00018-006-6333-y

Kaminen-Ahola, N., Ahola, A., Maga, M., Mallitt, K. A., Fahey, P., Cox, T. C., Whitelaw, E., & Chong, S. (2010). Maternal ethanol consumption alters the epigenotype and the phenotype of offspring in a mouse model. *PLoS Genetics*, *6*(1), e1000811. https://doi.org/10.1371/journal.pgen.1000811

Kang, H. J., Kawasawa, Y. I., Cheng, F., Zhu, Y., Xu, X., Li, M., Sousa, A. M. M., Pletikos, M., Meyer, K. A., Sedmak, G., Guennel, T., Shin, Y., Johnson, M. B., Krsnik, Ž., Mayer, S., Fertuzinhos, S., Umlauf, S., Lisgo, S. N., Vortmeyer, A., Weinberger, D. R., Mane, S., Hyde, T. M., Huttner, A., Reimers, M., Kleinman, J. E., & Šestan, N. (2011). Spatio-temporal transcriptome of the human brain. *Nature*, *478*(7370), 483–489. https://doi.org/10.1038/nature10523

Krawczyk, M., Ramani, M., Dian, J., Florez, C. M., Mylvaganam, S., Brien, J., Reynolds, J., Kapur, B., Zoidl, G., Poulter, M. O., & Carlen, P. L. (2016). Hippocampal hyperexcitability in fetal alcohol spectrum disorder: Pathological sharp waves and excitatory/inhibitory synaptic imbalance. *Experimental Neurology*, *280*, 70–79. https://doi.org/10.1016/j.expneurol.2016.03.013

Kroener, S., Mulholland, P. J., New, N. N., Gass, J. T., Becker, H. C., & Chandler, L. J. (2012). Chronic alcohol exposure alters behavioral and synaptic plasticity of the rodent prefrontal cortex. *PLoS ONE*, *7*(5), e37541. https://doi.org/10.1371/journal.pone.0037541

Lancaster, M. A., Corsini, N. S., Wolfinger, S., Gustafson, E. H., Phillips, A. W., Burkard, T. R., Otani, T., Livesey, F. J., & Knoblich, J. A. (2017). Guided self-organization and cortical plate formation in human brain organoids. *Nature Biotechnology*, *35*(7), 659–666. https://doi.org/10.1038/nbt.3906

Lancaster, M. A., Renner, M., Martin, C. A., Wenzel, D., Bicknell, L. S., Hurles, M. E., Homfray, T., Penninger, J. M., Jackson, A. P., & Knoblich, J. A. (2013). Cerebral organoids model human brain development and microcephaly. *Nature*, *501*(7467), 373–379. https://doi.org/10.1038/nature12517

Lange, S., Probst, C., Rehm, J., & Popova, S. (2017). Prevalence of binge drinking during pregnancy by country and World Health Organization region: Systematic review and meta-analysis. *Reproductive Toxicology*, *73*, 214–221. https://doi.org/10.1016/j.reprotox.2017.08.004

Laufer, B. I., Kapalanga, J., Castellani, C. A., Diehl, E. J., Yan, L., & Singh, S. M. (2015). Associative DNA methylation changes in children with prenatal alcohol exposure. *Epigenomics*, *7*(8), 1259–1274. https://doi.org/10.2217/epi.15.60

Lebel, C., Roussotte, F., & Sowell, E. R. (2011). Imaging the impact of prenatal alcohol exposure on the structure of the developing human brain. *Neuropsychology Review*, *21*(2), 102–118. https://doi.org/10.1007/s11065-011-9163-0

Liberzon, A., Subramanian, A., Pinchback, R., Thorvaldsdóttir, H., Tamayo, P., & Mesirov, J. P. (2011). Molecular signatures database (MSigDB) 3.0. *Bioinformatics*, *27*(12), 1739–1740. https://doi.org/10.1093/bioinformatics/btr260

Lindsley, T. A., Shah, S. N., & Ruggiero, E. A. (2011). Ethanol Alters BDNF-Induced Rho GTPase Activation in Axonal Growth Cones. *Alcoholism: Clinical and Experimental Research*, *35*(7), 1321–1330. https://doi.org/10.1111/j.1530-0277.2011.01468.x

Luo, C., Lancaster, M. A., Castanon, R., Nery, J. R., Knoblich, J. A., & Ecker, J. R. (2016). Cerebral Organoids Recapitulate Epigenomic Signatures of the Human Fetal Brain. *Cell Reports*, *17*(12), 3369–3384. https://doi.org/10.1016/j.celrep.2016.12.001

MacLean, B., Tomazela, D. M., Shulman, N., Chambers, M., Finney, G. L., Frewen, B., Kern, R., Tabb, D. L., Liebler, D. C., & MacCoss, M. J. (2010). Skyline: An open source document editor for creating and analyzing targeted proteomics experiments. *Bioinformatics*, *26*(7), 966–968. https://doi.org/10.1093/bioinformatics/btq054

Mandal, C., Halder, D., Jung, K. H., & Chai, Y. G. (2017). In utero alcohol exposure and the alteration of histone marks in the developing fetus: An epigenetic phenomenon of maternal drinking. *International Journal of Biological Sciences*, *13*(9), 1100–1108. https://doi.org/10.7150/ijbs.21047

May, P. A., Chambers, C. D., Kalberg, W. O., Zellner, J., Feldman, H., Buckley, D., Kopald, D., Hasken, J. M., Xu, R., Honerkamp-Smith, G., Taras, H., Manning, M. A., Robinson, L. K., Adam, M. P., Abdul-Rahman, O., Vaux, K., Jewett, T., Elliott, A. J., Kable, J. A., Akshoomoff, N., Daniel, F., Arroyo, J. A., Hereld, D., Riley, E. P., Charness, M. E., Coles, C. D., Warren, K. R., Jones, K. L., & Hoyme, H. E. (2018). Prevalence of fetal alcohol spectrum disorders in 4 US communities. *JAMA - Journal of the American Medical Association*, *319*(5), 474–482. https://doi.org/10.1001/jama.2017.21896

May, P. A., Gossage, J. P., Kalberg, W. O., Robinson, L. K., Buckley, D., Manning, M., & Hoyme, H. E. (2009). Prevalence and epidemiologic characteristics of FASD from various research methods with an emphasis on recent in-school studies. *Developmental Disabilities Research Reviews*, *15*(3), 176–192. https://doi.org/10.1002/ddrr.68

Merritt, C. R., Ong, G. T., Church, S. E., Barker, K., Danaher, P., Geiss, G., Hoang, M., Jung, J., Liang, Y., McKay-Fleisch, J., Nguyen, K., Norgaard, Z., Sorg, K., Sprague, I., Warren, C., Warren, S., Webster, P. J., Zhou, Z., Zollinger, D. R., Dunaway, D. L.,

Mills, G. B., & Beechem, J. M. (2020). Multiplex digital spatial profiling of proteins and RNA in fixed tissue. *Nature Biotechnology*, *38*(5), 586–599. https://doi.org/10.1038/s41587-020-0472-9

Mews, P., Egervari, G., Nativio, R., Sidoli, S., Donahue, G., Lombroso, S. I., Alexander, D. C., Riesche, S. L., Heller, E. A., Nestler, E. J., Garcia, B. A., & Berger, S. L. (2019). Alcohol metabolism contributes to brain histone acetylation. *Nature*, *574*(7780), 717–721. https://doi.org/10.1038/s41586-019-1700-7

Mitchell, A. L., Attwood, T. K., Babbitt, P. C., Blum, M., Bork, P., Bridge, A., Brown, S. D., Chang, H. Y., El-Gebali, S., Fraser, M. I., Gough, J., Haft, D. R., Huang, H., Letunic, I., Lopez, R., Luciani, A., Madeira, F., Marchler-Bauer, A., Mi, H., Natale, D. A., Necci, M., Nuka, G., Orengo, C., Pandurangan, A. P., Paysan-Lafosse, T., Pesseat, S., Potter, S. C., Qureshi, M. A., Rawlings, N. D., Redaschi, N., Richardson, L. J., Rivoire, C., Salazar, G. A., Sangrador-Vegas, A., Sigrist, C. J. A., Sillitoe, I., Sutton, G. G., Thanki, N., Thomas, P. D., Tosatto, S. C. E., Yong, S. Y., & Finn, R. D. (2019). InterPro in 2019: Improving coverage, classification and access to protein sequence annotations. *Nucleic Acids Research*, *47*, D351–D360. https://doi.org/10.1093/nar/gky1100

Nageshappa, S., Carromeu, C., Trujillo, C. A., Mesci, P., Espuny-Camacho, I., Pasciuto, E., Vanderhaeghen, P., Verfaillie, C. M., Raitano, S., Kumar, A., Carvalho, C. M. B., Bagni, C., Ramocki, M. B., Araujo, B. H. S., Torres, L. B., Lupski, J. R., Van Esch, H., & Muotri, A. R. (2016). Altered neuronal network and rescue in a human MECP2 duplication model. *Molecular Psychiatry*, *21*(2), 178–188. https://doi.org/10.1038/mp.2015.128

Negraes, P. D., Trujillo, C. A., Yu, N. K., Wu, W., Yao, H., Liang, N., Lautz, J. D., Kwok, E., McClatchy, D., Diedrich, J., de Bartolome, S. M., Truong, J., Szeto, R., Tran, T., Herai, R. H., Smith, S. E. P., Haddad, G. G., Yates, J. R., & Muotri, A. R. (2021). Altered network and rescue of human neurons derived from individuals with early-onset genetic epilepsy. *Molecular Psychiatry*, *26*(11), 7047–7068. https://doi.org/10.1038/s41380-021-01104-2

Pașca, A. M., Park, J. Y., Shin, H. W., Qi, Q., Revah, O., Krasnoff, R., O'Hara, R., Willsey, A. J., Palmer, T. D., & Pașca, S. P. (2019). Human 3D cellular model of hypoxic brain injury of prematurity. *Nature Medicine*, *25*(5), 784–791. https://doi.org/10.1038/s41591-019-0436-0

Patro, R., Duggal, G., Love, M. I., Irizarry, R. A., & Kingsford, C. (2017). Salmon provides fast and bias-aware quantification of transcript expression. *Nature Methods*, *14*(4), 417–419. https://doi.org/10.1038/nmeth.4197

Popova, S., Lange, S., Probst, C., Gmel, G., & Rehm, J. (2018). Global prevalence of alcohol use and binge drinking during pregnancy, and fetal alcohol spectrum disorder. *Biochemistry and Cell Biology*, *96*(2), 237–240. https://doi.org/10.1139/bcb-2017-0077

Quadrato, G., Nguyen, T., Macosko, E. Z., Sherwood, J. L., Yang, S. M., Berger, D. R., Maria, N., Scholvin, J., Goldman, M., Kinney, J. P., Boyden, E. S., Lichtman, J. W., Williams, Z. M., McCarroll, S. A., & Arlotta, P. (2017). Cell diversity and network dynamics in photosensitive human brain organoids. *Nature*, *545*(7652), 48–53. https://doi.org/10.1038/nature22047

R Core Team (2020). *R: A language and environment for statistical computing*. R Foundation for Statistical Computing.

Rasmussen, C., Andrew, G., Zwaigenbaum, L., & Tough, S. (2008). Neurobehavioural outcomes of children with fetal alcohol spectrum disorders: A Canadian perspective. *Paediatrics and Child Health*, *13*(3), 185–191. https://doi.org/10.1093/pch/13.3.185

Renthal, W., & Nestler, E. J. (2009). Chromatin regulation in drug addiction and depression. *Dialogues in Clinical Neuroscience*, *11*(3), 257–268.

Riley, E. P., Infante, M. A., & Warren, K. R. (2011). Fetal Alcohol Spectrum Disorders : An Overview. *Neuropsychology Review*, *21*, 73–80. https://doi.org/10.1007/s11065-011-9166-x

Riley, E. P., McGee, C. L., & Sowell, E. R. (2004). Teratogenic Effects of Alcohol: A Decade of Brain Imaging. *American Journal of Medical Genetics - Seminars in Medical Genetics*, *127 C*(1), 35–41. https://doi.org/10.1002/ajmg.c.30014

Roozen, S., Peters, G. J. Y., Kok, G., Townend, D., Nijhuis, J., & Curfs, L. (2016). Worldwide Prevalence of Fetal Alcohol Spectrum Disorders: A Systematic Literature Review Including Meta-Analysis. *Alcoholism: Clinical and Experimental Research*, *40*(1), 18–32. https://doi.org/10.1111/acer.12939

Sánchez-Alvarez, R., Gayen, S., Vadigepalli, R., & Anni, H. (2013). Ethanol Diverts Early Neuronal Differentiation Trajectory of Embryonic Stem Cells by Disrupting the Balance of Lineage Specifiers. *PLoS ONE*, *8*(5), e63794. https://doi.org/10.1371/journal.pone.0063794

Santillano, D. R., Kumar, L. S., Prock, T. L., Camarillo, C., Tingling, J. D., & Miranda, R. C. (2005). Ethanol induces cell-cycle activity and reduces stem cell diversity to alter both regenerative capacity and differentiation potential of cerebral cortical neuroepithelial precursors. *BMC Neuroscience*, *6*(59). https://doi.org/10.1186/1471-2202-6-59

Santos, R., Vadodaria, K. C., Jaeger, B. N., Mei, A., Lefcochilos-Fogelquist, S., Mendes, A. P. D., Erikson, G., Shokhirev, M., Randolph-Moore, L., Fredlender, C., Dave, S., Oefner, R., Fitzpatrick, C., Pena, M., Barron, J. J., Ku, M., Denli, A. M., Kerman, B. E., Charnay, P., Kelsoe, J. R., Marchetto, M. C., & Gage, F. H. (2017). Differentiation of Inflammation-Responsive Astrocytes from Glial Progenitors Generated from Human Induced Pluripotent Stem Cells. *Stem Cell Reports*, *8*(6), 1757–1769. https://doi.org/10.1016/j.stemcr.2017.05.011

Sawada Feldman, H., Lyons Jones, K., Lindsay, S., Slymen, D., Klonoff-Cohen, H., Kao, K., Rao, S., & Chambers, C. (2012). Prenatal Alcohol Exposure Patterns and Alcohol-Related Birth Defects and Growth Deficiencies: A Prospective Study. *Alcoholism: Clinical and Experimental Research*, *36*(4), 670–676. https://doi.org/10.1111/j.1530-0277.2011.01664.x

Slenter, D. N., Kutmon, M., Hanspers, K., Riutta, A., Windsor, J., Nunes, N., Mélius, J., Cirillo, E., Coort, S. L., DIgles, D., Ehrhart, F., Giesbertz, P., Kalafati, M., Martens, M., Miller, R., Nishida, K., Rieswijk, L., Waagmeester, A., Eijssen, L. M. T., Evelo, C. T., Pico, A. R., & Willighagen, E. L. (2018). WikiPathways: A multifaceted pathway database bridging metabolomics to other omics research. *Nucleic Acids Research*, *46*, D661–D667. https://doi.org/10.1093/nar/gkx1064

Stankiewicz, T. R., & Linseman, D. A. (2014). Rho family GTPases: Key players in neuronal development, neuronal survival, and neurodegeneration. *Frontiers in Cellular Neuroscience*, *8*(314). https://doi.org/10.3389/fncel.2014.00314

Stein, J. L., de la Torre-Ubieta, L., Tian, Y., Parikshak, N. N., Hernández, I. A., Marchetto, M. C., Baker, D. K., Lu, D., Hinman, C. R., Lowe, J. K., Wexler, E. M., Muotri, A. R., Gage, F. H., Kosik, K. S., & Geschwind, D. H. (2014). A quantitative framework to evaluate modeling of cortical development by neural stem cells. *Neuron*, *83*(1), 69–86. https://doi.org/10.1016/j.neuron.2014.05.035

Subramanian, A., Tamayo, P., Mootha, V. K., Mukherjee, S., Ebert, B. L., Gillette, M. A., Paulovich, A., Pomeroy, S. L., Golub, T. R., Lander, E. S., & Mesirov, J. P. (2005). Gene set enrichment analysis: A knowledge-based approach for interpreting genome-wide expression profiles. *Proceedings of the National Academy of Sciences of the United States of America*, *102*(43), 15545–15550. https://doi.org/10.1073/pnas.0506580102

Tateno, M., Ukai, W., Yamamoto, M., Hashimoto, E., Ikeda, H., & Saito, T. (2005). The effect of ethanol on cell fate determination of neural stem cells. *Alcoholism: Clinical and Experimental Research*, *29*(12 SUPPL.), 225–229. https://doi.org/10.1097/01.alc.0000190658.56149.d4

Thomas, C. A., Tejwani, L., Trujillo, C. A., Negraes, P. D., Herai, R. H., Mesci, P., Macia, A., Crow, Y. J., & Muotri, A. R. (2017). Modeling of TREX1-Dependent Autoimmune Disease using Human Stem Cells Highlights L1 Accumulation as a Source of Neuroinflammation. *Cell Stem Cell*, *21*(3), 319-331.e8. https://doi.org/10.1016/j.stem.2017.07.009

Trevino, A. E., Sinnott-Armstrong, N., Andersen, J., Yoon, S. J., Huber, N., Pritchard, J. K., Chang, H. Y., Greenleaf, W. J., & Pașca, S. P. (2020). Chromatin accessibility dynamics in a model of human forebrain development. *Science*, *367*(6476). https://doi.org/10.1126/science.aay1645

Trujillo, C. A., Adams, J. W., Negraes, P. D., Carromeu, C., Tejwani, L., Acab, A., Tsuda, B.,

Thomas, C. A., Sodhi, N., Fichter, K. M., Romero, S., Zanella, F., Sejnowski, T. J., Ulrich, H., & Muotri, A. R. (2021). Pharmacological reversal of synaptic and network pathology in human MECP2 -KO neurons and cortical organoids. *EMBO Molecular Medicine*, *13:e12523*. https://doi.org/10.15252/emmm.202012523

Trujillo, C. A., Gao, R., Negraes, P. D., Gu, J., Buchanan, J., Preissl, S., Wang, A., Wu, W., Haddad, G. G., Chaim, I. A., Domissy, A., Vandenberghe, M., Devor, A., Yeo, G. W., Voytek, B., & Muotri, A. R. (2019). Complex Oscillatory Waves Emerging from Cortical Organoids Model Early Human Brain Network Development. *Cell Stem Cell*, *25*(4), 558-569.e7. https://doi.org/10.1016/j.stem.2019.08.002

Trujillo, C. A., Rice, E. S., Schaefer, N. K., Chaim, I. A., Wheeler, E. C., Madrigal, A. A., Buchanan, J., Preissl, S., Wang, A., Negraes, P. D., Szeto, R. A., Herai, R. H., Huseynov, A., Ferraz, M. S. A., Borges, F. S., Kihara, A. H., Byrne, A., Marin, M., Vollmers, C., Brooks, A. N., Lautz, J. D., Semendeferi, K., Shapiro, B., Yeo, G. W., Smith, S. E. P., Green, R. E., & Muotri, A. R. (2021). Reintroduction of the archaic variant of NOVA1 in cortical organoids alters neurodevelopment. *Science*, *371*(6530). https://doi.org/10.1126/science.aax2537

Vaags, A. K., Lionel, A. C., Sato, D., Goodenberger, M., Stein, Q. P., Curran, S., Ogilvie, C., Ahn, J. W., Drmic, I., Senman, L., Chrysler, C., Thompson, A., Russell, C., Prasad, A., Walker, S., Pinto, D., Marshall, C. R., Stavropoulos, D. J., Zwaigenbaum, L., Fernandez, B. A., Fombonne, E., Bolton, P. F., Collier, D. A., Hodge, J. C., Roberts, W., Szatmari, P., & Scherer, S. W. (2012). Rare deletions at the neurexin 3 locus in autism spectrum disorder. *American Journal of Human Genetics*, *90*(1), 133–141. https://doi.org/10.1016/j.ajhg.2011.11.025

Valenzuela, C. F., Puglia, M. P., & Zucca, S. (2011). Focus on : Neurotransmitter Systems. *Alcohol Research & Health*, *34*(1), 106–120.

Vangipuram, S. D., Grever, W. E., Parker, G. C., & Lyman, W. D. (2008). Ethanol increases fetal human neurosphere size and alters adhesion molecule gene expression. *Alcoholism: Clinical and Experimental Research*, *32*(2), 339–347. https://doi.org/10.1111/j.1530-0277.2007.00568.x

Veazey, K. J., Carnahan, M. N., Muller, D., Miranda, R. C., & Golding, M. C. (2013). Alcohol-induced epigenetic alterations to developmentally crucial genes regulating neural stemness and differentiation. *Alcoholism: Clinical and Experimental Research*, *37*(7), 1111–1122. https://doi.org/10.1111/acer.12080

Zhang, Y., Liu, T., Meyer, C. A., Eeckhoute, J., Johnson, D. S., Bernstein, B. E., Nussbaum, C., Myers, R. M., Brown, M., Li, W., & Shirley, X. S. (2008). Model-based analysis of ChIP-Seq (MACS). *Genome Biology*, *9*(9), R137.1-R137.9. https://doi.org/10.1186/gb-2008-9-9-r137

Zhao, X., & Bhattacharyya, A. (2018). Human Models Are Needed for Studying Human

Neurodevelopmental Disorders. *American Journal of Human Genetics*, *103*(6), 829–857. https://doi.org/10.1016/j.ajhg.2018.10.009

Zhou, F. C. (2015). Dissecting FASD through the global transcriptome. *Alcoholism: Clinical and Experimental Research*, *39*(3), 408–412. https://doi.org/10.1111/acer.12655

Acknowledgements

Appendix 3, in full, has been submitted for publication of the material as it may appear in *Molecular Psychiatry*: Adams, J. W., Negraes, P. D., Truong, J., Tran, T., Szeto, R. A., Teodorof-Diedrich, C., Spector, S. A., Del Campo, M., Jones, K. L., Muotri, A. R.*, & Trujillo, C. A.* (2022). **Impact of alcohol exposure on neural development and network formation in human cortical organoids.** The dissertation author was the primary researcher and author of this paper.